

Monitoring Tropospheric Composition using Time of Flight Chemical Ionisation Mass Spectrometric Techniques

Thesis submitted in fulfilment of the requirements for the degree of
Doctor of Philosophy at the University of Leicester.

Author: Robert Stephen Blake.
Leicester.
November 2005.

UMI Number: U488029

All rights reserved

INFORMATION TO ALL USERS

The quality of this reproduction is dependent upon the quality of the copy submitted.

In the unlikely event that the author did not send a complete manuscript and there are missing pages, these will be noted. Also, if material had to be removed, a note will indicate the deletion.



UMI U488029

Published by ProQuest LLC 2013. Copyright in the Dissertation held by the Author.
Microform Edition © ProQuest LLC.

All rights reserved. This work is protected against
unauthorized copying under Title 17, United States Code.



ProQuest LLC
789 East Eisenhower Parkway
P.O. Box 1346
Ann Arbor, MI 48106-1346

The work described in this thesis was conducted at the Department of Chemistry of the University of Leicester under the auspices of the Earth Observation Science group between May 2002 and April 2005. The work is that of the author unless acknowledged in the text or references.

The thesis may be made available for consultation within the library of the University of Leicester.

A handwritten signature in black ink, appearing to read 'R S Blake', written in a cursive style.

Robert Stephen Blake
Kirby Muxloe
Leicester LE9 2EA

10th November, 2005

Monitoring Tropospheric Composition using Time of Flight Chemical Ionisation Mass Spectrometric Techniques

Robert S. Blake

November 2005

The use of proton transfer reactions (PTR) to quantify volatile organic compounds (VOCs) occurring in a variety of environments has increased in recent years. Here a 44.4 MBq ^{241}Am source is used to ionise water vapour generating H_3O^+ protonated water molecules. These donate protons to target VOCs in a drift-tube and the resulting positively charged ions are analysed using mass spectrometric methods. This thesis describes how proton transfer reaction products fed into a time-of-flight mass spectrometer (TOF-MS), can produce simultaneous mass spectra for the entire mass range of reacting species in an experiment and produce a mass resolution $m/\Delta m$ greater than 1000.

The scope of application of the investigation has been expanded to include the use of alternative chemical ionisation reagents with proton transfer reactions to form a broader based technique called chemical ionisation reaction mass spectrometry or CIRMS.

In the field, the PTR-TOF-MS has progressed from an experimental machine used at Weybourne, Norfolk in May 2004 to a fully developed research machine at the ACCENT International Intercomparison campaign at Jülich, Germany in January 2005. The object of the ACCENT Intercomparison was to compare detection efficiencies under refereed and controlled conditions of the participants' equipment for commonly occurring tropospheric VOCs. The PTR-TOF-MS produced accurate results for ten of the twelve samples tested, showed measurement consistency in all cases and achieved detection efficiencies of 1 ppbv or better in some cases.

Measurements of atmospheric VOC loadings at the University of Leicester show pronounced weekday and subdued weekend cyclic variations in atmospheric VOC loading and demonstrate the value of the equipment in monitoring Leicester's growing urban pollution.

The PTR-TOF-MS is shown to support chemical ionisation reactions using the reagents, NO^+ , O_2^+ , as in earlier selected ion flow tube (SIFT) work. In experiments using a selection of commonly occurring VOCs as analytes, NO^+ and, to a lesser extent, O_2^+ were found to be useful alternative reagents to H_3O^+ . The results obtained were similar to the SIFT work with the same reagents, but they show the influence of the increased collision energy introduced by the potential gradient applied to the drift-tube and demonstrate the advantages of the broader based CIRMS approach.

The value of switching to NO^+ or O_2^+ as alternative chemical ionisation reagents has been demonstrated for use in the time-of-flight mass spectrometry environment.

Acknowledgements

During the three years that I have been at Leicester University studying for the degree of PhD in Atmospheric Science, I have received help, encouragement and wise counsel from a very wide variety of people in both the Department of Earth Observation Science and the Department of Chemistry. They have succeeded in making my sojourn one of the most enjoyable in my life. The one regret I have is that I did not return to academic life earlier, but then if I did, I may not have been so fortunate. I am doubly fortunate in having a wife, a scion of a family that prizes academic excellence above all. It was with her encouragement, that I made the move to re-enter academic life, after retiring.

Because of the structure of the Atmospheric Science group, I was placed under the care of three supervisors, Drs Paul Monks, Andy Ellis and John Remedios. They have successfully guided me along the paths of righteousness and kept me more or less on the straight and narrow path. For them I give my special thanks for their help, encouragement, guidance and advice.

The technical staff at the Department of Chemistry have patiently put up with my presence and have wrought a series of technical miracles of the highest degree. Here I am thinking particularly of Keith Wilkinson, Gerry Butler, Carl Schiefferstein, Jack Patel and John Weald who have at some stage or other come up with solutions to the impossible. Then there are the occupants of the Atmospheric Chemistry Laboratory, my colleagues and friends who have impressed me with their amiability, *joie de vivre* and general all-round talent in matters scientific. Kevin Wyche, Chris Whyte, Mark Jacob and Alex Parker and all the other people who have spent some time at the laboratory, to them I say: Thank you, with your help and encouragement, I have managed to make what could have been a rough passage into one of consummate smoothness.

Robert Stephen Blake

Kirby Muxloe

September 30th, 2005

List of Contents

CHAPTER 1

1	Introduction and overview	2
1.1	Introduction	2
1.2	Structure of the thesis	3
1.3	The troposphere and its chemical processes	4
1.3.1	The troposphere	4
1.3.2	The main trace constituents of the troposphere	5
1.3.3	Origin of NMHCs	7
1.3.4	The tropospheric oxidation cycle	9
1.3.5	Hydrocarbon chemistry	12
1.3.6	Urban chemistry and smog	14
1.3.7	Study of VOCs and OVOCs	17
1.4	Proton Transfer Reaction Mass Spectrometry (PTR-MS)	18
1.4.1	Deployment	18
1.4.2	Hydronium (H ₃ O ⁺)	20
1.4.3	Cluster formation	22
1.4.4	Chemical ionisation	23
1.4.5	Swarm-tubes, drift-tubes and selected ion flow tubes	25
1.4.6	Standard format for comparison	27
1.4.7	Summary	28

CHAPTER 2

2	Instrumentation	30
2.1	Introduction	30
2.2	Time-of-flight mass spectrometry	30
2.2.1	Basics	30
2.2.2	Development of time-of-flight techniques	31
2.2.3	Linear mass spectrometers	32
2.2.4	Reflectron time-of-flight mass spectrometry	32
2.2.5	Reasons for choosing PTR-TOF-MS	33
2.3	Instrument description	34
2.4	Ion Sources	36
2.4.1	The hollow cathode hydronium generator	37
2.4.1.1	The hollow cathode and source drift regions	38
2.4.1.2	The Venturi Inlet	39
2.4.1.3	The drift-tube	41
2.4.1.4	Computer simulation	43
2.4.1.5	Electrical configurations	44
2.4.1.5.1	Configuration with non-floating power supplies	45
2.4.1.5.2	Configuration with floating power supply	46
2.4.1.6	Operating Conditions	47
2.4.1.7	Bench tests	48
2.4.1.8	Performance criteria	49
2.4.2	The 241Am Ion Source Hydronium Generator	51
2.4.2.1	Construction	53
2.4.2.2	Exit orifice	54

2.4.2.3	Electrical configuration	54
2.4.2.4	Operating conditions	55
2.4.2.5	Bench tests	56
2.4.2.6	Stability	57
2.5	Other features	58
2.5.1	Common Interface Flange	58
2.5.2	Microchannel plate detector (MCP)	59
2.5.3	Detection and processing	61
2.5.4	Operating the TOF-MS	62
2.5.5	Gas handling	65
2.5.6	Temperature control	68
2.5.7	Mass resolution	68
2.6	Control and analysis software	69
2.6.1	Supplied software	69
2.6.1.1	Grams/AI and the Kore extensions	69
2.6.1.2	Spectrum recalibration or rescaling	72
2.6.2	Additional software	73
2.6.2.1	MaxiSum and MaxiBgd	73
2.6.2.2	MaxiGroup	75
2.6.2.3	Spreadsheet-based analysis	75
2.6.2.4	MaxiAnalysis	76
2.6.2.5	MaxiPlot	76
2.7	Summary	77

CHAPTER 3

3	Characterisation	79
3.1	Introduction	79
3.2	Constraints	80
3.3	The controls of the PTR-TOF-MS and the ion source	81
3.4	Parameter optimisation to maximise the H ₃ O ⁺ count rate	83
3.5	Mass range of the PTR-TOF-MS	85
3.6	Microchannel plate performance	85
3.7	Apertures	86
3.8	Drift-tube dynamics	86
3.9	Effect of humidity in the sample gas	88
3.9.1	Cluster formation as a function of E/N	89
3.9.2	Varying the sample humidity	90
3.10	Operating stability and temperature effects	92
3.11	Drift-tube pressure	96
3.12	Determining the sensitivity of the PTR-TOF-MS	97
3.13	Background estimation	102
3.14	Fragmentation determination	102
3.14.1	Principles	102
3.14.2	Calibration and fragmentation	104
3.14.3	Headspace dilution experiments	104
3.14.4	Analysing headspace data	106
3.14.5	Fragmentation results	108
3.14.6	Gas standards	110
3.14.7	Sensitivity assignments	111
3.14.8	Discussion of the sensitivity results	112

3.15	Conclusion	115
------	------------	-----

CHAPTER 4

4	Initial application to atmospheric measurement	117
4.1	Introduction	117
4.2	Linearity, sensitivity and calibration experiments	118
4.2.1	Sensitivity and Detection Limits	118
4.2.2	Linearity of response	118
4.3	Early urban air measurements	119
4.3.1	Experimental procedure	119
4.3.2	Results	120
4.4	Bonfire night	122
4.4.1	Experimental procedure	123
4.4.2	Results	123
4.4.3	Discussion	126
4.5	The TORCH Campaign	127
4.5.1	The site	127
4.5.2	Experimental	130
4.5.3	Runtime history	130
4.5.4	Results	131
4.5.5	Other TORCH results	133
4.5.5.1	University of York	133
4.5.5.2	Combined results	134
4.5.6	Correlation analysis	139
4.5.7	Calibration and calculating concentrations	140
4.5.8	Errors and the level of confidence	142
4.5.8.1	Atmospheric detailed variation	142
4.5.8.2	Precision or Instrumental Limitation Error	142
4.5.8.3	Standard statistical error	143
4.5.8.4	Signal-to-noise ratio (S/N)	144
4.5.9	Some conclusions from the TORCH campaign	146
4.5.10	Determining an alternative range of E/N	148
4.6	Troposphere measurements in Leicester	149
4.6.1	Experimental conditions	150
4.6.2	Results	151
4.6.3	Discussion	154
4.6.4	Gas Chromatography simulation	155
4.7	Summary	156

CHAPTER 5

5	The ACCENT OVOC Intercomparison	159
5.1	ACCENT	159
5.1.1	The Aims of ACCENT	159
5.1.2	Initial workshop	160
5.1.3	The Target OVOCs	162
5.1.4	Experimental protocol	163
5.1.5	The timetable for the intercomparison	164
5.2	Logistics	166
5.3	The installation at Jülich	166

5.3.1	Container	166
5.3.2	Connection to the inlet manifolds	168
5.3.3	Radiation check	168
5.4	Calibration	168
5.4.1	The Bristol / Apel standard	169
5.4.2	Spectrum	170
5.4.3	Federal Atmospheric Laboratory (FAL)	171
5.4.4	Calibration factors	172
5.5	Experimental	174
5.5.1	Continuous running	174
5.5.2	Temperature control	174
5.5.3	Ongoing data processing	174
5.6	Results	175
5.6.1	Diurnal variation in the hydronium count rate	175
5.6.2	List of compounds investigated	176
5.6.3	Background	176
5.6.4	Yield spectra	178
5.7	Results for each target OVOC	180
5.7.1	Interpreting the ACCENT results	180
5.7.2	Compounds not included	182
5.7.3	Acetaldehyde (CH ₃ CHO)	182
5.7.4	Acetone ((CH ₃) ₂ CO)	184
5.7.5	Benzaldehyde (C ₆ H ₅ CHO)	186
5.7.6	Butanal (C ₄ H ₈ O)	188
5.7.7	1-butanol (C ₄ H ₁₀ O)	190
5.7.8	Hexanal (C ₆ H ₁₂ O)	192
5.7.9	MBO (2-Methyl-3-buten-2-ol) (C ₅ H ₁₀ O)	194
5.7.10	Methanol (CH ₃ COH)	196
5.7.11	Methyl Acetate (CH ₃ COOCH ₃)	198
5.7.12	MVK and Methacrolein (C ₄ H ₆ O)	200
5.7.13	1-propanol (C ₃ H ₈ O)	202
5.7.14	Toluene (C ₆ H ₅ CH ₃)	204
5.7.15	Overall summary of results	206
5.8	Reporting results	207
5.8.1	Statistical errors	207
5.8.2	Precision	208
5.8.3	Signal-to-noise ratios	208
5.9	Conclusions	209
5.9.1	Performance	209
5.9.2	Quality of the results	210

CHAPTER 6

6 Chemical ionisation reaction mass spectrometry (CIRMS)	212
6.1 Introduction	212
6.2 Previous investigations using alternative CI reagents	213
6.2.1.1 H ₃ O ⁺	214
6.2.1.2 NH ₄ ⁺	215
6.2.1.3 O ₂ ⁺	216
6.2.1.4 NO ⁺	217
6.3 Experimental section	218
6.3.1 Apparatus	218
6.3.2 Reagent handling	219
6.3.3 Analyte handling	220
6.3.4 Experimental procedure	220
6.4 Reducing interference from residual H ₃ O ⁺	221
6.5 Results	222
6.5.1 Interference from H ₃ O ⁺ clusters	224
6.5.2 Reactions with H ₃ O ⁺	224
6.5.3 Reactions of NH ₄ ⁺	227
6.5.4 Reactions of O ₂ ⁺	228
6.5.5 Reactions of NO ⁺	231
6.5.6 1-butene sensitivity measurements with some CI reagents	234
6.6 Discussion and Conclusion	236

CHAPTER 7

7 Final comments	241
7.1 Development Achievements	241
7.1.1 Hardware development	241
7.1.2 Ease of operation	241
7.1.3 Detection sensitivity	242
7.1.4 Managing fragmentation, temperature effects and time shifts	242
7.2 Scientific achievements	243
7.2.1 Detection sensitivity	243
7.2.2 Accuracy	243
7.2.3 The Leicester atmosphere	243
7.2.4 CIRMS	244
7.2.5 Insensitivity to detection	244
7.3 Ongoing challenges	244
7.3.1 Preamplifier failures	244
7.3.2 Transportation, formalities and red tape	244
7.4 Future development	245
7.4.1 Improving the hydronium count rate	245
7.4.2 Online standards	246
7.4.3 Dedicated instrument	246
7.5 Finally	247

APPENDICES

APPENDIX 1 TABLES

	249
A1.3 Characterisation	249
A1.5 ACCENT intercomparison	251

APPENDIX 2. PUBLICATIONS

	265
A2.1 Articles	265
A2.2 Letters, Posters and Short Communications	265

REFERENCES

References	268
-------------------	------------

Chapter 1

Introduction and overview

*If you steal from one author, it is plagiarism
If you steal from many, it is research.*

Wilson Mizner-American playwright (1876-1933)

1 Introduction and overview

“The determination of atmospheric trace gas concentration constitutes a technological challenge, since extreme sensitivity (some species have to be detected at mixing ratios as low as 10^{-13}) is desired simultaneously with high specificity, i.e. the molecule of interest usually must be detected in the presence of a large excess of other species.”

U. Platt, Phys. Chem. Chem. Phys. 1 (1999) 5409

1.1 Introduction

This thesis addresses the challenge set out above as applied to the detection of trace Non-methane hydrocarbons (NMHCs) in the troposphere and describes an additional technique for this purpose. Two classes of NMHCs are of interest, Volatile Organic Compounds (VOCs) which comprise the alkanes, alkenes and aromatics and an important VOC subgroup, Oxygenated Volatile Organic Compounds (OVOCs). The OVOCs include alcohols, ketones, aldehydes and ethers as well as assorted organic peroxides and acids. The thesis describes a new approach to the specification, design, construction, testing and deployment of an instrument that provides a real-time method for detecting a wide range of trace volatile organic species in a wide range of matrices. Important characteristics of such an instrument should be

- Good temporal resolution – ideally less than a tenth of the rate of change
- Capture data covering a wide mass range effectively simultaneously
- Good sensitivity, capable of detecting concentrations of 1 ppbv or less
- Resolution to distinguish molecules differing in mass by 1 Dalton or less
- Linear response spanning concentrations of sub-ppbv to tens of ppmv
- Long term stability and ease of operation
- Ease of transportation, if not portable then at least mobile.

It was decided that these requirements would be achieved by coupling an ion generator using the Proton Transfer Reaction (PTR) technique to a Time-Of-Flight Mass Spectrometer (TOF-MS). Proton transfer is a widely used chemical ionisation process. The most commonly employed source of protons are hydrated water ions (hydronium or H_3O^+) that act as proton donors to the trace species in a carrier gas so that they can be analysed by a mass spectrometer. The “reaction” part of PTR involves this proton

transfer occurring in a drift-tube where well defined kinetics ultimately allow the concentrations of trace species to be determined.

1.2 Structure of the thesis

Chapter 1, this chapter, continues with a brief overview of the main sources, processes and sinks involved in the chemistry of the troposphere. The discussion is biased towards VOCs (and OVOCs), as they are the species targeted for study in this thesis. This is followed by a brief overview of the techniques generally used to detect VOCs and OVOCs in the troposphere, and a short history of the development of the PTR-MS technique leading up to the development of the PTR-TOF-MS. The advantages of combining the PTR process with a time-of-flight mass spectrometer are discussed.

Chapter 2 is devoted to a description of the development of the new PTR-TOF-MS instrument. Full operating details of the various components of this instrument, including the types of ion sources investigated, are given in Chapter 3, which deals with the characterisation of the instrument.

Chapter 4 describes some of the early experiments carried out with the PTR-TOF-MS. Included in this chapter are details of the TORCH campaign, which was the first field campaign on which the PTR-TOF-MS was deployed. In this initial field campaign there was still much to be learnt about the instrument and the PTR-TOF-MS contribution to the campaign was not a success. Finally a week-long monitoring exercise of the troposphere near the centre of Leicester is described. In this exercise, the PTR-TOF-MS was at its present state of maturity, and so this exercise would be a model for future tropospheric work.

Chapter 5 describes the results from a later study, the ACCENT Intercomparison campaign at Jülich. The results that were obtained there were commended by the international referee at the campaign as being excellent for a technique being developed.

Chapter 6 describes work carried out to determine whether the PTR-TOF-MS could use alternative chemical ionisation reagents, including non-proton-donating species such as

NH_4^+ , O_2^+ and NO^+ . The resulting technique is referred to as chemical ionisation reaction mass spectrometry or CIRMS. The application of this technique to the detection of OVOCs is described and the advantages discussed.

Chapter 7 contains a discussion of the problems and achievements experienced with the PTR-TOF-MS and deals with some suggestions for future work.

1.3 The troposphere and its chemical processes

1.3.1 The troposphere

The earth's atmosphere can be divided into several layers. As shown in Figure 1.1 the troposphere is the layer starting at ground level and extending to an altitude of some 15 km. The layer above the troposphere is the stratosphere and the two layers are separated by the tropopause, a region with characteristics intermediate between the two. The chemistry of the troposphere is influenced by activities occurring at the surface of the earth as well as by solar radiation. There is relatively little interchange between the troposphere and the stratosphere, although in the past it was believed that ozone occurring in the troposphere filtered down from the stratosphere, but now it has been shown that activity within the troposphere is a more likely source.

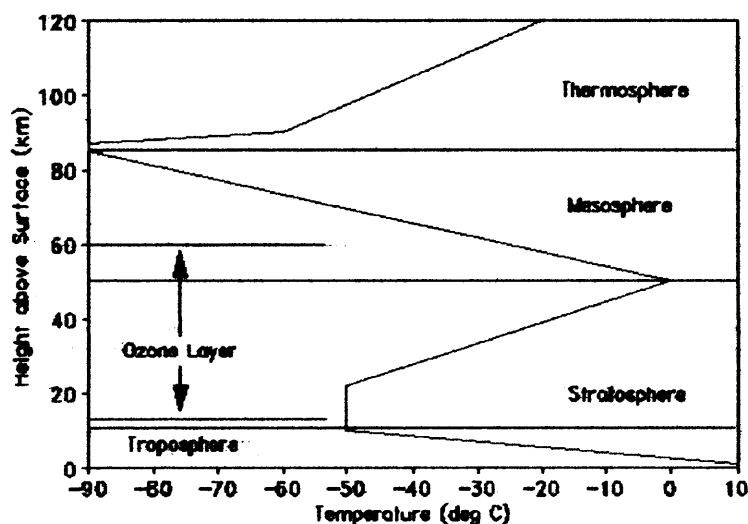


Figure 1.1 The layers in the Earth's atmosphere.

Atmospheric scientists have an active interest in the chemistry of the troposphere, and they have called on other branches of science, such as physics, to provide them with the tools to understand the mechanisms at work.

1.3.2 The main trace constituents of the troposphere

Apart from the main atmospheric gases oxygen, nitrogen, water vapour and CO₂, methane at 1700 ppbv is the most abundant hydrocarbon in the atmosphere (see Table 1.1).

Prior to the year 1800 the level of methane remained relatively constant at about 750 ppbv, and the rise since then coincides with such events as the industrial revolution and other human activities that are starting to change the composition of the atmosphere.

Table 1.1 Estimated sources and sinks of methane in Tg yr⁻¹ [Jackson, 2003].

Identified sources	Individual elements	Total
<i>Natural</i>		
Wetlands	115(50-150)	
Termites	20(0-50)	
Oceans	10(5-50)	
Other	15(10-40)	
Total identified natural resources		160(110-210)
<i>Anthropogenic</i>		
Fossil fuel related sources		
Natural gas	40(25-50)	
Coal mines	30(15-45)	
Petroleum industry	15(5-30)	
Coal combustion	7(1-30)	
Total fossil fuel related		100(70-120)
<i>Biospheric carbon</i>		
Enteric fermentation	85(65-100)	
Rice paddies	60(20-100)	
Biomass burning	40(20-80)	
Landfill	40(20-70)	
Animal waste	25(20-30)	
Domestic sewage	25(15-80)	
Total biospheric		275(200-350)
Total anthropogenic sources		375(300-450)

Identified sources	Individual elements	Total
Total identified sources		535(410-660)
<i>Sinks</i>		
Tropospheric OH	445(360-530)	
Stratospheric	40(15-45)	
Soils	30(15-45)	
Total sinks		515(430-600)
Total global burden	4850 Tg CH ₄	

In addition to methane a large variety of non-methane hydrocarbons (NMHCs) occur in the troposphere. While their relative abundance is lower than methane (typically of the order of ppbv or even pptv), many are far more active chemically and their effect on the environment makes them objects worthy of study. While methane has a lifetime of several years in the atmosphere some NMHCs, and especially some reaction intermediates, have lifetimes measured in hours or minutes.

Table 1.2 Sources of biogenic and anthropogenic NMHCs and some of the more common non-organic compounds [Jackson, 2003].

Compound	Natural sources	Anthropogenic sources
<i>Carbon-containing compounds</i>		
Carbon dioxide (CO ₂)	Respiration, oxidation of natural CO; forest destruction	Combustion of oil, gas, coal and wood; limestone burning
Carbon Monoxide (CO)	Forest fires; atmospheric oxidation of natural hydrocarbons and methane	Incomplete combustion of fossil fuels and wood; in particular motor vehicles, oxidation of hydrocarbons; industrial processes; blast furnaces
Light paraffins (C ₂ – C ₆)	Aerobic biologic source	Natural gas leakage; motor vehicle evaporative emissions; refinery emissions
Olefins (C ₂ – C ₆)	Photochemical degradation of dissolved oceanic organic material	Motor vehicle exhaust; diesel engine exhaust
Aromatic hydrocarbons	Insignificant	Motor vehicle exhaust; evaporative emissions; paints, petrol, solvents
Terpenes (C ₁₀ H ₁₆)	Trees, plants	

Compound	Natural sources	Anthropogenic sources
CFCs & HFCs	None	Refrigerants; blowing agents; propellants
<i>Nitrogen-containing compounds</i>		
Nitric oxide (NO)	Forest fires; anaerobic processes in soil; lightning	Combustion of oil and coal
Nitrogen dioxide (NO ₂)	Forest fires; lightning	Combustion of oil, gas and coal; atmospheric transformation of NO
Nitrous oxide (N ₂ O)	Emission from denitrifying bacteria in soil; oceans	Combustion of oil and coal
Ammonia (NH ₃)	Aerobic biological source in soil; breakdown of amino acids in organic waste	Coal and fuel combustion; waste treatment
<i>Sulphur-containing traces gases</i>		
Dimethyl sulphide (DMS)	Phytoplankton	Landfill gas
Sulphur dioxide (SO ₂)	Oxidation of H ₂ S; volcanic activity	Combustion of oil and coal; roasting sulphide ores
<i>Other minor trace gases</i>		
Hydrogen	Ocean; soils; methane oxidation; isoprene and terpenes via HCHO	Motor vehicle exhaust; oxidation of methane via HCHO
Ozone	In the stratosphere; natural NO – NO ₂ conversion	Man-made NO – NO ₂ conversion; supersonic aircraft
Water (H ₂ O)	Evaporation from oceans	insignificant

In addition to the hydrocarbons, other important components are ozone (O₃), the oxides of nitrogen (known collectively as NO_x, halogen compounds such as HCl, HBr and halo-carbon compounds such as the CFCs and gaseous sulphur compounds where H₂S and SO₂ are the most common. Short-lived radicals such as OH and the peroxy radicals HO₂ and the heavier RO₂ are also present, and play a vital part in many atmospheric chemical processes.

I.3.3 Origin of NMHCs

Anthropogenic NMHCs are produced as a result of human or industrial activity, and biogenic NMHCs are emitted from vegetation or natural processes such as volcanic eruptions or other natural causes. Some of the main natural and anthropogenic sources

are listed in Table 1.2. It is uncertain into which category forest and grassland fires would fall, as they could be the result of natural or human events.

Table 1.3 UK emissions of NMHCs for 1999 (from DEFRA, Digest of Environmental Statistics, 2001).

Source	k tonnes	% of total
Power stations	8	0
Refineries	1	0
Combustion in fuel extraction and transformation	1	0
Domestic	42	2
Commercial, public and agricultural	4	2
Iron and steel	1	0
Other industrial combustion	5	0
Production processes	212	12
Extraction and distribution of fossil fuel	259	15
Solvent use	572	27
Road transport	473	27
Off-road sources	56	3
Military	1	0
Railways	2	0
Shipping	2	0
Civil aircraft	3	0
Waste treatment and disposal	24	1
Agriculture and managed forestry	0	0
Forests	178	10
Total	1744	100

From Table 1.3 it can be seen that the total emission of NMHCs into the UK atmosphere is 1744 k tonne yr⁻¹ (1.74 Tg yr⁻¹). While the UK figure is small compared to the world-wide estimate of 142 Tg yr⁻¹ in 1990 [Middleton, 1995], the distribution of the pollutants is concentrated in a relatively small area.

An interesting figure is the relatively small contribution from biogenic sources (10%) and the large figure from motor traffic and solvent use, each contributing 27% to the UK total.

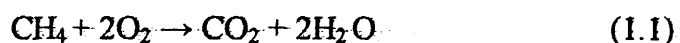
In spite of having a smaller relative abundance when compared to methane, the estimates for the annual global production of NMHCs (VOCs and OVOCs combined) are still substantial and a cause for concern.

NMHC emissions are due mainly to human activities, but it is hard to see how these contributions can be reduced substantially without affecting industrial activity in the UK. Nevertheless, it is important to monitor changes in NMHC emissions to provide information for use in future strategic planning.

The composition of biogenic NMHCs, emitted by plants depends on the types of vegetation, their distribution, seasons or even the time of day. Deciduous plants emit isoprene (2-methyl-1,3-butadiene) which is strongly temperature and light dependent, whereas conifers tend to emit terpenes, which exhibit no diurnal variations. Many OVOCs have biogenic origins, but partially oxidised OVOCs are created by the tropospheric oxidation cycle (see Section 1.3.4).

1.3.4 The tropospheric oxidation cycle

The chemistry of the troposphere is a slow combustion mechanism which, like the familiar type of combustion, is described by the reaction of the general form



using methane as an example. Here the process is mediated by radicals produced by the photolysis of ozone. The actual process of oxidation often comprises several steps in which intermediate oxygenated compounds are formed and then degraded in the next step of the process. In spite of the abundance of O_2 in the atmosphere, the oxidising capacity of the troposphere is determined by the atmospheric burden of O_3 , OH and H_2O_2 and transitory peroxy radicals, HO_2 and RO_2 .

The tropospheric oxidation cycle is initiated by the photo-dissociation of O_3 by light in the presence of water vapour to produce the primary source of OH radicals in the troposphere. Most of the shorter wavelength UV light is absorbed in the stratosphere but longer wavelengths can initiate the dissociation process so that



These reactions account for almost 70% of OH radical production in the troposphere [Cantrell, 1998]. The O(¹D) atoms that do not react with H₂O are quenched by collision with O₂ or N₂ molecules and end up in the ground state where they take no further part in OH production. The OH radicals formed are extremely reactive and will react with any hydrocarbons they encounter.

In conditions of low pollution (low NO_x) OH radicals react with CO or CH₄ molecules to produce peroxy radicals such as HO₂ or CH₃O₂. Peroxy radicals with their excess oxygen play an important part in the oxidation of NO to NO₂ and the production of oxygen-rich intermediates such as hyperoxides ([Monks, 2003] p161). They can also take part in reactions in which they effectively catalyze the destruction of O₃.



The OH radical formed will now react further either by



or with a molecule of CO

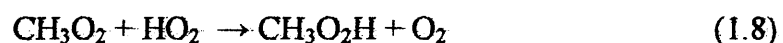


The hydrogen atom will now react with a molecule of O₂



giving rise to a catalytic cycle in which O₃ is destroyed and HO₂ is regenerated.

Alternatively, HO₂ can recombine to form H₂O₂ and oxygen or react with other organic peroxy radicals to form organic hyperoxides, e.g.



which are a sink for further peroxy radical activity. In conditions of high NO_x, the peroxy radical HO₂ forms part of a chain, which regenerates tropospheric ozone:



On the other hand



is also possible, so that for certain concentrations of NO, NO₂ and O₃ an equilibrium photo-stationary state occurs. The compensation point is defined as the NO_x concentration at which the two competing processes, one destroying and the other creating O₃, are in balance. In fact there are other loss processes that skew the equilibrium points.

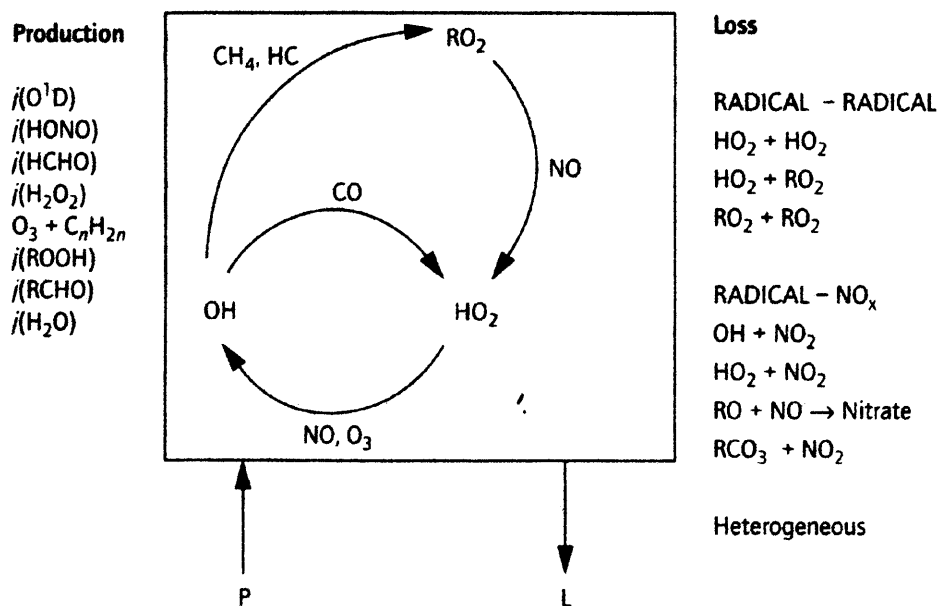


Figure 1.2 The tropospheric oxidation cycle for CH₄ and CO [Monks, 2003].

At night time, in the absence of light, ozone destruction ceases and its concentration in the boundary layer is restored by entrainment from the troposphere, in spite of some minor ozone-depleting processes such as



The conditions for the production and destruction of O₃ are summarised in Table 1.4.

Other peroxy radicals such as CH₃O₂ and other RO₂ can also contribute towards the oxidation of NO to NO₂, leading to regeneration of tropospheric O₃. An alternate sink channel for NO₂ is that it reacts with OH to form HNO₃.

Table 1.4 Summary of the conditions for O₃ creation and destruction in the troposphere.

	Low NO _x	High NO _x
Day	Ozone depleted (Equ. 1.12)	Ozone created (Equ. 1.9 –1.11)
Night	restored by entrainment	Restored by entrainment

The chemistry of NMHCs has close parallels to that of CH₄.

1.3.5 Hydrocarbon chemistry

The study of the behaviour of hydrocarbons in the troposphere is important because of the rôle they play in urban chemistry especially in urban pollution.

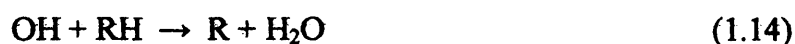
Methane is the most prevalent hydrocarbon constituent in the troposphere, currently 1700 ppbv, and so far the discussion of hydrocarbons has been confined to it and CO. At much lower concentrations, are the NMHCs from a variety of sources that play an important part in the chemistry of the troposphere.

The OH radical is the leading agent for the removal of NMHCs from the troposphere (Table 1.5). Seen from the perspective of the total combustion cycle, OH radicals are quick acting, but because a multitude of steps are needed to complete the combustion cycle, several environmentally undesirable intermediate OVOCs are formed along the way.

Table 1.5 Global turnover of tropospheric gases and the fraction removed by OH.¹

Trace gas	Global emission /Tg yr ⁻¹	Removal by OH /%
CO	2800	85
CH ₄	530	90
C ₂ H ₆	20	90
Isoprene	570	90
Terpenes	140	50
NO ₂	150	50
SO ₂	300	30
DMS - (CH ₃) ₂ S	30	90
CFCl ₃	0.3	0

The reactions that NMHCs undergo are analogous to those of methane. They are initiated by the reaction with OH radicals and follow a path in which alkoxy and peroxy radicals are chain propagators and OH is regenerated afterwards.



The chemistry is summarised in Figure 1.3 which is analogous to Figure 1.2 but considers the case of a general hydrocarbon R rather than the CH₄. The cycle is repeated until the end products are CO₂ and H₂O.

¹ Assuming mean global [OH] = 1x10⁶ molecules cm⁻³. Ehhalt, D., *Phys Chem Phys*, 24, 5401-8, 1999.

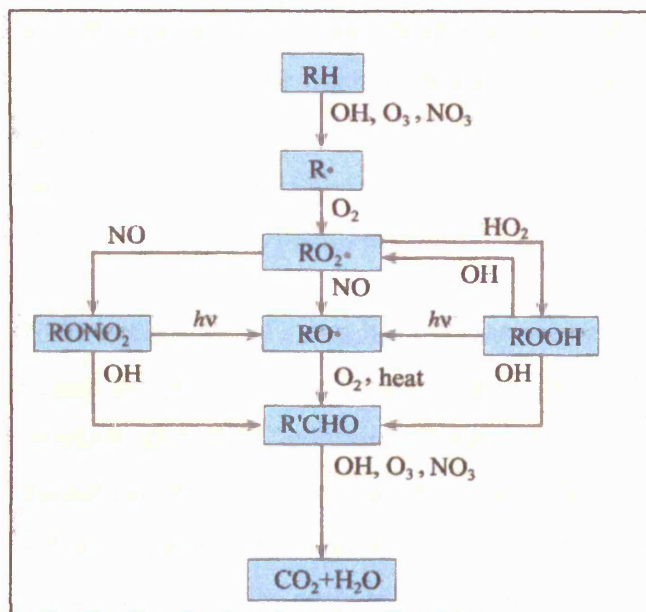


Figure 1.3 The tropospheric oxidation process.

1.3.6 Urban chemistry and smog

It has been claimed that interest in tropospheric chemistry and ozone photochemistry dates from the first appearance of photochemical smog. Smog is defined [Jackson, 2003] as a form of atmospheric pollution formed by the condensation of smoke and fog. It is formed as a result of high temperatures and sunlight promoting the rapid conversion of CO, NO, aromatic and other unburnt or partially oxidised VOCs and OVOCs into secondary pollutants including O₃. Other secondary pollutants are present as well. The term *smog* was first coined by Des Voeux to describe the mixture of smoke and fog that was prevalent in post-Industrial Revolution London.

Haagen-Smit [Haagen-Smit, 1950];[Haagen-Smit, 1952] working in Los Angeles in 1950, established that ozone, the primary ingredient in the smog found there, was not directly emitted from tailpipes or smokestacks, but was created in the atmosphere. Driven by sunlight, a photochemical reaction combined hydrocarbons from oil refineries and the partially unburned exhaust of motor traffic with nitrogen oxides, a combustion by-product, to form ozone.

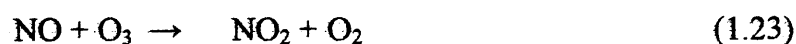
Haagen-Smit observed that in spite of early smoke control measures, residents still smelled a curious bleaching-solution odour in the air, and suffered severe eye irritation

on smoggy days. He was able to show that smog was produced by the reaction of oxides of nitrogen (NO_x) on some of the many hydrocarbon species present as traces in the atmosphere. Ozone was also found to be a major component of smog, although by contrast methane, despite being the most abundant hydrocarbon in the atmosphere, did not appear to have an active part in the phenomenon.

Since the early days, the occurrence of smog has become increasingly widespread, and although in Europe clean air policies have reduced particulate pollution from sources such as coal, hydrocarbon and NO_x, emissions from increasing motor traffic have resulted in the increased occurrence of hydrocarbon-based pollution or smog. In the UK, most industrial centres are pollution generators. The rise in the CO₂ level in the atmosphere from about 290 ppmv to the present 380 ppmv since the year 1800 has been ascribed in part to the rise of burning of fossil fuels but also to other forms of combustion of biomass ([Brasseur *et al.*, 1999] p170 *et seq.*).

It has become necessary to monitor the increase in atmospheric pollution constantly and to try and identify their sources and wherever possible, take steps to eliminate these. Extensive research has gone into establishing the mechanisms and intermediate products following the degrading of VOCs, OVOCs and the other organic compounds.

The following is a reaction scheme for photochemical smog formation. These reactions are all concurrent but not chained.





The reactions taking place can be summarised as representing the oxidation of VOCs which drives the formation of NO and NO₂. In the presence of sunlight the NO₂ can be dissociated to take part in the formation of O₃, while any O₃ already present can oxidise NO to NO₂.

In addition to the normal photolysis of O₃ (1.2) under polluted urban conditions there are additional sources of OH, such as the case with HONO emitted by motor car exhausts:



HO₂ is produced from the oxidation of formaldehyde under the influence of light, which can be summarised:

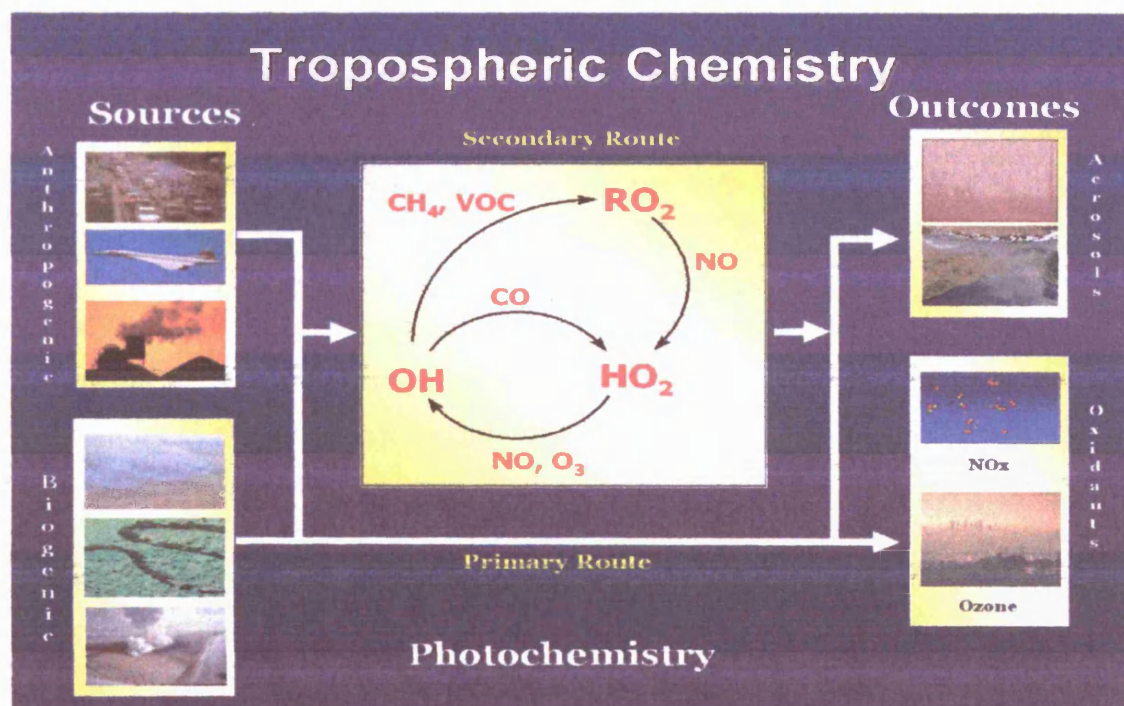
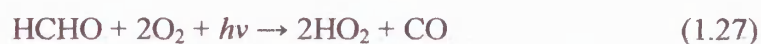


Figure 1.4 Summary of the sources, processes and sinks in tropospheric chemistry.

An interesting by-product of oxidation is peroxyacetylnitrate (PAN). This compound, CH₃C(O)OONO₂, is the end product of a series of reactions starting with acetaldehyde

and involving OH, O₂ and NO₂. Its lifetime at 25 °C is 30 minutes but 8 hours at 0 °C and several weeks at the temperatures encountered in the mid-troposphere. PAN created at ground level and transported into the mid-troposphere can travel long distances before returning to ground level. Once back at ground level, the ambient temperature is higher and the PAN decomposes releasing the NO₂ into the troposphere. PAN is generally taken to be a marker for tropospheric chemistry in action. The slide in Figure 1.4 sums up the main features of atmospheric chemistry.

1.3.7 Study of VOCs and OVOCs

At the University of Leicester research is in progress in the study of various facets of atmospheric chemistry. One of the established techniques is the Peroxy Radical Chemical Amplifier (PERCA) which is used to measure peroxy radical concentrations in the troposphere. Another group, using Solar Radiometers, measures the solar flux at ground level. The level of urban pollution has risen noticeably especially with the rise of motor traffic in the last 50 years. Monitoring the level of hydrocarbon emissions is needed to provide a basis for any future steps to limit or reduce urban pollution. A facility to study the emission of NMHCs, particularly VOCs and OVOCs, in urban environments, is an important adjunct to the existing equipment. Existing equipment such as GC-MS and GC-FID are able to measure both VOCs and OVOCs, but they cannot track rapid changes in species concentration.

OVOCs are of particular interest as they are often intermediate oxidation products formed during the tropospheric combustion process. These frequently are short-lived so it would be ideal to have equipment capable of fast response while capturing a wide mass range of species at the same time.

Table 1.6 lists the target OVOCs for this thesis. They were selected by a group of 30 European institutions in October 2004 at a workshop held under the banner of the ACCENT Initiative as representing the OVOCs most relevant to atmospheric pollution.

Table 1.6 List of target VOCs and OVOCs and their proton affinities ² for this thesis.

Mass /da	Species	PA /kJ mol ⁻¹	Formula
32	methanol	754.4	CH ₃ OH
44	acetaldehyde	769.0	CH ₃ CHO
58	acetone & propanal	812.0 & 784.9	C ₃ H ₆ O
60	1-propanol	787.4	C ₃ H ₈ O
70	MVK & methacrolein ³	834.7	C ₄ H ₆ O
72	butanal	792.7	C ₄ H ₈ O
74	methyl acetate	-	C ₃ H ₅ O
74	1-butanol	789.2	C ₄ H ₁₀ O
78	benzene	750.2	C ₆ H ₆
88	MBO ²	843.1	C ₅ H ₁₀ O
92	toluene	784.1	C ₆ H ₅ CH ₃
100	hexanal	-	C ₆ H ₁₂ O
106	benzaldehyde	834.0	C ₆ H ₅ CHO

1.4 Proton Transfer Reaction Mass Spectrometry (PTR-MS)

1.4.1 Deployment

Proton transfer reaction mass spectrometry (PTR-MS) is a technique that has already found a wide range of applications in analytical science. Developed in the mid-1990s, PTR-MS is a form of chemical ionization mass spectrometry based on proton transfer from a protonated reagent, most commonly H₃O⁺. Only those molecules with proton affinities in excess of that of H₂O can accept a proton from H₃O⁺, a criterion that excludes the major components of air such as N₂, O₂ and CO₂, but includes many trace gases including most VOCs. This discrimination enables trace gases to be detected without complications from intense background signals and confers high sensitivity, potentially sub parts per billion by volume. Furthermore, complications from fragmentation are modest since proton transfer is a relatively soft ionization technique.

² Taken from NIST, Standard Reference Database Number 69 (June 2005), National Institute of Standards and Technology, 2005, Zhou, J., and R. Zhang, *Atmos. Environ.*, 38, 2177-2185, 2004.

³ MVK : methylvinylketone; MBO: 2-methyl-3-buten-2-ol

Apart from a very recent study using an ion trap mass spectrometer [Prazeller *et al.*, 2003], quadrupole mass spectrometry (QMS) has been employed exclusively in all published PTR-MS work to date. However, quadrupole instruments have three significant disadvantages. First, the mass resolution ($m/\Delta m$) is modest, and is often little better than 100 in standard, low-cost, instruments. Second, the mass range is curtailed, with the upper limit rarely exceeding 1000 da. Third, and most serious of all, QMS systems are mass filters and therefore at any one instant in time they discard all signals except that in the designated mass channel. If the focus is on a small number of mass peaks, this is not a significant drawback. However, for a complex mixture where the aim is to monitor a large number of trace gases, QMS becomes highly inefficient.

By substituting a time-of-flight mass spectrometer, the objections raised here can be addressed. The PTR-TOF-MS has no obvious limit to the upper mass it is capable of detecting, and its mass resolution ($m/\Delta m$) has been shown to be an order of magnitude better [Blake *et al.*, 2004]. Finally, since the entire mass range is detected simultaneously, the PTR-TOF-MS is capable of tracking fast changing processes resulting in the production of complicated mass peak spectra.

Much of the pioneering work with PTR was performed by a group at the Institut der Ionphysik in Innsbruck [Howorka *et al.*, 1973; Lindinger *et al.*, 1998; Pahl *et al.*, 1971] who couple a hollow cathode ion source, providing hydronium ions to an electrically biased drift-tube where they react with the trace analytes present in a carrier gas.

The group has published extensively the results of their investigations into the behaviour of hollow cathode ion sources. The ion source consists of a hollow tubular cathode capped at either end by a flat anode. Saturated water vapour is leaked into the source and ions produced by the discharge inside the hollow cathode are extracted through an orifice in one anode. When a discharge occurs in the ion source, the plasma formed creates a region in which the outer electric field does not penetrate, and which concentrates around the central axis of the source. The concentration of H_3O^+ (hydronium) ions peak along the central axis of the ion source, so that the positive ions that emerge, consist predominantly of hydronium. The positive ions pass into a small

drift region where they react with more water vapour to produce an equilibrium mixture consisting of 99% hydronium ions [Pahl *et al.*, 1971].

1.4.2 Hydronium (H_3O^+)

In proton transfer reactions protonated water molecules (hydronium) donate the excess proton to a target molecule M so that the reaction (1.28) can be rewritten as



Proton transfer using H_3O^+ is favoured for atmospheric work because of several desirable characteristics.

Table 1.7 Reactions of H_3O^+ with various types of VOC [Smith and Španel, 2005].

Species	H_3O^+ reactions
Alcohols	MH^+ ; $(\text{M-OH})^+$
Diols	MH^+ ; $(\text{M-OH})^+$
Phenols	MH^+ ; $(\text{M-OH})^+$
Aldehydes	MH^+ ; $(\text{M-OH})^+$
Ketones	MH^+ ; $(\text{M-OH})^+$
Carboxylic Acids	MH^+ ; $(\text{M-OH})^+$
Esters	MH^+ ; $(\text{M-OR})^+$
Ethers	MH^+ ; $(\text{M-OR})^+$; $(\text{M-R})^+$
Organosulphur	MH^+ ;
Amines	MH^+ ; $(\text{M-NH}_2)^+$
Aliphatic hydrocarbons	$\text{H}_3\text{O}^+.\text{M}$ (alkanes); MH^+ (alkenes)
Aromatic hydrocarbons	MH^+ ;
Monoterpenes	MH^+ ; $(\text{M-R})^+$
Aliphatic halocarbons	MH^+ ; $\text{H}_3\text{O}^+.\text{M}$; $(\text{M-X})^+$; $(\text{M-X})\text{OH}^+$
Aromatic halocarbons	MH^+ ; $(\text{M-X})^+$

In principle H_3O^+ is a soft CI reagent and for many molecules the mass spectrum will be dominated by the protonated parent ion MH^+ . However, as will be seen in Table 1.7 other types of daughter ions can also be produced. For example, alcohols, aldehydes

and carboxylic acids tend to lose H₂O on protonation to form (M-OH)⁺. More complex fragments are extracted where the analytes are esters, ethers, amines, monoterpenes and halocarbons.

Finally, where the proton affinity of the analyte is just less than that of H₂O, some aliphatic hydrocarbons and halocarbons in the presence of a third molecule M can form an association complex as a result of a three-body reaction [Hunter and Lias, 1998], eg



Table 1.8 Proton affinities of common atmospheric components [Lindinger et al, 1998]

Species	Formula	Proton affinity /kJ mol ⁻¹
Hydrogen	H₂	100.9
Helium	He	177.8
Neon	Ne	203.3
Argon	Ar	369.0
Oxygen	O₂	420.9
Hydrogen	H₂	422.2
Krypton	Kr	424.7
Nitrogen	N₂	493.7
Xenon	Xe	496.2
Carbon dioxide	CO₂	540.6
Carbon monoxide	CO	592.9
Water	H₂O	691.2
Hydrogen sulphide	H ₂ S	705.0
Formaldehyde	HCHO	713.0
Benzene	C ₆ H ₆	750.2
Methanol	CH ₃ OH	754.4
Acetaldehyde	C ₂ H ₄ O	769.0
Ethanol	C ₂ H ₅ OH	776.6
Toluene	C ₇ H ₈	784.1
Propanal	C ₃ H ₆ O	784.9
1-propanol	C ₃ H ₈ O	787.4
Acetone	C ₃ H ₆ O	812.1
Ammonia	NH ₃	854.0

The suitability of using hydronium ions in the study of gas analysis was noted early on by [Lagg *et al.*, 1994]. Since the proton affinity of water is lower than the proton affinities of most common VOCs but above that of the major atmospheric gases makes it an excellent choice for atmospheric work. This is illustrated by the data in Table 1.7.

Certain families of VOCs are insensitive to proton transfer reactions. The lighter alkanes are a notable example, whereas the heavier ones undergo severe fragmentation [Wyche, 2005].

1.4.3 Cluster formation

Hydronium has the tendency to form hydrate clusters with one or more water molecules. It was found that with some species, clusters can affect protonation, ascribed to switching reactions [Praxmarer *et al.*, 1993]. On the other hand some species are unaffected by clustering. A problem arises when trying to analyse spectra in the presence of significant clustering, because of uncertainty over response of the different analyte species. Some react with monohydrate clusters but not at all with multihydrate clusters, and others such as benzene and toluene do not react at all with clustered hydronium. These and the behaviour of other species towards hydrate of H_3O^+ are summarised in a review article by [Smith and Španel, 2005].

Cluster formation in a drift-tube is determined by the value of E/N where E is the electric potential gradient in the drift-tube and N is the number density of the analyte and carrier gas in the drift-tube. It is measured in Townsends (Td) in units of V cm^2 . Raising E/N reduces clustering but fragmentation of the species increases. The choice of the optimum value of E/N , in which cluster elimination is balanced by the tendency of some analyte molecules to fragment, is discussed in Chapter 3, Section 3.9.

While fragmentation can complicate the interpretation of spectra, it can be used to circumvent the failure of proton transfer reactions to distinguish between isobaric compounds (same values of m/z). Glosik [Glosik *et al.*, 1993] points out in their SIFDT work on collision-induced dissociation of ions, that by varying the value of E/N , isobaric ions with different binding energies show different break-up patterns, a feature

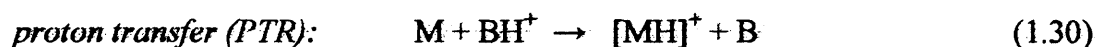
that can be used to differentiate between isobaric components. As an alternative, the use of other chemical ionisation reagents can be as effective.

1.4.4 Chemical ionisation

The traditional methods for ion production for use in mass spectrometry are Field ionisation (FI), electron ionisation (EI) and chemical ionisation (CI) the last of which has been widely used in recent years. EI is the most disruptive technique, causing such extreme fragmentation that interpretation of the results are frequently hindered by large numbers of daughter fragment ions. Fast Atom Bombardment (FAB) [*Caprioli and Suter, 1992*], matrix-assisted laser desorption/ionisation (MALDI) [*Baldwin, 1999*] and electrospray ionisation (ESI) [*Mann, 1990*] are other more recently developed ionisation techniques. Of these, the last two have proved highly successful for investigating macromolecules.

Both FI and CI have gentler ionisation mechanisms resulting in spectra which are simpler to interpret. In FI, the earlier of the two techniques, analyte ions ionised by powerful electric fields are mass-analysed to select the desired fraction. CI was developed from the early work of Talrose [*Talrose and Ljubimova, 1998* (reprint from 1952)] by Munson and Field [*Munson, 2000; Munson and Field, 1966*] into an analytically useful technique.

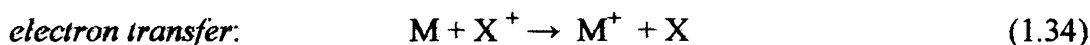
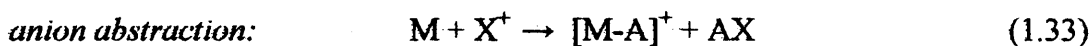
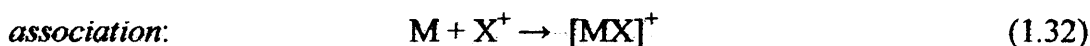
In CI, ions react with analyte gas molecules to form new ionised species. There are several ways in which these ion-molecule or molecule-molecule reactions can proceed:



reaction (1.28) is an example of this type of reaction.



in this type of reaction neither reactant is an ion.



An example of proton transfer between H_3O^+ ions (hydronium) and an analyte molecule (1.30) has been noted previously (1.28). It is of special interest as this CI mechanism is the main vehicle for investigation into atmospheric composition in this thesis, although investigations into the use of other alternative CI reactions using NO^+ , NH_4^+ and O_2^+ as precursors are described in detail in Chapter 6.

A principle route for NO^+ ions to react is via electron transfer (1.34), although, as discussed in Chapter 6, examples of hydride, hydroxide and even alkoxide ion extraction (1.33) as well as association formation (1.32) are also found.

O_2^+ ions, with a recombination energy of 12.06 eV, react via dissociative electron transfer. NH_4^+ ions can take part in proton transfer reactions (1.30) with analytes with proton affinity greater than $854.0 \text{ kJ mol}^{-1}$. Most commonly occurring VOCs have proton affinities below this value. So where a reaction of any sort is found, NH_4^+ ions form clusters with analyte molecules (1.32).

In proton transfer, the yield of the acceptor molecule $[\text{M.H}]^+$ achieved depends on the number of ion-molecule collisions that occur during the dwell time of the reactants in the reaction vessel. A longer dwell time can be obtained by mixing the ions and the analyte gas in a long drift-tube in which the reacting parties remain in contact longer, more molecular collisions occur and the number of proton transfers rises accordingly.

In the case of H_3O^+ , if the proton affinity of a target molecule exceeds that of H_2O then it has been shown that proton transfer reactions tend to proceed at an essentially collision-limited rate. In such circumstances the reaction rate coefficient k for the H_3O^+ reactions is given by k_c , the gas kinetic rate coefficient. This value can be calculated if the polarizabilities and dipole moments of the reactants are known [Su and Chesnavich, 1982]. Lindinger [Lindinger et al., 1998] preferred to rely on calculated values for rate coefficients where they had not yet determined them experimentally themselves. They claimed that these tended to agree better with their own experimental results (within 15%) than rate coefficients reported elsewhere in the literature.

In order to quantify the PTR yields it is necessary that the reactions should occur entirely within a volume of known and constant dimensions, such as a drift-tube.

1.4.5 Swarm-tubes, drift-tubes and selected ion flow tubes

In the 1960s and 1970s interactions between ions and neutral molecules were studied using beam experiments. Normally the incident ion beams' kinetic energies ranged from those corresponding to a few degrees Kelvin, typical of interstellar gas, to much higher temperatures such as those found in the ionosphere. In beam experiments, beams of ions are introduced into tubular reaction chambers filled with an analyte gas. The reaction rate coefficient can be derived, from the attenuation in the emergent ion current after traversing the column of the gas.

Problems arise with this approach for low ion energies in the sub-eV to a few eV range that are encountered in ion-neutral reactions in plasmas, because of the difficulty of producing and maintaining beams with well-defined energies. In spite of these difficulties significant results were obtained [*Friedrich et al.*, 1984; *Hierl et al.*, 1977; *Teloy and Gerlich*, 1974].

In the so-called swarm methods, a development of atomic beam techniques, an ion beam is introduced into a vessel filled with an inert carrier gas, typically helium at low pressure. The reactant ions diffuse and rapidly achieve an equilibrium distribution which they retain for the duration of their sojourn in the reaction vessel. The atomic beams are replaced, in effect, by a diffuse swarm of molecules travelling in all directions and whose energy distribution has achieved equilibrium. Traces of analyte gas are introduced into the tube where they undergo reactions with the reactant, and reduce the population of the reactant ions.

Swarm techniques were widely used to measure the characteristics of discharge afterglows [*Albritton et al.*, 1969; *Fehsenfeld et al.*, 1966; *Ferguson et al.*, 1969; *Märk and Oskam*, 1971; *McFarland et al.*, 1973; *Phelps and Brown*, 1952]. In the initial afterglow experiments a discharge of the carrier gas is initiated upstream at the entrance of a reaction chamber and the reagent gas is introduced a short way down. The discharge is sustained by the carrier gas, usually helium, and high densities of helium ions in a variety of excited states are produced. These react rapidly with the reagent

molecules, ionising them and often exciting these and other impurities in the chamber to create a visible ionised region, the afterglow, which extends beyond the discharge. Analyte gases are then introduced which reduce the current of reagent ions produced. Measurement of the decrease in the ion current is used to derive the reaction rates involved. Several alternative methods were tried with varying success to ensure that only a single type of reagent ion took part in the process at a time.

Two kinds of swarm experiments have been used to investigate plasma discharge afterglows: stationary afterglow and flowing afterglow.

In a stationary afterglow experiment the reaction products are measured by direct extraction from the reaction chamber [*Phelps and Brown, 1952*], [*Märk and Oskam, 1971*]. The reactants remain stationary in the reaction vessel and are sampled by sampling the contents at intervals. Measurement of the reaction products is cumbersome as they have to be inspected *in situ*. In spite of this, a great amount of data was assembled on proton affinities [*Fehsenfeld et al., 1976*], heats of formation and reaction rates

Märk and Oskam [*Märk and Oskam, 1971*] showed how to use a time-of-flight technique to map the spectrum of measured ions to their point of origin in the discharge afterglow, thereby converting the problem of measuring time-dependent quantities in the afterglow to one of measuring the distance travelled along the reaction vessel.

In flowing afterglow methods [*Fehsenfeld et al., 1966; Ferguson et al., 1969*], developed from static afterglow devices, the carrier gas flows through the reaction vessel at a constant rate and carries the reagent and analyte products with them. The reaction products are measured downstream as they leave the chamber.

The Selected Ion Flow Tube (SIFT) [*Adams and Smith, 1976*] is derived from the flowing afterglow work. In a SIFT, the emphasis moves away from discharges and afterglows and concentrates on ion-neutral reactions at thermal energies. Instead reagent ions are generated externally and mass-selected by a quadrupole filter, before injection into the flow-tube, thus overcoming the problem of ensuring that only one type of reagent at a time is active. The ions are thermalised by successive collisions

with the buffer gas in the flow tube. As the buffer gas is usually helium, thermal equilibrium is only achieved after the reactant ions have travelled some way along the flow tube. The ions rely for transport on the flow of the carrier gas through the flow-tube. The analyte molecules in gas or vapour form are introduced into the flow tube at a point where the reactant ions have achieved thermal equilibrium. Here they can intermix with the flood of reactant ions along the remaining length of the tube and have ample opportunity to react. In the SIFT-MS devices ions emerging from the flow tube downstream are analysed by a quadrupole mass filter.

In the case of drift-tubes, an electric gradient applied along a flow-tube fitted with a series of guide rings [Fairley *et al.*, 1999] is used in the place of the moving carrier gas flow used in the flow tube. The acceleration of the ions enhances the collision energy involved in interactions and guides the resultant ions toward the downstream end. The effect of the gradient is to enable the precursor ions to attain higher kinetic energy than in flow-tubes. In collision with analyte molecules, this extra energy can help to trigger reactions in some borderline cases.

In the configuration devised by the Innsbruck group [Lagg *et al.*, 1994] a hollow cathode ion source is coupled to an electrically biased drift-tube [Hansel *et al.*, 1995]. Introducing water vapour into a hollow cathode discharge vessel produced a variety of ions of which hydronium (H_3O^+) was a major component. Allowing these ions to have further contact with water vapour in a secondary chamber, resulted in a 99% pure supply of H_3O^+ ions. This technique formed the basis for their PTR-MS which has since achieved success in the market as an off-the-shelf device. A drift-tube is used in the PTR-TOF-MS to enable the reactant and analyte molecules to react before entering to time-of-flight mass spectrometer.

1.4.6 Standard format for comparison

In a mass spectrum the most prominent peak is that of hydronium at $m/z = 19$. Since hydronium is the precursor ion that is responsible for the creation of the observed spectrum, its peak height is reduced by the proton transfer reactions. In atmospheric work, where OVOCs are present in concentrations of ppbv, the effect on the hydronium concentration is small. The most likely factor that can affect the hydronium count rate is the formation of significant clusters with water molecules. If the observations are

made with a PTR-TOF-MS, this problem is not serious if operating at an E/N of 150 Td (defined in Section 1.4.3), where the contribution from water clusters amount to less than 5% of the total hydronium count.

Hence, providing the OVOC and VOC concentration is on the ppmv region or less, the peak count rates observed will rise and fall in step with the hydronium count rate. The convention for normalising data was first proposed by Warneke and co-workers [Warneke *et al.*, 2001] :

The sensitivity of PTR-MS with respect to a certain compound ... is defined as the number of the product ions produced at a trace gas mixing ratio of 1 ppbv and at an H_3O^+ signal of 1 million ion counts per second (ncps ppbv⁻¹).

The principle of normalising the counts observed has been extended to situations where other CI reactions are used. For normalisation the precursor ion specific to the type of chemical ionisation reaction is used as the base.

1.4.7 Summary

The initial sections of this chapter were devoted to a short overview of the chemical processes at work in the troposphere and in the latter half the history of the development of chemical ionisation methods were summarised. The characteristics of the proton transfer reaction (PTR) make it particularly suitable for monitoring VOCs and OVOCs present as traces, in the presence of the predominant components of the atmosphere. SIFT-MS could be used equally well in such a situation, but to date, they rely on quadrupole-based mass spectrometers which do not offer the simultaneity achievable with a time-of-flight mass spectrometer.

Chapter 2

Instrumentation

*Je n'ai fait celle-ci plus longue que parce que je n'ai pas eu
la loisir de la faire plus courte.*

- *Blaise Pascal, Lettres Provinciales (1657) no. 16*

2 Instrumentation

2.1 Introduction

This chapter is devoted to a description of the hardware and software systems that were developed for this research program. Several items were acquired from outside suppliers, whereas others were designed and constructed at the University of Leicester. Some experimental results are also included in this chapter to demonstrate key performance characteristics of the PTR-TOF-MS as an effective detector of trace Volatile Organic Compounds (VOCs) and Oxygenated VOCs (OVOCs).

This chapter starts with an overview of the field of time-of-flight mass spectrometry and explains why this technique is particularly useful for measuring rapid changes in the composition of the troposphere, and is able to cover a wide mass range simultaneously. It then describes the design, development and testing of a hollow cathode ion source and a ^{241}Am radioactive source. Other areas covered are the design and testing to drift-tubes and electric voltage divider chains used to apply an electrical accelerating gradient to propel ions through the drift-tubes. In the last section, the software needed to drive the instrument and to analyse the data produced by it are described. Some of it, for example the GRAMS/AI module which operates the PTR-TOF-MS was supplied with the body of the instrument, while other software, especially those modules for analysing the data were written in Leicester, or adapted from GRAMS/AI application modules.

2.2 Time-of-flight mass spectrometry

2.2.1 Basics

The technique of measuring the kinetic energy of a particle by determining the time it takes to travel a known distance was first developed in the mid 1940s [Stephenson, 1946]. The technique was used to measure the energy of neutrons emerging from nuclear reactors. The time-of-flight was measured by the time lag between two signals, one of which signals the start of the particle's journey and the other its arrival at a detector. For non-relativistic particles the kinetic energy E is given by

$$E = \frac{1}{2} mv^2 \quad (2.1)$$

where m is the particle's mass and v its velocity. For particles with the same mass travelling a distance s , the time taken to make the journey is

$$t = s \sqrt{\frac{m}{2E}} \quad (2.2)$$

The same relation could be applied to the case where particles with different masses start off with the same kinetic energy, and measuring their flight time gives a useful method of measuring their masses since

$$t \propto \sqrt{m} \quad (2.3)$$

2.2.2 Development of time-of-flight techniques

In 1946 Stevenson applied the time-of-flight principle to mass spectrometry [Stephenson, 1946]. In his application, ions were introduced into the space between the two plates of a capacitor and expelled when the capacitor was rapidly charged. A pulse derived from the charging current served as the start signal for the ions' journey. The process is shown diagrammatically in Figure 2.1

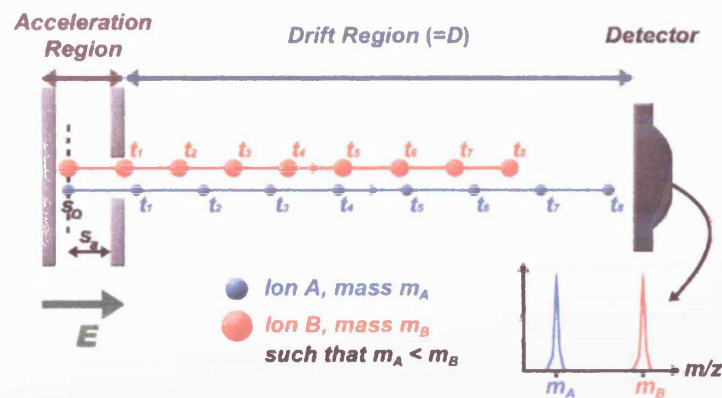


Figure 2.1 Diagram illustrating the principle of operation of a time-of-flight mass spectrometer [Whyte, 2003].

The best time resolution is obtained when all the particles are expelled from the capacitor with the same energy. In the initial implementation, the ions were not confined to a small volume in the space between the capacitor plates and thus acquired a spread of energies by virtue of their different starting positions between the plates. Consequently in the

earlier forms of time-of-flight mass spectrometry, the mass resolution was so degraded that the technique was of little practical use.

2.2.3 Linear mass spectrometers

By placing a charged grid some distance from the source of the ions an acceleration field is produced, so that the ions achieve a focus along their flight path where the slower and faster ions converge. Boesl *et al* [Boesl *et al.*, 1992] calculate that the convergence occurs at a point equal to twice the acceleration distance along the beam, which often occurs inconveniently close to the source.

Wiley and McLaren [Wiley and McLaren, 1955] showed that with the addition of a second acceleration field, (a second electrode or grid) the first-order space focus could be moved further away so that longer flight times were possible. Mass resolutions, $m/\Delta m$, as high as 4650 have been obtained by Opsal *et al.* [Opsal *et al.*, 1985], and mass resolutions of 1000 are fairly easily attainable with a sufficiently long flight tube. The Wiley-McLaren configuration is still widely applied today in time-of-flight mass spectrometers.

Further developments in the positioning of the accelerating electrode grids made it possible to minimise second order effects, so that acceptable mass resolution was obtained in very short length flight paths. For example, Boesl [Boesl *et al.*, 1994] reported obtaining $m/\Delta m = 850$ in an instrument with a flight path of only 13 cm.

2.2.4 Reflectron time-of-flight mass spectrometry

Alikanov [Alikanov, 1957] and Mamyrin [Mamyrin *et al.*, 1973] proposed a novel method for compensating for the effect of differing flight times. They applied an electric repulsion field gradient at one end of the flight tube, which slowed down, then repelled and finally reversed the ions' flight direction. As explained in the previous section, injected ions with the same mass can have a spread of initial kinetic energy. In the reflectron the more energetic ions penetrate the repulsion field further and follow a longer flight path than the less energetic ones (Figure 2.2). By suitably arranging the repulsion field, it is possible to eliminate the leads and lags so that all the ions of a particular type in a bundle reach the detector at the same time. The reflectron's

decelerating field is obtained by using one or more charged grids. Normally a fixed gradient field is used.

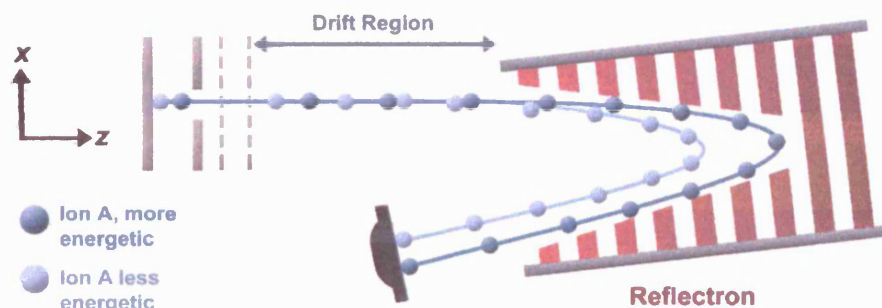


Figure 2.2. Diagram of a reflectron time-of-flight analyser [Whyte, 2003]. The decelerating electrodes at the one end reverse the direction of travel of the ions. For ions of the same mass, the more energetic ones follow a longer path so that all reach the detector simultaneously.

The kinetic energy spread is minimised at the injection phase by applying the first and second order focussing acceleration electrodes [Wiley and McLaren, 1955].

Extremely high mass resolutions were obtained with reflectron-based mass spectrometers. Bergmann *et al.* [Bergmann *et al.*, 1989] reported achieving a mass resolution of 35000.

2.2.5 Reasons for choosing PTR-TOF-MS

As discussed in Chapter 1, proton transfer reaction mass spectrometry (PTR-MS) is a relatively new technique that has already found a wide range of applications in analytical science [Critchley *et al.*, 2004; Hansel *et al.*, 1995; Lindinger *et al.*, 1998a; Lindinger *et al.*, 1998b; Prazeller *et al.*, 2003]. Developed in the mid 1990s, PTR-MS is a form of chemical ionization mass spectrometry based on proton transfer from a protonated reagent, most commonly hydronium (H_3O^+). Only those molecules with proton affinities in excess of that of H_2O can accept a proton from H_3O^+ , a criterion that excludes the major components of air such as N_2 , O_2 and CO_2 , but includes many trace gases, including most Volatile Organic Compounds (VOCs) and Oxygenated VOCs (OVOCs). Hence trace gases can be detected without interference from intense background signals and makes it possible to construct an instrument with high detection sensitivity (sub-parts

per billion). Furthermore, complications from fragmentation are minimal since proton transfer is a relatively soft ionization technique.

Apart from a very recent study using an ion trap mass spectrometer [Prazeller *et al.*, 2003], quadrupole mass spectrometry (QMS) has been employed exclusively in all published PTR-MS work to date. However, quadrupole instruments have three significant disadvantages. First, the mass resolution ($m/\Delta m$) is modest, and is often little better than 100 in standard, low-cost, instruments. Second, the mass range is curtailed, with the upper limit rarely exceeding $m/z = 1000$. Third, and most serious of all, QMS systems are mass filters and therefore at any one instant in time they discard all signals except that in the designated mass channel. If the focus is on a small number of mass peaks, this is not a significant drawback. However, for a complex mixture where the aim is to monitor a large number of trace gases, QMS becomes highly inefficient. The PTR-TOF-MS offered a means to avoid these limitations.

2.3 Instrument description

Hydronium ions, produced in an ion source using the Proton Transfer Reaction (PTR) protonate VOC and OVOC in a drift-tube prior to analysis in a mass spectrometer [Boschetti *et al.*, 1999; Hansel *et al.*, 1995; Howorka *et al.*, 1973; Lindinger, 1973; Lindinger *et al.*, 1998b] and [Pahl *et al.*, 1971]. When referring to the TOF-MS and its attached ion source it is denoted as PTR-TOF-MS. At times the abbreviated term TOF-MS is used when concerning functions that involve TOF-MS devices in general.

A schematic of the configuration of the instrument is shown Figure 2.3. The basic elements of the instrument are an ion source, a drift-tube, an ion transfer region, and a reflectron time-of-flight mass spectrometer [Alikanov, 1957; Mamyrin *et al.*, 1973; Weickhardt *et al.*, 1996; Wiley and McLaren, 1955].

Hydronium ions generated in a radioactive or hollow-cathode discharge source are fed into the drift-tube where they react with the gaseous sample to be analysed [Hansel *et al.*, 1995].

The processes involved can be represented by the reactions



for reagent ion generation, and



for the production of the protonated analyte. A typical sample would be air containing a mixture of VOCs and OVOCs [de Gouw *et al.*, 2003a; de Gouw *et al.*, 2003b]. On leaving the drift-tube, protonated VOCs and OVOCs along with any unreacted hydronium ions enter a set of ion transfer optics that guides them to the pulsed ion extraction unit of the TOF-MS.

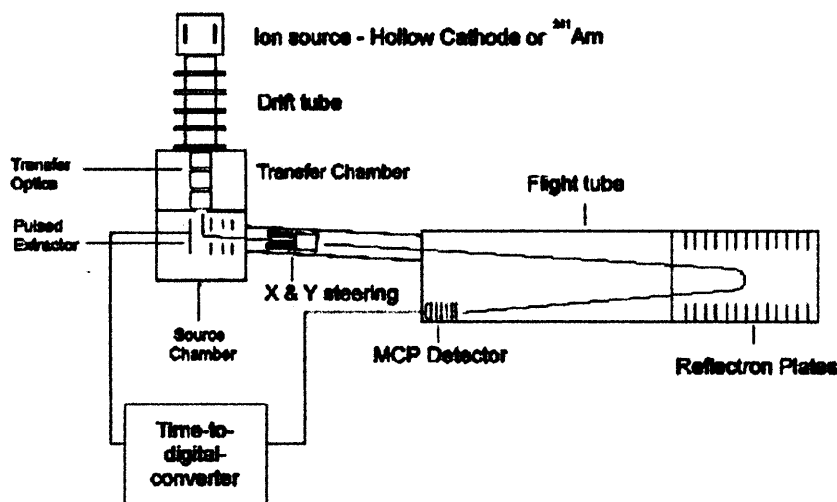


Figure 2.3 Diagram of the PTR-TOF-MS.

The ion transfer optics consist of a three-element einzel lens that focusses the ions into a narrow beam between the back plate and extraction grid of the TOF-MS. The potential on the grid is rapidly switched to drive ions into the flight tube and after passing through spatial focusing electrodes and between X and Y steering plates the ions enter a large bore reflectron equipped with a dual micro-channel plate (MCP) detector. The anode of the MCP detector is connected to a purpose-built preamplifier with a built-in discriminator that generates an ECL logic pulse whenever the pre-selected signal threshold is exceeded.

The MCP output is sent to a time-to-digital converter (TDC) with 2 ns time bins. The TDC processes the input data to construct an arrival time histogram. The TDC also provides the trigger pulse to the extraction grid of the TOF-MS for initiating the flight time sequence. Repetitive scans are essential to attain meaningful ion count statistics and for a scan range of 0-300 Daltons (da) approximately 10^4 scans per second can be accumulated.

Pumping in the first differential pumping region, the transfer optics chamber, and the TOF-MS is carried out using individual turbomolecular pumps.

A small mechanical pump attached to its downstream end is used to evacuate the drift-tube. Three turbomolecular pumps maintain the vacuum in the system. Two pumps each with a capacity of 70 litres sec^{-1} pump the plenum chamber below the drift and the transfer chamber. The third pump with a capacity of 150 litres sec^{-1} is attached to the source chamber.

2.4 Ion Sources

In this section, two different approaches to generate hydronium ions are described. They differ in the method by which hydronium ions are generated, but both make use of drift-tubes where hydronium ions can protonate molecules present in the gas sample being analysed.

The first method is based on the pioneering hollow cathode discharge work of Lindinger and co-workers [*Hansel et al.*, 1995; *Howorka et al.*, 1973; *Lindinger*, 1973; *Lindinger*, 1986; *Lindinger et al.*, 1998b; *Pahl et al.*, 1971]. The hollow cathode design has been widely used and has gained a reputation for stability and simplicity of operation. Ideally a floating power supply was needed to drive the hollow cathode discharge, and a separate power supply for the various bias voltages used in the source and drift-tube. Although a possible power supply was found early on in the work, it needed modifications, so that it was necessary to resort to the unconventional method of operation described in Section 2.4.1.5.1. Some while afterwards, when the floating supply was available, the electrical configuration was changed to the one described in Section 2.4.1.5.2.

The second approach is based on the work of Hanson *et al.* [Hanson *et al.*, 2003], who used α -particles from a radioactive ^{241}Am source, reacting with water molecules in water-saturated nitrogen to produce the hydronium ions. The hydronium ions produced then protonated sample ions in a drift-tube. Although the hydronium ion count-rates achieved by this method were less than those achieved with the hollow cathode approach, its operation was exceptionally stable, and the PTR-TOF-MS can run almost continuously for months with only minimal attention. The device is described in Section 2.4.2.

2.4.1 The hollow cathode hydronium generator

The design of the hollow cathode hydronium generator was based on that described by the Innsbruck group [Hansel *et al.*, 1995; Howorka *et al.*, 1973; Lindinger, 1973; Lindinger, 1986; Lindinger *et al.*, 1998b; Pahl *et al.*, 1971].

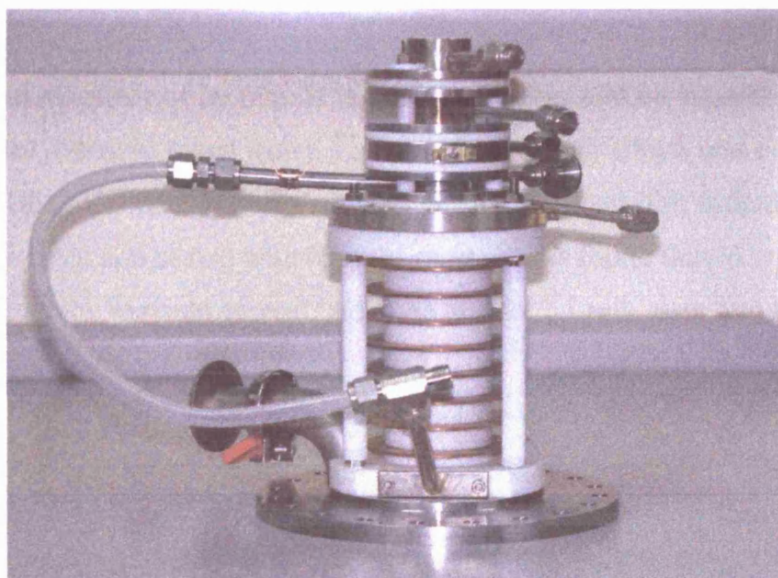


Figure 2.4 The hollow cathode ion source and drift-tube fully assembled.

The design has been described in the literature in general terms only as the originators were marketing an off-the-shelf product, which was protected by several patent applications. The ion source described here was designed and built based on information gleaned from published work only. In the following sections the various parts of the hollow-cathode hydronium generator are described: the hollow cathode discharge assembly, the source drift region (SD), the drift-tube where the hydronium ions reacted

with the sample gas and the two alternative electrical circuits used to power the generator.

2.4.1.1 The hollow cathode and source drift regions

The hollow cathode hydronium ion generator consists of an ionisation chamber in which water vapour is ionised by an electric discharge. The water vapour is drawn from the headspace of a sample of de-ionised water (15 M Ω -cm) and leaked into the hollow cathode through a needle valve. While it is difficult to perform fine adjustments to the water vapour flow with the needle valve, once it is set up, it needs no further adjustment. The pressure of water vapour in the hollow cathode area, (typically 0.15 mbar) is monitored with a Pirani gauge attached to the source drift electrode. An additional Pirani gauge measures the drift-tube pressure (Section 2.4.1.3).

The hollow cathode consists of a stainless steel tubular section with a length of 25 mm with an internal diameter of 30 mm. It is capped at either end by stainless steel Anodes, one of has a molybdenum insert with a 1 mm orifice through which ions can pass into the rest of the device. The anodes were isolated electrically from the cathode by means of Macor ceramic discs and sealed with Viton o-rings. It was found that in order to maintain a stable discharge the ionising current had to be at least 2.5 mA, with 5 to 8 mA being the normal operating range.

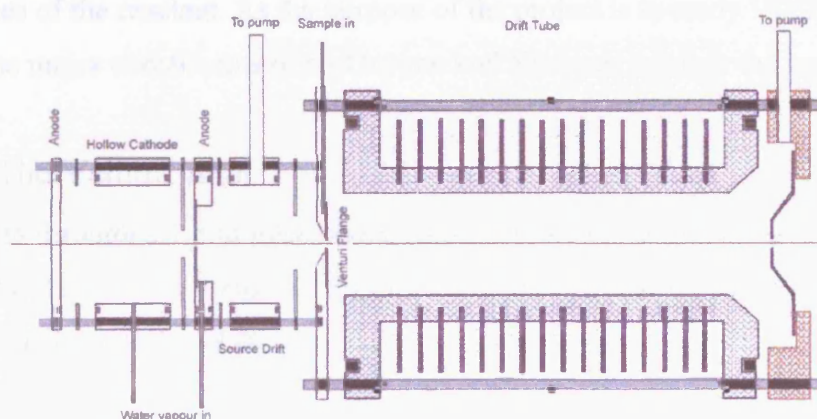


Figure 2.5 Exploded view diagram of the hollow cathode, source drift chamber, the Venturi flange and the drift-tube. The bias voltage applied to the drift-tube is 1000 V.

Pahl and co-workers [Pahl *et al.*, 1971] found that in a hollow cathode discharge of water vapour, a plasma is formed in which hydronium ions predominate along the central axis. The so-called negative glow concentrates along the central longitudinal axis of the hollow cathode and pulls away from the walls. Inside the plasma, there is virtually no field gradient and it was usually referred to as the field-free region. Pahl *et al.* [Pahl *et al.*, 1971] showed that the distribution of hydronium ions reaches a maximum on the axis of the negative glow.

The ion source employed in the present work is held at positive potentials, up to 1000 V relative to ground and ions are extracted into a region where the potential is some 300 V lower.

All the ions extracted from the hollow cathode discharge entered a small source drift chamber (SD) where they have further opportunity to react with water vapour and optimise the yield of hydronium ions [Hansel *et al.*, 1995], which was found to approach 99% of the total ion yield. In the initial trials, water vapour was introduced into the source drift region as well, but it was found that water feeding through from the hollow cathode region was sufficient for the purpose.

After the source drift chamber, the ions enter a 100 mm drift-tube where they protonated the reactants in the chosen sample gas. The sample gas (inert in a proton-transfer sense) contain traces of the reactant. As the purpose of the project is to study VOCs and OVOCs in the air, the major constituents of air Oxygen and Nitrogen serve as the inert carrier.

2.4.1.2 The Venturi Inlet

The Ions pass through a 1 mm inlet from source drift region to the drift-tube. The sample gas enter the drift-tube through a ring of 12 holes surrounding the ion inlet aperture [Fishman and Grabowski, 1998].

The effect of this arrangement is to create a Venturi effect so that the tendency of the sample gas to diffuse backwards into the source drift region is reduced.

2.4.1.3 The drift-tube

The hydronium ions produced in the drift-tube are accelerated by the electric field of the drift-tube. The dimensions of the drift-tube are based on the published work of Linsinger who performed numerous in-depth investigations on various methods, the interaction of ions in drift-tubes [Linsinger 1933, Linsinger 1936]. Most drift-tube designs for PTR work have been based on Linsinger's design.

Assembly Venturi Plate and Annulus



Figure 2.6 Side view of the Venturi flange showing the gas passage. The annular cover plate containing the gas outlets is shown in red.

The drift-tube consisted of a PTFE cylinder with a series of copper guide rings on the inner surface. Most Venturi designs are complicated and required high precision engineering [Dupeyrat *et al.*, 1982], but Fishman *et al* showed how a relatively simple arrangement performed almost as well. They found that 12 small diameter conventional holes arranged in a circle around the main inlet, gave results rivalling the more complicated arrangement which called for a closely machined annular groove surrounding the central ion inlet [Fishman and Grabowski, 1998].

The Venturi flange consists of two parts (Figure 2.6 and Figure 2.7). The base consists of a flange in which the gas channels are machined, and a bronze insert flange with the array of 12 holes 0.34mm in diameter. The insert flange seals on an o-ring. The sample gas, under pressure, enters the drift-tube as a series of high-speed jets directed away from the central orifice where the hydronium ions enter the drift-tube.



Figure 2.7 The Venturi flange.

2.4.1.3 The drift-tube

The hydronium ions protonated the VOC and OVOC ions in the sample gas in the drift-tube. The dimensions of the drift-tube are based on the published work of Lindinger who pioneered many of the advances in proton transfer reaction techniques. He performed numerous in-depth investigations on swarm methods, the interaction of ions in drift-tubes [Lindinger, 1973; Lindinger, 1986]. Most drift-tube designs for PTR work have been based on his work.

The drift-tube consisted of a PTFE cylinder with a series of copper guide rings on the outside. The guide rings were located in grooves in the body of the drift-tube, so that the wall thickness under the guide rings was 5 mm. Graduated potentials of up to 1000 Volts are applied to the guide rings from a resistor chain. This provides the potential gradient for moving the ions down the drift-tube.

The drift-tube design used was first proposed by Soppart and Baumbach [Soppart and Baumbach, 2000] for an IMS system. They obtained satisfactory performance from drift-tubes in which the guide rings surrounded the drift-tube on the outside, rather than intrude into the interior. The one-piece drift-tube design eliminates contamination from the several o-rings needed in a segmented system and reduces the number of individual segments and potential leak sites in the structure. The connection for the Pirani pressure monitor is on the drift-tube exhaust line. The location is not ideal as a pressure reading at that point is likely to be lower than the actual drift-tube pressure. This is an item that will have to be addressed in future designs, but was tolerated during the initial work. There is the risk that unwanted charge build-up could occur in the interior of the drift-tube and cause premature sparking.

It is necessary to consider the effect on the voltage gradient inside the drift-tube of the intervening layer of PTFE. This gradient accelerates the ions towards the exit aperture as well as reducing the occurrence of cluster formation with water molecules.

Consider the potential gradient between any two guide rings. In one case they just reach the interior of the drift-tube and in the other one they surround the drift-tube and are separated from the interior by a 4 mm layer of PTFE (Figure 2.8). The latter situation can

be represented by a capacitor containing two different types of dielectric: vacuum and PTFE as shown in the left hand side of the diagram. Their permittivities are ϵ_1 and ϵ_2 are 1.0 and 2.1 and thickness d_1 and d_2 respectively. The system resembles 3 capacitors in series. Where the guide rings protrude into the interior, the potential gradient between a pair of plates is (right hand of diagram):

$$\Delta v = v_0 - 0 \quad (2.6)$$

Where the field rings merely surround the drift-tube, the potential is (left hand diagram):

$$\Delta v = v_1 - v_2 = v_0 \cdot \frac{2\epsilon_1 d_2}{\epsilon_2 d_1 + 2\epsilon_1 d_2} \quad (2.7)$$

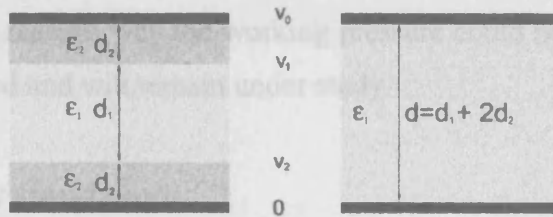


Figure 2.8 Single and multiple dielectric capacitors.

The field inside the drift-tube can be represented by a series of equipotentials which curve out into the interior of the drift-tube from one guide-plate to the next. These equipotentials are components of the electric field generated by a potential gradient. The path of an equipotential through an inhomogeneous medium affects the voltage partition within that medium. So, for example as d_2 increases, d_1 decreases. If the permittivity of d_2 is twice as much as that of d_1 , the voltage partition changes even faster in favour of d_2 . The value of d_1 for an equipotential which barely reaches the inside of the drift-tube is 0, and the voltage drop ΔV (from $v_1 - v_2$) is 0 also. In the simplified case where the field has to traverse a PTFE-vacuum-PTFE dielectric, given that $d_2 = 5$ mm and $d_1 = 15$ mm we find that $\Delta V = 0.75$ or the potential gradient is 75% of the strength where there is no intervening PTFE.

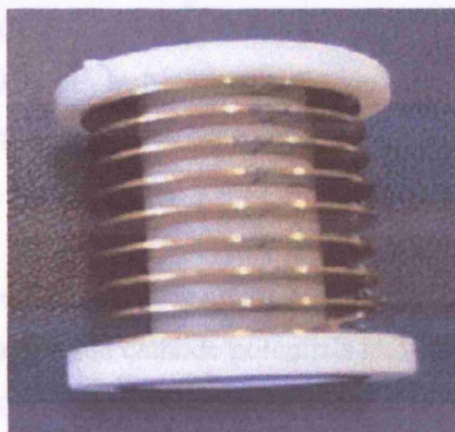


Figure 2.9 The PTFE drift-tube with the guide rings fitted.

The entry pressure of the sample gas was adjusted with a needle valve and was replaced with a 100 sccm mass flow controller at a later stage. The internal drift-tube pressure of the water vapour plus the sample gas was maintained at between 0.4 to 0.6 mbar. While it was possible to raise the pressure further, it appeared to affect the total yield of the source adversely. The reasons why the working pressure could not be raised beyond this value were not resolved and will remain under study.

2.4.1.5. Electrical configurations

2.4.1.4. Computer simulation

In order to test the feasibility of alternative designs for the hollow cathode source and its drift-tube, several alternative configurations were simulated on computer using SIMION v7.0. SIMION is a computer simulation package that can be used to model the effect of electric fields on ion trajectories.

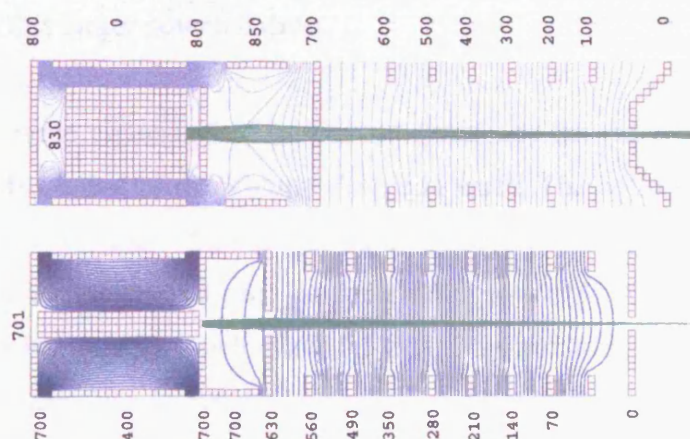


Figure 2.10 Two SIMION runs simulating the geometry of the hollow cathode hydronium generator.

In the simulation examples shown in Figure 2.10, the influences of different exit plates, plane or conical were evaluated. In both cases the ion trajectories were focussed into a narrow beam, and the choice of the flat exit plate was chosen for simplicity in manufacture.

It was assumed that hydronium ions were created in the hollow cathode region on the left side of the diagram. The anode and cathode potentials had no influence on the hydronium ions in the negative glow region and ions emerged with zero or close to zero energy. The size of the negative glow area in the hollow-cathode discharge did not affect the ion trajectories once they exited through the aperture in the anode.

The ion beam was strongly focussed by the field in the source-drift region and held in a tight beam during their path in the drift-tube. In the examples shown in Figure 2.10, the potentials modelled were slightly lower than those used in practice. Similar results were obtained assuming initial ion energies up to 3 eV.

2.4.1.5 Electrical configurations

The ion source was held at high potential – typically 1 kV. The drift-tube Venturi flange operated at several hundreds of Volts below that. It was found that the potential difference across the source drift region had to be larger than indicated by the models. This was probably due to improved extraction rather than better focussing. Since the potential along the drift-tube was kept constant at 600 Volts, the anode potentials were raised to provide this larger potential drop.

The guide rings were connected to a resistor chain and provided a constant voltage gradient ranging from that of the Venturi flange to earth. The hollow cathode discharge was handled by an in-house 1.5 kV supply capable of delivering up to 25 mA current. Normally, the discharge currents used ranged from 5 to 8 mA. A second 1.5 kV power supply fed the resistor chain which drew 1.5 mA. The resistor chain provided the bias voltages of the anodes, the source drift electrode and the drift-tube (see Figure 2.11 and Figure 2.12).

Ideally, the hollow cathode discharge should have been powered by a floating power supply and the bias requirements for the source and drift-tube provided by a separate supply. A floating power supply was not available initially so an inelegant method of biasing the ion source and the drift-tube was tried. Although crude, finicky and cumbersome, it worked acceptably; certainly well enough to operate the PTR-TOF-MS for days at a time without undue attention.

The electrical arrangements to power the hollow cathode source were updated when the floating power supply became available. The change to the new supply was implemented, although more effort went into making the first approach work. The advantages of each method are described below.

2.4.1.5.1 Configuration with non-floating power supplies

The original electrical configuration is shown below in Figure 2.11. The ion source was held at a positive potential up to 1.0kV relative to ground.

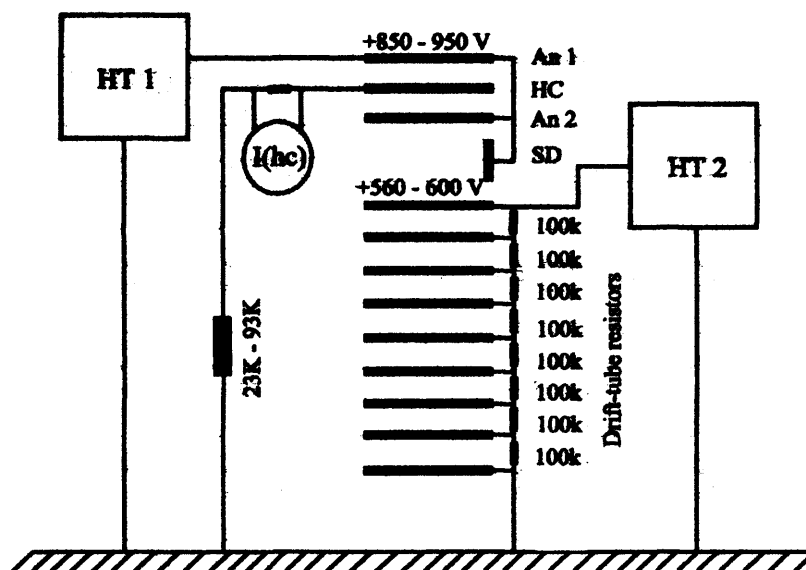


Figure 2.11 The original power supply configuration. The cathode resistor (switchable from 47 kΩ in 22 kΩ steps to 93 kΩ) in power supply HT 1 limits the current as well as raises the anode potential. Power supply HT 2 provides the drift-tube potential gradient. A voltmeter spanning a 1 kΩ resistor in the cathode circuit measures the discharge current.

A switchable cathode resistor was chosen to maintain the hollow cathode in the region of 5 to 8 mA and the anode voltage ranged between 800 and 1000 Volts. The cathode resistors could be selected by means of a rotary switch in steps of 22 k Ω . The voltage supplied to the Venturi inlet was provided by a second power supply and was at the top of a potential divider chain applied to the drift-tube electrodes. Typically, the Venturi inlet flange was biased to some 350 Volts below the anode voltage. It provided a voltage gradient to extract ions from the hollow-cathode discharge and to accelerate them. Varying this voltage was found to be the most effective way of regulating the ion current of the ion source.

Initially the SD voltage was held at the same level as the Venturi flange, but it was found that this tended to encourage the hollow-cathode discharge to migrate to the source drift region. When the SD electrode was connected to the second anode, the discharge was less inclined to migrate.

Whenever the discharge moved into the source drift region, apart from a dramatic rise in count rate, the spectrum measured showed a very strong O₂⁺ peak which dwarfed the hydronium peak. The condition also produced a significant increase in background noise. It was thought that the effect was the result of the discharge in the SD region attacking the walls of the electrodes in the SD region.

2.4.1.5.2 Configuration with floating power supply

In the revised biasing system the ion source was still held at a high positive potentials up to 1.0 kV relative to ground, but it was supplied from a 2 kV supply via a 1 M Ω dropping resistor. The resistor served to drop the voltage at the anode to 1 kV and also to quench potential sparking.

The source drift chamber could be adjusted to any potential between the second anode and the Venturi flange. It was found to perform better close to the anode potential, as arcing tended to occur when it was closer to the Venturi potential. The bias resistor chain of the ion source and drift-tube was housed in a box in which each component was removable. It was relatively easy to change the value of any of the resistors in the chain.

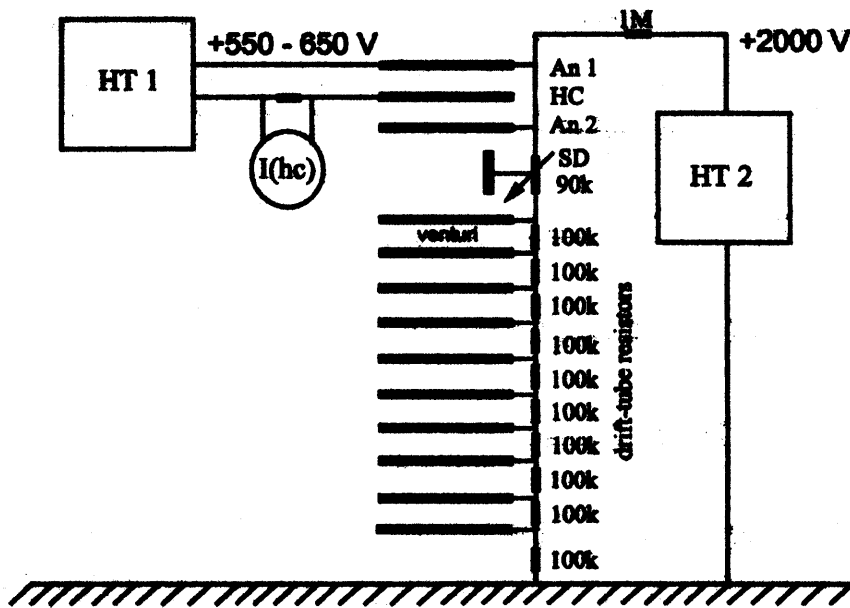


Figure 2.12 Floating power supply HT 1 handles the hollow cathode discharge, while power supply HT 2 supplies the bias requirements of the rest of the system through potential divider chain.

The current drawn by the divider chain was less than that required for the hollow cathode supply, and the initial voltage exceeded the maximum output of the home-grown power supply. In its place a Stanford Research PS350 supply was used that was capable of delivering up to 5000 Volts at 5 mA. The accompanying diagram depicts the electrical bias configuration (Figure 2.12).

The hollow cathode discharge was powered by a floating power supply HT 1. The voltage of HT 1 was adjusted to produce a discharge current of 5 mA. The bias voltage supplied by the SRS PS350 was slowly raised until the anode voltage was about 850 Volts and the Venturi flange about 640 Volts. The applied voltage HT 2 at this stage was about 1700 to 1800 Volts.

There was not sufficient time to test the new configuration properly. An opportunity has not yet presented itself by this time of writing (September 2005).

2.4.1.6 Operating Conditions

The ion source operated best at drift-tube pressures between 0.4 to 0.6 mbar. Above and below that pressure range, the hydronium count dropped sharply. When the pressure was low the hollow cathode discharge was extinguished and when it was high, increased

recombination of the ions set in and reduced the hydronium yield. Ionicon maintain the drift-tube pressures in their systems at of 2 mbar, greater than used in the current instrument.

The new electrical biasing arrangement was tested for a few days only. It was possible to establish that it was more stable in operation and simpler to operate than with the original biasing system.

The gas pressure measurement in the device was taken from the source drift area using a Pirani gauge connected through an insulated PTFE tube. Typical working pressures were 0.2 mbar water vapour and 0.6 mbar with the sample gas. The contribution of the sample gas at this measuring point was expected to be low as the Venturi flange was downstream from the source drift region, and the drift-tube exhaust port at the far end of the drift-tube, back-streaming of the sample was diminished. Gas flow into the drift-tube was maintained with a mass flow controller, and no direct pressure measurements were made of the pressure in the drift-tube.

Provision has now been made to measure the pressures for future work at the input lines of the water vapour and the sample gas.

2.4.1.7 Bench tests

When the ion source and drift-tube were first mounted onto the TOF-MS, no output was observed. It was then decided to test the ion source and drift-tube separately before trying again.

A special flange was made up which made provision for pump attachments as well as a Faraday cup to measure the current from the ion source.

Initially the ion source was mounted without the drift-tube and the source drift section. These were then added back one by one as testing proceeded. The charge collected would be fed into a Keithley Model 427 charge sensitive amplifier, and the output measured on a voltmeter. Since the output was essentially DC output, the time constants on the amplifier were set at the maximum.

The first experiment consisted of the hollow cathode mounted on the Faraday cup using air as the ionisation gas. Next, water vapour was introduced, and finally the source drift section and drift-tube were added.

The pressure of water vapour and air in the system was 0.35 mbar and the hollow cathode discharge current kept at 5 mA. Under these conditions a current of about 300 pA was observed. The observed current increased when the top anode (anode 1) was held at a slightly higher potential with respect to exit Anode 2. The positive ions entered the source drift region through an aperture in Anode 2 and an ion current of 500 pA was measured.

With the assembly mounted on the TOF-MS it was found that when the bias conditions were used which corresponded to the maximum Faraday cup readings, arcing in the source drift region or even the drift-tube itself occurred.

2.4.1.8 Performance criteria

When operating steadily, the hydronium count registered in the PTR-MS-TOF was in the region of 3500 to 4000 counts per second. Higher hydronium count rates could be obtained by increasing the bias of the MCP detector, but with higher biases this increase is masked by other events. In Section 2.5.2 the most of the observed higher count-rates are due to the non-linear behaviour of the detector whose distorted output caused the TDC to register two events (slightly time-shifted) instead of one.

The effect of varying the potential of the source drift region could not be investigated in detail with this configuration, as it was possible that its optimum setting could lie somewhere between that of the Venturi flange and Anode 2.

The hollow cathode ion source showed satisfactory stability during operation over periods of days, with its yield varying less than 3% in 25 hours.

The three spectra in Figure 2.13 show the stages of breakdown in the operation of the ion source. In the bottom figure, the hollow cathode discharge was confined to the

hollow cathode chamber, while in the centre spectrum, arcing in the SD region is making a contribution to the output as evidenced by the increased prominence of the O_2^+ and NO^+ peaks. Finally in the top section of the diagram arcing is now occurring lower down in the ion source. This generated substantial background noise, as seen in the left hand side of the top spectrum. The noise seriously degrades the resolution of the other peaks. When operating normally hydronium count rates of the order of 4000 per second were observed.

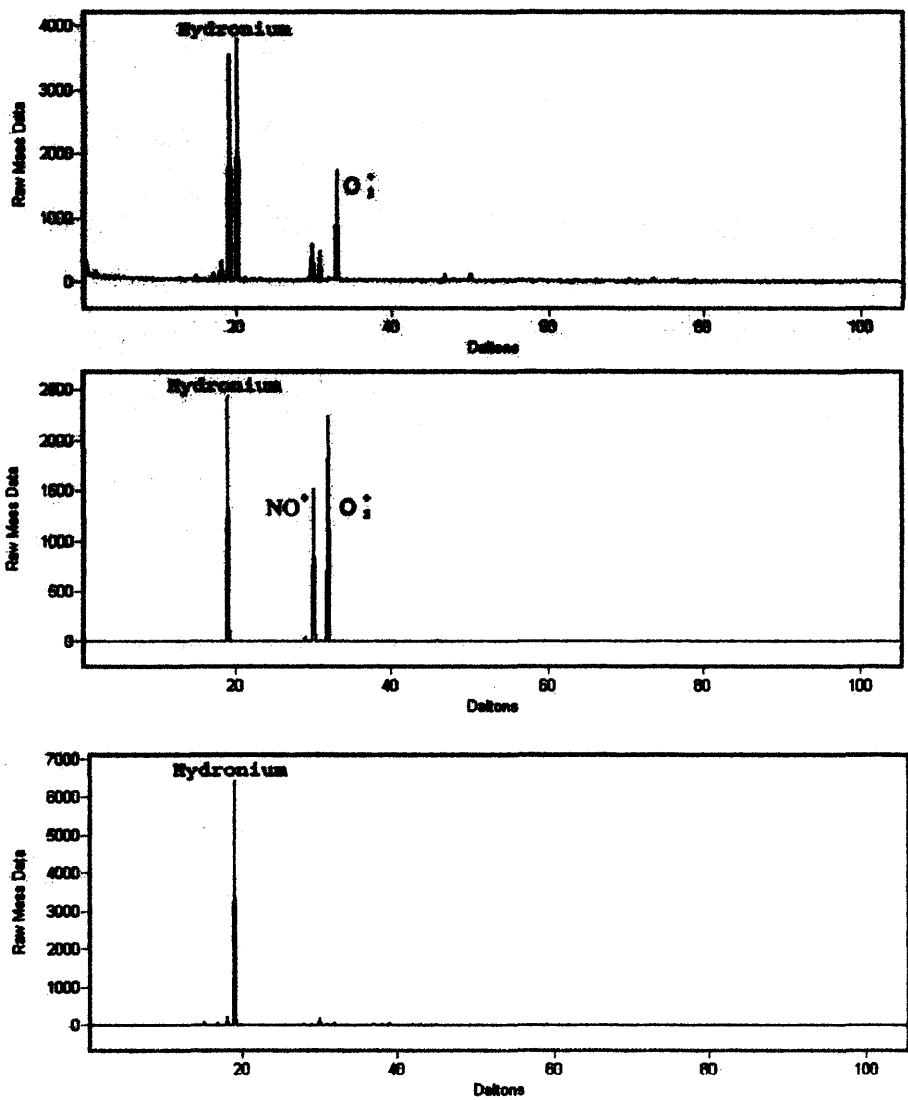


Figure 2.13 Spectra obtained when discharge was confined to the hollow cathode (bottom), when the discharge was partially in the source drift region (centre) and when the discharge was starting to strike in the drift-tube (top).

2.4.2 The ^{241}Am Ion Source Hydronium Generator

An ion source and drift-tube assembly based on a published paper by Hanson *et al.* [Hanson *et al.*, 2003] was designed and constructed at the University of Leicester. The ion source used a radioactive strip of ^{241}Am (half-life 432 years) in a stainless cylinder (~44.4 mBq, standard film, NRD Incorporated, Grand Island, NY). The alpha particles emitted were used to ionise water vapour to generate H_3O^+ ions. The ion source was held at a high positive potential up to 3.0 kV relative to ground.

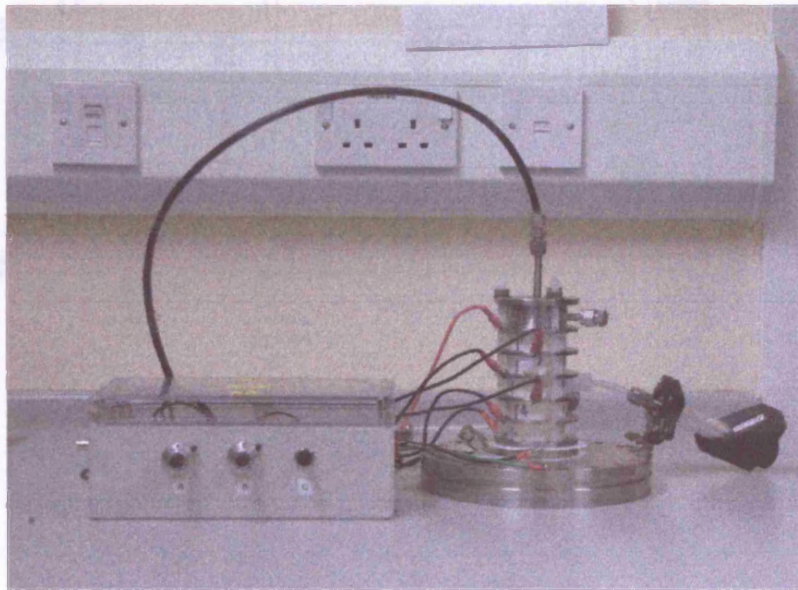


Figure 2.14 The ^{241}Am ion source and drift-tube fully assembled. The gas inlet could be either at the side of the source or as shown here, at the top of the ion source.

Zero-grade nitrogen (BOC, BTCA 178 grade) saturated with water vapour was introduced into the top of the ion source. The flow rate of the nitrogen was controlled by a mass flow controller to feed between 12 to 52 sccm. The water vapour was protonated to form hydronium ions (H_3O^+). The hydronium ions were drawn into the drift-tube by the potential gradient on the guide rings.

Figure 2.15 is a diagram of the assembly. The drift-tube is 10 cm long and is constructed of stainless steel guide rings separated by static dissipative Teflon cylinders, with Viton O-rings between the two. The sample to be analyzed was continuously injected at a flow rate of 200-275 sccm into the upstream end of the drift-tube and the pressure in the drift-

tube was maintained at 6 mbar and later at 7.9 mbar. Positive ions from the ion source are drawn into the drift-tube by a voltage gradient and proton exchange reactions with the sample gas take place as the mixture proceeds along the drift-tube. The ions leave the drift-tube via a 200 μm orifice in a stainless steel plate and pass through a small differential pumping plenum chamber before entering the ion transfer optics of the TOF-MS.

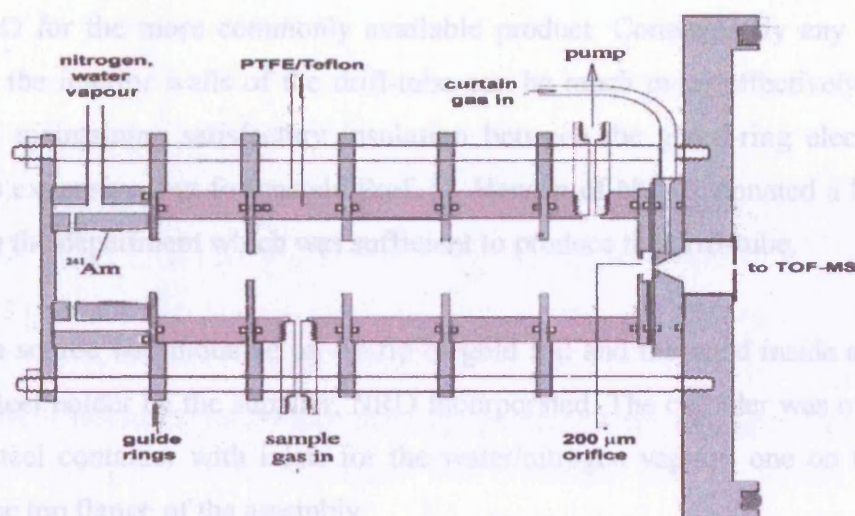


Figure 2.15 Diagram of the ^{241}Am -powered ion source and drift-tube.

Simulation tests using SIMION (Figure 2.16) confirmed that a part of the emergent ion beam could be focussed in a tight beam. Hanson *et al.* [Hanson *et al.*, 2003] assume that about 20% of the ions created are focussed and arrive at the exit orifice. The rest are lost to the walls of the ion source.

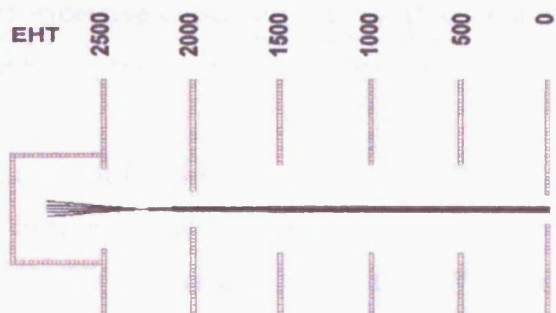


Figure 2.16 SIMION simulation of the ion beam in the ^{241}Am source.

2.4.2.1 Construction

The special PTFE used in the drift-tube was a material that was important to the operation of the ion source. Semitron ESD 500 (Quadrant EPP) is a specially formulated PTFE used for static dissipation applications. It has a surface resistivity of $10^{10} - 10^{12} \Omega$, (or the commonly used but dimensionally incorrect unit Ω/Square) which is much lower than $10^{15} \Omega$ for the more commonly available product. Consequently any build-up of charge on the interior walls of the drift-tube can be much more effectively dissipated, while still maintaining satisfactory insulation between the guard-ring electrodes. The material is expensive, but fortunately Prof. D. Hanson of NCAR donated a block of the material to the department which was sufficient to produce the drift-tube.

The ^{241}Am source was mounted on a strip of gold foil and mounted inside a cylindrical stainless steel holder by the supplier, NRD Incorporated. The cylinder was mounted in a stainless steel container with inlets for the water/nitrogen vapour, one on the side the other on the top flange of the assembly.

The stainless steel guide rings had 8 mm holes on their outer circumference, to allow the source and drift-tube assembly to be held together by three 6 mm diameter threaded nylon studs.

Provision was made to allow dry gas to be leaked into the source at the last guide ring. The purpose of this 'curtain' gas is to provide a region of dry gas at the exit of the source which strips water molecules from clusters that occur in the system. So far this feature has not been used since excessive clustering was avoided by a suitable combination of sample gas pressure and EHT (for example 6.0 mbar/3000 V or 7.9 mbar/2700 V).

Both ion sources and their drift-tubes share a common interface flange for mounting on the TOF-MS (see also Section 2.5.1). The base of the drift-tube is insulated from the common interface flange with a sheet of 0.8 mm thick PTFE so that it can be biased above earth potential. The adjustable bias focuses the ion beam but also imparts kinetic energy to the emerging ions, which has to be compensated for when entering the transfer optics of the TOF-MS (see Section 2.5.4).

2.4.2.2 Exit orifice

The exit orifice from the drift-tube is a 200 μm diameter hole in the centre of a 1 inch diameter stainless steel plate. Several aperture plates were supplied by MicroMetrics of Lincoln with orifice diameters of 50, 100, 200 and 300 μm . The laser drilling technique used by MicroMetrics produce cleaner holes than can be produced using a conventional drill.

2.4.2.3 Electrical configuration

Figure 2.17 shows the electrical circuit arrangement for the ^{241}Am source and drift-tube. The ion source and drift-tube was held at a positive potential relative to earth. Initially, this was 2500 Volts, but this was raised to 3000 Volts, as this proved more effective in suppressing the formation of water clusters around the charged reagent as well as the product ions. The source holder and the top guide rings were held at fixed potentials by the resistor chain, whereas on the bottom two electrodes, their bias voltages could be altered by means of two 100 k Ω ten-turn potentiometers. The adjustment of these potentiometers was quite critical as they had a strong focussing effect on the emerging ion beam.

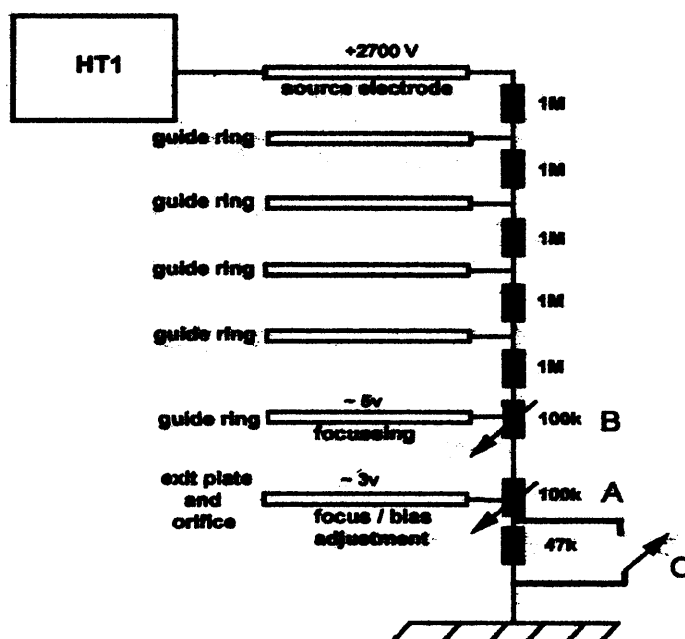


Figure 2.17 Resistor chain supplying the bias requirements of the ^{241}Am source and drift-tube.

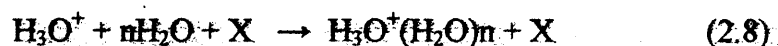
During tests the top electrode was taken up to 4200 Volts without problems, but the drift-tube pressure also had to be raised to 8 mbar to avoid sparking. As long as the drift-tube was at its normal operating pressure of 6.0 mbar, the system showed no propensity to spark or flash over. However if a flash over did occur, it upset the stability of the system and it needed an hour or more to recover.

When starting up the source, the EHT was raised slowly until the event counter of the Kore acquisition program detected counts (see Figure 2.28). At low voltages, this was likely to be due to a multi-clustered form of hydronium. A count detector window was set to accept counts due to hydronium events ($m/z = 19$) and the other to accept all mass events greater than $m/z = 19$. Once a signal was detected, the HT was raised further, continuously readjusting the PTR-TOF-MS for maximum counts. As the HT applied increased, cluster formation diminished until single hydronium signals predominated. The wide-open event counter window was then adjusted to select only the counts of mono-hydrated hydronium clusters at $m/z = 37$. Conditions in the instrument could then be optimised to improve the H_3O^+ count rate.

2.4.2.4 Operating conditions

High purity de-ionised water (15 M Ω -cm) was used as the source of water vapour and purged before use. N_2 carrier gas was bubbled through it and fed into the ion source via a mass flow controller at a flow rate of 50 sccm. Zero grade nitrogen (BOC, 99.998%) passed through an Alltech activated charcoal hydrocarbon trap was served as the carrier gas for the water vapour. Zero air (BOC, BTCA 178 grade) scrubbed through a self-indicating hydrocarbon trap was used for some calibration scans.

With water vapour present in the system, some VOCs and OVOCs neutrals or ions form clusters with water molecules which can hinder protonation directly, or influence the course of reactions indirectly by swapping water molecules between reagents and analytes by ligand switching. H_3O^+ ions readily form multi-hydrate clusters by means of termolecular reactions of the type



The effect of the third body in the reaction (2.8) is to stabilise the resultant hydrated ion from subsequent dissociation into its constituents [Smith and Španel, 1996] [Španel and Smith, 1995].

Increasing the electric field by raising the applied EHT along the drift-tube causes clusters to break up, but increasing the density of water vapour enhances cluster formation. Every attempt was made to minimise cluster formation. An alternative approach was to use a leaner water vapour mixture, but this reduced the protonation yield if the water vapour density were reduced too much.

The route chosen to reduce cluster formation was to increase the EHT, while leaving the drift-tube pressure unchanged. The PTR-TOF-MS was operated at an E/N of 190 – 200 Townsends (Td) where 1 Townsend = 10^{-17} Volts cm^2 . The quantity E/N is the ratio of the applied electric field E in Volts/cm and N is the molecule density. A systematic investigation into the technique of cluster reduction is described in a later chapter.

A disadvantage of operating at high E/N is that fragmentation of some VOCs and OVOCs could be significant. In Chapter 6 it is shown that fragmentation under certain circumstances could be a useful aid in helping to identify mixtures of isobaric compounds.

In the early stages of operation, the PTR-TOF-MS ran at ambient temperature (approximately 23 °C), but in the current version the ion source and drift-tube are heated to constant temperature above ambient (40°C) to minimise the effects of outside temperature variation on the reaction rates in the drift-tube. Experiments have shown that this effect was small in the case of hydronium and is discussed in Chapter 3.

2.4.2.5 Bench tests

The orifice plate in the drift-tube was the penultimate element in the potential divider chain and not tied to earth. It was a convenient point to measure the ion current arriving at the aperture plate. A guide ring masked the aperture plate, that exposed a circular area 5 mm in diameter to the incident ions.

The current signal from the orifice plate was fed into a Keithley Model 427 current amplifier and the output read on a voltmeter. The amplifier was set at maximum gain, 10^{10} V/A, and the rise time set to maximum, so as to allow the current signal, which was mainly DC, to be detected. The ion current collected on the aperture plate was 500 picoamps. The measured current was comparable to that reported by Hanson and co-workers [Hanson *et al.*, 2003].

The ion source and drift-tube were mounted on a flange to which a Faraday cup was attached. Firstly, the current gathered by the aperture plate was measured, and an attempt was made to see if the current in the Faraday cup could be measured. Since the diameter of the aperture in the plate was only 200 μm , the current passing through to the Faraday cup would be reduced by a factor of 625 of that which could be measured on the aperture plate. There would be a further reduction in any detected current for geometric reasons because the collector plate in the Faraday cup would not be able to collect the entire ion current.

The expected current due to particles passing through the orifice and collected in the Faraday cup would be 1/625 at most or less than 1 picoamp. The actual signal measured in the Faraday cup was 4.4 pA. This reading did not change when the drift-tube bias was removed, so it was concluded that the signal observed was due to noise.

It is interesting to note that with the hollow-cathode source, readings in the Faraday cup reached 500 pA. The hydronium yield of the ion source when measured on the TOF-MS was similar to the yield from the ^{241}Am case. Clearly the ion current observed was due to some other activity. On the TOF-MS it was found that when the bias conditions were used which corresponded to the maximum Faraday cup readings, arcing in the source drift region or even the drift-tube itself occurred.

2.4.2.6 Stability

It was important that the PTR-TOF-MS should be stable in the long term and so several experiments were performed to check its stability.

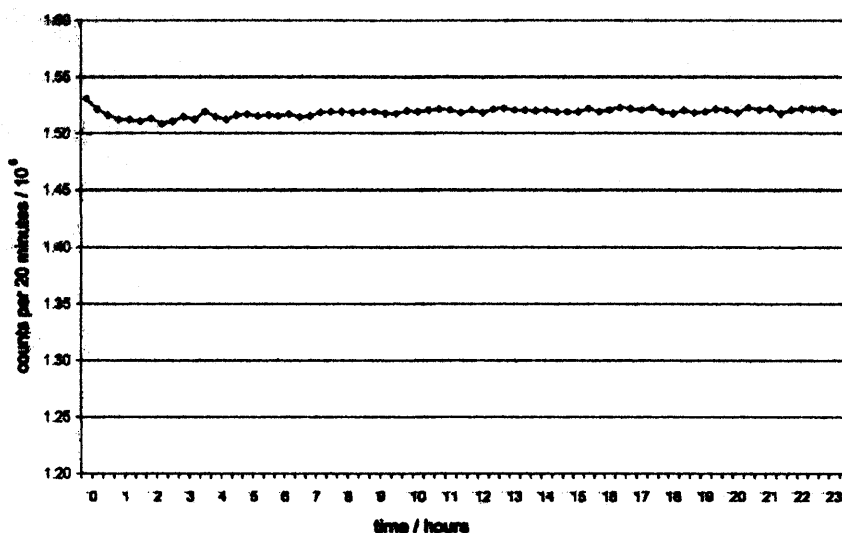


Figure 2.18 The hydronium yield at a constant temperature of 40 °C.

The long term behaviour of the ion source is demonstrated in Figure 2.18. In the first hour of running, the ion source exhibited a slight drop in performance, before a steady operating state was established. Thereafter the ion source settled down to a steady operation. This behaviour was valid in conditions of steady external temperature. In Section 3.10 the output of the ion source was found to be temperature dependent, so care had to be taken to ensure that the operating temperature of the equipment remained constant throughout.

2.5 Other features

This section deals with features that are common to both the hollow cathode and the ²⁴¹Am versions of the PTR-TOF-MS.

2.5.1 Common Interface Flange

The hydronium ion source and drift-tube were mounted onto the TOF-MS via a pair of Conflat CF160 flanges specially machined so that they formed a plenum chamber. Each ion source had its own version of the flange forming the top part of the plenum chamber, while the flange forming the bottom half was shared. To reduce the load on the turbo pumps in the TOF-MS, this intermediate plenum chamber was used to provide an extra pumping stage before the ions passed into the transfer optics of the TOF-MS. A Varian V70 turbo pump evacuated the plenum chamber

The bottom flange has a 5 mm exit aperture, and has provision for smaller apertures to be fitted. A major criterion for the exit aperture size is that it should be as large as possible, while still ensuring the pressure in the body of the TOF-MS does not exceed 10^{-6} bar (at which point protective interlocks would switch off the MCP detector). Although the drift-tube pressure in the Americium source is normally 6 mbar, the exit orifice from the drift-tube with a diameter of $200\mu\text{m}$ slows the leakage rate into the main body of the PTR-TOF-MS. A 3 mm bottom flange aperture was sufficient to limit the pressure in the body of the PTR-TOF-MS to 2.7×10^{-7} bar.

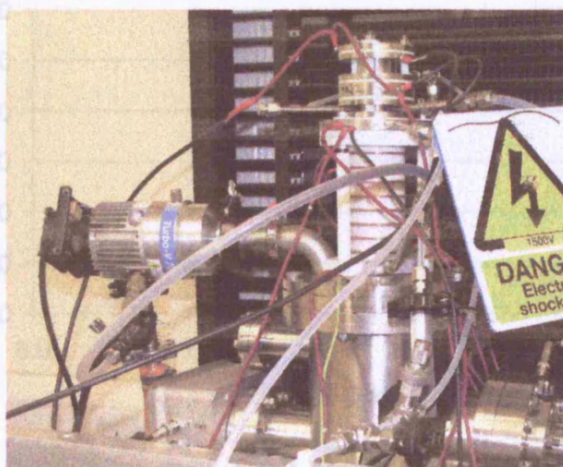


Figure 2.19 The ^{241}Am source is mounted on the common flange. The Varian VR70 turbo pump which evacuates the plenum chamber is clearly visible.

For the hollow cathode source a 2 mm exit orifice was found to be suitable. The hollow cathode drift-tube with its internal pressure of 0.4 – 0.6 mbar has a 1 mm diameter exit aperture into the source drift region, which in turn has a 2 mm orifice leading to the drift-tube. The MS-TOF pressure usually varies between 4×10^{-7} to 5×10^{-7} mbar depending on the drift-tube pressure used.

2.5.2 Microchannel plate detector (MCP)

The MCP sensitivity is adjusted by a positive excitation bias from 0 to 3000 Volts determined by a ten-turn potentiometer with the full-scale setting (10.0) corresponding to the maximum bias.

As the detector ages the output count rate decreases so that it is necessary to raise the bias to compensate. The ion count rate increases substantially as the bias is raised.

From the data in Figure 2.20 it appears that the count rate rises smoothly up to a bias potentiometer setting of about 9.0 (2700 Volts) after which the count rate shows signs of saturation. The accompanying figure shows the increase in hydronium peak count rate as a function of increasing MCP bias.

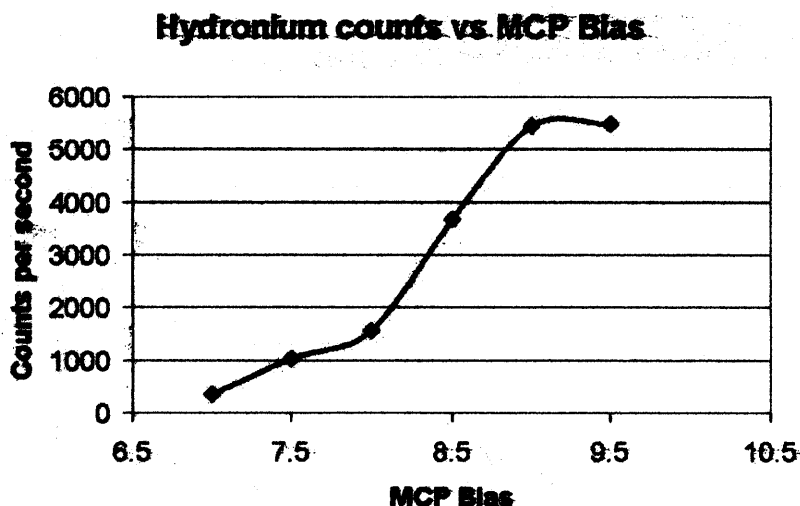


Figure 2.20 The hydronium count rate is strongly dependent on the bias applied to the MCP detector. The x-axis represents the settings of the bias potentiometer, which has a scale of 0 – 10.

While the curve suggests that it is safe to operate at a bias potentiometer setting of almost 9.0, a large part of the apparent count rate appears to due to a non-linearity in the MCP's response. An event causes the time-to-digital converter (TDC) to generate a double pulse, one slightly displaced in time from the main peak.

When operating at a scan range of up to $m/z = 143$, the apparent hydronium count rate can approach 10000 counts per second (about double the value seen at a bias of 7.7). However by readjusting the system dead-time from 2 ns to 4 ns the observed count rate halves, so it is likely that the high count rate observed may include spurious events or even a malfunction in the TDC.

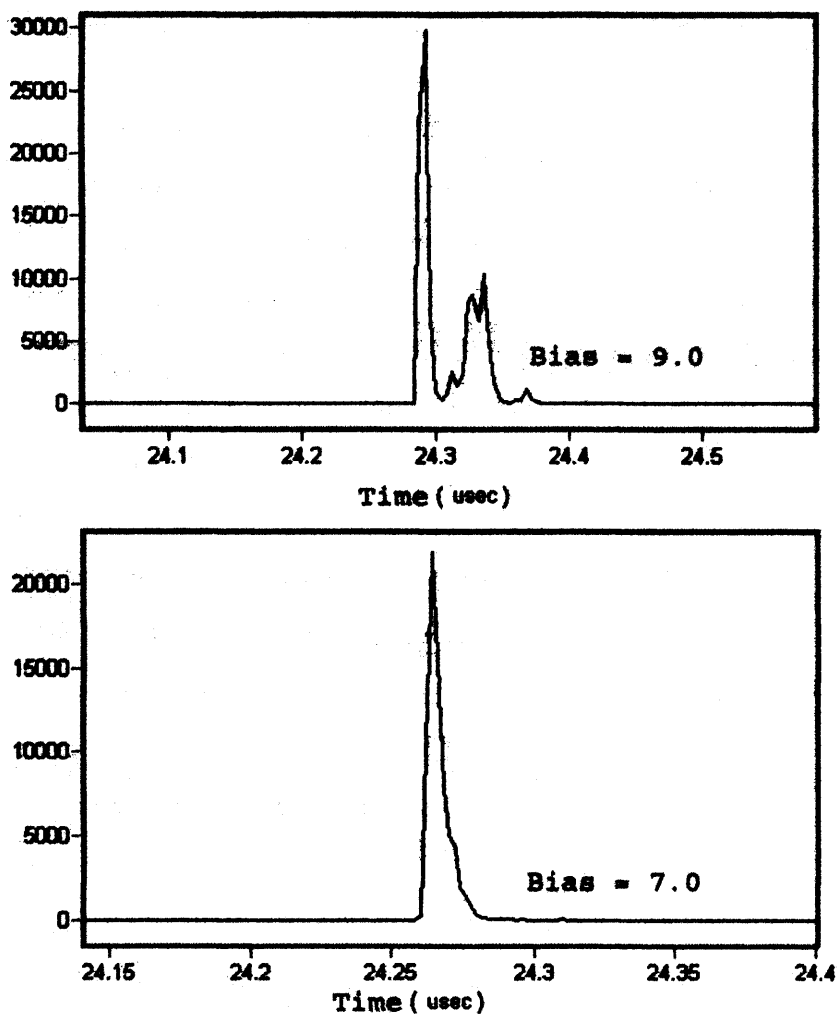


Figure 2.21 Hydronium time peaks seen with when MCP bias potentiometer was set to 9.0 (top) and 7.5 (lower).

The double pulse depicted at the top of Figure 2.21 still means a single event has been captured, but depending on the scan time range used, the second pulse lies outside the dead time of the system and so gives rise to a second ghost event. It was found that the MCP bias setting should not exceed a bias potentiometer setting of 7.7 (2310 Volts). The effect of overloading is to create a second time peak in the response of the TDC.

2.5.3 Detection and processing

A time-to-digital converter (TDC) sorts the measured ion flight times into a series of 2 ns time bins. The TDC was designed and built by Kore Technology of Ely. Time scans are triggered by the ion extractor pulse in the TOF-MS, which is generated from a trigger

pulse from the TDC. The output of the TDC is fed into a PC *via* a purpose-built interface (also by Kore Technology) for data capture and subsequent display and analysis.

The main analysis software tool was GRAMS/AI produced by Thermo Galactic Inc, Salem, New Hampshire, USA. GRAMS/AI provides powerful handling and manipulation facilities for the processing of spectral data. The package is extremely versatile and has extensive facilities and entry points for user customisation. Kore provided the control program, linked to GRAMS/AI, with which the user controls the operation of the TOF-MS and can view the captured data either as a time-of-flight scan or a mass spectrum histogram.

The Kore application provides facilities that include the ability to

- group time bins as 2, 4, or 8 ns time bins.
- set the mass range to be captured from 100 atomic mass units (da) to 1000 and beyond.
- determine the length of each acquisition for each run.
- initiate a scan cycle.
- fine-tune the conversion coefficients for converting time spectra to mass spectra.
- display the count rate in two preset time or mass windows.

GRAMS/AI provides a high level programming language, Array Basic for producing customised programs to extend the functionality of GRAMS/AI.

Many of GRAMS/AI's features are written in this language, as indeed, are the KORE utilities. The language is interpretive and so it is simple to read the source code of the existing utilities and modify them. The recommended procedure to learn the language is to modify an existing utility. Code modules are grafted onto an existing Array Basic application to extend their functionality. This speeds up the analysis of the data considerably.

2.5.4 Operating the TOF-MS

The TOF-MS has a control panel with multi-turn potentiometers to allow adjustment of the various electrical bias voltages for the TOF-MS and for fine-tuning its performance

(Figure 2.22 and schematic in Figure 2.23). The potentiometers all work off a common rail set at -2000 Volts so that any voltage drift would affect all the parameters in proportion. The resistors in the common rail proved to be sensitive to temperature variations and caused problems whenever there was a large variation in operating temperature. A high voltage DC power supply (Stanford Research SF350) capable of giving up to 5000 Volts and 5 milliamps supplies the negative 2000 volt bias. Under typical operating conditions the common rail draws 3.98 milliamps.



Figure 2.22 The Bias Control Panel of the TOF.

Figure 2.22 depicts the user controls of the PTR-TOF-MS and Figure 2.23 shows in detail the wiring of the instrument as well as the location of the items controlled from the panel in Figure 2.22.

Three potentiometers (T.Extract, T.Lens & Backplate) control the input section of the TOF-MS. They control the DC bias for the extractor plate, the back plate and the einzel lens. The bias adjustment for the MCP is also on this panel.

Two potentiometers (X & Y) control the settings for the X- and Y-deflectors that steer the beam into the reflectron and finally there are two potentiometers controlling the retardation voltages of the reflectron grids. These last two (Retard & Reflect) control the reflectron's decelerating field and have a pronounced effect on the ion flight times. If touched it was always necessary to recalibrate the TOF-MS.

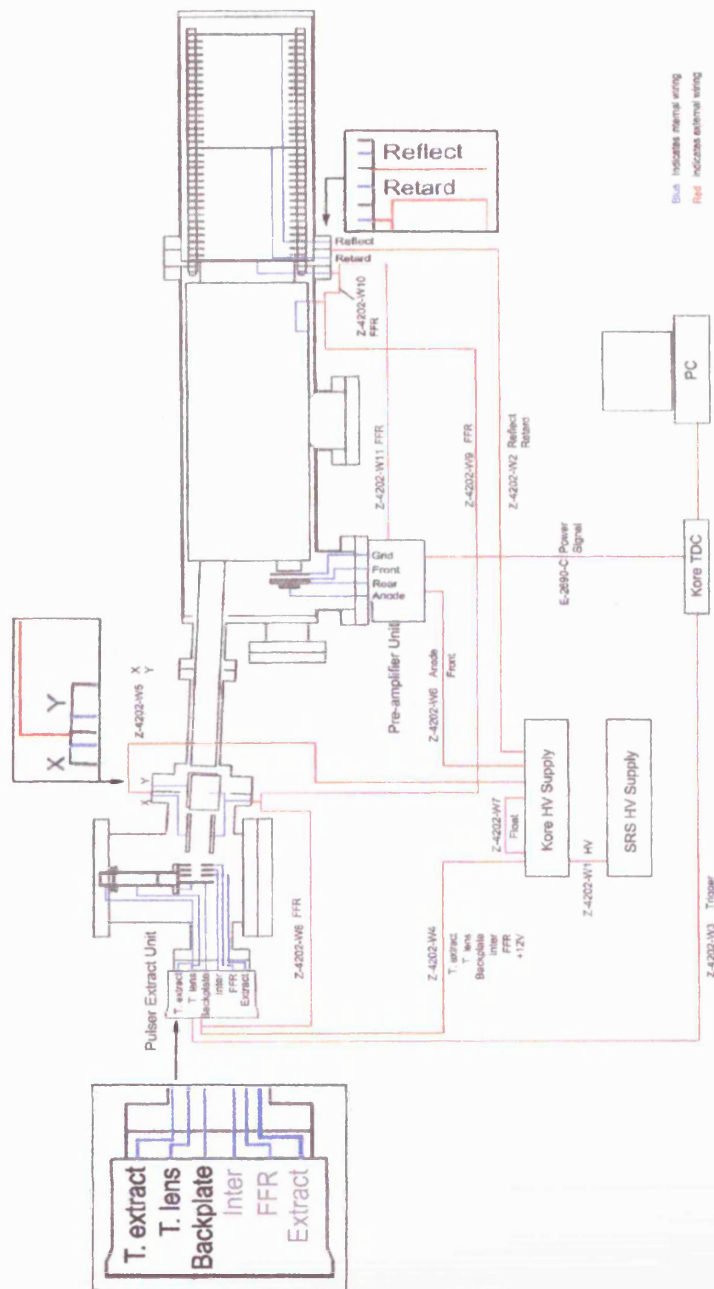


Figure 2.23 Schematic of PTR-TOF-MS showing internal and external wiring. The user adjustment potentiometers are highlighted and enlarged for easy identification.

Initially problems were encountered with the X-deflector settings, as there was insufficient adjustment provision at the top of end of the range. Kore investigated the problem and concluded that whereas the entry optics to the TOF-MS assume that the incoming ions have near-zero kinetic energy, in fact the ions still have some residual velocity on entering. Kore's solution was to apply a positive bias to the internal field-free region of the TOF-MS to counteract the energy of the incoming ions. A Thurlby EL561

regulated power supply with a range of 0 to 56 Volts (positive or negative) supplied the necessary positive bias. In normal operation it was set to about 38 Volts. Occasionally it was necessary to adjust the setting slightly to optimise the ion count rate.

Under a temperature-controlled environment the instrument settings of the TOF-MS do not need readjustment for several months. However in the field where there might be large working temperature variations, drifting in the mass readings can be observed. After discussions with Kore, it was concluded that the drift was most likely due to temperature effects on the resistor common rail. The main effect observed was a shift in the time-of-flight of the ions: by as much as 0.5 da. Ideally the instrument should have had a separate regulated supply for each of the adjustment parameters, but this would have been very expensive. The backbone of resistors used in the current model of the TOF-MS was not stable enough to avoid the problem. Fortunately, there was a way to eliminate the problem. By performing many short duration runs that could be summed together after appropriate mass rescaling, it was possible to overcome the data analysis problems caused by time shifts entirely and avoid having to retune the TOF-MS on a regular basis.

2.5.5 Gas handling

Both types of ion source require water vapour to function. In the case of the hollow cathode source, pure water vapour was fed into the ion source through a needle valve. In the case of the ^{241}Am source, zero-grade nitrogen (BOC, BTCA 178 grade) saturated with water vapour was used as the reagent mixture and the mixture passed through a mass flow controller at the rate of 50 sccm into the ion source.

Pure water vapour for the hollow cathode source was drawn from the headspace of a glass container filled with high purity deionised water (15 M Ω -cm) and metered through a needle valve rather than through a mass flow controller. An inline filter (7 micron) was placed in the line to prevent water droplets from entering the system. The partial pressure of water vapour in the source was 0.2 mbar.

For the ^{241}Am source, Zero-grade nitrogen was bubbled through a vessel containing high purity deionised water (15 M Ω -cm). The saturated gas was drawn off from the headspace

and leaked into the ion source via a 50 sccm mass flow controller and fed into the ion source at the rate of 6 – 12 sccm.

Experiments with inline filters to remove water droplets were unsatisfactory as occasionally droplets of water did collect at the input of the mass flow controller. A simple water trap was inserted. It was more reliable than the in-line filter. The water trap consisted of a test tube into which a metal stopper (with an o-ring seal) was fitted. Two tubes passed through the stopper, one was the inlet, and the other connected to the input of the mass flow controller. Any water droplets penetrating as far as the water trap, collected at the bottom of the test tube. The system worked faultlessly.

The sample gas containing the VOCs and OVOCs was atmospheric air. Since the purpose of the project was to detect contamination in the atmosphere, the atmosphere was the obvious choice as a working fluid for the sample gas.

Initially, the sample gas for the hollow cathode source was metered through a needle valve, and later replaced with a mass flow controller for better control. In the hollow cathode source the internal pressure was the main criterion used to judge gas flow.

In the case of the ^{241}Am source, mass flow controllers were always used to govern gas flow. The most common flow rate used was 200 sccm of sample gas to 12 sccm of saturated water vapour.

A special unit shown in Figure 2.24 was developed to incorporate the two mass flow controllers and needle valve used to manage the gas flow into one unit. It occupied half the space of a 19" chassis tray, leaving space for the drift-tube temperature regulator and a turbo pump controller.

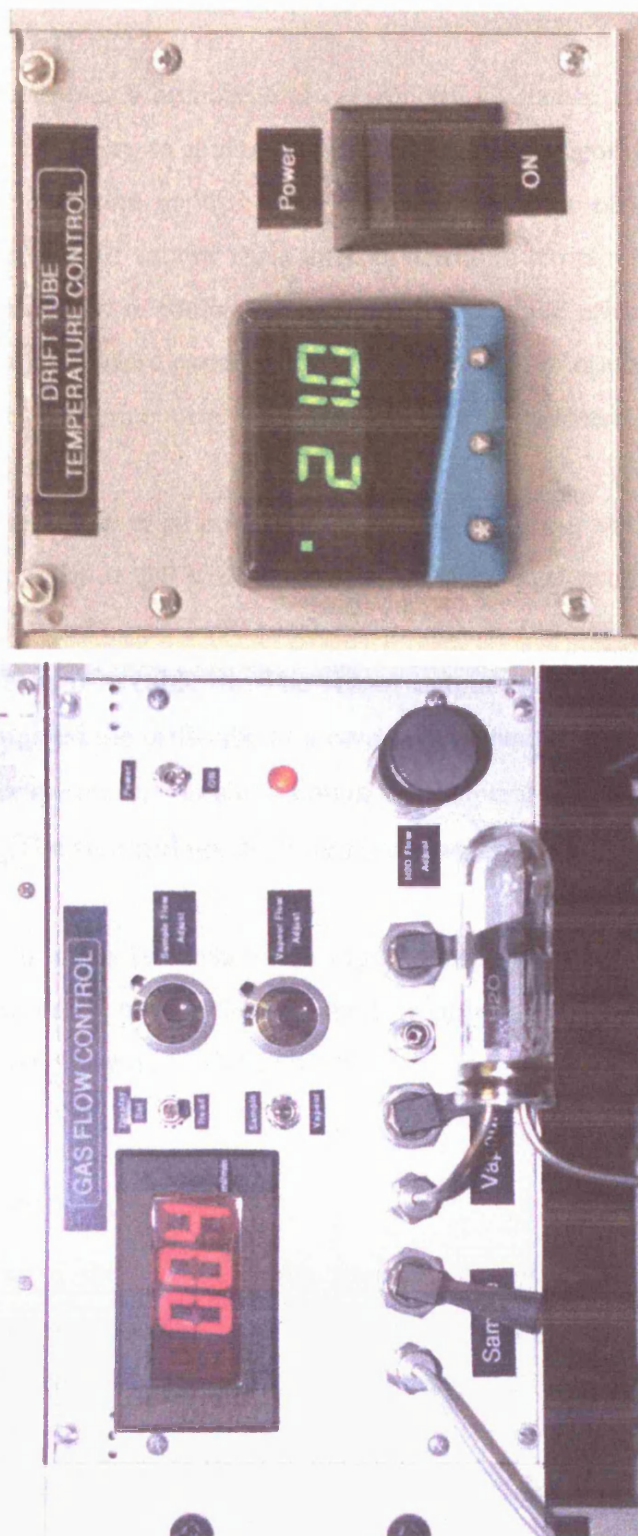


Figure 2.24 The gas handling module and the drift-tube temperature controller.

2.5.6 Temperature control

Some groups, for example, Wareneke and co-workers [Wareneke *et al.*, 2001] reported finding that it was necessary to maintain the drift-tube and incoming sample gas at a constant elevated temperature in PTR-TOF-MS experiments in order to counteract the effects of atmospheric water vapour variations. In addition, temperature fluctuations can cause significant variations in protonation rates and introduce errors into experimental results. A simple way to assure experimental consistency is to operate the experimental instruments at a constant temperature above the ambient temperature.

To achieve this, a 1m length of silicone-coated heating wire was wound around the drift-tube. It was powered by a 24 Volts DC supply and could produce 40 Wm^{-1} . The temperature was measured by a PT100 patch sensor attached to one of the PTFE rings on the drift-tube by means of a cable tie. The sensor output was fed into a CAL9300 PID controller that maintained the drift-tube at a constant temperature. Once equilibrium was established at any temperature, it could maintain the temperature to within 0.1° C . up to a maximum of 50° C . The standard operating temperature was chosen to be 40° C .

The temperature control unit (also shown in Figure 2.24) was fitted to the ^{241}Am source, the source most commonly used. When the hollow cathode source is redeployed in the future, the heating control device will be attached.

2.5.7 Mass resolution

The mass resolution of the TOF-MS was found to be $m/\Delta m > 1000$. Some factors contributed to this satisfactory figure: the speed and stability of the electronics as well as the long flight tube of the reflectron portion of the instrument.

There may be slight broadening of the peak as a result of recalibration if the spectrum has shifted significantly. In Figure 2.25 the results are shown for a peak at $m/z = 121$. Similar $m/\Delta m$ figures were obtained for peaks in the $m/z = 40$ region.

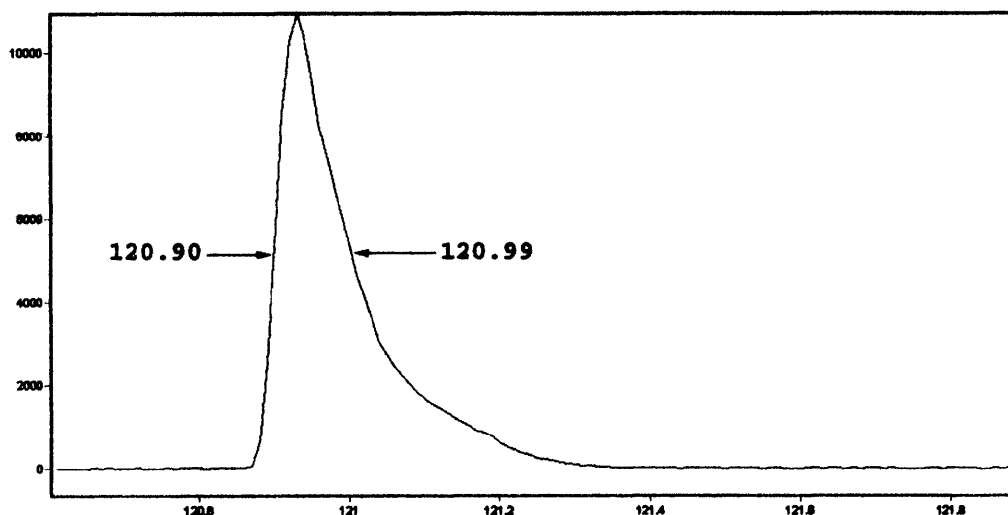


Figure 2.25 Measured resolution of the PTR-TOF-MS. Here $m/\Delta m = 1344$ at $m/z = 121$.

2.6 Control and analysis software

The TOF-MS was supplied with data acquisition and manipulation software. Additional software was needed and wherever possible spreadsheets were used to process the data and produce charts. The following sections describe the software used for data acquisition and subsequent processing. The applications are arranged in the order in which they were applied to analyse data from the PTR-TOF-MS.

2.6.1 Supplied software

2.6.1.1 Grams/AI and the Kore extensions

The control and acquisition program for the PTR-TOF-MS was developed by KORE as a user application linked to GRAMS/AI. In GRAMS/AI parlance this program was called a Workbook. The main features of the workbook were spelt out in Section 2.5.3 :

- Group incoming data into 2, 4, or 8 ns time bins.
- Set the mass range.
- Determine the time of data acquisition for each run.
- Initiate a run cycle.
- Fine-tune the conversion coefficients for converting time spectra to mass spectra.
- Display the count rate in two preset windows – invaluable for optimising the instrument.

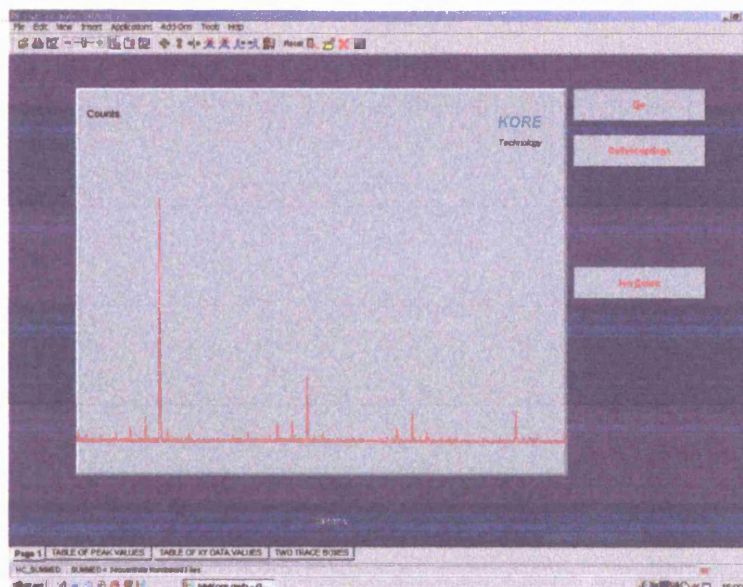


Figure 2.26 The KORE data acquisition program supplied by KORE. It controls the PTR-TOF-MS and displays captured data as a time series or as a mass histogram.

Whenever GRAMS/AI was loaded on the computer controlling the PTR-TOF-MS, this workbook was loaded by default.

In a typical on-screen mass spectrum as shown in Figure 2.26 above, the display can be expanded along the x- or y-axis so making it possible to zoom in on low intensity peaks covering a small range of atomic mass units.

Data could be displayed with flight times or mass units along the x-axis. The conversion from the time to mass domain was done in real time using the conversion equation

$$m = \left(\frac{t_i - t_0}{C_b} \right)^2 \quad (2.9)$$

The conversion coefficients can be recalculated between scans. The calibration procedure requires two peaks of known mass to be identified in a scan, and the variables t_0 and C_b are then calculated. The recalibration procedure is initiated by selecting the 'collect options' button and then the 'advanced' button on the dialogue box which is shown in Figure 2.27. The calibration routine used a wizard to guide the user through the process.

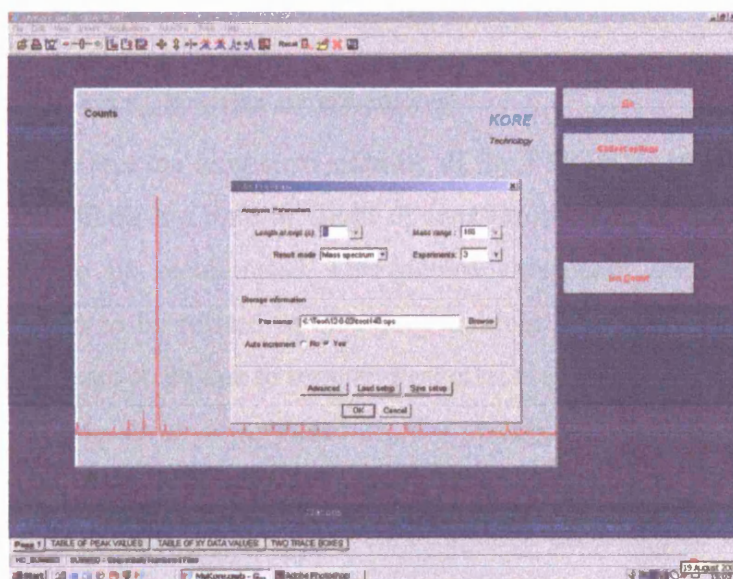


Figure 2.27 The control panel for adjusting settings in the KORE data acquisition program.

The 'ion counts' button run an application that is useful when setting up the PTR-TOF-MS. It displays a large prominent window with large numbers indicating the number of counts detected in two mass ranges or windows (Figure 2.28).

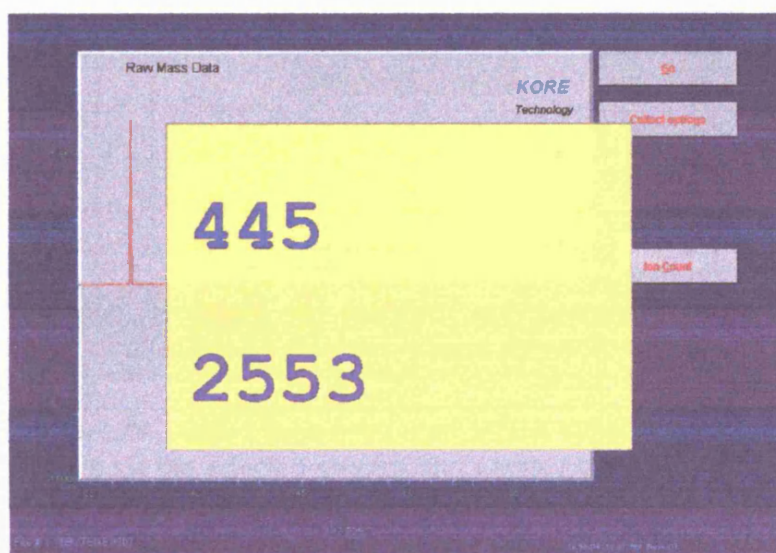


Figure 2.28 Ion counter is a useful aid when setting up the PTR-TOF-MS. The figures displayed are purposely large to make aid visibility.

Each window can be adjusted to register counts between an upper and lower mass value. Normally the lower window is set to cover the range of 18.5 to 19.5 Da. for hydronium and the upper one $m/z = 36.5$ to 37.5 for the hydronium monohydrate cluster.

2.6.1.2 Spectrum recalibration or rescaling

Several factors can affect the long-term stability of the PTR-TOF-MS. Changing any of the potentiometers affects the time of flight of ions through the TOF-MS, and requires the PTR-TOF-MS to be recalibrated. Unexpected significant time drifts have been observed which seem to be related to changing ambient temperature. The cause of the problem is now believed to be due to temperature effects on the resistor backbone. While the trend of the time drifts are related to the changes in temperature, they occur erratically. Nevertheless the time drifts are gradual, and do not affect short runs of a minute. However, for longer scans, where data might be accumulated for several hours, drifting is a real problem.

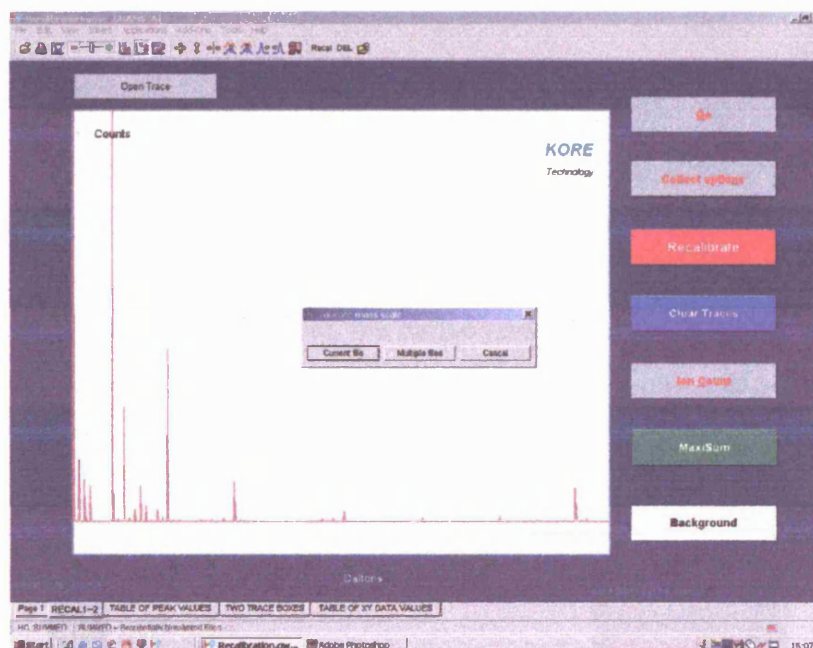


Figure 2.29 A post processing application supplied by KORE rescales all the selected spectra and compensates for any time shifts between runs.

Fortunately KORE have a facility in their general software that can rescale time and mass spectra (Figure 2.29). Its operation is similar to the calibration wizard where two peaks of known mass are identified and used to calculate the calibration constants.

As shown diagram in Figure 2.29, the user has a choice of rescaling up to 255 spectra at a time. There is a slight loss of peak resolution, but since resolution of the TDC of the TOF-MS was 0.01 da, the effect of rescaling was small.

2.6.2 Additional software

Additional software was needed to facilitate the rapid analysis of the data produced by the PTR-TOF-MS. The standard unit of data acquisition was a one-minute scan, which generated 1440 files per day.

2.6.2.1 MaxiSum and MaxiBgd

The MaxSum and MaxiBgd applications were not supplied by KORE Technology. They were developed by the writer from standard GRAMS/AI application. GRAMS/AI applications are written in Array Basic, so are relatively simple to extend for additional functionality.

The two programs perform group and sum operations on mass spectra, sorting them into 180 mass unit bins from mass 19 to mass 198. For each mass unit the window of acceptance of MaxiSum is 0.35 da starting at $X-0.15$ da and extending to $X+0.20$ da for any integral mass number X . In effect, the native resolution of the GRAMS/AI (100 bins per da) is reduced to 1 da, but makes allowance for the fact that peaks spread on either side of the integer values.

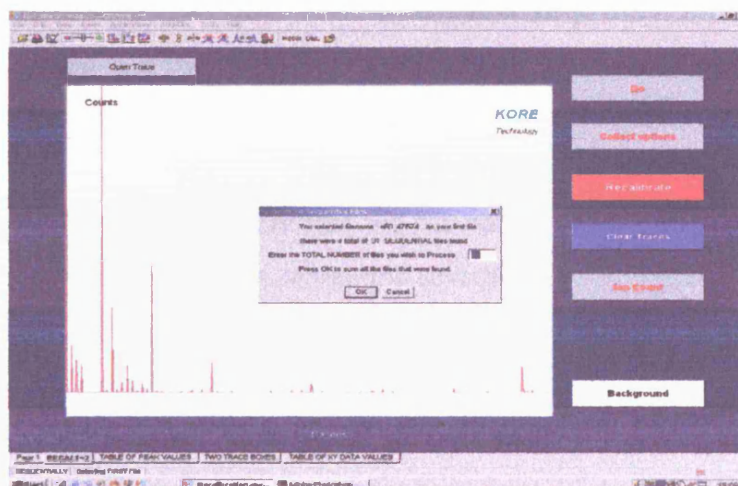


Figure 2.30 The MaxiSum application divides a spectrum into 1 da bins.

Array basic can only produce strings of text records that contain up to 17 items per record, so the MaxiSum produces its output as an intermediate binary (.byn) file where there is no limitation in record size. A further step is needed (Section 2.6.2.2) to convert this into the desired text readable format (.csv).

The mass resolution of the PTR-TOF-MS is sufficiently large ($m/\Delta m > 1000$) that it was possible to estimate the background contribution with good accuracy, by selecting a portion of spectrum midway between integral mass numbers. The peaks are sufficiently well resolved so that there are flat plateaus of background counts between them.

So, for any peak at position X , MaxiPeak captures the extents from $X-0.15$ to $X+0.20$ (the peaks), whereas MaxiBgd deals with the extents $X-0.55$ to $X-0.20$ (between the peaks). Apart from the different area of focus, the two programs are identical.

GRAMS/AI spectra data consist 100 points for each atomic mass unit. The position for each peak in the spectrum is calculated by the program using the linear relationship between the GRAMS/AI spectra data X and the value of the corresponding ion mass Y :

$$Y = aX - b \quad (2.10)$$

The value of a is 100.0 in ideal circumstances and b has a threshold value in the region of 1225. In the past, because of the time drift, a could vary from 99.7 to 100.3. After spectrum recalibration was introduced, a was always 100.0 and b was 1227. The values of a and b were obtained from the best fit for several experimental runs.

Both MaxiPeak and MaxiBgd require that the file names of the files to be processed be numbered consecutively. In a folder containing several series of spectra, it is necessary to select the first run in the series to be summed (it need not be the first one). The programs count the remaining number of files in the series and the user selects all or part of that number for summing. The format of the output of the two programs is identical. The first set or line of 180 numbers are the mass numbers from 19 to 198. For each spectrum summed there is another set or line of 180 numbers containing the summed peak or background values for 19 to 180 da. In addition, the program also produces a summed spectrum record in GRAMS/AI format.

2.6.2.2 MaxiGroup

MaxiGroup is a self-contained program written in Visual Basic. Its function is to convert binary .byn files into .csv text files that are readable by Excel. It can also divide up the records in the file into groups and sum them.

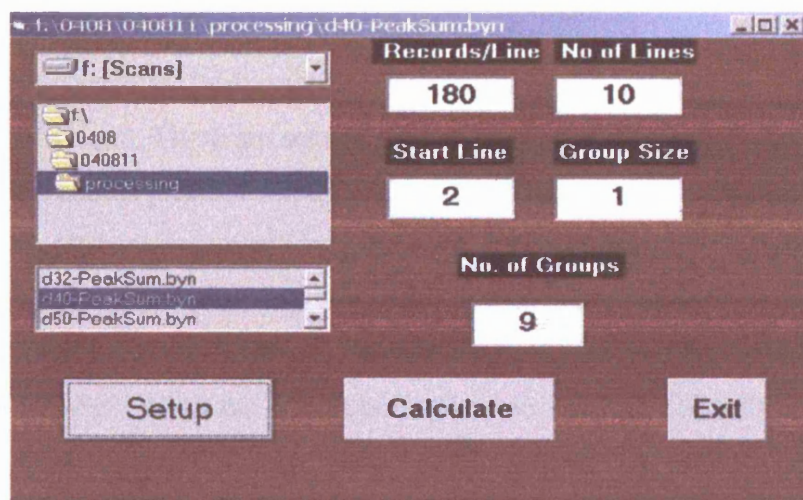


Figure 2.31 The MaxiGroup application converts the binary files to text files which were readable by Excel.

The 1440 spectra of one minute scans taken in a 24 hour day were rescaled, then grouped into 60s and summed with MaxiPeak to produce 24 summed spectra in GRAMS/AI format. The procedure was repeated using MaxiBgd. The resulting summed spectra processed with MaxiGroup to produce two sets of .csv files each with 24 lines, one for each hour of the day.

2.6.2.3 Spreadsheet-based analysis

Microsoft Excel is a convenient tool for performing useful tasks in evaluating captured data. This section describes these functions in outline.

Two Excel projects were created. The first one analysed and processed the data, and the second one used data from the first one and tabulated the results in graphic form. The two programs were not combined to avoid over complication. The two projects were called MaxiAnalysis and MaxiPlot.

A third project, MaxiCorrelation, was unwieldy and was not developed further. It calculated correlations between every mass number and displayed only situations where the correlations exceeded a value set by the user (usually > 0.75). The problem with the output was that it was difficult to read as it required a triangle with 180 entries on a side.

2.6.2.4 MaxiAnalysis

Maxi Analysis processes Peak and Background data copied from the .csv text files created by MaxiGroup. There are separate input tables, one for peak counts and the other for background counts (see Section 2.6.2.1). The data input for each consists of a header record with the atomic mass numbers 19 to 198 followed by up to 24 lines of data, one for each hour of the day with values for each corresponding atomic mass number. Partial tables are allowed but this requires manual manipulation to ensure that the data is properly aligned. First of all the data is normalised to 10^6 ncps following the convention of de Gouw *et al.* [de Gouw *et al.*, 2003a], i.e. scaled to represent the peak heights corresponding to 10^6 hydronium counts. Next, for each of the mass numbers, the corresponding background counts are subtracted from the peak counts.

$$Diff = Peak - Background \quad (2.11)$$

Then the error at each point is calculated:

$$Err = \pm \sqrt{Peak + Background} \quad (2.12)$$

Finally three output tables is calculated for *Diff*, *Diff+Err*, *Diff-Err*. These values serve as input for Maxiplot.

2.6.2.5 MaxiPlot

MaxiPlot uses the charting function of Excel to plot selected peak spectra. The upper and lower bounds are also plotted (Figure 2.32). Where the sensitivity of the PTR-TOF-MS for a particular species is known, the input values can be scaled to represent actual concentrations as concentrations of parts per billion by volume (ppbv).

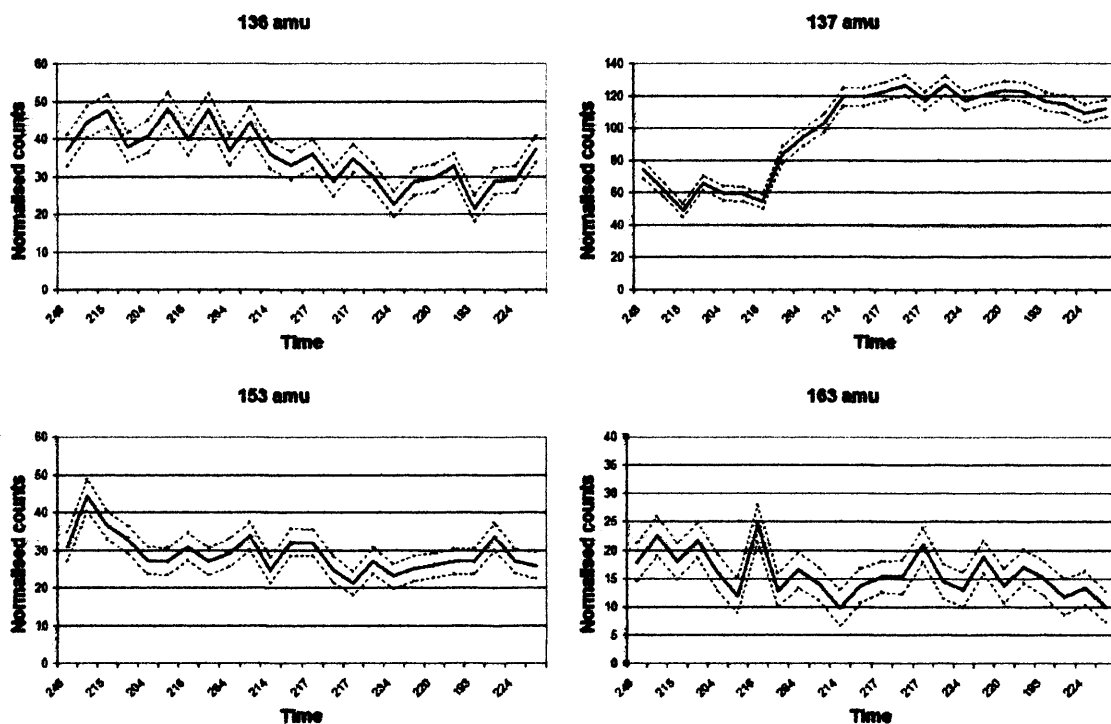


Figure 2.32 Typical output from MaxiPlot. The upper and lower bounds of the peak values are shown as dotted lines. These spectra show hourly yields for 24 hours.

2.7 Summary

In this chapter, the structure and mode of operation of the PTR-TOF-MS was described. It also contained details of the two ion source techniques investigated and the design, construction and implementation on the PTR-TOF-MS. The ^{241}Am powered source was finally chosen as the way forward because of the simplicity of operation it offered. Some details of the long term stability of the configuration was mentioned, and this has been borne out since, as the instrument rarely needs adjustment, and occasional cleaning.

In the next chapter, the exercise of characterising the PTR-TOF-MS is described. This will include determining the ideal settings for the reflectron as well as the optimum drift-tube bias and pressures, as well as the optimum flow rates for the analyte and reagent gases.

Chapter 3

Instrument characterisation

*He who stops being better, stops being good.
- Oliver Cromwell 1599 - 1658*

3 Characterisation

3.1 Introduction

The new PTR-TOF-MS is controlled by several interactive variables as well as several constraints. In addition, the attached ion source needs to be tuned to achieve the optimal settings of water vapour pressure, analyte pressure and drift-tube voltage. It was found that once the instrument was tuned, most of the variables needed no further adjustment, and they have needed little modification for over two years of almost continuous operation.

Like most projects that start with small beginnings, when the ^{241}Am source was first mounted onto the PTR-TOF-MS, the observed hydronium count rate was very low, and substantial improvements in performance were needed. The very first trace obtained using the ^{241}Am ion source is shown in Figure 3.1. It depicts the data captured during a one minute run and sampling the laboratory air. At the time the PTR-TOF-MS running environment had not yet been optimised. Since the hydronium count rates have been increased some 100-fold. Initially contributions from other contaminants such as O_2^+ were present.

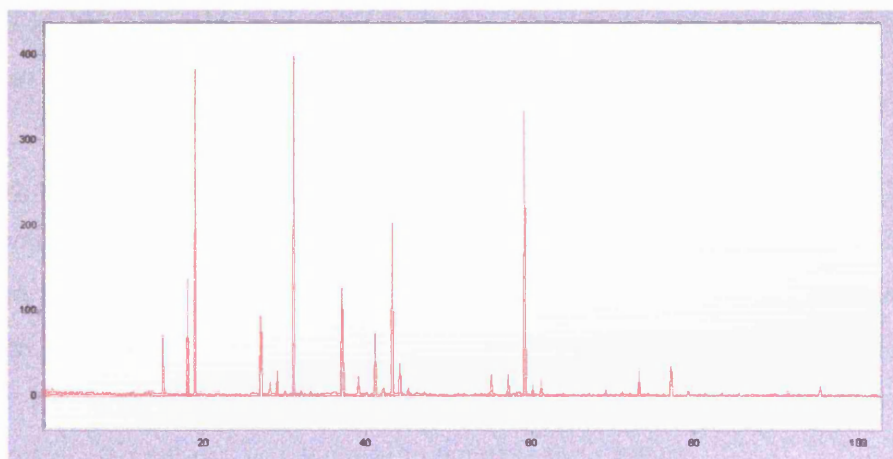


Figure 3.1 The first spectrum produced by the ^{241}Am -powered ion source. The spectrum is of historic interest only.

Currently, the count rate observed for the main hydronium group at $m/z = 19$ regularly exceeds 200,000 counts per minute. Further development holds the promise of even better

performance. Count rate improvements of an order of magnitude appear possible with better ion focussing of the ion beam as it leaves the drift-tube to enter the PTR-TOF-MS.

This chapter describes characteristics of the PTR-TOF-MS and the work done to ensure that it performs with long-term stability and reliability. Other matters covered in this chapter include the optimisation of the variables controlling the operation of the PTR-TOF-MS, the effects of humidity on cluster formation, the effects of the ambient temperature on the equipment response, and the sensitivity of the equipment in counts per ppbv.

3.2 Constraints

The performance of the PTR-TOF-MS with its PTR source is limited by several constraints:

- By design, if the pressure in the flight-tube of the PTR-TOF-MS exceeds 10^{-6} mbar, the instrument is programmed to suspend the operation of the MCP detector to protect it from damage or deterioration of its useful life.
- The optimum size of the aperture between the source drift-tube and the PTR-TOF-MS is 200 μm , which in turn limits the sample gas pressure in the drift-tube to 8 mbar.
- The ratio E/N (defined in Chapter 2, Section 2.4.2.4) influences the type of reactions occurring in the drift-tube. For low values (<120 Td) water molecules tend to form clusters with the hydronium ions that can affect the rate of proton transfer to some analyte species. On the other hand when it is too high (> 200 Td), the increased energy in collisions causes greater fragmentation of the analyte species. This subject is discussed in detail in this chapter.
- A region of differential pumping was required between the drift-tube and the PTR-TOF-MS to keep the pressure in the latter at an acceptably low level. This transfer chamber was evacuated by a small (70 l s^{-1}) turbo pump maintaining a typical pressure of 4×10^{-4} mbar.

- The intermediate transfer chamber was at earth potential and to propel the ions from the drift-tube towards the entrance of the PTR-TOF-MS, the drift-tube exit aperture plate was kept at a positive potential relative to earth.
- On entering the PTR-TOF-MS, the ions had to be slowed down so that their dwell time traversing the entrance aperture of the PTR-TOF-MS was as large as possible, as this affected the duty cycle of the device. This was achieved by applying a positive bias to all the internal elements (also known as the field-free region) of the PTR-TOF-MS to counteract the potential of the drift-tube exit.
- The yield from the ion source improved as the electric field along the drift-tube was increased. However, since there was a limit to maximum pressure of the sample gas in the drift-tube, in practice values of E employed were limited to those that gave a reasonable E/N .

While there are probably a family of settings which would be suitable for operation, the need to maximise the ion yield, along with minimising clustering and ion fragmentation, produced a *primum optimorum* series of curves of the settings for the best operation.

3.3 The controls of the PTR-TOF-MS and the ion source

Power for the PTR-TOF-MS is supplied by a Stanford Research Systems SR350 unit which supplies a potential of -2000 volts to the main voltage divider rail. Voltage taps off the rail that supply the different parts of the instrument. The critical voltage taps are adjustable by means of ten-turn potentiometers. The important electrical adjustment settings of the PTR-TOF-MS are shown in Table 3.1, where the voltage ranges are given along with typical potentiometer settings. In addition, since the potentiometers are linear, typical settings are given as percentages of their maximum range. The components of the PTR-TOF-MS referred to in Table 3.1 are detailed in Chapter 2, Figure 2.3.

The X & Y deflectors needed adjustment, whenever the drift-tube operating environment, such as E/N , was altered. The MCP bias was always set to zero before switching off and reapplied after start-up. The other potentiometers rarely needed attention.

Table 3.1 Potentiometer settings for TOF operation [Kore Technology, 2003]. The location and function of the items is given in Figure 2.23 and Section 2.5.4 in Chapter 2.

Item	Range /V	Settings /%	Function
T-Extract	0 / -20	95.5	Extracts ions from ion source
T-Lens	-70 / -270	41.8	Lens focussing ions into PTR-TOF-MS
Backplate	0 / -20	32.1	Entrance to TOF from transfer section
Extractor	0 / -400	fixed	Extracts ion bundles into the TOF flight-tube
X, Y	-1920 / -2080	50.1, 47.3	X & Y deflectors to steer beam
Reflect	-300 / -300	50.1	Reflect plate of reflectron
Retard	-900 / -1100	100.0	Used to adjust reflectron
MCP	n/a	77	Bias for the MCP detector

A second Stanford Research Systems SR350 supplied the drift-tube positive bias and has run as high as 4100 V at times. A Thurlby EL561 power supply (0-50 volts adjustable) biased the interior field-free region of the PTR-TOF-MS to counteract the incoming ion energy caused by the positive drift-tube exit voltage.

Table 3.2 Ion source and drift-tube controls and their function.

Item	Range /V	Function
Thurlby	0 - 50	Counter-bias PTR-TOF-MS typically 35 V
A	16 - 50 or 0 - 34	Bias drift-tube exit voltage
B	0 - 200	Bias of final stage of drift-tube
C	0 - 16	Switch to short A/Ground bias resistor
Drift-tube	0 - 4100	Drift-tube bias set on SR350

The output of the Stanford Research Supply SRS350 is fed to a voltage divider using a resistor chain to bias the guide rings and two potentiometers - A and B - for maintaining the drift-tube above earth potential and adjusting the focussing at the last two stages of the drift-tube (see Table 3.2, and Figure 3.2 for details). Figure 2.18 has been reproduced here as Figure 3.2 for ease of reference.

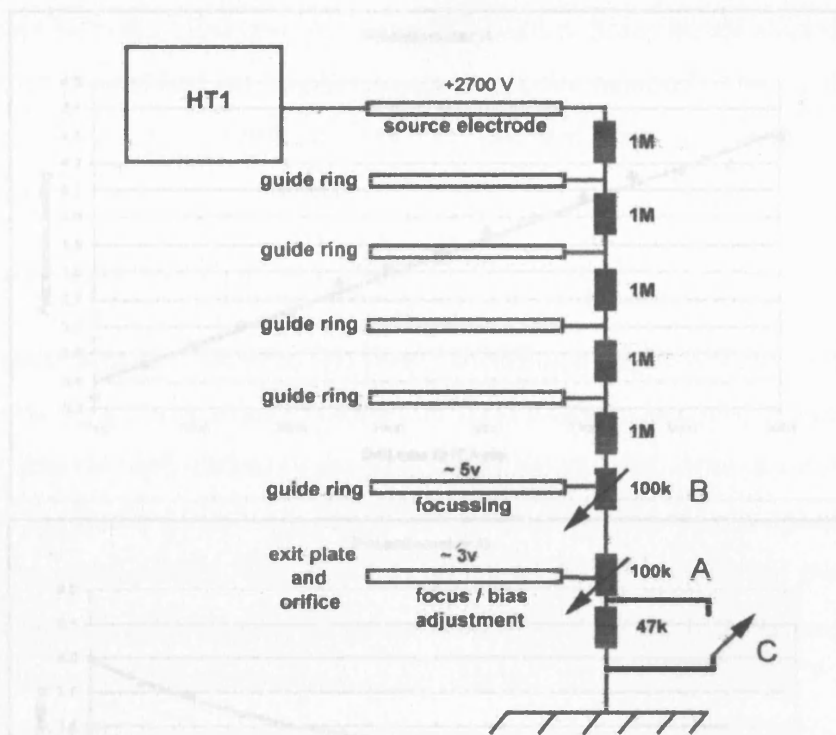


Figure 3.2 The electrical biasing configuration for operating the ion source. The resistances A and B are ten-turn variable potentiometers. This figure can also be found in Chapter 2 as Figure 2.17.

During operation, adjustments are kept at a minimum. When changes are necessary they consist of selecting an operating voltage on the SR350, in the range of 2000 – 3000 volts and then adjusting potentiometer A and the Thurlby settings to maximise the hydronium yield of the PTR-TOF-MS. Occasionally potentiometer B needed adjusting. The choice of bias settings for MCP are discussed later in Section 3.6.

3.4 Parameter optimisation to maximise the H_3O^+ count rate

The purpose of the potentiometers A and B is to modify the potential on the exit flange and the final guide ring of the ion source. The voltage on A determines the final potential of the drift-tube relative to earth, whereas B adjusts the focussing of the ion beam as in the final section of the drift-tube. Changing the electrical bias of the whole drift-tube will affect the potential distribution along the drift-tube, so that A and B may need adjustment. Hence the voltage supplied by the Thurlby supply will need readjustment.

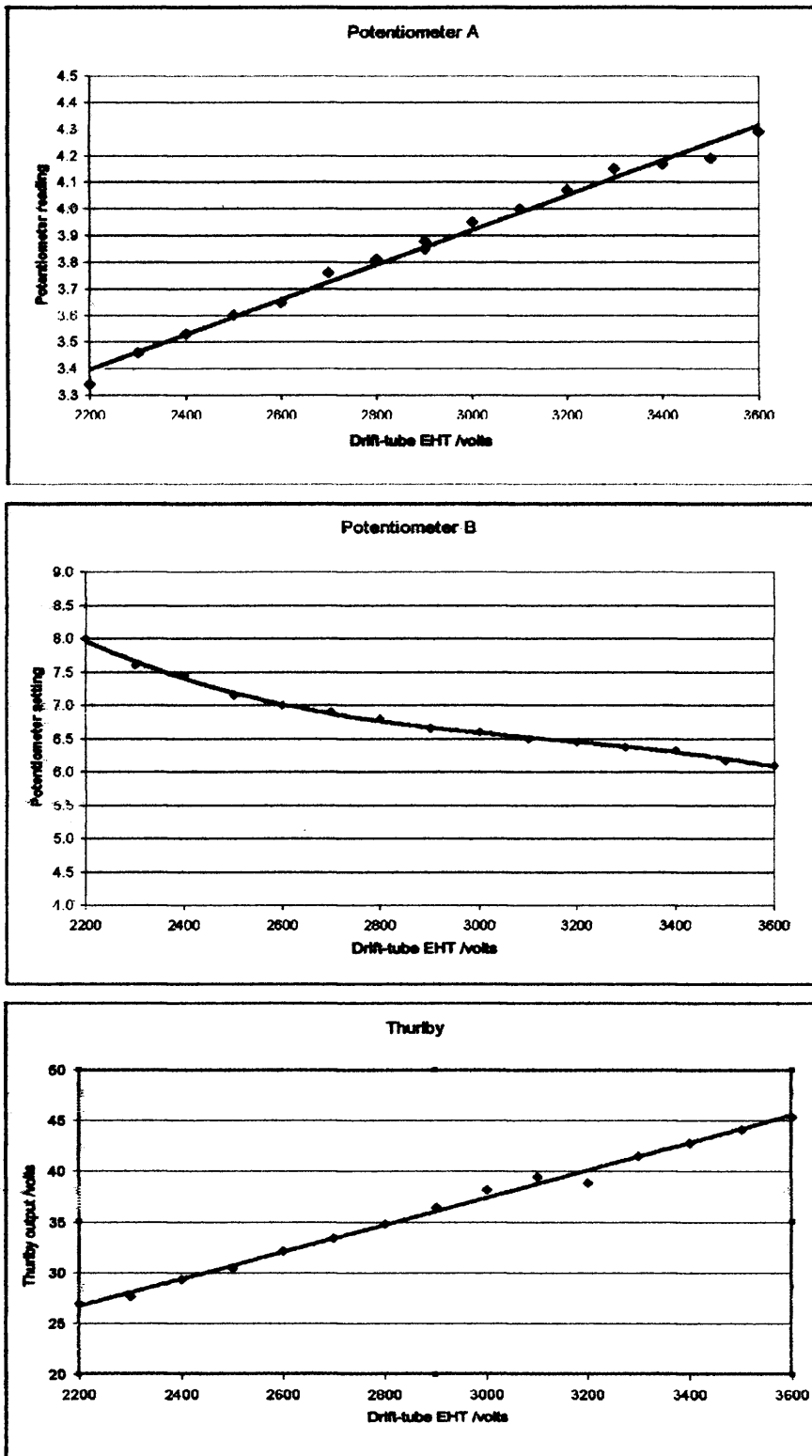


Figure 3.3 a, b & Thurlby. Settings of the potentiometers A & B and the voltage output from the Thurlby power supply to cater for different drift-tube voltages.

It is possible to produce a family of plots showing possible values of A, B and the Thurlby supply. However it was found that it was possible to narrow these down to a linked set of

values (Figures 3a, b & c) that give the best performance. Some minor alterations of one or other parameter is possible, but in practise, these are not required. The toggle switch C is always open. Closing the switch sets the exit aperture plate of the drift-tube to earth potential, a feature not currently needed.

3.5 Mass range of the PTR-TOF-MS

The data capture program, supplied by Kore Technologies, is developed as an application based on Grams AI from Galactic Systems Inc. It offered a preset selection of mass ranges, from $m/z = 100$ to 1000 Daltons (da) that could be selected from a drop-down menu. Alternatively a specific mass range could be obtained by choosing a specific ion flight-time/dead-time combination from the advanced section. The shorter the mass range selected, the greater is the number of scans the PTR-TOF-MS performs per second. The system dead-time depends on the mass range selected. It can be as low as 2 ns up to mass range 143, whereafter the system automatically increases the dead-time to 4 ns for the range of $m/z = 144 - 300$ and 8 ns for scan ranges beyond. For most work, the PTR-TOF-MS was set for a mass range of 143, which corresponds to a scan time of 66 μ s and a dead-time of 2 ns.

3.6 Microchannel plate performance

Signals from the MCP detector are fed through a preamplifier, amplified and passed on to a time to digital converter (TDC) which converts the analogue signal into a digital pulse for pulse counting. The pulses detected by the MCP are used to calculate the ions flight time in the flight-tube. The start pulse of a time sweep is initiated by the TDC and is fed to the extractor plate of the PTR-TOF-MS where it sends a group of ions on its way in the reflectron. The dead time setting of the electronics determines how soon it will be able to process another arrival.

As discussed in Chapter 2, Section 2.5.2, the output spectra showed that at a bias setting in excess of 80% of the maximum, the MCP registers a dual event for each single event. While using the lower dead time of 2ns, the system could not suppress the secondary event but by increasing the dead time to 4ns, the spurious event was suppressed. Clearly the MCP was not functioning correctly under these conditions. It was found that up to 80% of the maximum MCP bias, the phenomenon did not appear, but we were advised by KORE that

this bias setting was still excessive and could seriously affect the MCP's useful life. then The MCP bias was reduced to 77% of maximum and no recurrence of dual events has been observed since.

3.7 Apertures

The choice of optimum aperture sizes for the drift-tube exit and the bottom of the differential pumping section required extensive investigation. Clearly the larger the apertures used in the system, the greater the ion throughput. Unfortunately the PTR-TOF-MS requires a vacuum of better than 10^{-6} mbar, which places limits on the permissible drift-tube pressure and in turn limits the choice of aperture sizes.

The two apertures with the most influence on throughput and pressure differentials are situated at the exit of the drift-tube feeding into the intermediate transfer chamber and between the transfer chamber and the PTR-TOF-MS itself.

The optimum value of the drift-tube exit aperture was 200 μm . Alternative apertures with diameters of 100 and 300 μm diameter were tried. The former reduced the ion count by a factor of four, while the latter let too much gas pass so that it was necessary to reduce the drift-tube gas pressure that in turn reduced the ion count rate.

The exit aperture from the transfer chamber was 5 mm in diameter, although there was provision to narrow it down further to reduce the gas flow into the PTR-TOF-MS. It was found that when a smaller aperture was used here (3 mm and 4 mm diameter) the pressure rise in the PTR-TOF-MS was slightly improved, but the count rate of the transmitted ions dropped to about half its original value, so that it appeared the beam entering the PTR-TOF-MS is essentially unfocussed.

3.8 Drift-tube dynamics

As mentioned earlier, the formation of hydrated hydronium clusters, $\text{H}_3\text{O}^+(\text{H}_2\text{O})_n$ is a potential problem in the drift-tube. Cunningham and co-workers [Cunningham *et al.*, 1972] estimate the cluster binding energy for the monohydrate cluster to be 1.37 eV. Cluster formation can be reduced by increasing E/N . If the electric field E along the drift-tube is

increased, the average collision energy will be increased leading to H₂O molecules being dislodged from the cluster with H₃O⁺.

The mean free path of a molecule in a gas in a drift-tube is given by

$$\lambda = \frac{RT}{\sqrt{2} \pi d^2 N} \quad (3.1)$$

Where λ is the mean free path of a molecule with notional diameter d travelling in a gas at pressure P and temperature T . In addition R and N are respectively the gas constant and number density of molecules. If we consider the situation of a drift-tube in which the gas pressure P is 8 mbar and the molecular diameter d is 3.0 Å, the mean free path of a molecule is 1.6×10^6 cm. In its journey along a 10 cm drift-tube a hydronium ion, and any other heavier one as well, will undergo 6.25×10^6 collisions and under these conditions it quickly reaches a terminal velocity. The energy acquired after several collision will be sufficient to fragment any ion clusters and De Gouw [de Gouw *et al.*, 2003a] has proposed techniques to estimate the distribution of cluster ions in a drift-tube.

When moving under the influence of an electric field an ion with mobility μ attains terminal velocity

$$v_d = \mu E \quad (3.2)$$

where E is the electric field in $V\text{ cm}^{-1}$ while μ , the mobility of the ion is in $\text{cm}^2\text{ V}^{-1}\text{ s}^{-1}$. The mobility μ is related to the reduced mobility μ_0 , the mobility at NTP, by the relation

$$\mu_0 = \left(\frac{P}{P_0} \right) \left(\frac{T_0}{T} \right) \cdot \mu \quad (3.3)$$

which is equivalent to

$$\mu_0 = \left(\frac{N}{N_0} \right) \cdot \mu \quad (3.4)$$

from which it follows that

$$v_d = \mu_0 N_0 \left(\frac{E}{N} \right) \quad (3.5)$$

Extensive data on the reduced mobilities of ions have been published by Dotan [Dotan *et al.*, 1976]. From the above expressions the terminal velocity of an ion can be calculated as well as the average energy it contributes to a collision.

The collision rate with clusters is proportional to the density N of target molecules in the drift-tube so that the ratio E/N can be used as quantity for determining both the extent of clustering and ion fragmentation characteristics. For convenience, values of E/N are expressed in Townsends (Td), one Td being equal to 10^{-17} V cm². The range of E/N favoured for most PTR-MS work is usually between 120 and 150 Td.

Molecules of the sample gas, which act as the carrier of the analyte, are responsible for most of the collisions with the hydronium ions. In the centre-of-mass frame the kinetic energy involved when a hydronium ion travels at velocity v_d is given by

$$\text{KE}_{\text{cm}} = \frac{1}{2} m_s v_d^2 + \frac{3}{2} k_B T = \frac{3}{2} k_B T_{\text{eff}} \quad (3.6)$$

where k_B is Boltzmann's constant and T_{eff} represents the energy or "effective temperature" of the collision. A simple program was produced to enable rapid evaluation of the centre of mass energies involved in a reaction, It takes account of the operating conditions of the PTR-TOF-MS. In the environment in which the PTR-TOF-MS operates, the kinetic energy term is typically of the order of 0.3 eV while the thermal energy term is 0.03 eV. DeGouw [de Gouw *et al.*, 2003a] mentions that in a limited number of cases, the effective temperature describes the internal energy of the ion reactants. Referring to work by Lau [Lau *et al.*, 1982] to measure the equilibrium constants of the hydronium/water association/dissociation, they showed that for E/N values above 120 most hydronium clusters are effectively eliminated. Warneke [Warneke *et al.*, 2003] had further comments on the degree to which theory and experiment agreed, but for regions of E/N greater than 120 Td interference from clusters could be expected to be small.

3.9 Effect of humidity in the sample gas

This explanatory section is intended to serve as an introduction to the next stage of the characterisation of the PTR-TOF-MS, namely to examine the significance of hydronium

cluster formation and its influence on the choice for the working environment on the PTR-TOF-MS

Several experiments were performed on different occasions to explore the influence on cluster formation of humidity present in the sample gas. In particular it was important to examine the effect of humidity on the distribution of $\text{H}_3\text{O}^+(\text{H}_2\text{O})_n$ for $n = 0, 1, 2$ or higher in order to select the ideal E/N when operating. Initially saturated water vapour is fed into the ion source, which contributes to the water vapour loading of the system as a whole. Then in addition, the sample gas, if drawn from the atmosphere in the field, will contain an unpredictable quantity of water, which can result in seriously increased cluster formation. Two types of experiment were carried out. The first was to get an idea of the degree cluster formation can play under typical operating conditions. The second set of experiments were designed to show the effects of varying relative humidity of the sample gas on cluster formation, to help establish in what range of E/N cluster formation could be kept less than 20%.

3.9.1 Cluster formation as a function of E/N

This experiment's aim was to examine cluster formation with varying E/N .

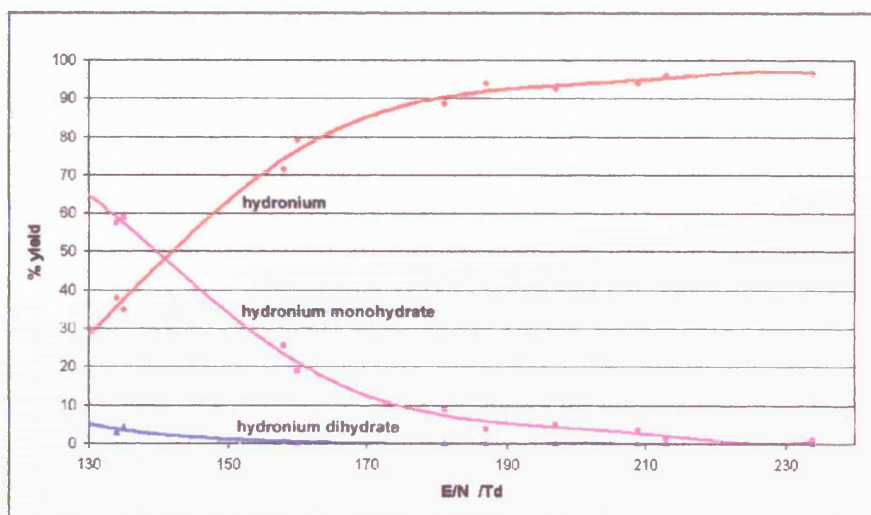


Figure 3.4 Relative population of hydronium and hydrate clusters for an E/N range of 130 to 230 Td. The humidity level was high to emphasise clustering behaviour.

The relative humidity was kept constant and relatively high (60% at 23 °C), while E/N was varied by changing the drift-tube pressure (N) or the electric field (E) so E/N ranged from

130 to 235 Td. The results are depicted in Figure 3.4 where it was found that the presence dihydrate of hydronium was small throughout the range, but the monohydrate became significant below 160 Td.

Initially the PTR-TOF-MS was run at 190 Td although this was lowered to 170 Td when it was realised that excessive ion fragmentation was occurring. Improvements in the voltage gradient resulted in a new set of results (Section 3.9.2) with smaller contributions from cluster formation.

3.9.2 Varying the sample humidity

The next set of experiments set out to investigate the effect of sample moisture conditions such as could be encountered outside the controlled laboratory environment.

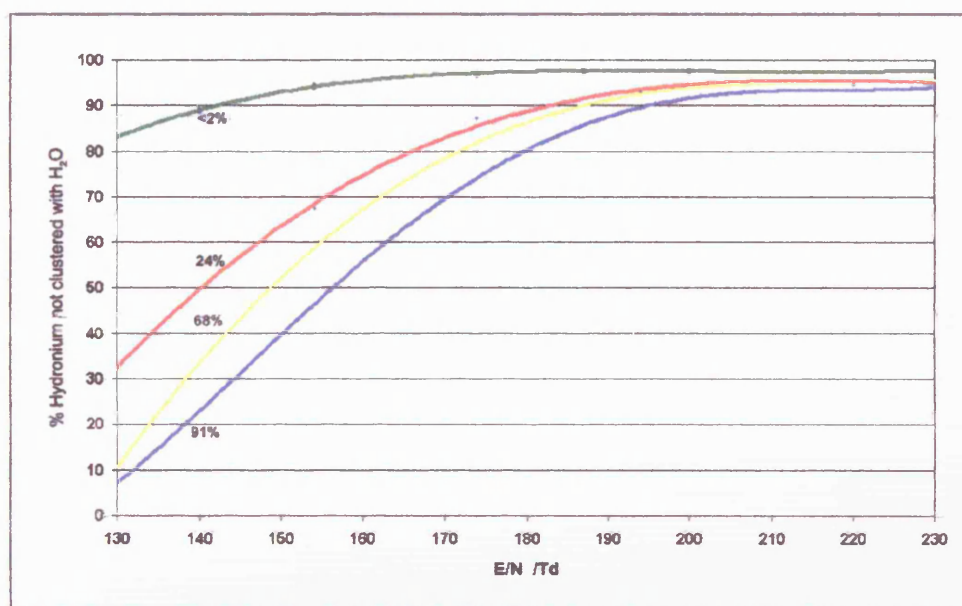


Figure 3.5 Variation in the percentage of hydronium ions not forming clusters with H_2O compared to the total hydronium yield for a range of E/N . The curves show the effects of a range of relative humidity in the sample gas, ranging from less than 2% to 91%.

The relative humidity of the sample gas was measured with a General Eastern model 1311DR chilled mirror sensor feeding into a General Eastern Hygro M4 Dewpoint Monitor. For each sample type, mass spectra were taken for a range of E/N values from 130

to 230 Td. In Figures 3.5 and 3.6 the effect of relative humidity on the percentage population of non-hydrated hydronium is shown.

The extreme example where the relative humidity was 91% is not expected to occur in practice. Now that the drift-tube and inlet lines are heated up to 40 °C to remain above ambient, this situation is unlikely to recur.

It was decided to try to work at the lower value of E/N , 150 Td, to bring the system closer into line with other workers in the field and a new investigation was started.

A new set of experiments was performed in less detail after it was found that the voltage gradient on the drift-tube was not constant and it was important to see what the effect would be once this was rectified. Care was taken to ensure that E/N was the same for all the stages of the drift-tube. No attempt was made to produce ultra-dry air. When these experiments were carried out, it had already been established that the PTR-TOF-MS was sensitive to changes in the ambient temperature, and modifications were applied to ensure that the drift-tube and the inlet tubes were kept at a controlled 40 °C.

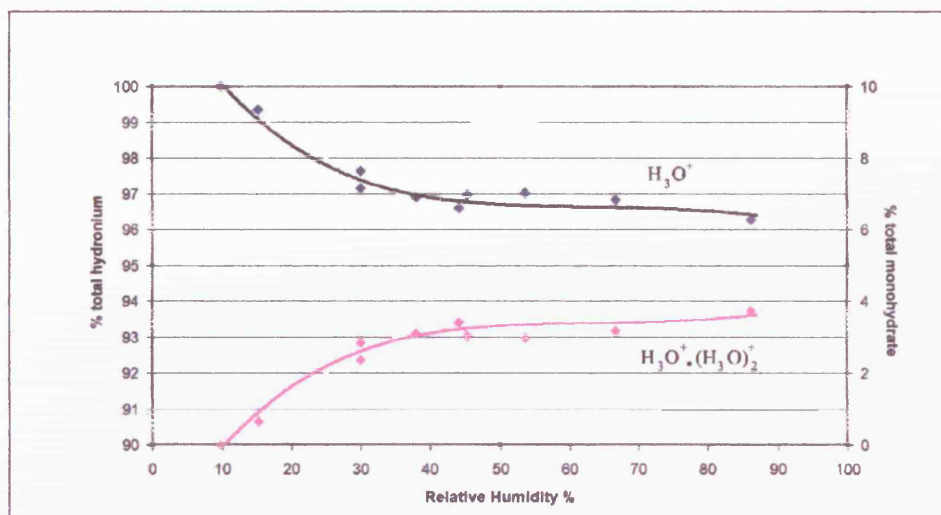


Figure 3.6 Percentage of H_3O^+ and $H_3O^+(H_2O)_n$ at varying relative humidity and at an E/N of 150 Td.

Water vapour samples with dewpoints measured in the range of 0 to 37 °C were taken from the headspace of a flask that was cooled or heated on an electric heating mantle as required. From Figure 3.6 it can be seen that cluster formation is now lower than that previously observed, so that it is feasible to operate at an E/N of 150 Td or possibly even lower. De Gouw [de Gouw *et al.*, 2003b] achieved even greater cluster suppression where the presence of hydronium clusters at 120 Td were all but eliminated. The effect on reactions of the 4% contribution from the hydronium monohydrate observed in the second set of experiments is insignificant.

The design of the ion source does allow the migration of a larger amount of water vapour into the drift-tube compared to the hollow cathode designs widely used in PTR-MS devices, so that it is necessary to operate at slightly higher values of E/N . So, for example the PTR-TOF-MS is run at 150 Td instead of 120 Td which is favoured by other groups. However, it is possible to do useful science under these conditions, and there is always the possibility of lowering the working E/N in the future. Changing the working E/N is simple, but the amount of recalibration, sensitivity measurements and fragmentation determination, makes it a non-trivial undertaking.

3.10 Operating stability and temperature effects

A small temperature dependence of the hydronium yield was observed in a series of experiments lasting several weeks. The yield was found to decrease by 2.5% for every 10°C rise in operating temperature.

The 24 hour stability of the hydronium count rate is shown in Figure 3.7. The operating temperature of the equipment was maintained at the laboratory temperature of 23 °C throughout. The output of the ion source remains constant to within 2% providing there is no change in the operating temperature of the drift-tube.

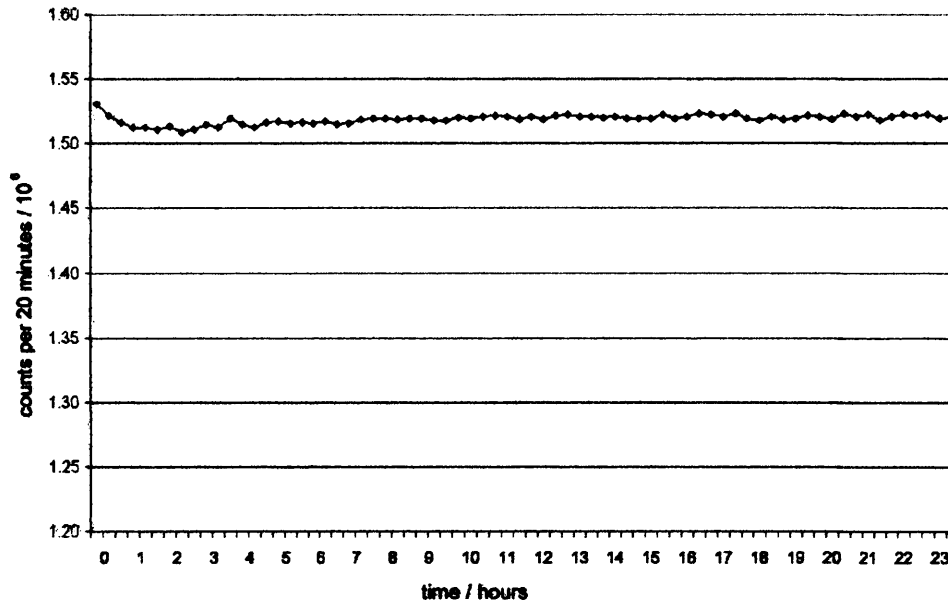


Figure 3.7 The hydronium yield at constant temperature exhibits good long term stability. This example was taken over a period of 24 hours. The first few points were measured before the drift-tube had stabilised at 40 ° C.

If the drift-tube temperature is raised hydronium count rate will be affected by the change of the gas density in the drift-tube. At first sight this is in contradiction of the prediction of the Arrhenius Equation, that the count rate should rise, but since the prime source of ions is a radioactive source which is not affected by changes in temperature, this does not apply. In effect, with a rise in the temperature in the ion source, the density of the target water molecules drops for a given pressure, so the target for the alpha particles is correspondingly reduced.

It could be argued that when an α -particle loses all its energy in the nitrogen/water gas, the total ion production should be the same, no matter what the gas density is in the ion source. At normal atmospheric pressure, α -particles like those emitted by the ^{241}Am source (5 MeV) have a range of 3 cm but this range is inversely proportional to the gas density. The range of an α -particle in the ion source with a gas pressure of approximately 8 mb, is closer to 375cm, and in traversing the diameter of the ion source it will only lose a portion of its initial energy. Furthermore, its total energy loss until it is absorbed by the walls of the ion source, is governed by the number of collisions it undergoes on the way. Since all the better known α -particle sources emit their particles in this energy range and beta particles have a far lower energy loss rate, dE/dx , there are few other alternatives to choose from.

So, the next step was to determine the size of this effect experimentally. Since hydronium production is dependent on the number density of water molecules in the ion source, it is reasonable to expect the hydronium production rate to fall when retaining a constant drift-tube pressure and increasing the temperature.

The hydronium count rate was found to fall as predicted, as the drift-tube temperature was raised from 25°C to 40 °C (Figure 3.8). The calculated count rate decrease based on the application of the ideal gas equation which could be expected for the same temperature rise is plotted in red in the same figure.

While the sensitivity of the PTR-TOF-MS instrument was found to be affected by large ambient temperature changes, the actual changes observed in the field are larger than can be explained by the observed change in sample gas temperature alone.

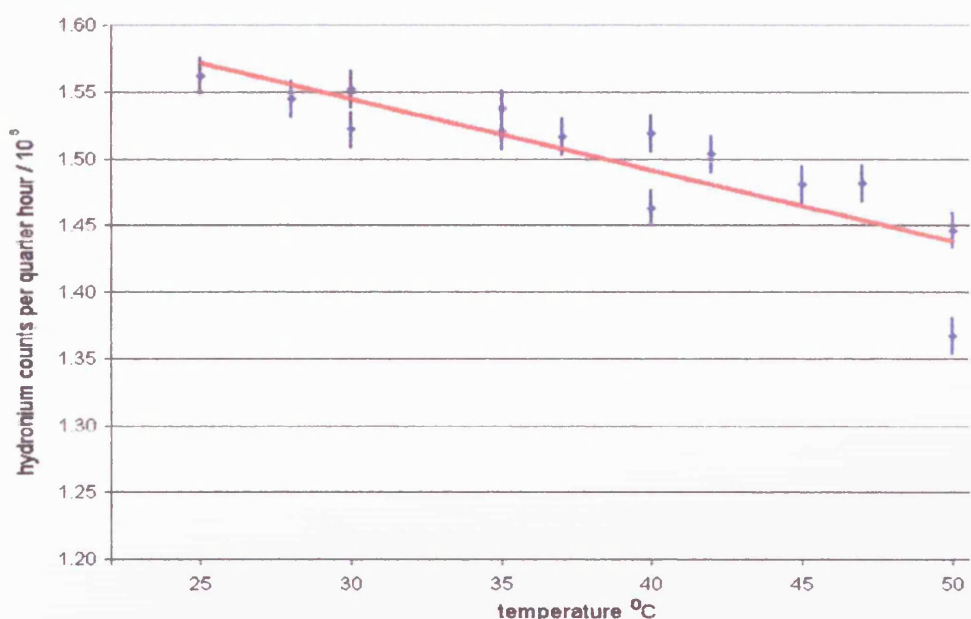


Figure 3.8 The hydronium count rate depends on the prevailing temperature in the drift-tube and falls as the number of sample molecules decrease with rising temperature. The red curve is not a fit of the data but rather a curve proportional to the particle density in the drift-tube.

Figure 3.9 illustrates a situation where the intensity of a methanol peak was measured over a period of four weeks. In the lower panel the outside temperature over the same period is

shown. There is a clear cyclic strong cyclical effect on the count rate observed in the PTR-TOF-MS instrument. The peak intensity exhibits far greater swings than can be accounted for by the difference in temperature alone. The most likely reason is the daily variation in the tropospheric hydrocarbon loading, but other possibilities should also be considered.

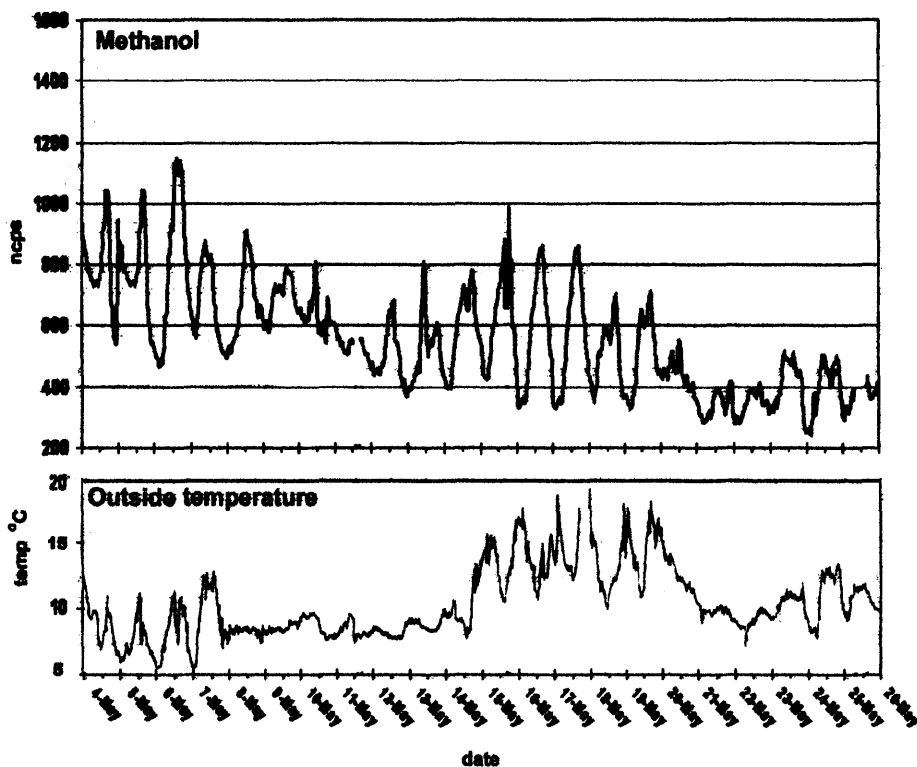


Figure 3.9 Yield variations were observed in conditions of large swings in ambient temperature.

An alternative possible explanation for these large swings in sensitivity could be the result of temperature-dependent drifts in components of the voltage divider chains, which regulate the operation of the PTR-TOF-MS. Such fluctuations would cause variations in the ion trajectories through the PTR-TOF-MS. The manufacturers, KORE Technology, confirmed that a preferred, more stable and far more expensive option would have been to use separate power supplies for each ion optic element.

In addition to sensitivity changes, the apparent ion flight-times also changed, but fortunately these time shifts could be corrected with post-processing software. The time

shifts were generally found to be temperature-related but occasionally they occurred spontaneously. It is now practice to collect data using one-minute scans, so that time shifts can be detected and corrected.

In temperature-controlled environments sensitivity changes were not observed. As a consequence of the temperature effect, it was decided to ensure that the gas inlet lines and the drift-tube would be maintained at a constant 40 °C. This temperature was chosen partly because it is higher than any ambient temperature the PTR-TOF-MS instrument is ever likely to encounter. In addition, a reasonably higher temperature helps to avoid sample condensation on the walls of the inlet lines and the drift-tube.

Each inlet line was twinned with a two metre length of silicone rubber coated heating wire and encased in a silicone-rubber sheath material. A one metre length of the same wire was wound round the drift-tube. The wires were powered by DC switched power supplies and the temperature controlled with Cal 9300 RID temperature controllers. Normally the equilibrium temperature was reached within ten minutes.

Some temperature dependence was still observed even after the addition of a temperature stabilised system, and the swings in performance were about ±5% for the duration of the campaign (Section 5.5, Chapter 5) and only 2% during the data acquisition periods. A more stable performance requires operating the instrument in a temperature controlled laboratory.

3.11 Drift-tube pressure

The pressure in the drift-tube is monitored by a Pirani gauge. Normally the accuracy of these devices in the region of 5 – 20 mbar is at best 20%. In order to determine E/N accurately, it is necessary to use a previously calibrated gauge. The calibration of the Pirani gauge involved two steps. Firstly, a baratron (Chell CPD1-A) pressure transducer was used for initial calibration which yielded the following relation:

$$P_{\text{pirani}} = 1.09 \times P_{\text{baratron}} + 0.64 \quad (3.7)$$

The second step was to calibrate the baratron against an instrument which provided absolute pressure readings. A McCloud gauge provides absolute pressure readings. It is not feasible to connect it to the PTR-TOF-MS permanently, as it would be difficult to operate

with the high voltages surrounding the drift-tube, so it was used to calibrate the baratron instead. Once calibrated, the baratron could be used to calibrate any Pirani gauge before it is taken into service.

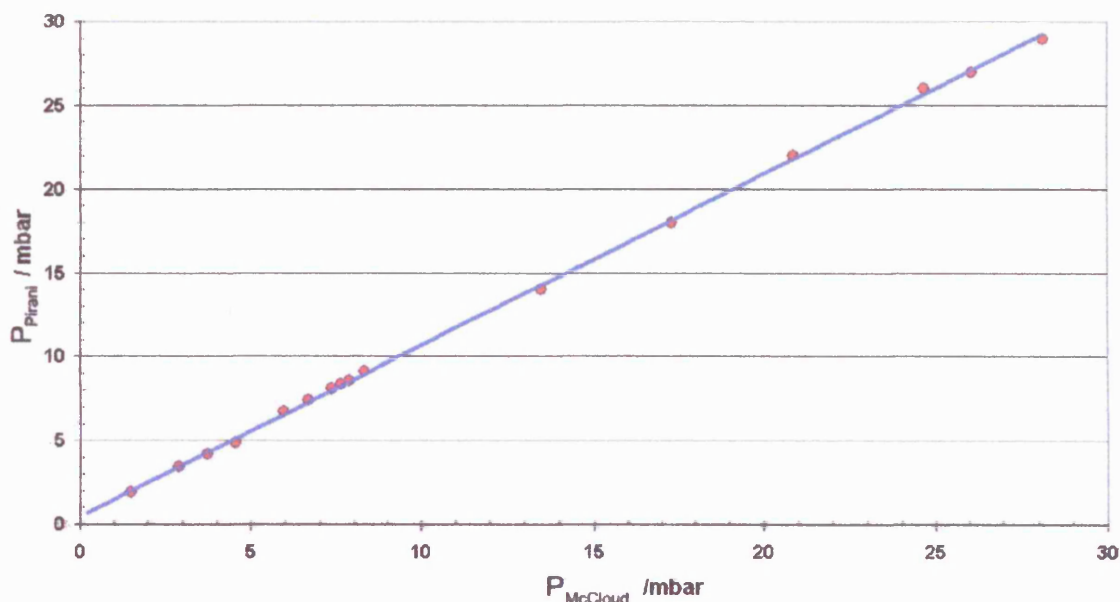


Figure 3.10 Plot of the pressure as measured by the Pirani gauge used on the PTR-TOF-MS versus the pressure as measured using a McCloud gauge.

Having calibrated the baratron against the McCloud gauge, the Pirani/baratron calibration figures were updated to take account of the McCloud/baratron results. The resulting P_{pirani} vs P_{McCloud} plot is shown in Figure 3.10. The resulting relationship between the Pirani gauge and the readings of the McCloud gauge were

$$P_{\text{pirani}} = 1.02 P_{\text{McCloud}} + 0.48 \quad (3.8)$$

As a consequence the pressure reading of 8.5 mbar on the Pirani which is the normal operating pressure of the drift-tube, is in fact 7.9 mb or 7% lower than first believed.

3.12 Determining the sensitivity of the PTR-TOF-MS

In order to be useful in the field, it is necessary to know the sensitivity of the PTR-TOF-MS for those species it is likely to detect. The starting point for determining the sensitivity of the equipment was to obtain gas samples of known concentration.

Several attempts were made to manufacture standards by leaking the vapour of an analyte into an evacuated vessel until the pressure inside reached a few millibars, then filling it with nitrogen to bring it up to atmospheric pressure, thereby effecting a first stage dilution. For several cycles thereafter the vessel is partially evacuated and refilled with N₂, each cycle reducing the concentration of the analyte in the mixture. Several attempts were made to produce a sufficiently dilute standard mixture by this procedure. However this multiple dilution technique produced erratic results especially for dilutions less than 100 ppmv. The problem with the dilution apparatus was persistent leaks in the gas canister and the associated pipe-work, which become significant over the several days required to produce a sufficiently dilute mixture.

An alternative approach was to use commercial standards with known composition. These are expensive and need to be selected with care to ensure that interference between species are minimised. There are certain classes of hydrocarbons such as the alkanes that a PTR-TOF-MS is unable to detect, because they are reluctant to accept protons from hydronium.

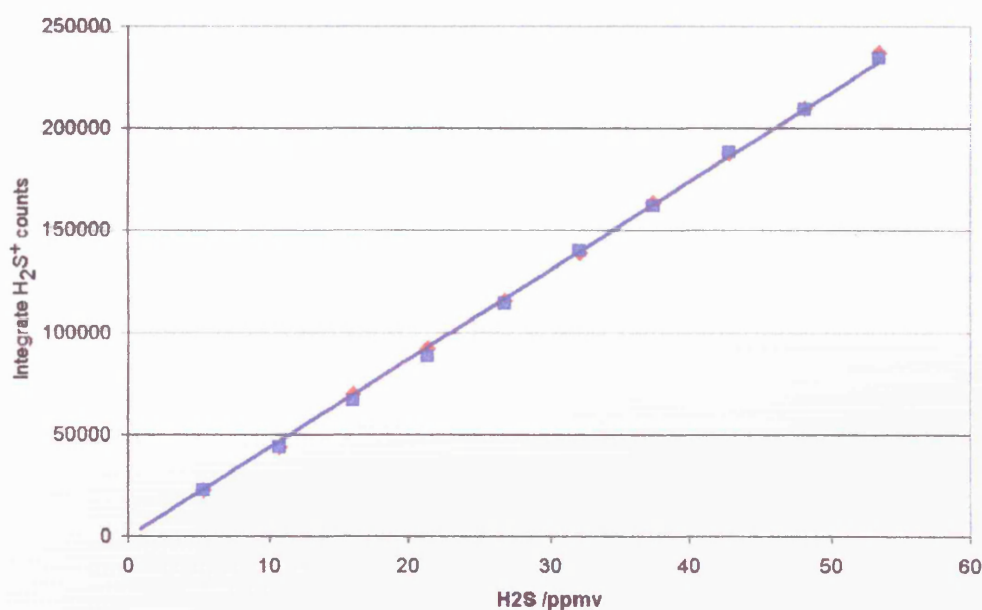


Figure 3.11 H₂S calibration results showing the excellent linear response in nitrogen (●) and zero air (■) carrier gases.

In the first attempt at measuring the sensitivity of the instrument, a 53.47 ppmv H₂S (BOC α -spectra seal) mixture was used. The mixture was supplied by Horiba (UK). A commercial diluter (also supplied by Horiba) was used to vary the output concentration of H₂S down to 5.35 ppmv.

Experiments with a series of dilutions showed a linear response from the PTR-TOF-MS (Figure 3.11) for the reaction



From the slope the sensitivity was found to be 4.4 counts per ppbv at an E/N of 180 Td.

The experiments were carried out with BOC BTCA 178 zero-air air as well as BOC zero-grade nitrogen (99.99% pure) to check if the measurements using the air differed from those obtained with nitrogen. The data measured showed that there was no measurable effect from changing gases.

More recently a standard of 1-butene (1 ppmv in Nitrogen) was used to test the linearity of the PTR-TOF-MS using a variety of Chemical Ionisation (CI) reagents: H_3O^+ , NO^+ and O_2^+ . A gas diluter consisting of two calibrated mass flow controllers with 100 sccm and 5 slpm (5000 sccm) capacity respectively were coupled to give a common output section. Nitrogen gas (BOC zero-grade) was fed into the larger mass flow controller while the rate of the 1-butene flow was controlled by the other.

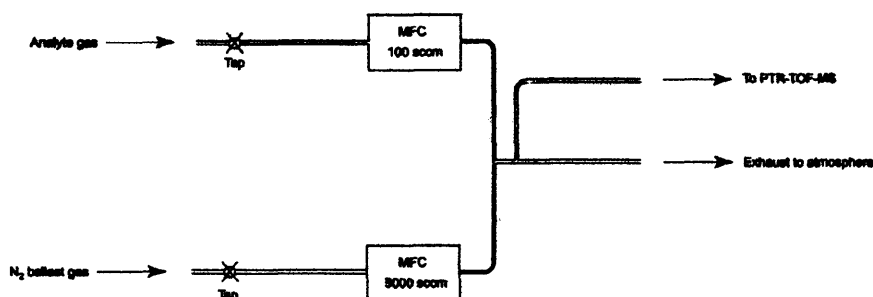


Figure 3.12 Schematic of the gas mixture diluter.

The two outputs were joined and a sample for the input into the PTR-TOF-MS was taken before the rest of the gas was exhausted into the atmosphere. The mass flow controllers were calibrated by timing the flow of known volumes of N_2 . These were carried out immediately prior to the construction of the diluter and found to be linear in agreement with the manufacturer's 2% specification.

Table 3.3 Typical dilution rates using a diluter. Certain values of the final analyte concentration can be obtained by more than one combination of the mass flow controller settings.

Analyte flow sccm	MFC 1 % maximum	Diluent (N ₂) flow sccm	MFC 2 % maximum	Dilution factor	Analyte conc. ppbv
100	100	0	0	0	1000.0
100	100	500	10	6	166.7
50	50	500	10	11	90.9
100	100	2500	50	26	38.5
100	100	5000	100	51	19.6
50	50	2500	50	51	9.9
10	10	500	10	51	19.6
50	50	5000	100	101	9.9
5	5	500	10	101	9.9
10	10	2500	50	251	4.0
10	10	5000	100	501	2.0
5	5	2500	50	501	2.0
5	5	5000	100	1001	1.0

With the 5 slpm mass flow controller fully open and the smaller one at 5% of maximum capacity (5 sccm) a dilution factor of up to 1:1000 could be obtained. Since the PTR-TOF-MS required an input flow of 275 sccm, the flow of N₂ through the diluter was not reduced to below 500 sccm. So with the 1-butene standard a mixture range of 1 to 100 ppbv was available, in addition to the 1ppmv concentration obtained by using the undiluted standard mixture. Some typical settings are shown in Table 3.3.

The total detection sensitivity of the PTR-TOF-MS for 1-butene for is 12.1 ncps ppbv⁻¹ and the partial sensitivity when using the peak at 57 amu is 6.1 ncps ppbv⁻¹. So it is not an ideal test gas, especially at low concentrations, where it was found there was interference from contamination. The useful limit of detection was in the region of 2 ppbv at which point the errors in the measurement exceeded the accuracy of the measurement.

The dilution curve using H₃O⁺ was based on the protonated 1-butene peak at 57 da, and in case of O₂⁺ the $m/z = 56$ peak was used. For the NO⁺ data, the peak due to the associated complex C₄H₈.NO⁺ at $m/z = 86$ was chosen. In order to arrive at a figure for the sensitivity of the PTR-TOF-MS it is necessary to know the fragmentation behaviour of product ion

for 1-butene at the E/N used in the experiment for each CI reagent. At 150 Td 1-butene exhibits fragmentation and has significant contributions at $m/z = 57$ (53 % $M+H^+$), $m/z = 41$ (35% $(M-CH_3)^+$) and $m/z = 39$ (12% $C_3H_3^+$). The results obtained using any of these peaks were inconsistent and indicative of serious interference from other sources. The only peak which behaved as expected was that of $C_4H_8.NO^+$ at $m/z = 86$.

Table 3.4 Sensitivity for detection of 1-butene using H_3O^+ , NO^+ and O_2^+ as reagents.

Reagent	Ncps ppbv ⁻¹
H_3O^+	6.5
NO^+	5.9
O_2^+	7.7

The slope of the diluter plot using the $m/z = 57$ peak was 6.4 ncps ppbv⁻¹, and since the peak used accounts for 53% of the total counts the actual sensitivity for detection of 1-butene is $6.4 \cdot 100/53 = 12.1$ ncps/ppbv.

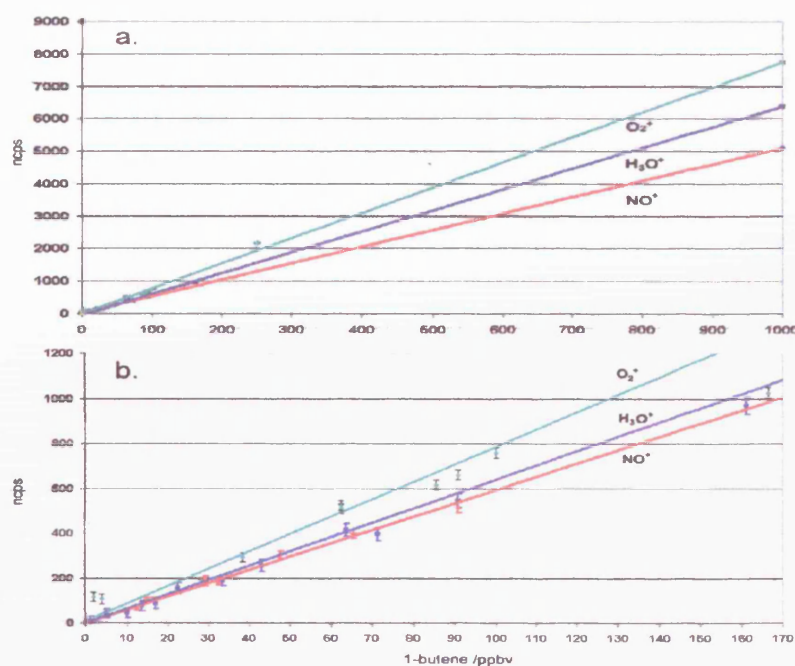


Figure 3.13 1-butene sensitivity plots. The top plot (a) shows the full range of dilutions used, while (b) shows the lower end of the plots in more detail.

3.13 Background estimation

Most spectra contain unwanted contributions from other sources, such as contamination in the system or the analyte sample. Sometimes it is sufficient to perform background runs in which the carrier gas (usually N₂) containing an analyte is replaced by the carrier gas alone, in the hope that this will only contain structure from system impurities and the impurities in the sample gas.

When using a diluter, a background signal can be derived from plotting the observed counts against the dilution and producing a trend line of the form

$$Y = aX + b \quad (3.9)$$

to obtain the best straight line fit to the points. Here Y is the observed counts at the peak and b the offset from the origin of the graph. The background contribution is given by the value of b . If there were no interference, b would be zero and the curves would pass through the origin of the graph. The statistical error is given by

$$\delta Y = \sqrt{Y + b} \quad (3.10)$$

Where the background is large, the error term can approach the actual count in size, which limits the low end sensitivity. One way to resolve the problem would be to increase the acquisition time, so that the statistical error is reduced. In the case where the 1-butene was diluted to 1 ppbv, the limited supply of 1 ppmv gas remaining, did not allow this option, so that the lowest dilution for which a valid data point was obtained was at 2 ppbv.

3.14 Fragmentation determination

3.14.1 Principles

Highly exothermic reactions enhance the tendency of analytes to fragment as shown in Figure 3.14 for toluene. Fragmentation can give information about the internal structure of molecules.

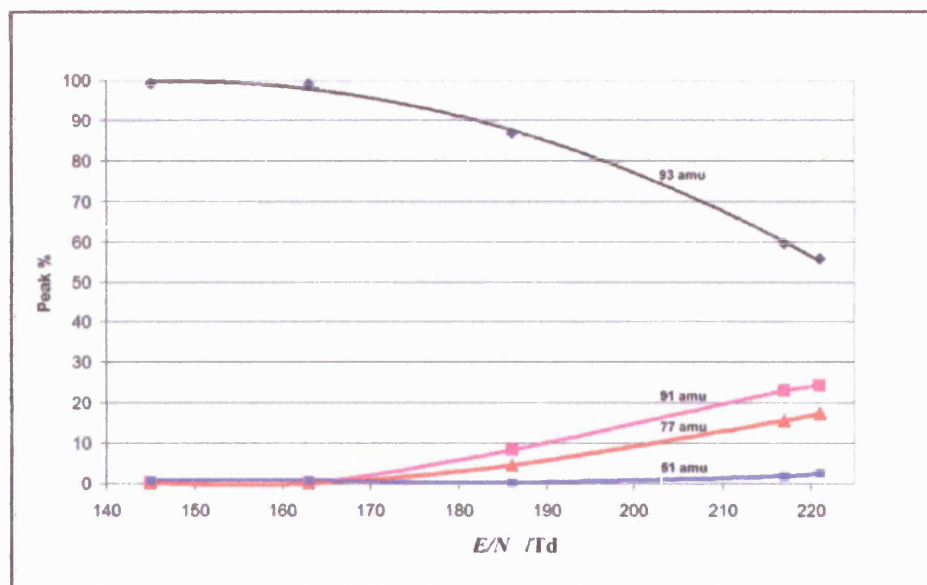


Figure 3.14 For values of E/N below 160 Td toluene shows little tendency to fragment.

In the PTR-TOF-MS, the count rate $[RH^+]$ resulting from a CI reagent X^+ reacting with an analyte with concentration $[R]$ can be calculated from the pseudo first-order equation

$$[RH^+] = kt [X^+].[R] \quad (3.11)$$

where $[X^+] \gg [R]$ and $kt[R] < 1$. Here $[R]$ is the concentration of the trace substance, $[X^+]$ and $[RH^+]$ are equivalent to the observed count rates of the reagent and analyte, k is the reaction rate coefficient and the time t the reactants drift time in the drift-tube. If the concentration of $[R]$ (and $[RH^+]$) rises, the pseudo first order conditions described earlier in this paragraph, will no longer apply and product yield calculations can no longer be accurately described by Equation 3.11.

If one expresses the yields of peaks in a spectrum $[R_x^+]$ as ratios of another prominent peak $[R_{ref}^+]$ as a reference, when $[R_{ref}^+]$ decreases with time the observed values of the $[R_x^+]$ can be expressed

$$[R_x^+] = a[R_{ref}^+] + b \quad (3.12)$$

The values of the slope a and the intercept b describe the relationship between $[R_x^+]$ and $[R_{ref}^+]$. The values for a and b can be obtained graphically from a series of spectra in which

the analyte concentration [R] decreases with time. In the relation above the slope a is the relative intensity of two peaks. Here

$$b = b_{\text{Rref}} - b_{\text{Rx}} \quad (3.13)$$

is due to the background which can have contributions from either peak. Branching ratios extracted using this correlation method agreed well with the traditional approach in which estimates of background contributions are subtracted prior to any further processing.

3.14.2 Calibration and fragmentation

For calibration purposes it is not necessary to know the fragmentation behaviour of an ion, given that the concentration of the analyte is known, and the trace of the analyte has a well defined peak which can be used to determine a calibration factor.

On the other hand, when trying to calculate the sensitivity of the PTR-TOF-MS to detect an analyte, or the rate coefficient for the reaction, it is necessary to determine the total yield of a reaction. Frequently an ion will fragment in such a way that some of the fragmentation products are obscured by other peaks. If the data is used to calculate rate coefficients, it is necessary that the contribution from all the reaction products be known. Similarly, when no calibration standard is available, and it is necessary to calculate the yield, then a knowledge of the fragmentation behaviour of the analyte is essential.

3.14.3 Headspace dilution experiments

When running at $E/N = 150$ Td, many analytes will fragment after a collision with a hydronium ion and produce several daughter fragments. If the main aim of an experiment is to determine sensitivity as well as the rate coefficient of the reaction, then it is necessary to take into account all the fragmentation products occurring (Equation 3.11). It is difficult to detect fragmentation products below 32 da, because of the presence of large peaks arising from hydronium, NO^+ and O_2^+ , and their isotope companion peaks.

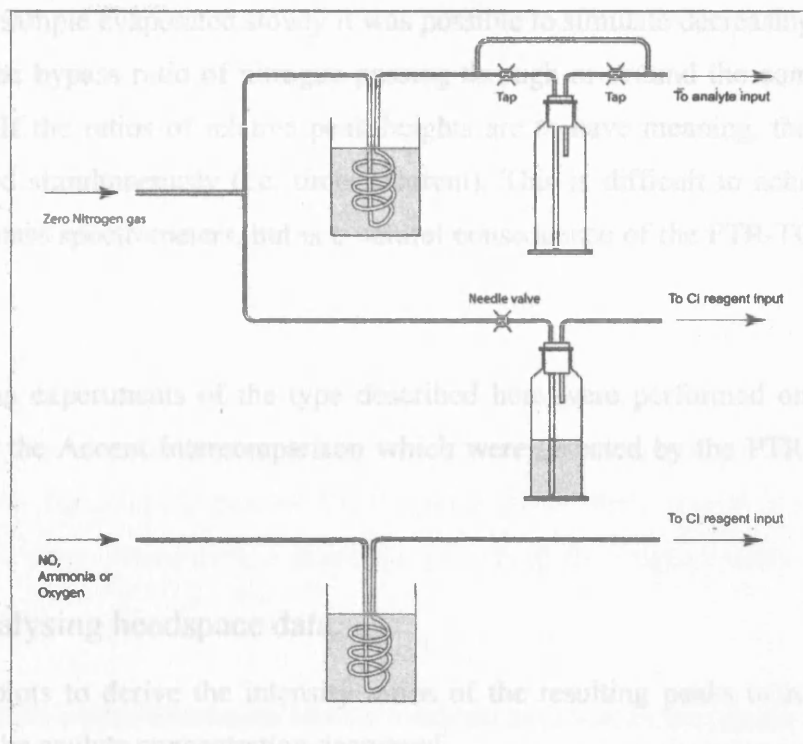


Figure 3.15 Equipment for running headspace experiments. The flask can be isolated from the stream of N_2 when changing analytes, to minimise introducing outside air into the system.

If on the other hand, the main aim of the experiment is to derive a figure that can be used to measure the detection sensitivity of the PTR-TOF-MS for a particular analyte, then it is only necessary for an analyte to produce at least one prominent peak to use as a reference. The experiments described here have this aim in mind and a simple way to obtain a sample for analysis is to use a dilute mixture of its headspace vapour.

Samples of analyte were introduced into a Dreschell flask. The headspace vapour from the analyte was flushed out with a stream of zero-grade nitrogen and fed into the analyte input of the drift-tube. Initially the sample concentration was very high and all the hydronium concentration was not able to cope with the excess analyte concentration. However, once the analyte concentration dropped sufficiently the hydronium peak reappeared and once it had regained about 90% or more of its original amplitude, the experiment could commence.

A series of one-minute time scans were collected for analysis until the peak amplitude of the analyte had dropped to less than 5% of its size when the experiment started.

If an analyte sample evaporated slowly it was possible to simulate decreasing concentration by varying the bypass ratio of nitrogen passing through or around the container with the test analyte. If the ratios of relative peak heights are to have meaning, they should have been recorded simultaneously (i.e. time-coherent). This is difficult to achieve with most varieties of mass spectrometers, but is a natural consequence of the PTR-TOF-MS's mode of operation.

Fragmentation experiments of the type described here were performed on those species specified for the Accent Intercomparison which were detected by the PTR-TOF-MS (see Chapter 5).

3.14.4 Analysing headspace data

Correlation plots to derive the intensity ratios of the resulting peaks to each other were extracted as the analyte concentration decreased.

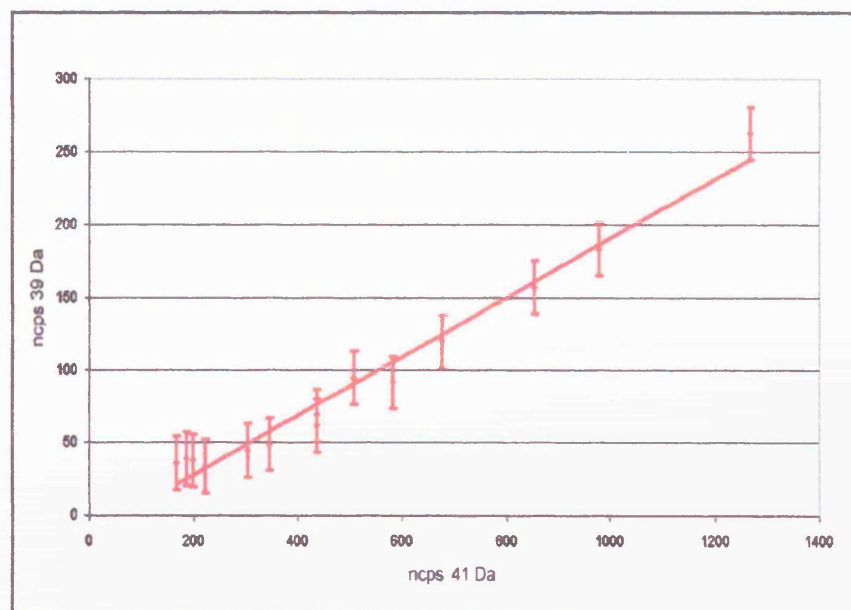


Figure 3.16 The peaks at $m/z = 39$ and 41 are groups characteristic of the fragmentation of methacrolein.

In the fragmentation experiments, the analyte concentration is very high and conditions of Equation 3.11 do not apply initially. With high analyte concentrations more complicated

processes such as self-protonation can occur. The anomalous reactions die away rapidly, and, PTR reactions start to predominate.

Once the analyte concentration falls below a few parts per million (ppmv), it is possible to examine the relationships between peaks, by plotting the intensity of one peak against that of another.

Where both peaks in a graph can be identified as originating from the same analyte and reaction type, the slope of the line will indicate the relative intensity of fragmentation of one peak with the other. When all the daughter peaks, their origins and their relative intensity have been determined, a complete picture of the fragmentation pattern can be obtained.

Where the points on the correlation plot lie either on a vertical or horizontal line, there is no correlation at all between the two peaks and one of them is due to a system contamination. In Figure 3.17 the intensity of the peak at $m/z = 31$ does not share a common origin with the peak at $m/z = 41$ and so its intensity remains constant whereas the other peak's intensity falls with increasing dilution of the analyte.

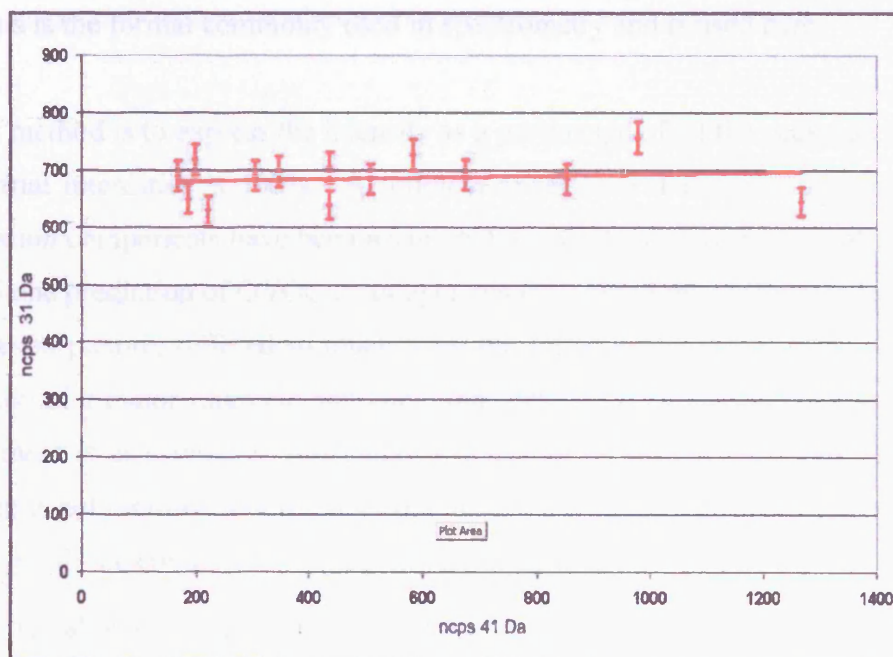


Figure 3.17 This plot compares the yields of peaks at $m/z = 31$ and 41 observed when using NO^+ as the reagent with methacrolein.

Extensive fragmentation experiments were carried out, with a number of analytes using H_3O^+ as the reagent. This work formed part of the OVOC Intercomparison campaign performed at Jülich, Germany in January 2005 (see Chapter 5).

The scope of the investigation was extended even further, this time using NO^+ , NH_4^+ and O_2^+ as reagents to see if other chemical ionisation reaction mechanisms could accentuate structural differences between isobaric twin species. Details are included the Chapters 5 and 6.

3.14.5 Fragmentation results

For the experiments described here, the drift-tube voltage was 2700 volts and the sample gas pressure was 7.9 mbar corresponding to E/N of 150 Td.

The fragmentation results obtained from the headspace experiments described in this section are shown in Appendix 1, Tables A1.3.1 and A1.3.2. There are two ways in which the results can be presented. The first way is to assign a value 100 to the most intense peak in the group, and all daughter groups' intensities are expressed as a percentage of that group. This is the format commonly used in spectrometry and is used here.

The other method is to express the intensity as a percentage of all the peaks, so that the sum of the partial intensities is 100%. A problem arises here if it is not certain that all the fragmentation components have been accounted for. Certainly, from some of the results in Chapter 5 one prediction of OVOC loading (1-butanol) based on our knowledge of the total fragmentation picture, differed so much from the actual value, that it was probable that a contribution of a major fragment had gone undetected. As mentioned before, if the aim of an experiment is determine an instrument's detection sensitivity, then total fragmentation knowledge is not required, but if one hopes to extract a value for the reaction rate, then the intensities of all the component fragments need to be known.

Appendix 1, Table A1.3.1 covers fragmentation products of the OVOCs with masses in the range $m/z = 27$ to 57, while, Table A1.3.2 contains the results for those with masses of $m/z = 59$ to 107.

The 1-butene sample was supplied as a gas and its fragmentation pattern was obtained from the diluter data. For the headspace experiments using the liquid OVOC samples the dilution method described in Section 3.14.3 was used.

In order to establish the sensitivity of the PTR-TOF-MS in terms of counts ppbv⁻¹, it was necessary to use standards of known concentration.

Table 3.5. Composition of the NPL 30 component standard mixture. Mixture consists mainly of alkanes, some alkenes and many isobaric species.

VOC/OVOC	da.	ppbv
ethyne	27	9.26
ethene	29	4.36
ethane	31	8.35
propyne	41	2.58
propene	43	4.19
propane	45	3.71
1,3-butadiene	55	5.56
1-butene	57	4.12
but-1-ene	57	4.1
trans-2-butene	57	1.39
cis-2-butene	57	2.75
n-butane	59	1.94
1-butane	59	1.23
isoprene	69	2.99
trans-2-pentane	71	4.77
cis-2-pentane	71	2.45
n-pentane	73	1.14
1-pentane	73	1.42
benzene	79	5.5
2 methyl pentane	87	1.83
3 methyl pentane	87	2.83
n-hexane	87	4.86
cyclohexane	87	3.21
toluene	93	4.25
n-heptane	101	2.47
o-xylene	107	1.42
n-xylene	107	2.16
ethylbenzene	107	1.74
124-trimethylbenzene	121	1.09
135-trimethylbenzene	121	1.28

3.14.6 Gas standards

The following standards were available:

- A National Physical Laboratory 30 component standard gas mixture, consisting mainly of alkanes and several isobaric species. A few items were useful, although there were indications that there was more than one contributor to most peaks.
- A standard mixture of 1-butene gas with a concentration of 1ppmv in nitrogen.
- 10ppmv standard of methanol in nitrogen,

Table 3.6 The standard produced by Apel-Riemer Associates for the Bristol University group and used by the Leicester group for calibration.

OVOC	Mass /da	Concentration ppbv
methanol	32	522
acetaldehyde	44	453
ethanol	46	542
acrolein	55	468
Butane	58	548
propanal	58	480
acetone	58	536
1-propanol	60	532
methacrolein	70	432
MVK	70	511
butanal	72	504
MEK	73	510
1-butanol	74	491
MBO	88	540
1-butanol	74	491
pentanal	86	481
hexanal	100	476

- A multi-OVOC standard produced by Apel Riemer Associates, Denver, USA and supplied to the University of Bristol. This mixture will be referred to as Apel/Bristol.
- The FAL (Federal Atmospheric Laboratory, Zürich) synthetic standard mixture generator which produced standards of ethanol, isoprene and acetaldehyde.

Table 3.7 OVOC concentrations of the gas mixture produced by the FAL synthetic standard generator

OVOC	Mass /da	MH+ /da	ppbv
Benzene	78	79	21.7
Toluene	92	93	10.5
Isoprene	68	69	8.9
MVK	70	71	19.2
Methacrolein	70	71	9.2
Cis-3-Hexanal	100	101	39.9
Hexanol	102	103	19.5

3.14.7 Sensitivity assignments

Despite the fragmentation which occurred for many compounds, it was possible to make unambiguous sensitivity assignments for most of the target species (see Table 1.2, Chapter 1). Several species such as benzene, toluene, benzaldehyde, acetaldehyde, and methanol showed slight or no tendency to fragment, so that it was straight forward to calculate the PTR-TOF-MS sensitivity in these cases.

Other situations were more complicated and required additional manipulation to arrive at a figure for detection sensitivity. Butanal undergoes substantial fragmentation with a prominent peak at $m/z = 55$ which overlaps with one of the major fragmentation products of hexanal. The hexanal contribution at $m/z = 55$ can be deduced from the size of its other prominent daughter at $m/z = 83$. This can be subtracted from the total size of the $m/z = 55$ peak to obtain the value of the butanal contribution.

Propanol overlaps with daughter fragments from acetaldehyde, 1-butene and pentanal at $m/z = 41$ and at $m/z = 43$ from ethyl acetate. There was no pentanal or 1-butene present in the Bristol/Apel standard, which reduced the number of overlapping components which had to be taken into account. Both the $m/z = 41$ and 43 peaks were used to calculate the sensitivity for 1-propanol, and near-identical results were derived from the examination of both peaks. Despite this good agreement, it appeared that a hidden fragmentation product resulted in the figure obtained for its sensitivity being too low.

3.14.8 Discussion of the sensitivity results

A summary of the detection sensitivities can be found in Table 3.8. A subset of these were used for OVOC assignments for the Jülich Intercomparison campaign in January 2005.

The peaks obtained from the Bristol/Apel mixture to assign the sensitivities of the PTR-TOF-MS ranged from 87000 (benzene) to 350000 (MVK and methacrolein), so that the statistical error for each peak from this source is less than 0.3%. The FAL standard runs had lower peak counts, and it was used to obtain a calibration point for toluene which had a peak of 1078 unnormalised counts. The statistical error in this point is thus 3.04%.

In ideal conditions the count rate observed for each species can be calculated using Equation 3.11. In practise it is necessary to include a quantity F into the equation to account for other factors which affect the detection efficiency of the equipment. These factors include the duty cycle of the instrument, mass-dependent efficiency factors and incomplete accounting of all the fragments created by the fragmentation of the analyte species. Gilmore and Seah [Gilmore and Seah, 2000] have discussed the detection efficiency of the microchannel plate for varying combinations of ion mass and incident energy, and there are indications of reduced detection efficiency of heavier species.

For this reason Equation 3.11 needs to be modified to

$$[RH^+] = kt [X^+].[R].F \quad (3.14)$$

where F accounts for the difference between theory and practise. The values observed for F do not follow a predictable pattern and need to be established experimentally. If a molecule fragments, some of the resulting fragments may contain overlapping groups from other

species or they may fall below the recorded mass range, and so escape detection. For example, any fragments with masses of $m/z = 19, 37, 32$ or 30 are dwarfed by large contributions from H_3O^+ , $H_3O^+ \cdot H_2O$, O_2^+ and NO^+ respectively. Normally $F < 1$, but some instances of $F > 1$ were observed, which could be due to two reasons: either the value of the reaction rate k used was incorrect, or more likely, some undetected daughter fragments were not taken into account when calculating the total number of counts per ppbv.

High values of F resulted in underestimation of 1-butanol component in the Accent OVOC Intercomparison campaign (see Chapter 5), whereas good agreement was obtained for the other OVOCs, including methyl acetate, the sensitivity was derived from the calculated yield. The 1-butanol case is interesting especially as it was the one case of the species tried, where the sensitivity was calculated in two ways and such good agreement was achieved. The only explanation is that a major fragmentation channel was hidden and thus not included.

High values of F resulted in underestimation of 1-butanol component in the Accent OVOC Intercomparison campaign (see Chapter 5), whereas good agreement was obtained for the other OVOCs, including methyl acetate, the sensitivity was derived from the calculated yield. The 1-butanol case is interesting especially as it was the one case of the species tried, where the sensitivity was calculated in two ways and such good agreement was achieved. The only explanation is that a major fragmentation channel was hidden and thus not included.

From the point of view of using the PTR-TOF-MS as a measurement device, the only requirement is that the calibration data should offer at least one well-defined group which can be made to represent a known concentration of the species. If the aim of an experiment is to derive reaction coefficients, then it would be advisable to run the PTR-TOF-MS at low values of E/N (100 Td or lower) to minimise the complications introduced by fragmentation. In fact a SIFT, which does not rely on electric fields, would be the preferred device for the task. If the main purpose of an experiment is to detect OVOC and VOC concentrations, and the characteristics of the reaction are known then the PTR-TOF-MS will perform satisfactorily.

Table 3.8 Sensitivity in ncps ppbv⁻¹ of PTR-TOF-MS to OVOCs sampled at Jülich, Germany in January 2005.

mass /da	species	k $10^{-9} \text{ cm}^3 \text{ s}^{-1}$ (2)	ppbv ⁻¹ (1)	ppbv ⁻¹ (2)	ppbv ⁻¹ (3)	Notes (4)
32	methanol	2.33	42.9	29.2	40.2	a
44	acetaldehyde	3.36	102.0	43.1	79.7	b
46	ethanol	2.26	-	29.9	-	c
58	acetone+propanal	3.00	61.5	38.5	62.6	b
60	1-propanol	2.47	68.3	31.3	62.8	b
70	MVK/methacrolein	3.83/3.53	44.9	47.5	37.4	b,d
72	butanal	3.49	50.4	59.8	42.3	b
74	methyl acetate	2.00	-	40.1	33.7	e
74	1-butanol	2.47	63.0	31.7	20.5	b
86	MBO	3.40	40.7	54.2	18.3	b
92	toluene	2.12	27.0	27.2	26.0	b
100	hexanal	3.74	18.3	48.0	19.0	b,d
106	benzaldehyde	4.12	11.8	55.0	45.1	f

The accumulation time to detect 1 ppbv of any VOC or OVOC depends on the hydronium count rate and the detection efficiency of the PTR-TOF-MS for the particular species. In Table 3.6 the range of the OVOCs measured sensitivities was found to vary from 16.1 ncps ppbv⁻¹ to 79 ncps ppbv⁻¹ for a hydronium count of 10⁶. As an example, consider the case of toluene with a detection sensitivity of 25.7 ncps ppbv⁻¹. Currently the PTR-TOF-MS operates with a hydronium count rate of about 4000 s⁻¹ so the time to register a single count at $m/z = 93$ is 9.7 seconds. Depending on the background, this could be regarded as statistically significant, but an accumulation of 5 counts would exceed the 2 (95%) level

¹ Measured sensitivity

² Calculated sensitivity using published or assumed values for the rate coefficients

³ Sensitivities reported to ACCENT for evaluation

⁴ Key to symbols:

(a)Methanol standard 10ppmv Kore Technologies; (b) Apel/Riemer standard by kind permission of the University of Bristol; (c.) Not reported; (d) FAL standard on site (e) calculated, assumed rate coefficient = $3.0 \times 10^{-9} \text{ cm}^3 \text{ s}^{-1}$; (f) calculated from published rate coefficient $4.12 \times 10^{-9} \text{ cm}^3 \text{ s}^{-1}$. Zhou, J., and R. Zhang, *Atmos. Environ.*, 38, 2177-2185, 2004.

and 9 counts would reach the 3σ level. The accumulation time required would be 1 minute for the former and less than 2 minutes for the latter.

3.15 Conclusion

In this chapter, the behaviour of the PTR-TOF-MS has been determined in sufficient detail to enable it to be operated under normal conditions such as those likely to be encountered in the UK or Europe. Detection sensitivities have been obtained for the list of target hydrocarbons which are of use in the following chapters. In the following chapters, some experimental results are presented dealing with atmospheric observation campaigns (Chapter 4) as well as the ACCENT Intercomparison campaign in which groups from several European organisations took part. Chapter 4 will cover atmospheric observations performed during the early life of the PTR-TOF-MS as well as some performed a year later, when the instrument was better understood.

Chapter 4

Laboratory work and the TORCH campaign

Every noble work is at first impossible

Thomas Carlyle 1795-1881

4 Initial application to atmospheric measurement

4.1 Introduction

As with any new technique, it is important to characterise the performance and explore some of the applications. This chapter describes some of the initial work with the PTR-TOF-MS in relation to atmospheric measurements.

The PTR-TOF-MS was ready for service at the beginning of November 2003 and the first overnight run was performed on Bonfire night, November 5th. Given the proximity to Bonfire night, it was felt that it would be interesting to sample the Urban air that night. The findings of this initial experiment, along with other preliminary experiments are included in this chapter. At the time no one was sure whether the PTR-TOF-MS was stable enough to run unsupervised for a whole night!

As it turned out, the equipment performed faultlessly and in the months following, the machine was kept running for increasingly longer periods, so that during the Weybourne TORCH and the Jülich ACCENT campaigns (see Chapter 5) the PTR-TOF-MS ran continuously for the entire duration of the campaigns.

The TORCH campaign was the first occasion where the PTR-TOF-MS was used in any extensive measurement campaign alongside other devices – GC-FID, GC-MS and PTR-MS. The campaign lasted for five weeks starting on 23rd April and ending on 29th May 2004. The PTR-TOF-MS gathered data from May 5th to May 25th.

Several lessons in the behaviour of the PTR-TOF-MS were learnt and modifications to the equipment and the data post-processing procedures were devised and subsequently incorporated. Section 4.5 deals with the performance of the PTR-TOF-MS in the TORCH campaign and in Section 4.6 results of the first week-long study of the Leicester atmosphere performed on August 15th to August 22nd 2005 are described. All the performance improvements that had been acquired from the date of its first entry into service had been applied to the PTR-TOF-MS prior to the experiment.

4.2 Linearity, sensitivity and calibration experiments

4.2.1 Sensitivity and Detection Limits

The initial step in the reduction of the data is to normalise all the peaks in a trace to a nominal hydronium count rate of 10^6 s^{-1} so that all yields are given as normalised counts per second or ncps. The sensitivity of the PTR-TOF-MS for a particular species is defined as ncps per parts per billion by volume or ncps ppbv⁻¹. This follows the convention of Warneke *et al* [Warneke, *et al.*, 2001]. This practice has been widely adopted to eliminate fluctuations due to variation in equipment performance thus creating a common platform for comparing results.

4.2.2 Linearity of response

It is important that the linearity and sensitivity of the PTR-TOF-MS be commensurate with the task: to have the capability of determining species concentrations of 1 ppbv or lower. If the device responds linearly to variations in concentration, then it is possible to interpolate or perhaps even extrapolate with confidence starting from points of known concentration.

In order to establish the linearity of the PTR-TOF-MS, experiments were performed with H₂S and 1-butene as analyte gases. The experiments were part of the characterisation exercise to determine the linearity in the response of the PTR-TOF-MS as well as to establish a lower detection limit (Section 3.12, Chapter 3). It was found that the PTR-TOF-MS's response was linear and proportional within experimental error to the concentration of both H₂S and 1-butene.

With regard to sensitivity, the experiment using H₂S did not tax the low-end sensitivity of the PTR-TOF-MS as much as 1-butene did, as at its most dilute, its concentration was still 5.4 ppmv. With 1-butene, background noise limited the ultimate detection limit of the equipment to 2 ppbv.

The lower detection limit of the PTR-TOF-MS was later found to be far lower when, given the right conditions in Section 4.6 and also Chapter 5, it had no problem identifying concentrations of OVOCs 200 -300 pptv unambiguously.

4.3 Early urban air measurements

A large body of tests were done on the PTR-TOF-MS to determine its performance limits, and at the same time to explore the facilities and limitations of the Grams/AI software that controlled the running of the system.

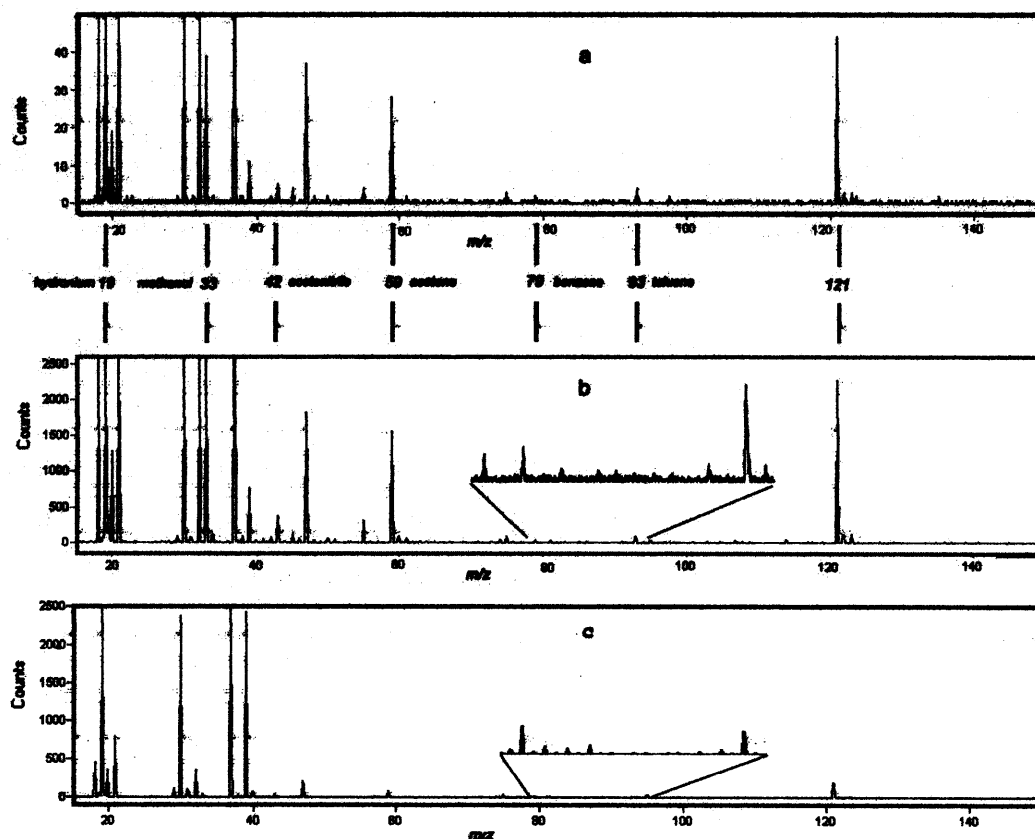


Figure 4.1 PTR-TOF-MS scans of urban air covering the range $m/z = 10-150$ (a & b) and a background spectrum (c). The traces have been normalised to 10^6 hydronium counts. The spectra are discussed in Section 4.3.1.

4.3.1 Experimental procedure

Air was drawn from outside of the laboratory building and fed into the PTR-TOF-MS through a ¼" Teflon tube. Since the Chemistry Department is situated about one mile from the centre of Leicester, substantial quantities of VOCs and OVOCs were expected to be present.

Examples of the spectra of the Leicester atmosphere are shown in Figure 4.1. In the figure, trace (a) at the top was accumulated in one minute (6×10^5 scans) whereas trace (b) was obtained over one hour (3.6×10^7 scans). An expanded view of part of the one-hour spectrum is also shown in traces (b) and (c). Trace (c) is a background spectrum (one hour average) using nitrogen (BOC zero-grade 99.99% pure) as the analyte. The peak at $m/z = 121$ is due to a contaminant from the viton o-rings used in the system. It is usually reasonably weak, but a very useful marker for recalibration the PTR-TOF-MS.

For the blank spectrum, the analyte gas was fed through an activated charcoal hydrocarbon trap and a liquid nitrogen trap. In later work, it was found that the presence of the trap made no difference to the resulting spectra, as the PTR-TOF-MS does not detect alkanes or lower molecular weight alkenes.

4.3.2 Results

The mass resolution is in excess of $m/\Delta m \gg 1000$. In all the spectra, the strongest peak by far is that of the hydronium (H_3O^+) ion with a raw count rate in the range of 2.4 to 3.0×10^5 counts per minute. Much weaker, but still off-scale in the plot are peaks from monohydrated hydronium ($\text{H}_3\text{O}^+(\text{H}_2\text{O})$) at $m/z = 37$, NO^+ at $m/z = 30$ and O_2^+ at $m/z = 32$. Several trace-level organic species can be identified above the noise level even in the 1-minute spectrum. These include protonated toluene ($m/z = 93$) and benzene ($m/z = 79$) as well as stronger signals of protonated methanol and acetone. Using published thermal rate coefficients [Lindinger, *et al.*, 1998], the peak intensities of the VOCs in the air sample corresponded to: 10 ppbv for toluene, 6 ppbv for benzene, 119 ppbv for acetone/propanal and 29 ppbv for methanol. A strong signal was seen at $m/z = 121$, at least some of which seems to arise from emissions attributable to Viton O-rings. Later calibration work confirmed that the derived concentration values were not unreasonable.

The concentrations determined for methanol and acetone are high compared with previously measured average values in urban air. However, given that the air was sampled outside a Chemistry Department, it is possible that it was contaminated by

solvent emissions from the department. Subsequent measurements in locations well away from the Chemistry Department, such as the Atmospheric Research Station at Weybourne, confirmed this supposition (Section 4.5.7).

The 3-D diagrams of the type shown in Figure 4.2 and 4.3 are useful to give a quick inspection of Trace (b) in Figure 4.1 demonstrates the excellent signal-to-noise ratio that can be achieved with longer data acquisition times. On a one-hour time scale it is possible to detect concentrations below 1 ppbv, indeed in later experiments (for example, Acetaldehyde in Table A5.1) this was proved experimentally where concentrations of 500 pptv and less were unambiguously identified using 40-minute sampling periods. In Section 4.6.2 concentrations of 200 – 300 pptv were confirmed with sampling runs of only ten minutes.

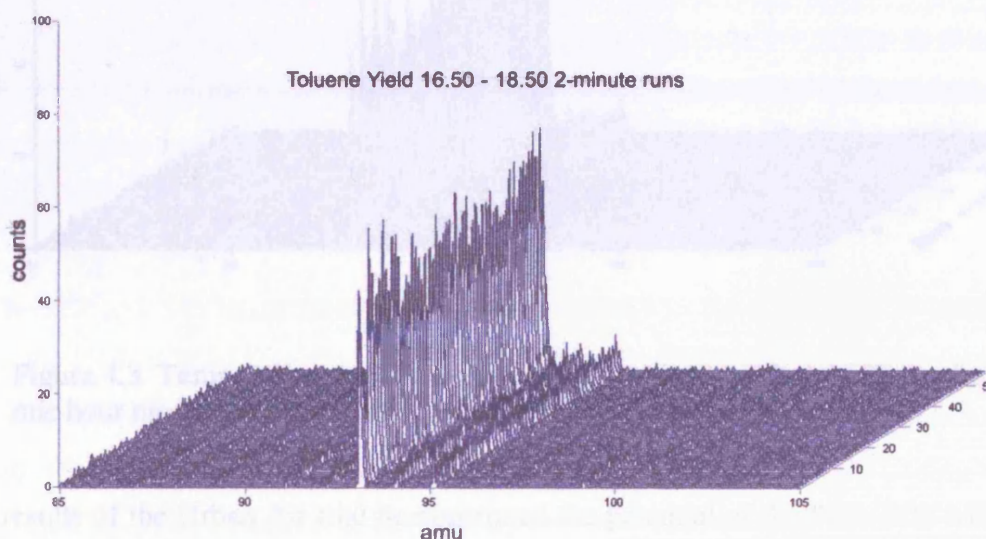


Figure 4.2 Profile of toluene signal of a run over an hour period from 16.50 to 17.50. Each peak shows the intensity in a one-minute period.

Figure 4.2 depicts the minute by minute variation for toluene over a period of one hour from 16.50 to 17.50 when traffic activity is high. Considering the low level of counts recorded, it is not possible to draw any conclusions from the count rate over the period, as the structure observed could be due to statistical variations.

Looking over a broader mass range, Figure 4.3 shows the minute-by-minute variation of acetone, benzene, toluene and the $m/z = 121$ peak over the same period. Here too no

major fluctuations in intensity were observed, suggesting that the sources of these organic compounds are not varying rapidly.

The 3-D diagrams of the type shown in Figure 4.2 and 4.3 are useful to give a quick overview of trends in changes of VOC concentration, but for numerical analysis conventional 2-D diagrams of counts versus time for each mass number are preferable.

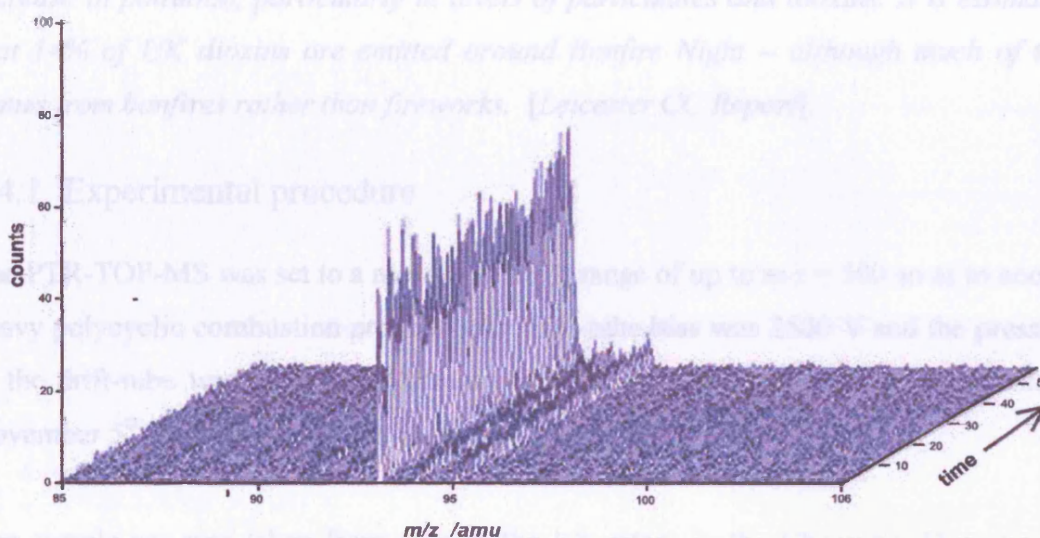


Figure 4.3 Temporal response for species between $m/z = 50$ and 150 for the one hour measurement period 16.50 to 17.50.

The results of the Urban Air trial demonstrated the potential of the PTR-TOF-MS as a sophisticated and powerful monitoring tool for trace VOCs and OVOCs in the atmosphere. Further work was required to develop it into a real-time measurement instrument for VOC and OVOC detection in the atmosphere.

4.4 Bonfire night

The measurements performed on November 5th 2003, formed the first night-time unattended PTR-TOF-MS run, using samples of outside air drawn from outside the Department of Chemistry from a point about 3 metres above ground level. Traditionally bonfires are held throughout the country and since the use of fireworks figure prominently in the festivities, it would seem that the contribution to atmospheric pollution would be measurable, seeing that it is easily detected by smell. The PTR-TOF-MS was not expected to have the versatility of a human nose. The exact emissions

will depend on the type of firework, but as the main component of fireworks is gunpowder, sulphur compounds are expected. Our original expectations were over-optimistic as the following extract on the impact of the Bonfire night activities shows. It forms part of publications by a number of UK County Councils. *Fireworks are also likely to produce small amounts of particulate matter, metal oxides and organic compounds (including minute amounts of polycyclic aromatic hydrocarbons, dioxins and furans). On and around Bonfire Night in the UK there is often a noticeable increase in pollution, particularly in levels of particulates and dioxins. It is estimated that 14% of UK dioxins are emitted around Bonfire Night – although much of this comes from bonfires rather than fireworks. [Leicester CC Report].*

4.4.1 Experimental procedure

The PTR-TOF-MS was set to measure a mass range of up to $m/z = 500$ so as to accept heavy polycyclic combustion products, the drift-tube bias was 2500 V and the pressure in the drift-tube was 6.0 mbar. Data acquisition started at 17.00 on the afternoon of November 5th with a series of 2-minute runs.

The sample gas was taken from outside the laboratory in the Chemistry Department, while the PTR-TOF-MS itself stayed in the 23 °C temperature-controlled environment of the laboratory. The inlet port consisted of an inverted funnel at the end of the sample tubing which helped prevent rain and moisture inadvertently entering. In hindsight, the inlet could have been positioned elsewhere, since it was in a fairly sheltered position, where the air was quite stagnant. It was also close to the solvent store which could add significantly to the permanent contamination background detected. On the other hand, a great deal of firework and bonfire activity could be expected in Victoria Park, which adjoined the University Main Campus. Victoria Park is situated on a high point in Leicester and is notorious for the wind blowing in all directions, so that there was a good chance that any activity in or near the park would ultimately reach the inlet port of the PTR-TOF-MS.

4.4.2 Results

The key results for the Bonfire Night measurements are summarised in Figures 4.4 and 4.5. These show measured temporal profiles for a variety of mass channels. Individual

two-minute scans were summed into 10-minute groups to help improve the statistics, although some temporal resolution would be sacrificed. Background contributions were subtracted before plotting. The root mean square errors (rms) for the resulting peaks resulting from error propagation were calculated from the expression

$$\text{Error} = \sqrt{\sigma_p^2 + \sigma_b^2} \quad (4.1)$$

Where σ_p and σ_b are the rms errors for the peak and background respectively [Lindberg, 2000].

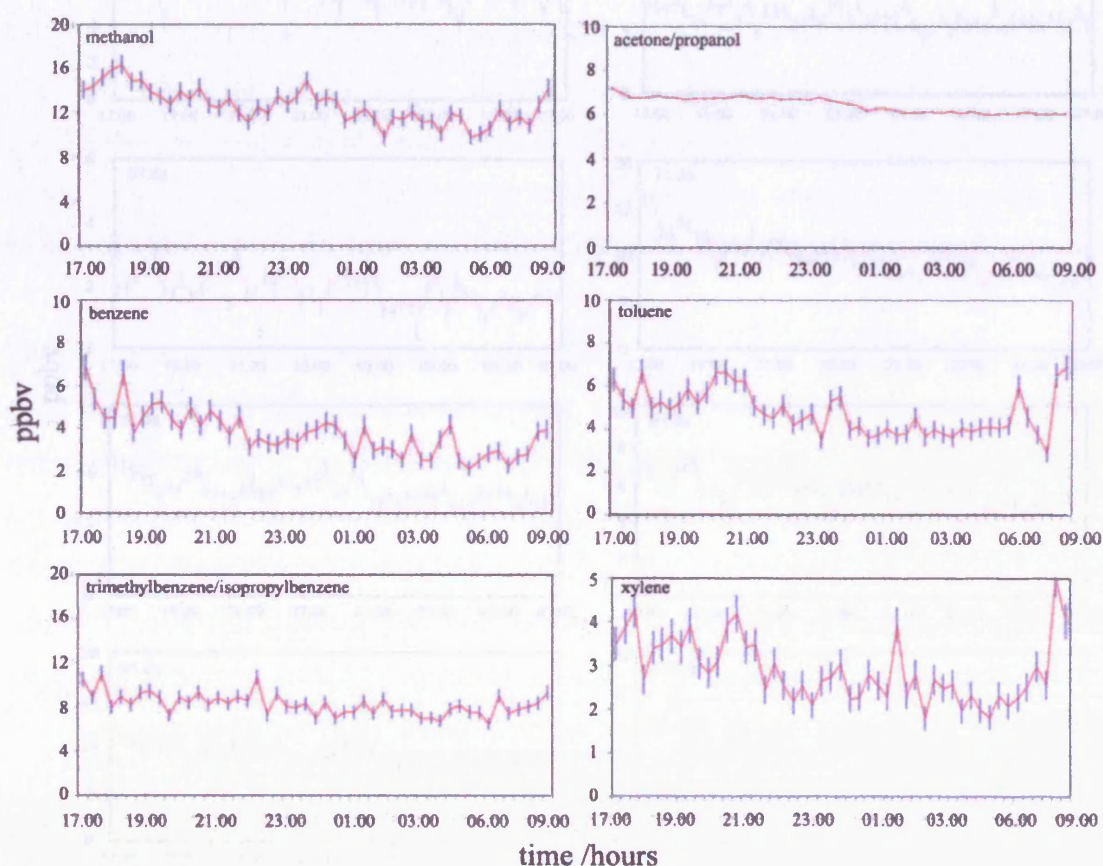


Figure 4.4 Temporal profiles of the identified species present in the Bonfire night atmosphere. The vertical lines on each point at 10 minute intervals show the rms errors.

The level of OVOC and VOC emissions would be expected peak between 17.00 and 22.00 and then tail off during the night. To calculate the concentrations of some well-known species (Figure 4.4), published thermal rate coefficients [Lindinger, *et al.*, 1998] were used to calculate the yields in the familiar units ppbv or in one case ppmv. For

the unidentified groups shown in Figure 4.5, a default value for the thermal rate coefficient of $k = 3.0 \times 10^{-9} \text{ cm}^3 \text{ s}^{-1}$ was used to convert yields to ppbv or ppmv.

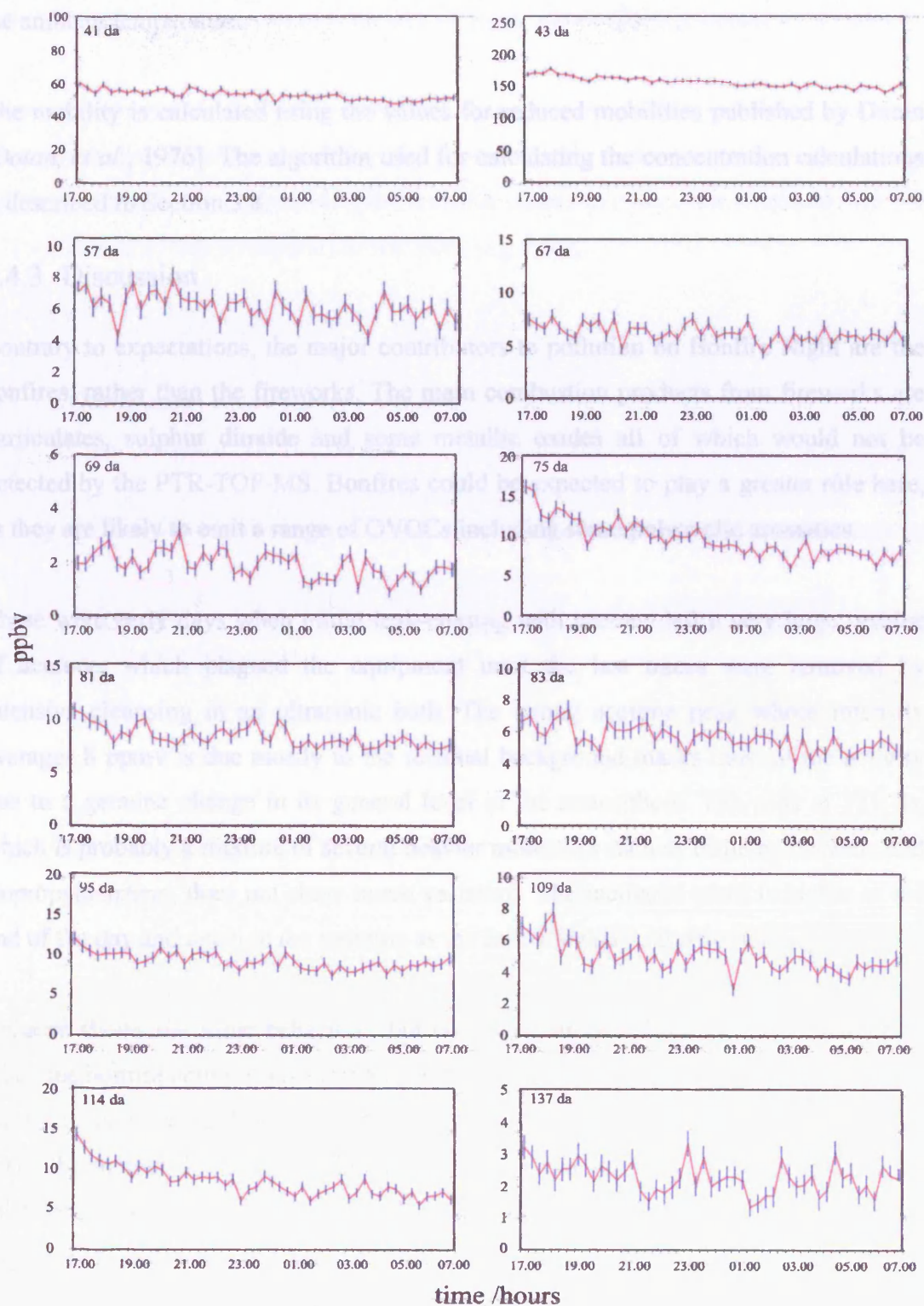


Figure 4.5 Unidentified species present in the Bonfire Night atmosphere.

Where groups have been identified, the yields in ppbv are calculated using published thermal rate coefficients, drift-tube bias and length, ion mobility and pressure as well as the ambient temperature.

The mobility is calculated using the values for reduced mobilities published by Dotan [Dotan, *et al.*, 1976]. The algorithm used for calculating the concentration calculations is described in Section 3.8.

4.4.3 Discussion

Contrary to expectations, the major contributors to pollution on Bonfire Night are the bonfires, rather than the fireworks. The main combustion products from fireworks are particulates, sulphur dioxide and some metallic oxides all of which would not be detected by the PTR-TOF-MS. Bonfires could be expected to play a greater rôle here, as they are likely to emit a range of OVOCs including some polycyclic aromatics.

These were early days when initial leak-chasing with acetone left a very large residue of acetone, which plagued the equipment until the last traces were removed by intensive cleansing in an ultrasonic bath. The strong acetone peak whose intensity averages 8 ppmv is due mostly to the residual background masks most of the activity due to a genuine change in its general level in the atmosphere. The peak at 121 da, which is probably a mixture of several heavier molecules such as trimethylbenzene and isopropylbenzene, does not show much variation. The methanol yield is higher at the end of the day and again in the morning as the following day's traffic starts up.

Toluene shows the same behaviour, but comes up strongly between 18.30 and 21.00 when the bonfire activity was most active. The Xylene peak at $m/z = 107$ behaves much the same as Toluene. Benzene had a few spikes in its trace that occurred at various times throughout the night. All in all, the activity was not very pronounced. Had the inlet been more strategically placed, more pronounced features could have been expected.

The spectra for the unidentified masses were also relatively featureless, although for the $m/z = 137$ group there were peaks later in the evening at 23.00 and some peak activity

occurred in the $m/z = 83$ and 109 mass channels at 19.00. The increased activity of the $m/z = 139$ and 109 peaks could be due to cyclic hydrogen emissions from the bonfire activities but there is some doubt whether they are statistically significant.

In conclusion, the PTR-TOF-MS did not detect any large fluctuations in the mass channels it was monitoring. While disappointing, the negative results indicate that whatever pollution was generated, it was of a nature that was not detectable by the PTR-TOF-MS in this configuration and sampling mode.

4.5 The TORCH Campaign

4.5.1 The site

TORCH, an acronym for Tropospheric ORganic CHemicals, consisted of two campaigns held in successive years, at Writtle, Essex and at Weybourne, Norfolk.

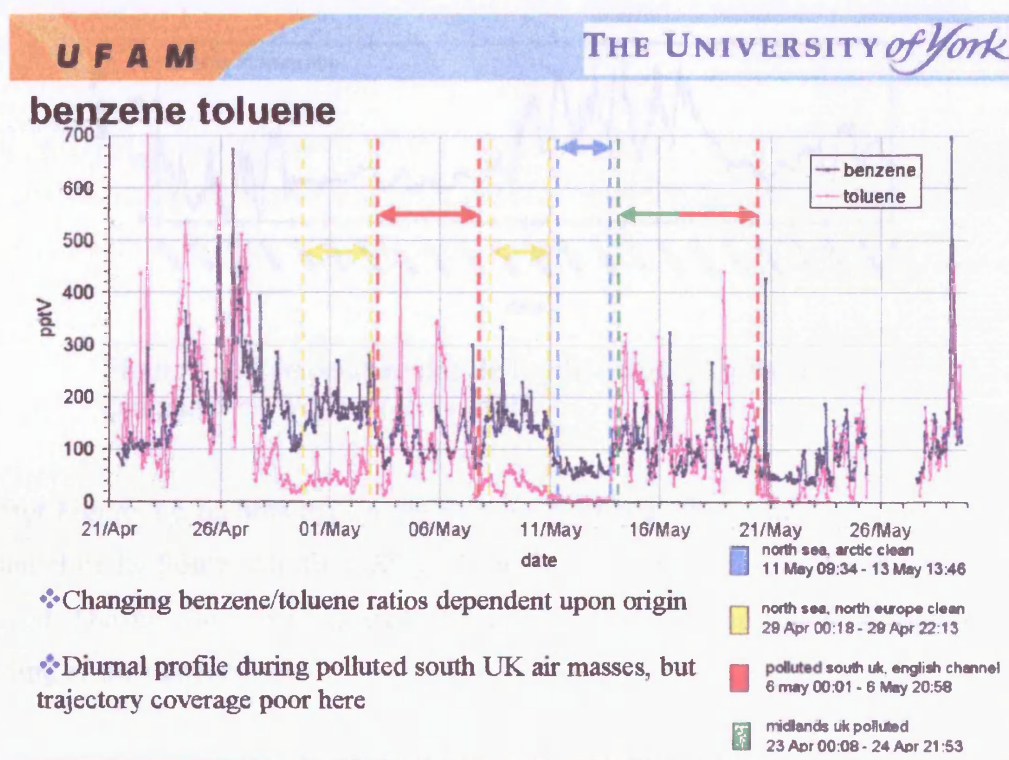


Figure 4.6 Chart of the influence of the prevailing conditions on the origin of species. Courtesy of University of York [Hopkins, 2004]

The principal aim of the two campaigns was to monitor the eastward progress of pollution plumes from the main industrial centres of London and the West Midlands.

Groups from several UK Universities employing a variety of techniques collaborated in the venture. For the campaign at Weybourne in May 2004, the PTR-TOF-MS was considered to have reached a sufficient state of development, to deploy it in a field campaign.

The campaign site at the Weybourne Atmospheric Observatory (WAO) was organised and hosted by the University of East Anglia based in Norwich. The main purpose of the observatory is to monitor the air flows from the north, and much of the work there is done in collaboration with similar installations on Svalbard, so it was not surprising that during the period of the campaign, the wind frequently blew in from that direction.

Climatologists predicted that for a fair proportion of the time during the Torch Campaign at Weybourne, the wind would be expected to blow in from of London or the West Midlands, and bring with it a rich mixture of OVOCs and VOCs.

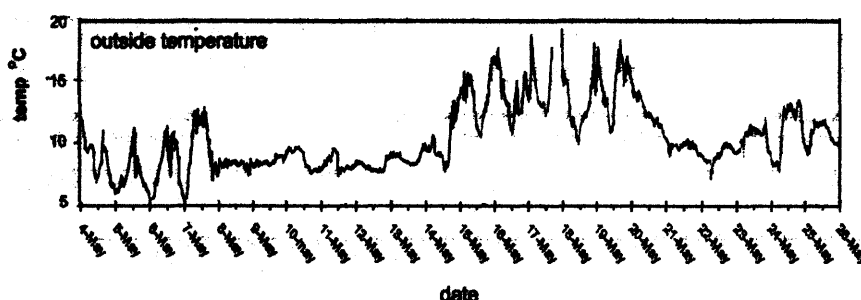


Figure 4.7 Temperature profile for the duration of the TORCH campaign at Weybourne, Norfolk.

In fact Figure 4.6 records that in the first week of May there was air from the English Channel in the South, and from May 15th to 22nd polluted air from the Midlands finally arrived. During these periods daily temperatures rose (Figure 4.7) as did the VOC loading of the atmosphere.

Input sample gas from the atmosphere was taken from several towers on the site. To supply the equipment in the main experimental building, the air was taken from the top of a permanently installed tower and fed via a glass conduit to a common manifold. A second removable tower about ten metres high and lower than the main tower was erected approximately 20 metres further inland. It served the participants not situated in

the main building, which were housed in containers situated around the main building. The PTR-TOF-MS was connected to the subsidiary tower. It can be seen on the far left of Figure 4.8.



Figure 4.8 The TORCH site at Weybourne. The PTR-TOF-MS was housed in the Portacabin on the far right. The inlets for all the Leicester instruments were mounted on the temporary tower on the left.

The original accommodation allocated to Leicester University was found to be unsuitable, and a Portacabin was hired to house the PTR-TOF-MS. About 5 days were lost before it was delivered and ready for service.

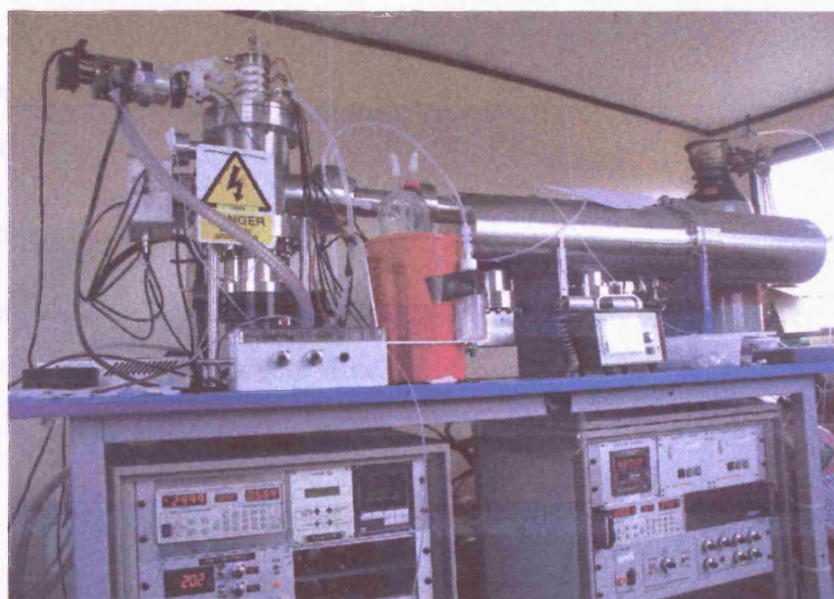


Figure 4.9 The PTR-TOF-MS as installed in the portacabin at Weybourne.

The Portacabin was situated behind the other installations on the landward side, and was too far from the common manifold used by the other PTR-MS devices on the site. It was very spacious but had no air conditioning. The windows could not be opened sufficiently to cope with the hot weather so the performance of the PTR-TOF-MS was affected as a consequence.

Once installed in its new environment, the PTR-TOF-MS ran continuously and without problem, once some initial electronic problems had been sorted out.

4.5.2 Experimental

At the time of the Weybourne campaign, the EHT across the drift-tube of the PTR-TOF-MS was 2500 V and the drift-tube pressure 6.0 mbar. The E/N varied with the ambient temperature, which ranged from 10 to 30 °C inside the Portacabin. This was higher than the range recorded by the outside temperature monitor, so that E/N actually varied between 168 and 178 Td.

The reactant gas used was zero-grade nitrogen bubbling through a Dreschell flask containing 15M Ω demineralised water. At the time the bubbler was at the ambient temperature. The water vapour was fed into the ion source of the PTR-TOF-MS at the rate of 53 sccm. The sample gas was drawn in from the top of the inlet tower through 20 m of ¼" PFA tubing and fed into the ion source at the rate of 275 sccm. To avoid spurious moisture from entering the system, the intake end of the tube was connected to an inverted funnel.

4.5.3 Runtime history

As the temperatures rose, it was noticed that the time-of-flight mass spectra shifted such that the ion flight times decreased. At its worst, the spectra showed a shift of as much as 0.4 da. in a period of 30 minutes. The shifts were sporadic, and seemed more related to a change of state in one of the electronic components, than a gradual shift caused by changes in temperature. After consultations with KORE Technology, who gave assurances that they would supply software for *post facto* recalibration of the results, it was decided that it was feasible to continue gathering data with one-minute scans and correct the drifting effect in the data analysis after the campaign was over. At

one stage the use of scan times longer than a minute was considered, but after the sporadic time shifts were detected, it was decided stick to one-minute scans.

4.5.4 Results

Figure 4.10 shows the strongly cyclic nature of the signals in specific mass channels which appear to be linked to the changes in the ambient temperature.

The building in which the PTR-TOF-MS was finally housed had no air conditioning and the windows could not be opened sufficiently to prevent temperature swings in excess of that recorded by the temperature log and the performance of the equipment was seen to be heavily temperature-dependent. The yield fluctuations observed are quite dramatic, often varying by as much as a factor of two.

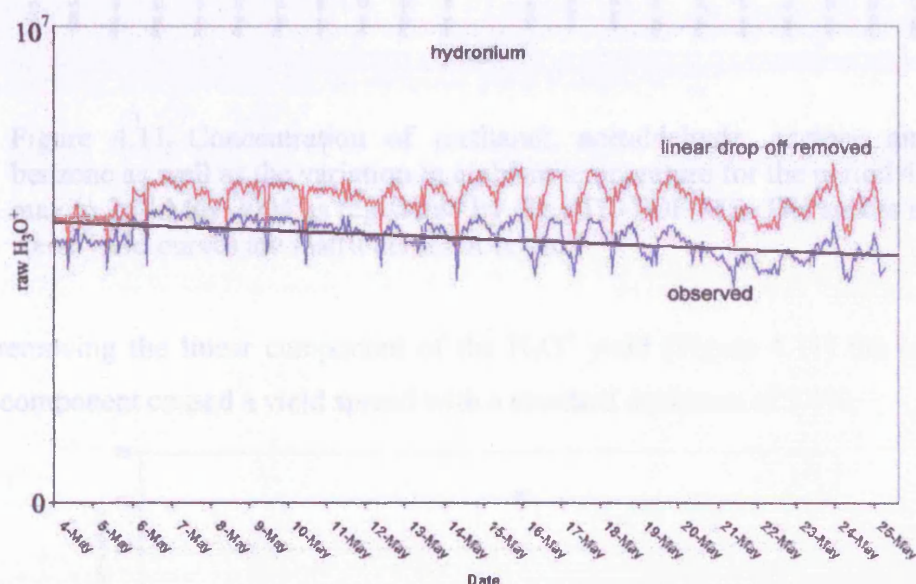


Figure 4.10 The hydronium count rate versus time. The oscillations in the count rate are superimposed on a steadily decreasing background which is illustrated by the straight line.

The hydronium output of the ion source also showed some temperature-linked behaviour superimposed on a slow linear drop of 8.9% in output over the period 4th May to 25th May. Part of the rapid change could be due to the amount of water vapour in the reactant gas which would be affected by the temperature of the bubbler.

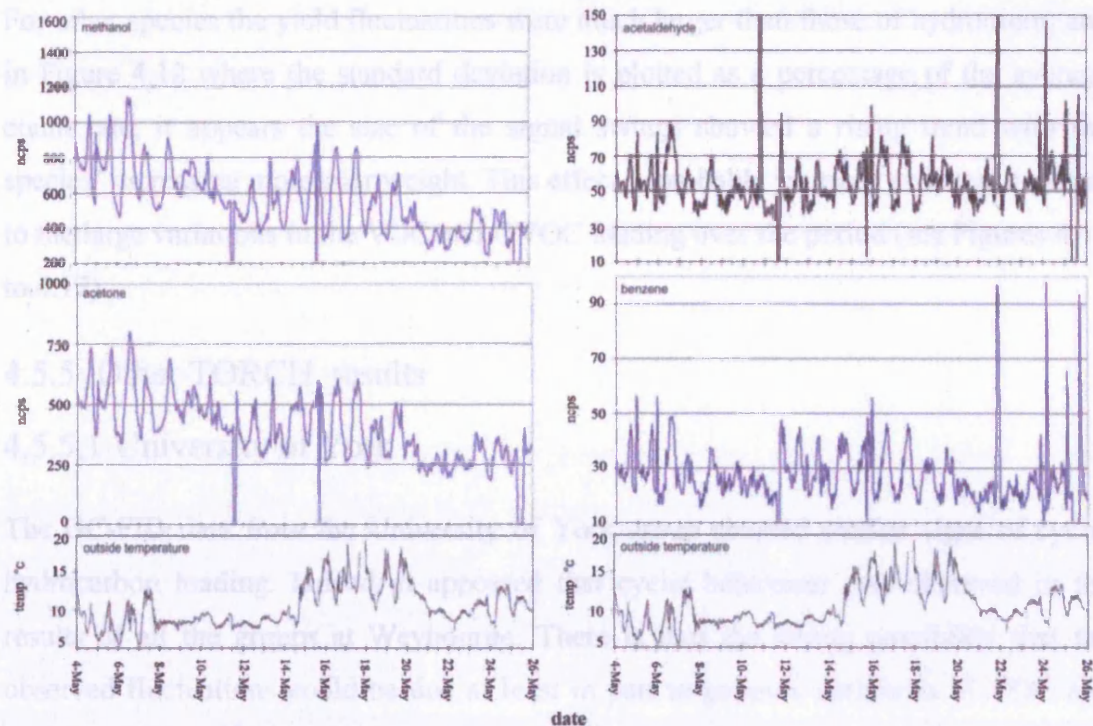


Figure 4.11 Concentration of methanol, acetaldehyde, acetone and benzene as well as the variation in ambient temperature for the period 4th May to 25th May 2004 as registered by the PTR-TOF-MS. The spikes in some yield curves are instrumental in origin.

After removing the linear component of the H_3O^+ yield (Figure 4.11) the remaining cyclic component caused a yield spread with a standard deviation of 5.4%.

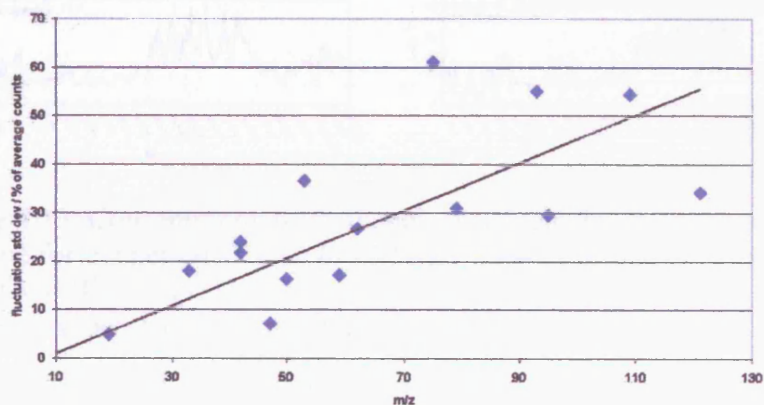


Figure 4.12 The percentage standard deviation of the species plotted as a function of species mass. The variation could be due to diurnal increases of species loading in addition to any temperature effects.

For other species the yield fluctuations were much larger than those of hydronium, and in Figure 4.12 where the standard deviation is plotted as a percentage of the average count rate, it appears the size of the signal swings showed a rising trend with the species' increasing molecular weight. This effect is probably spurious as it could be due to the large variations in the VOC and OVOC loading over the period (see Figures 4.14 to 4.17).

4.5.5 Other TORCH results

4.5.5.1 University of York

The GC-FID data from the University of York group showed similar signs of cyclic hydrocarbon loading. Indeed, it appeared that cyclic behaviour was observed in the results of all the groups at Weybourne. There is thus the strong possibility that the observed fluctuations could be due at least in part to genuine variations of VOC and OVOC loading and not only due to ambient temperature swings.

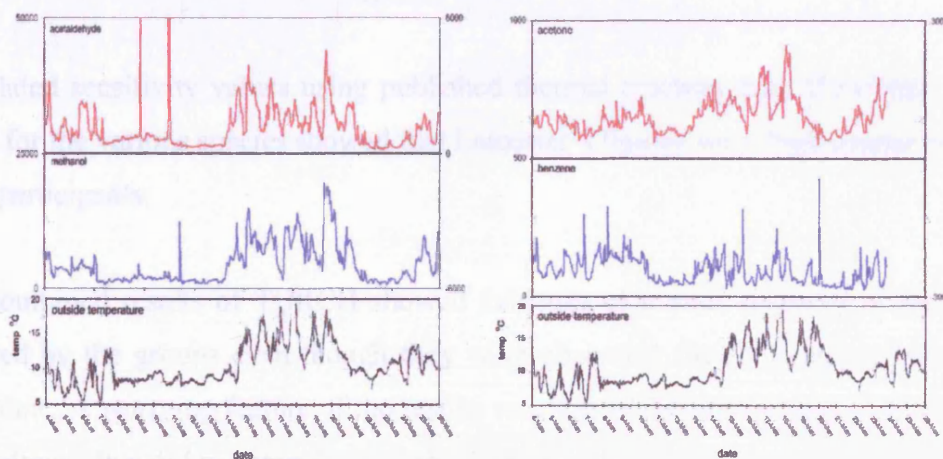


Figure 4.13 Concentration of methanol, acetaldehyde, acetone and benzene for the period 4th May to 25th May 2004 as measured by the York GC-FID group. The bottom panel (black) is a record of the ambient temperature variation during this period

In Figure 4.13 some PTR-TOF-MS results are shown together with the plot of the ambient temperature and the similarity between the two types of data is immediately apparent. The sharp rise in yields in the period between May 13th and May 23rd occurred when the prevailing wind blew from the West Midlands and the English

Channel (from the industrialised South), bringing with it the industrial effluent generated there.

Since the wind blew from the land, its temperature was higher than that for wind blowing in from the sea, or from the North. The results obtained during this period were the most interesting of the entire campaign.

4.5.5.2 Combined results

The results reported by the TORCH participants are summarised below in the diagrams Figure 4.14 to Figure 4.17 spanning the period of high VOC and OVOC activity experience during the period May 13th to 23rd. In the case of the Leicester results shown in the diagrams, these were not normalised or reduced to ppbv at the time of the compilation, as no reliable calibration figures were available at the time. So the Leicester results were plotted using the scale on the right hand side derived from native counts.

Calculated sensitivity values using published thermal reaction rates [*Lindinger, et al., 1998*] for the various species showed that Leicester's figures were high compared to the other participants.

The combined results of TORCH showed evidence of a wide disparity of the results reported by the groups even though they were observing the same atmosphere at the same time. A worrying feature of the results was that while most groups observed yield fluctuations, they did not appear to overlap well at all. Atmosphere samples were drawn from three towers that were situated within 20 metres from each other.

The tower serving the PTR-TOF-MS was 10 metres high while the tower feeding the main Atmosphere Research Laboratory building was 15 metres high and situated closer to the seashore. It would be surprising if the variation on OVOC and VOC loading could vary as much as was observed purely because of the placement of the inlet towers. Unfortunately the York PTR-TOF-MS was out of action for most of the duration of the TORCH campaign. This was disappointing as it was hoped that the campaign would be an opportunity to compare the response of two similar devices. The

large spread in the results shown below, suggest that Leicester's results were not as bad as originally thought.

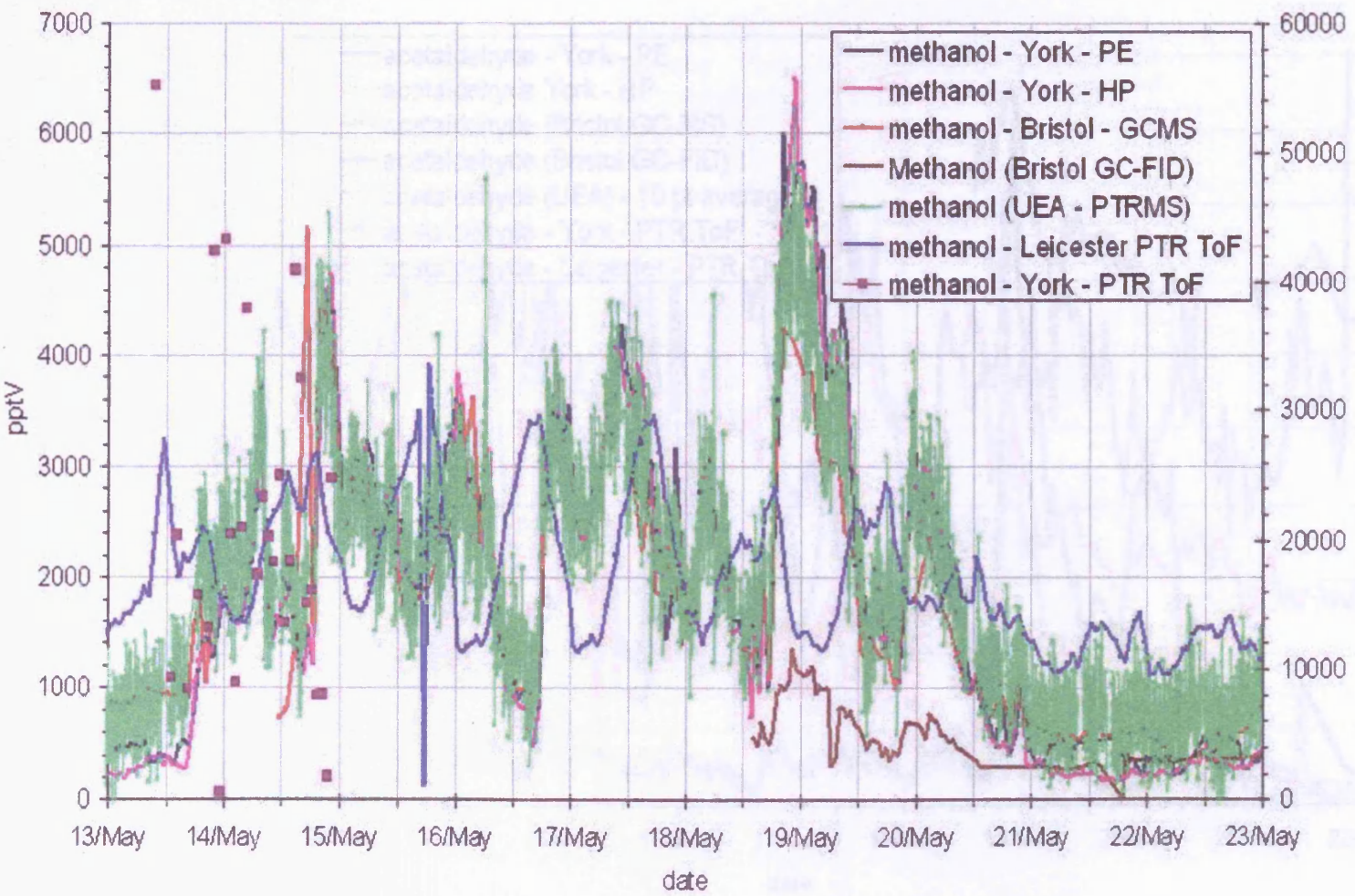


Figure 4.14 TORCH combined results for Methanol. Courtesy of University of York [Hopkins, 2004].

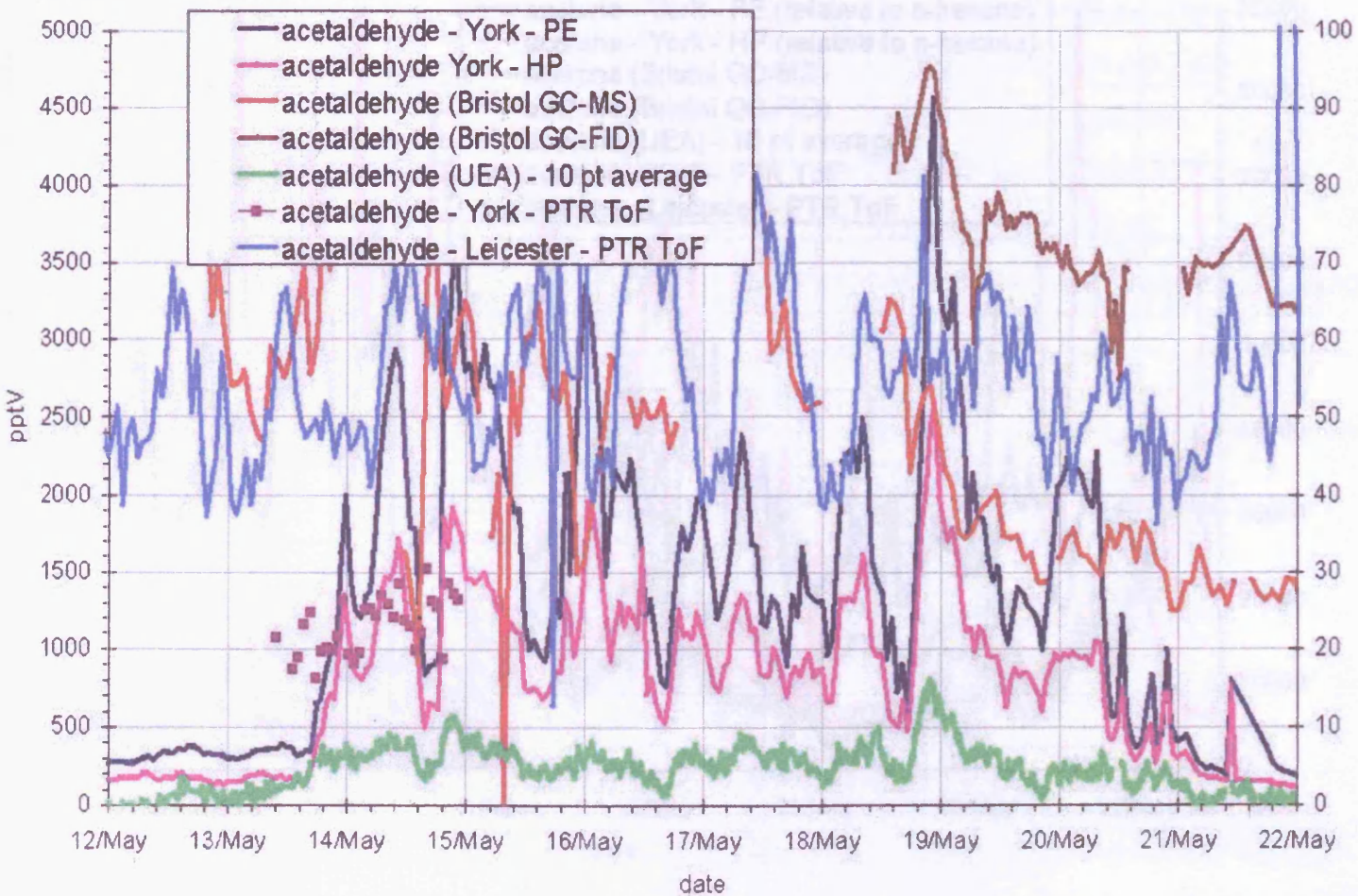


Figure 4.15TORCH combined results for acetaldehyde. Courtesy of University of York [Hopkins, 2004].

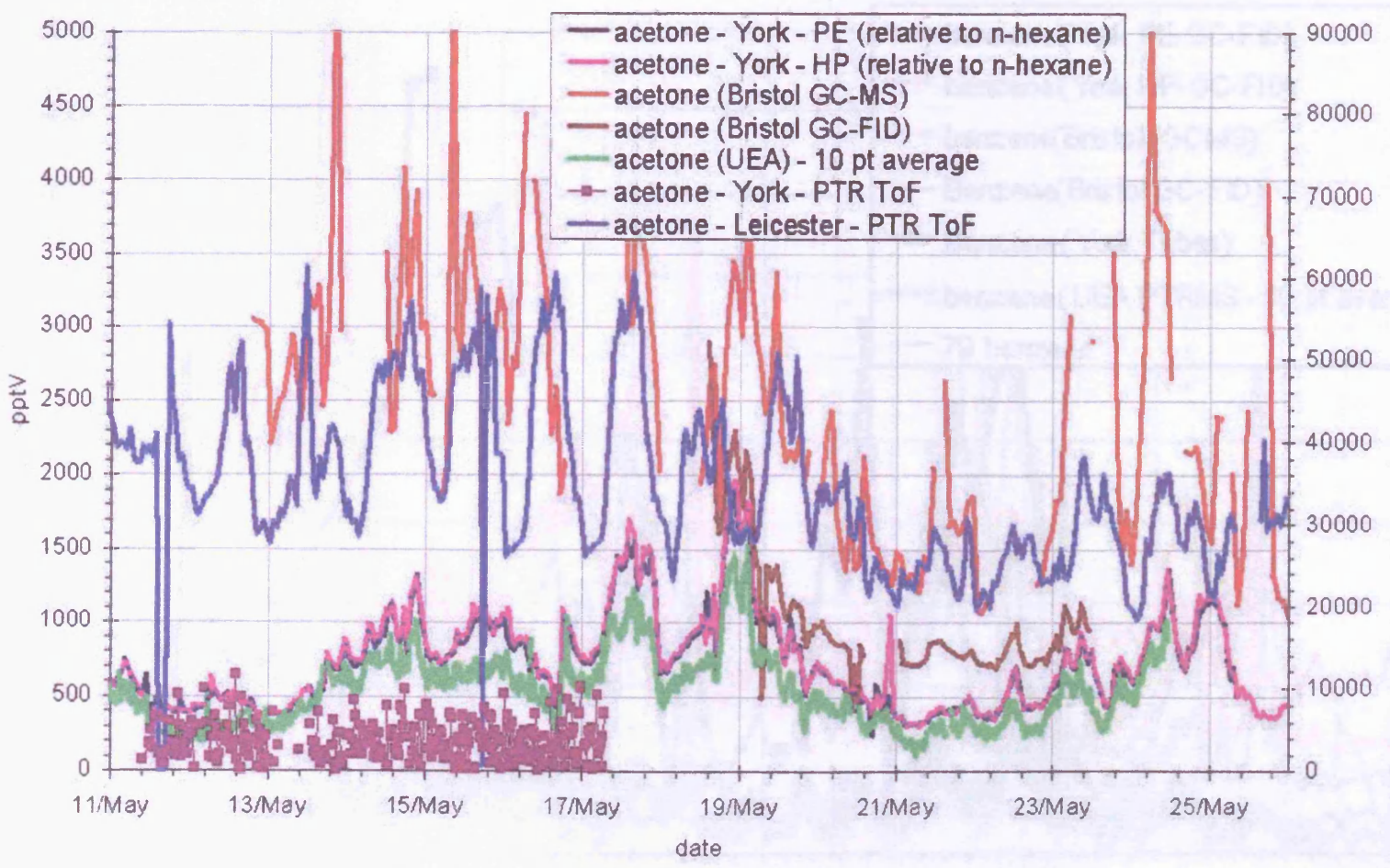


Figure 4.16 TORCH combined results for acetone. Courtesy of University of York [Hopkins, 2004].

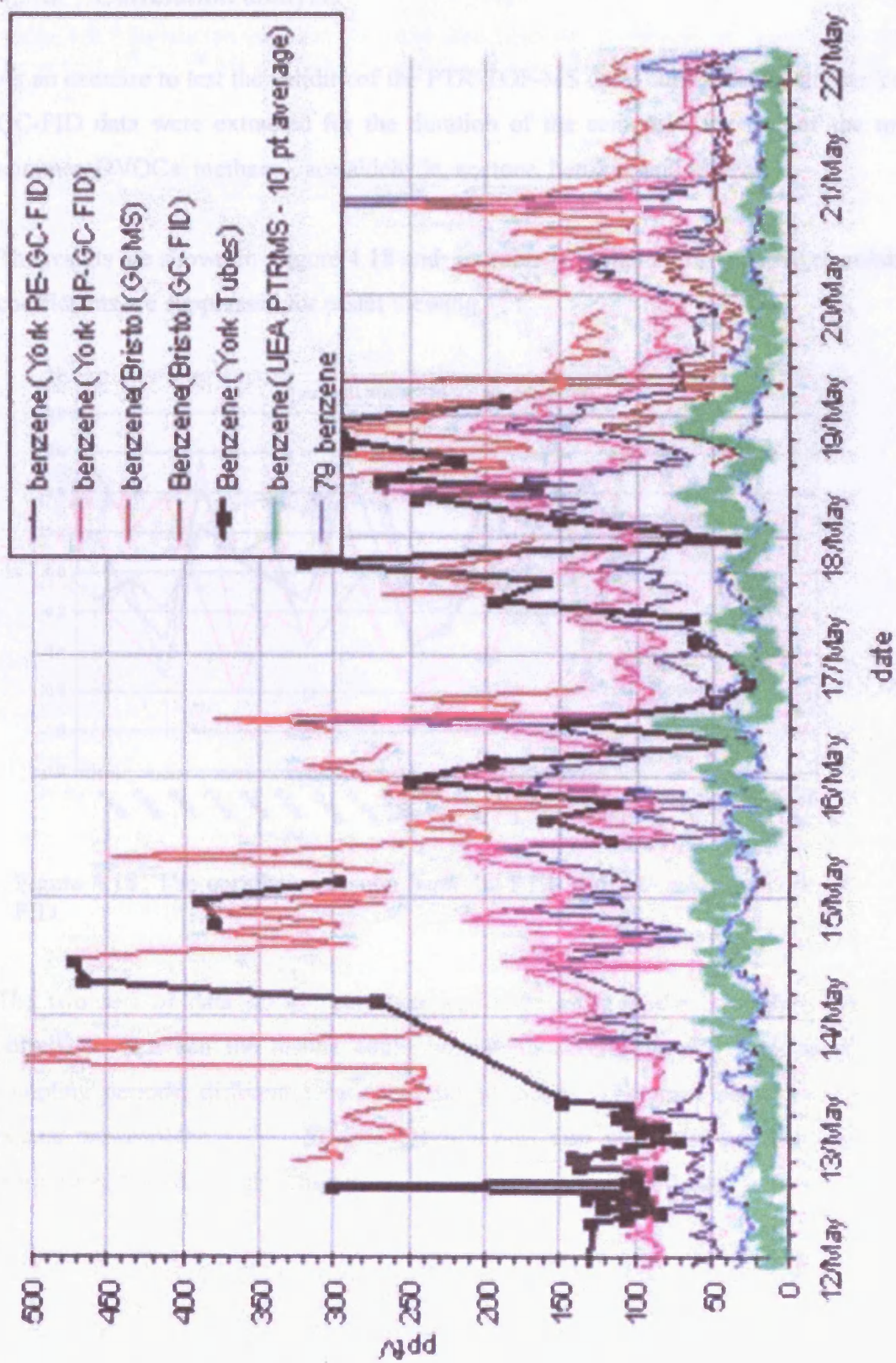


Figure 4.17 TORCH combined results for benzene. Inexplicably, Leicester's results were omitted. Courtesy of University of York [Hopkins, 2004].

4.5.6 Correlation analysis

Table 4.1. Correlations between the York and Leicester daily runs at Westhousey Farm

As an exercise to test the validity of the PTR-TOF-MS data, correlations with the York GC-FID data were extracted for the duration of the campaign for five of the most common OVOCs, methanol, acetaldehyde, acetone, benzene and toluene.

The results are shown in Figure 4.18 and in Table 4.1 where 0 or negative correlation coefficients are suppressed for easier viewing.

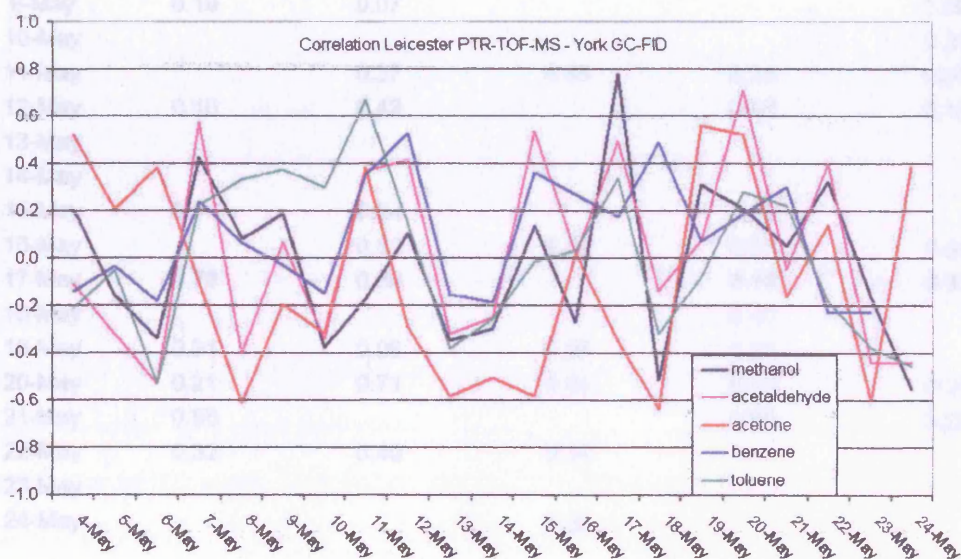


Figure 4.18 The correlation results from the PTR-TOF-MS and the York GC-FID.

The two sets of data do not correlate well over most of the campaign. The poor correlation between the results could be due to several factors, such as different sampling periods, different location of sample inlets. The most positive correlation occurs between the 15th – 20th May, which was also when the weather was at its warmest and the day/night temperature swings were more significant.

Table 4.1 Correlation between the York and Leicester daily runs at Weybourne for the period 4th – 25th May. The best correlations were obtained for the period of 15th – 20th May.

Date	Methanol	Acetaldehyde	Acetone	Benzene	Toluene
4-May	0.20		0.52		
5-May			0.21		
6-May			0.38		
7-May	0.42	0.58		0.24	0.22
8-May	0.08			0.06	0.33
9-May	0.19	0.07			0.38
10-May					0.30
11-May		0.37	0.38	0.35	0.67
12-May	0.10	0.42		0.53	0.14
13-May					
14-May					
15-May	0.14	0.54		0.38	
16-May		0.01	0.02	0.27	0.04
17-May	0.78	0.50		0.18	0.33
18-May				0.49	
19-May	0.31	0.08	0.58	0.07	
20-May	0.21	0.71	0.53	0.19	0.28
21-May	0.05			0.30	0.22
22-May	0.32	0.40	0.14		
23-May					
24-May			0.39		

4.5.7 Calibration and calculating concentrations

Two calibration standards were used at Weybourne: a 30-component VOC standard gas from BOC and a Bristol/Apel standard. Neither standard was ideal, as both contained components that complicated matters. The 30-component standard consisted of a mixture of alkanes and isobaric compounds. The PTR-TOF-MS has a very low sensitivity for detecting alkanes, and it is not able to resolve the components of isobaric mixtures. The Bristol/Apel was designed for use in Gas Chromatography and contained several isobaric constituents. At the ACCENT Intercomparison campaign (Chapter 5) a new Bristol/Apel calibration mixture was used which proved to be better suited to the requirements of a PTR-TOF-MS.

The results obtained were not very consistent although they did agree with the calculated values within 20%.

The other groups at the Weybourne campaign reported wildly varying yields (as shown in Figure 4.14 to Figure 4.17). Although the VOC yield curves for the period looked similar in shape the results differed widely in reported concentrations. This was particularly noticeable in the results for acetone in Figure 4.16, where the results seemed to fall either into a high or a low concentration group.

The results for May 17th were chosen for further processing as on this day, the PTR-TOF-MS results showed the strongest correlation with the York results (Figure 4.19). Calculated values for the sensitivities were used because of the suspect nature of the calibration results.

The background owing to contamination of the PTR-TOF-MS was low and at all times well below the peaks attributed to methanol, acetaldehyde, acetone, benzene and toluene. A set of detection sensitivities (in ncps ppbv⁻¹) were calculated using published thermal rate coefficients [Lindinger, *et al.*, 1998] and applied to the Weybourne data to give an indication of the order of magnitude of the final results.

Table 4.2 VOC/OVOC peak values on 17th May 2004 recorded by the PTR-TOF-MS and the highest value reported by other groups. The asterisk refers to data from York GC-FID only.

VOC/OVOC	Leicester /ppbv	Highest other /ppbv	Lowest other/ppbv
Methanol	33.9	14.1	0.5
Acetaldehyde	2.2	3.5	0.25
Acetone	18.6	>5.0	0.5
Benzene	2.2	>0.3	<0.05
Toluene	3.1	0.2*	<0.05

The Leicester results were found to be between two to three times higher than reported by the other groups as seen by some typical results in Table 4.2. The lowest approximate figures reported for that day are also shown. It is interesting to note that

the two main inlets servicing the groups were at different heights, but no more than 20 metres apart. The group whose findings were closest to those of the PTR-TOF-MS, was the Bristol GC-MS group.

4.5.8 Errors and the level of confidence

All measurements are prone to error from various sources, so it is important to obtain an estimate of the effect of these on the reliability of experimental data. The PTR-TOF-MS data are gathered as a series of runs or scans usually of one-minute duration. In turn these are grouped together into larger sampling periods for further manipulation. While grouping of successive data runs will tend to produce smoother spectra, the more rapidly varying features which appear in the ungrouped data will be lost. Yet, it is from an examination of the underlying detail that it is possible to gain a measure of the degree of confidence in the data. The following three quantities can be used to measure the validity and reliability of data produced by the PTR-TOF-MS for atmospheric research:

4.5.8.1 Atmospheric detailed variation

Rapid and genuine atmospheric variations in species concentrations visible in successive one-minute data runs are smoothed out when these are grouped together. The standard deviation of the ungrouped data gives a measure of large random and genuine fluctuations in the underlying spectra. The fluctuations can be due to genuine changes in atmospheric composition as well as normal statistical variation and the limits in the precision of the apparatus. The atmospheric detailed variation is obtained by obtaining the standard deviation of the ungrouped data. The determination of the relative contribution of the limits to precision is discussed next.

4.5.8.2 Precision or Instrumental Limitation Error

The figure for precision attempts to define the ability of the PTR-TOF-MS to yield similar results for successive measurements of the same item. The instrumental limitation error (ILE) defines the limit to the precision of the instrument once other sources of error have been accounted for. The ILE will start to predominate once the

contribution from the statistical variation diminishes with increased peak size, leaving the ILE as the major contributor in the combined error.

A figure of merit for this criterion can be obtained by examining the average standard deviation of groups of one-minute calibration runs using gas standards with concentrations of the relevant species, present in much higher concentrations than those expected to appear in the experimental conditions. The reasoning behind this is that the contribution of the normal statistical variation in the calculation of the standard deviation diminishes with large count rates, whereas the contribution of the ILE to the precision of the equipment, does not change. Where the count rate in a particular mass channel is extremely high, the variation in the standard deviation of the observed counts approaches the limiting precision of the equipment performing the measurement. The standard deviation obtained in this way can be applied to subsequent experimental results to indicate the precision of the measurement

Calibration runs were performed on two occasions, 11th May in the middle of the campaign and the other on 25th May at the end of the campaign, which made it possible arrive at a figure for the precision or ILE of the PTR-TOF-MS. The contribution of the ILE ranged from 2.9% to 3.1% depending on the species.

4.5.8.3 Standard statistical error

The standard statistical error (standard deviation) is calculated by taking the square root of the summed one-hour spectra. The spread in these are smaller than in the previous case of the atmospheric detailed variation, because of the smoothing effect of grouping into longer accumulation times. The standard deviation described here is termed the 'standard statistical error' to distinguish it from the standard deviation referred to in the 'atmospheric detailed variation' referred to in Section 4.5.8.1.

In the results for May 17th are shown in Figure 4.19 with the contributions of the standard error, the atmospheric detailed variation error and the ILE shown in blue, black and red error bars respectively. Predictably the error bars due to atmospheric variation are greater than the instrumental limitation error.

4.5.8.4 Signal-to-noise ratio (S/N)

The signal-to-noise ratio of a data item is given by the ratio of the mean value to the standard deviation.

The one-minute data was scaled to 10^6 hydronium cps before manipulation and rescaled after grouping. The data was normalised so as to maintain the same ratio to hydronium throughout. Since one-hour spectra are summed and averaged one-minute spectra, the signal-to-noise ratio can be obtained from the ratio of the summed data points to the standard deviations for the same underlying datasets from which the points are derived.

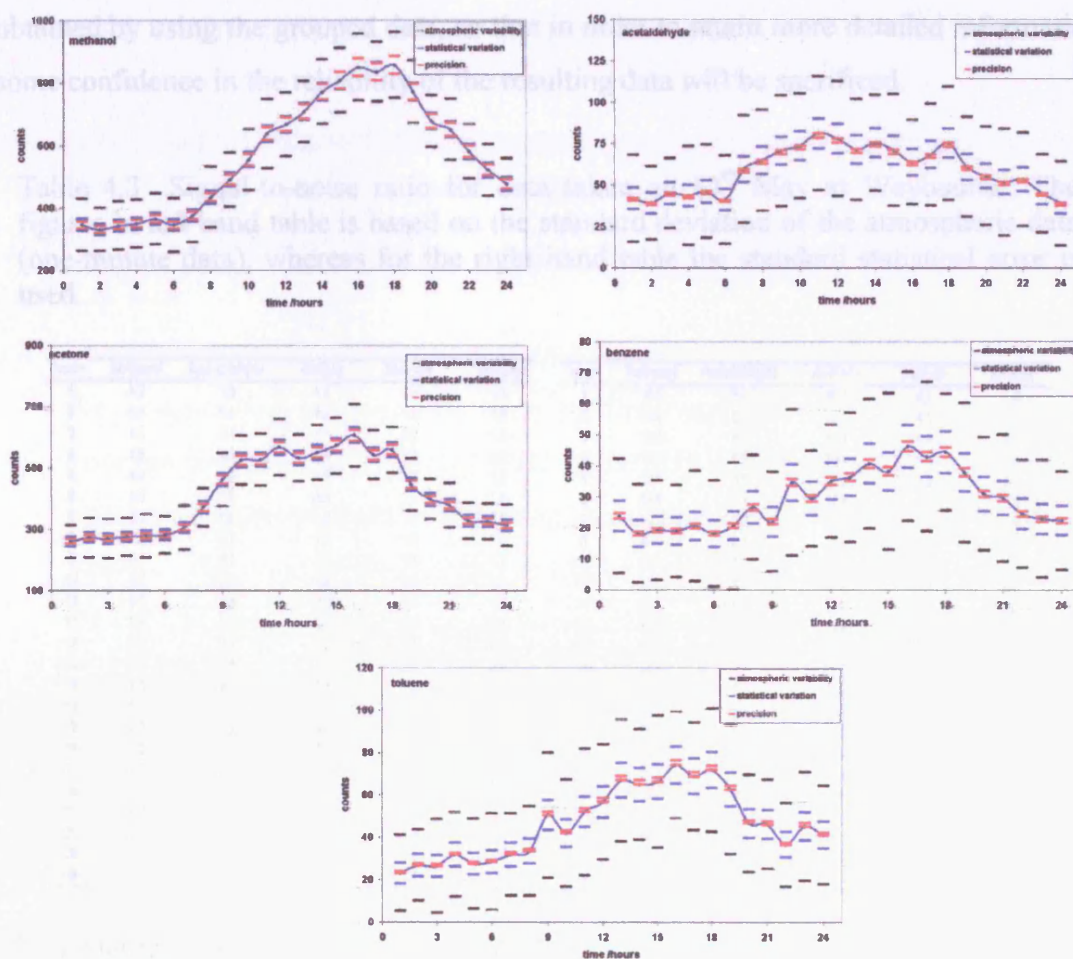


Figure 4.19 Results for a typical day at Weybourne (17th May 2005). The bars depict the statistical variations (blue), the atmospheric variations (black) and the precision (red) limits of the measurement.

The signal-to-noise ratio is a useful means of expressing confidence in the validity of a set of data. For normally distributed data, the standard deviation is a measure of the variability of a set of data for which 66% of the data points can be expected to fall within one standard deviation or 99% within three standard deviations of the mean value [Wayne, 1994]. Ideally one would look for a signal-to-noise ratio of 3 or higher where three standard deviations would equal the value of the mean height used in the signal-to-noise calculation. For larger values of the signal-to-noise ratio, the mean height of the data is greater than three standard deviations, and can be distinguished from the statistical noise.

If the underlying standard deviation is used, the signal-to-noise ratio is lower than that obtained by using the grouped data, so that in order to retain more detailed information some confidence in the reliability of the resulting data will be sacrificed.

Table 4.3 Signal-to-noise ratio for data taken on 17th May at Weybourne. The figures in left hand table is based on the standard deviation of the atmospheric data (one-minute data), whereas for the right hand table the standard statistical error is used.

hours	Methanol	Acetaldehyde	Acetone	Benzene	Toluene	hours	Methanol	Acetaldehyde	Acetone	Benzene	Toluene
1	4.2	1.8	4.9	1.3	1.3	1	18.6	8.5	16.1	4.8	4.8
2	4.9	1.8	4.2	1.1	1.6	2	18.2	8.3	16.5	4.3	5.2
3	4.5	2.1	4.1	1.2	1.2	3	18.5	8.7	16.4	4.4	5.1
4	4.8	1.5	4.4	1.3	1.6	4	18.7	8.8	16.6	4.4	5.6
5	4.4	1.8	4.0	1.2	1.3	5	19.1	8.8	16.7	4.5	5.2
6	4.0	1.5	4.6	1.1	1.3	6	18.8	8.4	16.8	4.3	5.3
7	4.4	1.8	4.2	1.0	1.6	7	19.4	7.7	17.5	4.5	5.6
8	4.5	2.1	5.9	1.8	1.8	8	20.8	8.1	19.2	5.2	5.8
9	5.7	2.1	5.3	1.4	1.7	9	22.1	8.4	21.5	4.7	7.1
10	5.7	2.3	6.6	1.5	1.7	10	23.5	8.8	22.9	5.9	6.5
11	5.7	2.4	6.2	1.9	1.7	11	25.2	9.0	23.0	5.4	7.2
12	6.5	2.2	6.1	1.9	2.1	12	26.8	8.8	23.8	5.9	7.5
13	7.2	2.4	7.0	1.7	2.3	13	26.8	8.4	23.1	6.0	8.2
14	7.5	2.6	6.1	2.0	2.5	14	27.8	8.7	23.5	6.4	8.1
15	7.8	2.1	6.3	1.5	2.1	15	28.4	8.4	23.9	6.2	8.1
16	8.0	2.5	6.0	1.9	2.9	16	29.1	8.0	24.6	6.8	8.6
17	8.7	2.2	6.8	1.8	2.7	17	28.9	8.3	23.3	6.6	8.3
18	8.2	2.2	7.6	2.4	2.5	18	29.3	8.7	23.6	6.7	8.5
19	7.7	2.0	5.3	1.7	2.0	19	27.8	7.8	21.1	6.2	7.9
20	6.1	1.9	6.1	1.7	2.0	20	26.0	7.4	19.9	5.6	6.8
21	6.7	1.6	5.2	1.4	2.2	21	25.5	7.2	19.4	5.4	6.8
22	6.7	1.9	5.6	1.4	1.9	22	24.1	7.3	18.1	4.9	6.0
23	6.4	1.9	5.5	1.2	1.8	23	22.8	6.7	18.0	4.8	6.7
24	5.8	1.5	4.6	1.4	1.8	24	21.8	6.2	17.7	4.7	6.4

The signal-to-noise ratios using the raw (one-minute) and summed standard deviations are shown side by side in Table 4.3. The improvement in the signal-to-noise ratio achieved by assembling runs into larger groups is clear, especially as it can give a feel for the minimum group size that can still give meaningful results. This theme is developed further in Section 5.8.3, Chapter 5.

4.5.9 Some conclusions from the TORCH campaign

While a great deal of insight into the working of the PTR-TOF-MS was gained during the TORCH campaign at Weybourne, the results obtained could not be converted with confidence into species concentration in ppbv, using the calibration results taken at the time, so calculated values for the PTR-TOF-MS sensitivity using published reaction rates were used instead.

The lessons learnt at TORCH were applied to later studies described in Chapters 5 and

6. The specific lessons of value were:

- The PTR-TOF-MS was found to be capable of detecting concentrations of suitable VOCs or OVOCs down to the several ppbv level. The sensitivity could be increased if a higher hydronium count rate could be achieved.
- Problems with excess hydronium cluster formation were not encountered during the all the campaigns.
- The anomalously large VOC concentrations observed with the PTR-TOF-MS at Weybourne could be accounted for by the fact that it was drawing its input from a different location, quite close to the University of Bristol GC-FID container, which also obtained results which were higher than most of the other installations. However the range of the results reported by other groups varied so widely that the PTR-TOF-MS results could not be automatically be considered unfeasible.
- While the calibration data obtained at ACCENT cannot be used to extract species concentrations from the TORCH results, it is possible to argue for the use of calculated yields as being at least as acceptable an alternative. What is puzzling about the TORCH results is why they are so high, when the ACCENT results (Chapter 5) are so close or even on the low side of the official results.
- The most serious problem highlighted in the TORCH campaign was the lack of suitable standard gas mixtures, specially designed for the PTR-TOF-MS. The

standard borrowed from the University of Bristol, contained several isobaric species and alkanes that are not detected by the PTR-TOF-MS.

- In spite of the problems, good spectra were obtained on a regular basis, and the equipment ran extremely smoothly for long periods of time. Over a period of weeks the hydronium count rate dropped by 8.9% in three weeks of running, as a result of increasing contamination. After cleaning all the components of the ions source in a hydrosonic bath, the original performance returned.
- The PTR-TOF-MS consistently reported higher VOC loadings than the other collaborators in the TORCH campaign. The results can be considered to lie at the high end of a widely varying set of results from the other groups.

Problems which needed attention were:

- The PTR-TOF-MS is sensitive to the ambient temperature, which not only affects the total count rate of the machine, but also causes shifts in the time-of-flight of ions.
- The shifts in time-of-flight can be corrected post-processing of the campaign data, and the effect of time shifts during data acquisition can be contained by performing one-minute scans only which can be grouped and averaged at a later date as required.
- The TORCH campaign demonstrated the effect of varying ambient temperature on the operation of the PTR-TOF-MS thus confirming the findings of several other workers using PTR-MS (see for example [Dommen, *et al.*, 2003] and [Steinbacher, *et al.*, 2006]). It was decided that in the future steps would have to be taken to maintain the temperature of the inlet lines and the drift-tube above ambient temperature.

Subsequently the following modifications were applied to the PTR-TOF-MS. The drift-tube now operates at 40 °C to insulate it from changes in the ambient temperature; the water vapour bubbler, and both inlet lines from the mass flow

controllers to the ion source are also heated to 40 °C; finally two 5 metre heated pipelines were added to ensure that analytes and the nitrogen feeding the bubbler all operated at the same temperature.

- It was not possible to heat the whole body of the PTR-TOF-MS to 40 °C, although that would be preferable. The serious time shifts and temperature variations experienced at Weybourne were not observed in the laboratory, while it may not be practical to heat the whole body and control electronics of the PTR-TOF-MS to 40 °C, efforts would have to be made in the future to limit changes in the ambient temperature.
- A re-evaluation of the operating conditions of the PTR-TOF-MS was needed for future work. This is described in the next section.

4.5.10 Determining an alternative range of E/N

During the TORCH campaign the drift-tube bias was 2500 volts, the pressure in the drift-tube 6mb and the ambient temperature 23 °C, corresponding to an E/N of 170 Td. The saturated reactant gas was fed into the ion source at the rate of 12 sccm, and the sample gas typically set to 200sccm raised the internal pressure in the ion source to 6mb.

In August of 2004 experiments were carried out to determine the operating limits of the PTR-TOF-MS and at the same time, observe the behaviour of the PTR-TOF-MS running at different values of E/N .

Tests were run to see the effect of raising the bias by steps up to 4100 volts, and increasing the drift-tube pressure. The main factor limiting the drift-tube pressure was the pressure in the main body of the TOF-MS, which could not be allowed to exceed 10^{-6} mbar. The drift-tube voltage could be raised until the Thurlby counter-voltage reached the device's maximum output of 50V. At this point E/N was 280 Td and substantial fragmentation occurred with most species, so for a while the bias was reduced to 3000V. Now E/N was 205 Td, and fragmentation reasonable but still on the high side.

As a result of further fragmentation studies of benzene, acetone, toluene, ethanol, acetaldehyde and acetonitrile, it was found that at 150 Td very little or no fragmentation occurred, so the running conditions of the PTR-TOF-MS were modified once more. The new drift-tube bias was set to 2700 volts, the drift-tube pressure to 7.9 mbar so that E/N was now 150 Td. After recalibration of the drift-tube gauge, it was found that the pressure reading of 8.5 mbar corresponded to a real pressure of 7.9 mbar. The reactant gas flow rate was changed to 53 sccm and the sample flow rate set to 275 sccm.

In the future, it may well be desirable to reduce E/N to the region of 120-130 Td. In order to do that, would entail obtaining a new set of fragmentation data for all the species of interest, and producing a complete set of revised sensitivities for all of them as well. In order to do this, it will be necessary to obtain a new set of in-house calibration standards.

4.6 Troposphere measurements in Leicester

Leicester is a medium size city situated in the Eastern Midlands of England, where levels of traffic have increased significantly in the past decade. Automotive exhaust fumes and other increases in industrial effluent have resulted in a deterioration of the quality of the atmosphere. In this section an experiment is described, which it is hoped will become routine in the future. The aim of the experiment was to measure the hydrocarbon loading of the local atmosphere over an extended period, in this case a week. Over this period, the PTR-TOF-MS ran continuously and without interruption for the week of August 15th to 22nd 2005.

A new inlet line to draw sample air from the exterior had been installed some weeks previously, extending from the laboratory at ground level to the roof of the Chemistry building. Perhaps this location was not ideal as there was the chance of large contributions from the venting chimneys of the department, but since mid-August fell in the summer holiday period, chemical activity in the laboratories had come to a virtual standstill.

4.6.1 Experimental conditions

The ambient temperature in the laboratory was maintained at 23 °C throughout, and the sample air drawn from outside passed through a 5 metre pre-heating tube that was maintained at a controlled temperature of 40 °C and then fed to the PTR-TOF-MS at 275 sccm. The reactant gas consisted of a stream of zero-grade N₂ bubbled through a flask containing 15 MΩ demineralised water and fed into the PTR-TOF-MS at 50 sccm. The flask containing the demineralised water was maintained at a constant 40 °C. The mass flow controllers that regulated the input flow of the reactant and sample gases were connected to the PTR-TOF-MS through PTFE tubes heated to 40 °C.

The PTR-TOF-MS was set up with a mass range of $m/z = 20$ to 143 and otherwise to run under the conditions as were used for the ACCENT Intercomparison held at Jülich as described in Chapter 5. The OVOCs detection sensitivity figures obtained there could be used to convert the observed ncps to ppbv with the assurance that the results would be realistic.

As has become standard practice with the PTR-TOF-MS, data was acquired as a series of one-minute scans, which could later be clustered as required, in this instance into ten-minute groups. It was found that while grouping the scans into one-hour groups, as was done for the TORCH campaign, would certainly improve the statistical error for the groups detected. The use of 10-minute groups allowed sufficiently high counts per peak could be obtained without losing too much information on rapidly changing events.

Estimates of the intrinsic background contribution from the system were obtained using zero-grade nitrogen as the analyte. Background runs were performed before and after the main experiment in runs lasting two and twenty three hours respectively. Data and background counts were normalised to ncps, although the size of the rms errors were based on the their counts before normalisation. The errors were scaled down by the same factor as the data. Data capture commenced in earnest on Monday, August 15th at 09.07 and finished the following Monday at 09.06.

4.6.2 Results

The spectra shown in Figure 4.20 and Figure 4.21 were obtained by summing the entire week's data as well as the background runs and then normalising them. There were strong residual traces from previous experiments in the PTR-TOF-MS.

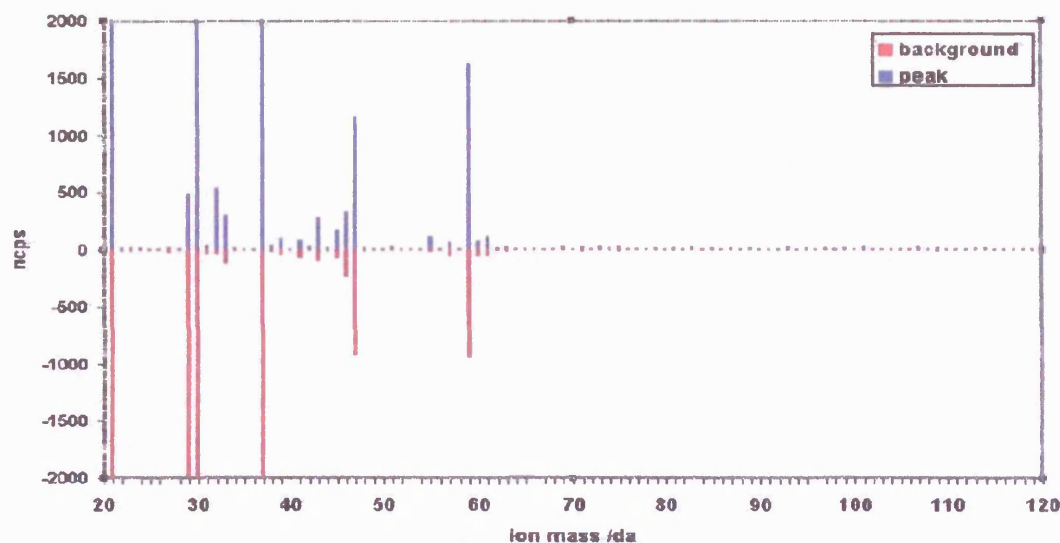


Figure 4.20 Normalised peaks and background traces depicting the more intense groups. Some of the background peaks are due to machine contamination and cannot be ignored.

The yields are shown in two parts, the first one showing the more intense groups lying below $m/z = 60$, and the second part depicting the peaks from the weaker constituents.

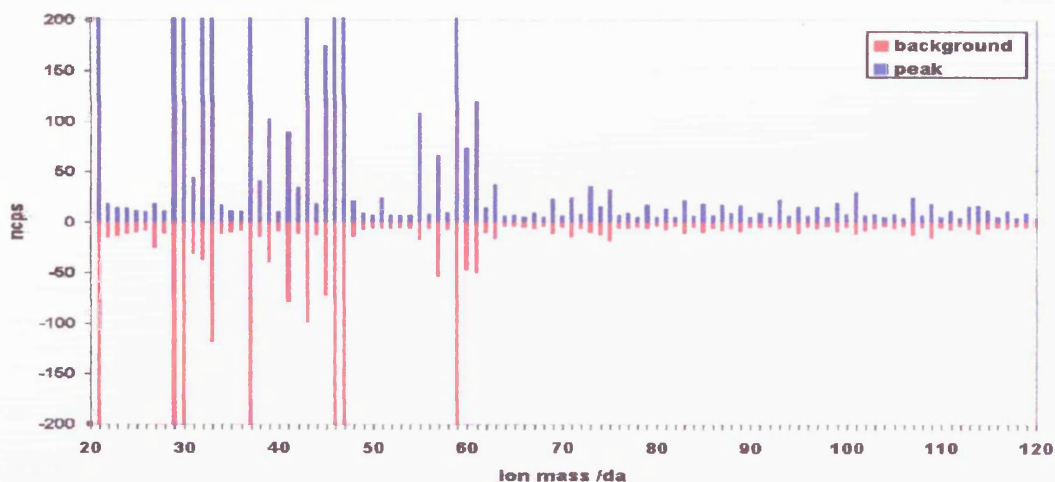


Figure 4.21 Normalised peaks and background traces of the weaker groups. Here the scale of the diagram has been altered to highlight the less intense peaks to show that it is also necessary to compensate for background contributions.

The main purpose of the experiment was to measure the yields of the VOCs and OVOCs detected by the PTR-TOF-MS over the period of the experiment. Several groups were identified unambiguously and their yield curves are shown in Figure 4.22. These are groups whose constituent peaks did not overlap with other peaks and for whom the detection sensitivity data was known (see also Chapter 5 which deals with the ACCENT Intercomparison.).

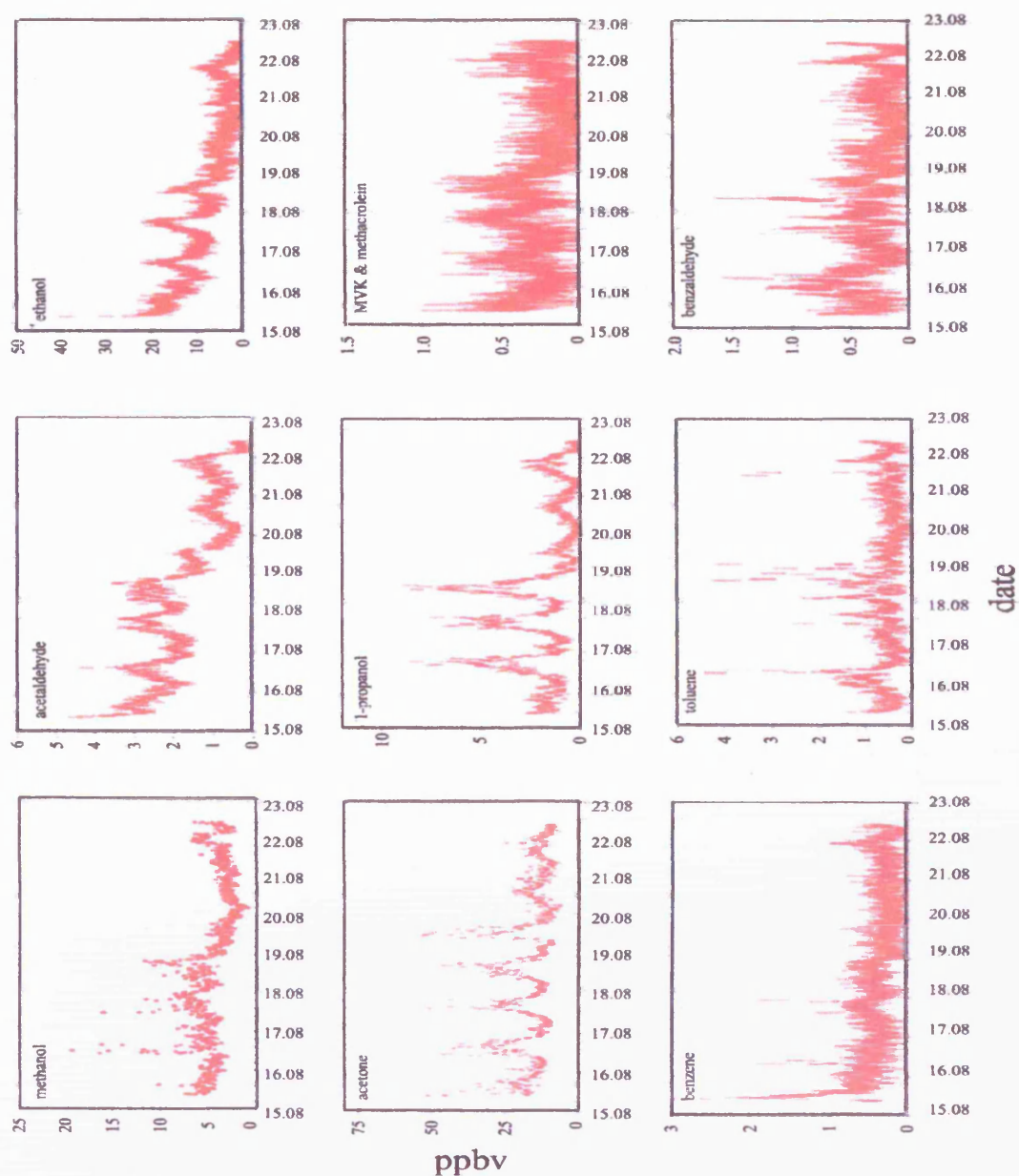


Figure 4.22 Weekly yield of the groups that could be identified unambiguously.

A feature of the yields of the all the groups in the spectrum is the strong dependence on the time of the day. During the weekdays the increase in yield is apparent, as is the much lower level of activity during the weekend, the last two days of the experiment.

Additional yield plots are contained in Figure 4.23. These peaks could not be identified unambiguously, either because there was known to be interference from other peaks, or because no calibration data was available to permit unambiguous identification.

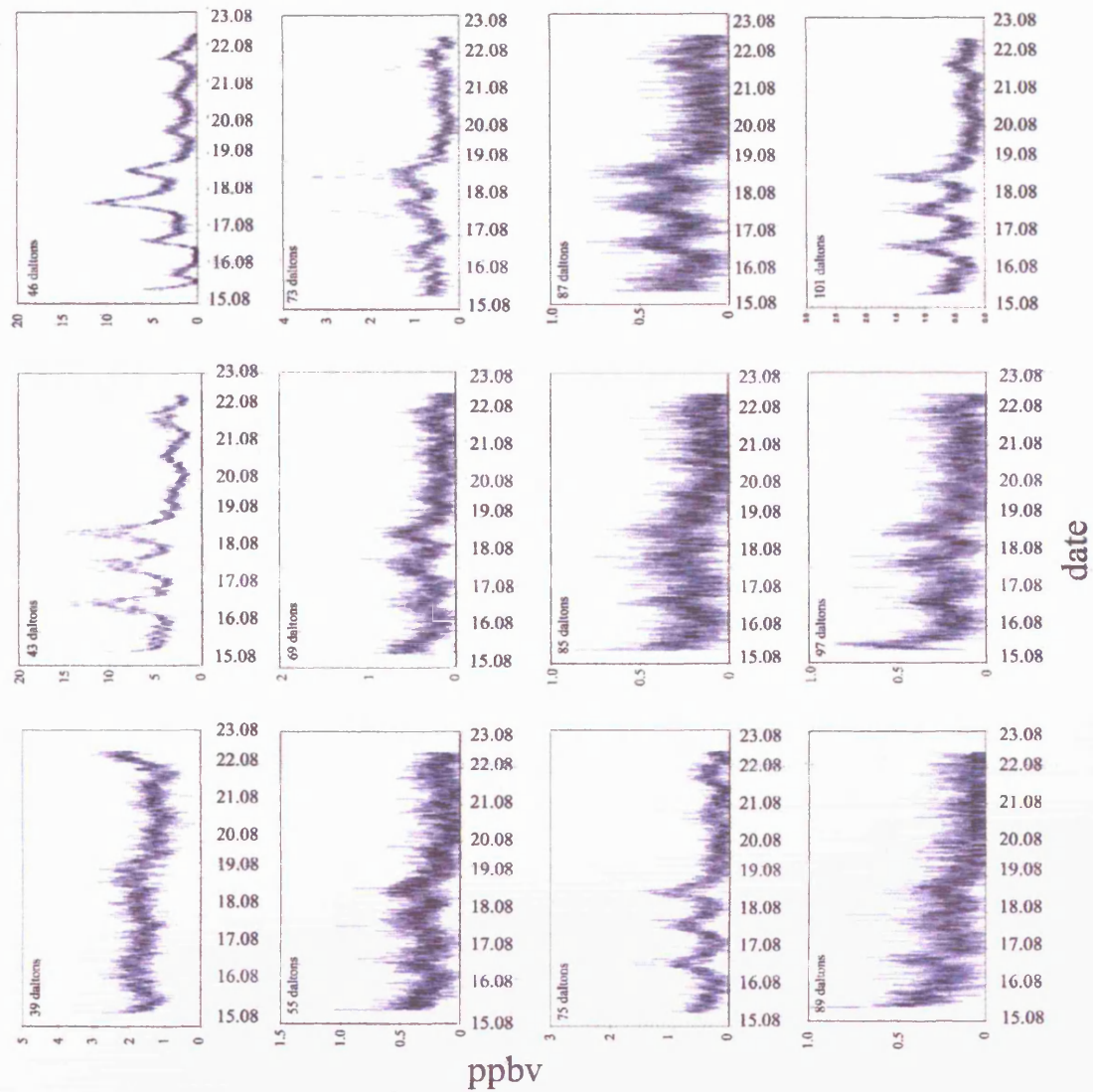


Figure 4.23 Weekly yield of the groups that could not be identified unambiguously.

A default value for the detection sensitivity of $40 \text{ ncps ppbv}^{-1}$ was used to convert normalised counts in these spectra to the more meaningful ppbv. The value chosen was typical of the species tested at Jülich.

4.6.3 Discussion

The fragmentation results obtained in fragmentation experiments (Section 3.14.4, Table A3.1 and A3.2) were used to extract the identities of the species. They cover mainly the target hydrocarbons (Table 1.2), so are far from complete.

From Figure 4.22 it can be seen that methanol, ethanol and acetone showed very high levels of concentration, reaching peak yields of more than 20 ppbv in the case of acetone. These peaks sat on top of large residual peaks, which, if not adequately estimated would result in artificially high concentrations for these species. There could be traces of this effect in the acetaldehyde and ethanol results. By contrast, acetone and methanol showed no signs of such a gradually diminishing background. Benzene, toluene and benzaldehyde and the isobaric twins MVK and methacrolein were easily identifiable as there was no interference in their peaks from other species. The analysis of the species shown in Figure 4.23 is more complicated.

The pronounced diurnal yield peaks and troughs found for all species cannot be explained by residual contamination. Similarly, the weekend reduction in yield would indicate that the peaks are derived from industrial or some other anthropogenic activity, some of which could originate from the Chemistry Department.

The peak found at $m/z = 43$ is known to have contributions from fragment ions from many sources: 1-propanol, acetaldehyde, MVK, methacrolein and 1-butanol, so that it is not possible to assign it a unique identity. The $m/z = 39$ peak is known to be associated with the fragmentation of methacrolein.

The peaks at $m/z = 69$ and 87 are most likely MBO or isoprene species that are emitted by vegetation. They are not very strong groups, occurring at about 300 – 500 pptv, which is not surprising, as there is only a moderate density of vegetation in the immediate vicinity.

The minor group at $m/z = 73$ (approximately 500 pptv) could be due to a minor fragment of butanal, whose major fragment occurs at $m/z = 55$ which it shares with the hydronium cluster $(\text{H}_3\text{O}^+)(\text{H}_2\text{O})_2$. Similarly hexanal which would have a small peak at $m/z = 101$ (1.3%) and a strong peak at $m/z = 55$ (42%) does not fit the observed peak

strengths. Since both the $m/z = 55$ and 101 peaks are of similar magnitude, we can conclude that little if any hexanal is present.

The weak peak at $m/z = 75$ (200 – 1000 pptv) could be assigned to methyl acetate, but it is not known whether there are other contributing groups present here. The remaining groups could not be identified with certainty.

4.6.4 Gas Chromatography simulation

Gas Chromatography (GC) is a particularly powerful technique for identifying VOCs and OVOCs in the troposphere. The technique is able to identify isobaric doublets and other species where PTR do not perform satisfactorily. In comparison with the PTR implementations, GC is slow. Typically in any hour of observation, samples of the troposphere are gathered for a period of 5 minutes, and the GC spends the remaining 55 minutes processing the data to produce a result. PTR devices and the PTR-TOF-MS in particular are better at recording transitory fluctuations in species concentration than any GC device. This feature can be demonstrated by a simulation exercise using the 10-minute groups for some of the compounds studied here.

To simulate the behaviour of the GC, one out of six points of a PTR-TOF-MS plot were chosen to represent GC data and highlighted on the PTR-TOF-MS plot. The fact that 10-minute samples are used instead of 5-minute ones does not diminish the point of the simulation, which is to demonstrate while GC does in fact give a good representation of the average activity in the troposphere, it can miss out on some interesting transient variations.

Three examples of OVOC were chosen to demonstrate the effect: methanol, acetone and 1-propanol. In the left hand panels of Figure 4.24 the weekly spectra are shown with the simulated GC data shown in blue on top of the PTR-TOF-MS data which is in red. In the panels on the right hand side of the figure, the activity of the two midweek days are magnified, to demonstrate the difference in detection ability, while at the same time confirming the value of the GC technique.

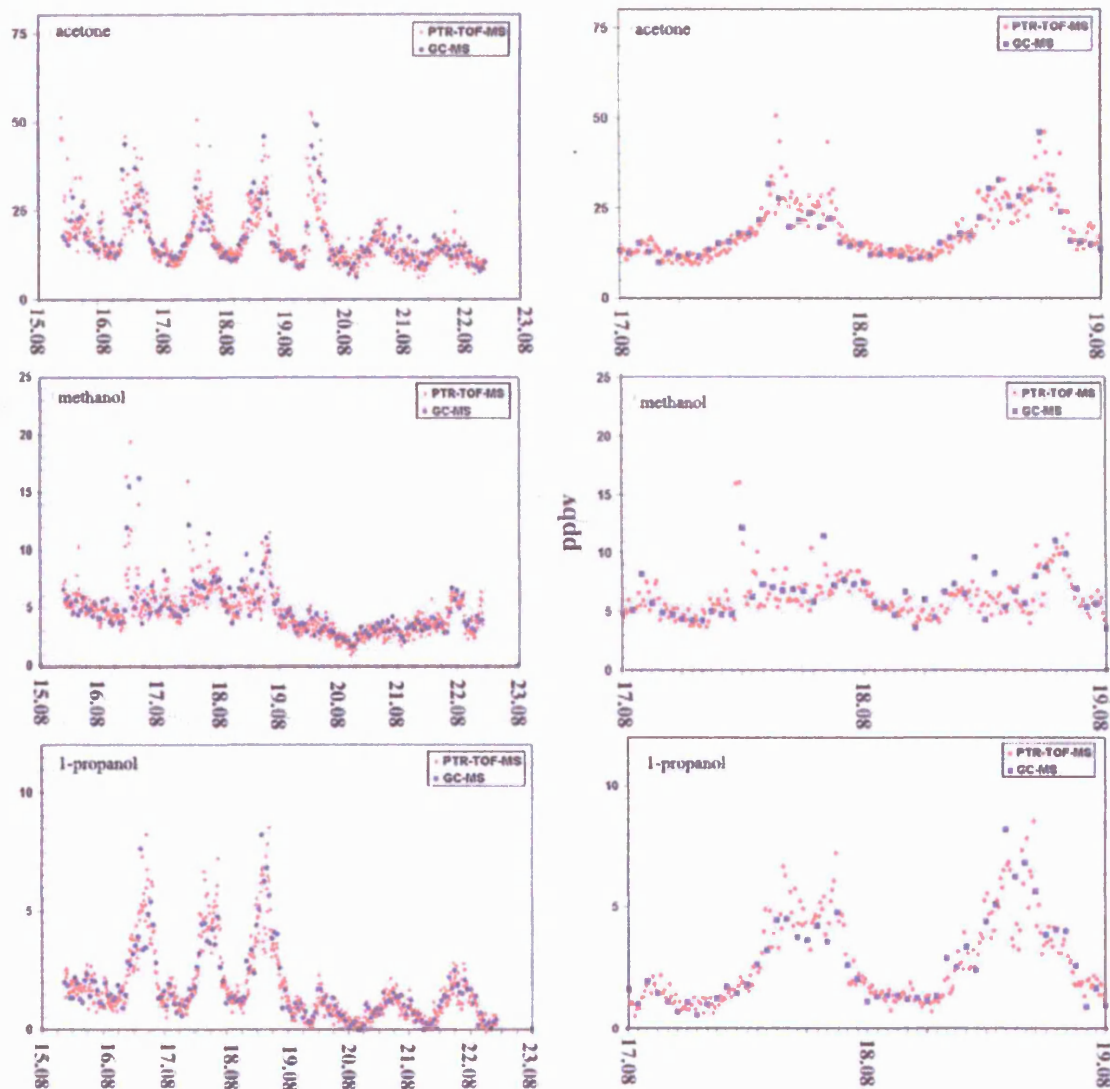


Figure 4.24 Superimposed plots of the PTR-TOF-MS yield curves for three OVOCs chosen at random, and plots representing the response from a simulated GC-MS. The diagrams on the left show the results for a whole week and those on the right the results for two midweek days.

4.7 Summary

The PTR-TOF-MS has demonstrated its worth as a versatile research tool because of the unique characteristics it offers the experimenter. Its mass resolution far exceeds that of any commercially available quadrupole-based PTR-MS and the detection of ppbv levels of selected VOCs and OVOCs are attainable often in less than a minute. For sample times of 10 minutes it was found that the equipment is capable of unambiguously detecting levels in the 200 – 500 pptv range.

However the primary advantage is the PTR-TOF-MS's ability to perform multichannel data acquisition permitting simultaneous data capture across the entire mass range. It will allow study of the complex interplay between many trace gas components to be determined in real-time measurements.

This chapter has traced the development of the PTR-TOF-MS from the time when it first started to monitor the troposphere to the present. In that time many lessons were learnt on how to improve the performance of the equipment, and in the final experiment it has been shown to be a capable device, well equipped to perform its duty as a member of the Atmospheric Science Group at Leicester University.

The next chapter covers the ACCENT Intercomparison campaign held at Jülich, Germany in January 2005. Chronologically it should be slotted in between the TORCH campaign and the Leicester atmospheric experiment, but due to the importance the intercomparison exercise played in defining the capabilities of the PTR-TOF-MS, an entire chapter is devoted to the campaign.

Chapter 5

The ACCENT Intercomparison campaign

Jülich, Germany, January 24th – 28th 2005

It's true hard work never killed anybody,

but I figure, why take the chance?

Ronald Reagan (1911 – 2004)

...

.

5 The ACCENT OVOC Intercomparison

5.1 ACCENT



5.1.1 The Aims of ACCENT

ACCENT, an acronym of Atmospheric Chemical Change the European NetWork of excellence, is a pan-European research endeavour covering every aspect of research into the atmosphere. ACCENT covers several fields of investigation and for each of these, there are many participants, from all over Europe (in and out of the EU) using a variety of different techniques.

In order to maintain the interchangeability of data, it is necessary to stage Quality Assurance Intercomparison campaigns for the various interest groups falling under the ACCENT banner. Participating groups gather to perform measurements on a common set of phenomena, compare the results and establish a common basis for data exchange. The campaign described in this chapter was a formal blind intercomparison in which twelve groups took part and which was supervised by an independent referee.

The opening paragraph of the Accent Workshop Protocol dated October 2004 sets out the aims of the work described in this chapter:

The frame of the intercomparison:

For various fiscal reasons, the implementation of the OVOC intercomparison had to be finished before February 2005 because of the demands of ACCENT. Comparable intercomparisons (AMOHA, NOMHICE) began with only few compounds and expanded over 4 to 5 years to more complex mixtures. Since it is the first OVOC intercomparison

and there are only four months left for the set up, the OVOC intercomparison is aimed to be basic and “simple” in the sense of a quality assurance of “less is more”.

5.1.2 Initial workshop

An initial planning workshop was held at the Jülich Research Centre, near Jülich, North Rhine Westphalia, Germany on October 12th and 13th 2004. This was the first time all the potential participants could meet and discuss matters of mutual interest including the selection of target OVOCs for the intercomparison. The participating groups employed a wide variety of techniques.

Proton Transfer Reaction (PTR) Mass spectrometry:

- University of Leicester
- Federal Atmospheric Laboratory Agroscope, Zürich, Switzerland (FAL)
- University of Innsbruck, Austria
- Forschungszentrum Jülich, Germany

Gas chromatography:

- University of Bristol
- University of York
- FAL Agroscope
- Swiss Federal Laboratory for Material Testing and Research, Switzerland (EMPA)
- Forschungszentrum Karlsruhe – IFU, Germany
- Forschungszentrum Jülich, Germany

Off-line techniques (cartridges and solid phase micro extraction):

- Institut für Troposphärenforschung, Germany
- Norsk Institutt for Luftforskning, Norway (NILU)
- Fundación Centro de Estudios Ambientales del Mediterráneo, Spain (CEAM)

Hantsch method formaldehyde estimation:

- University of Bremen, Germany
- Forschungszentrum Jülich, Germany
- Forschungszentrum Karlsruhe – IFU, Germany

Finally, the Forschungszentrum Jülich also conducted some DOAS work.

Of the three UK participating groups, the Universities of York and Bristol used GC-FID and GC-MS equipment. The third member, Leicester proposed the use of PTR-TOF-MS.

With the exception of the Leicester entry, the PTR devices were quadrupole-based PTR-MS supplied by Ionicon, an Austrian company based in Innsbruck.

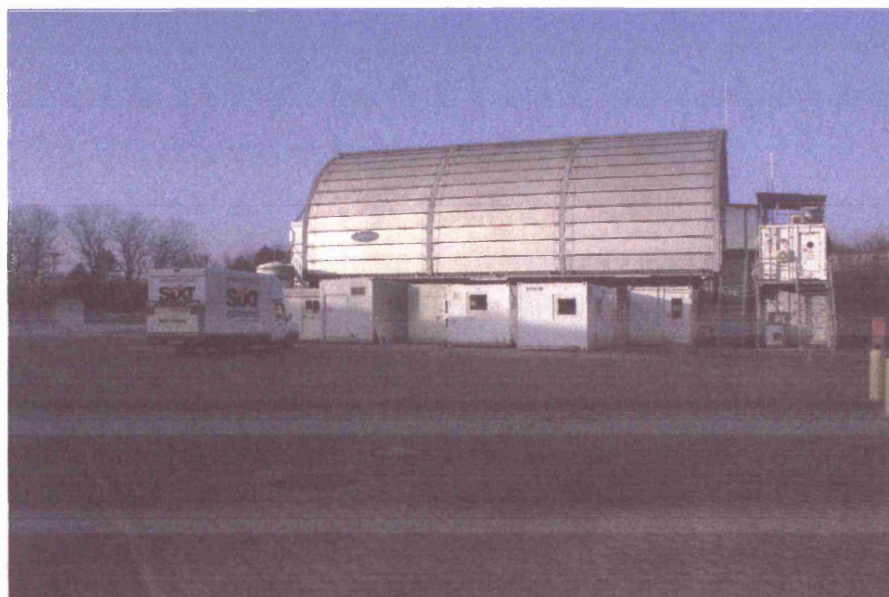


Figure 5.1 The SAPHIR facility at the Jülich Research Centre, Germany.

The intercomparison was held at the Jülich Research Centre situated near Jülich, Germany. The SAPHIR chamber at Jülich is particularly suited for this type of work. It consists of a 300 m³ PTFE bag into which gas of controlled composition can be introduced and fed to experimenters through a series of manifolds. The bag is housed in a large structure (Figure 5.1) with shutters which can be opened to the sky if required. There is sufficient space beneath the bag to permit full size containers, holding the groups' experiments, to park underneath the installation. The bag could not be heated, which limited its operating environment to that determined by the ambient temperature. Ultra-pure nitrogen (N7.0) and oxygen stored in large tanks to one side are used to create the artificial atmospheric environment to order.

5.1.3 The Target OVOCs

The following extract (see also Table 1.2) from the Accent Workshop Protocol summarises the rationale for the choice of target compounds thus:

“Because of their major importance formaldehyde, acetaldehyde, methacrolein, methyl vinyl ketone (MVK), methanol, ethanol, acetone, and 2-methyl-3-buten-2-ol(MBO) should be included in the list. Furthermore, formaldehyde can be measured by DOAS. The alcohols 1-propanol and 1-butanol, and benzaldehyde will be measured too.

Some compounds were excluded because they complicate the measurements of other compounds with the PTR-MS. Propanal, pentanal, and 2-propanol interfere with acetone, MBO and 1-propanol, respectively.

High boiling compounds like heptanal, octanal, and acetic acid butyl ester may condense on the cold surface of the SAPHIR chamber during winter measurements and were excluded. Butanal might cause problems in PTR-MS when measuring other aldehydes and was excluded, too.

Glyoxal, methylglyoxal, butanedial, 4-oxo-pentanal, hydroxyacetone, verbenone, and α -terpineol can only be measured by few participants and were excluded from the component list.

Eucalyptol is only of minor importance in atmospheric chemistry and will not be measured too. To monitor the dilution of the mixture by the experiment flow through the chamber butane and toluene will be added because they can be measured by most of the groups.”

The final list of compounds that were to be intercompared are listed in Table 5.1

Table 5.1 List of target compounds for the Jülich intercomparison. The reaction rate coefficients (at 300° K) for H₃O⁺ as the reagent ion are taken from [Lindinger *et al.*, 1998], [Zhou and Zhang, 2004] and [Ennis, 2004].

Species	Mass /da	Rate coefficient <i>k</i> 10 ⁻⁹ cm ³ s ⁻¹
methanol	32	2.33
acetaldehyde	44	3.36
acetone	58	3.00
1-propanol	60	2.47
MVK	70	3.83
methacrolein	70	3.53
butanal	72	3.49
methyl acetate	74	-
1-butanol	74	2.47
MBO	86	3.40
toluene	92	2.12
hexanal	100	3.74
benzaldehyde	106	4.12

Due to the differing detection abilities of each technique, it was unlikely that all the groups would be able to measure all the components of the proposed mixture. So, for example while butane was included in the mixture for those groups interested in measuring alkanes, it was not included in the list of Leicester target species. PTR devices are insensitive to alkanes so that other approaches such as Gas Chromatography are used to detect their presence in mixtures.

5.1.4 Experimental protocol

“Design of the experiments:

For all experiments the construction of the SAPHIR chamber has to be taken into account: Complete mixing of compounds injected into the chamber takes about 30 min. During this time concentration gradients in different parts of the chamber are possible. Furthermore, to avoid concentration gradients owing to high flow rates it was decided to measure at discrete concentration plateaus.

As the minimum individual analytical cycling time for some systems is 1 hour (GC systems), the time for a concentration plateau should not be less than 3 hours. A possible time schedule for an experiment includes one hour of equilibration after addition of compounds, 3 hours of measurements at a concentration plateau, and one hour of dilution and stabilisation at a new concentration level. These phases (measurements and dilution) will be repeated three times the day. The total experiment is then approx. 12 hours. Mixing ratios of circa 6, 2, and 0.6 ppbV denoted as concentration plateaus was accepted by all groups.”

The intercomparison would be refereed by Eric Apel, of UCAR, Boulder, Co, USA, an acknowledged expert in the field of gas mixtures.

5.1.5 The timetable for the intercomparison

The planned order of the experiments is shown in Figure 5.2. The participating groups could start to install their equipment a week before the official start of the intercomparison. The first day of the official intercomparison was Monday January 24th, and experiments were for five days until January 28th. One day was allowed to dismantle the equipment.

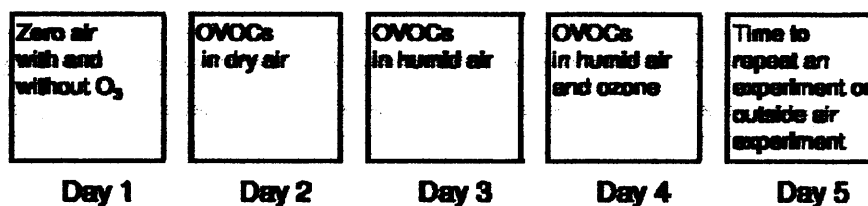


Figure 5.2 Proposed order of the intercomparison campaign.

During the night prior to each day's experimental runs, SAPHIR was flushed with synthetic air to remove all traces of the previous day's run. It was planned to conduct five experiments.

On the morning of the first day SAPHIR was filled with dry synthetic air, for the first part of the day's experiment. For the second stage, water vapour was injected to create a moist atmosphere to test the response of the experimental equipment to increased

humidity in the sample gas. Finally ozone was added to the mixture for the last part of the first day's experiment.

After the initial start-up procedure each day a new mixture of OVOCs was introduced into SAPHIR, and after an initial period to allow thorough mixing, the experiments started. The slope in the OVOCs yield seen in Figure 5.3 arose from the fact that as all the groups were drawing about 40 litres a minute of the gas mixture from SAPHIR, the loss was made good by adding synthetic air to prevent the SAPHIR envelope from collapse. In so doing, the OVOCs concentration declined slowly, approximately 10 – 15% for a three hour session.

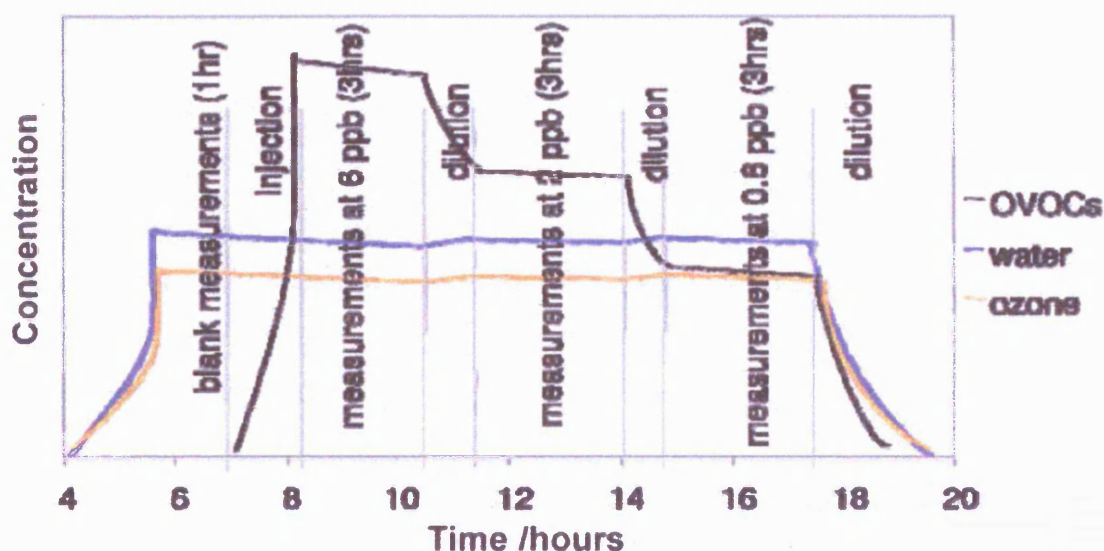


Figure 5.3 Typical behaviour of the OVOC concentration from SAPHIR as a function of time. The coloured lines indicate the presence of humidity and ozone. The diagram, taken from the ACCENT descriptive material, is not to any scale and is purely illustrative of the process.

On day 2, the first part of the experiment consisted of experiments with dry air. Initially SAPHIR was filled with synthetic air, and a mixture of OVOCs was introduced and after allowing an hour for the mixture to gain equilibrium the experiments commenced. After about two hours, the mixture was diluted by bleeding a part of the existing gas from SAPHIR and replacing it with synthetic air, to obtain the desired dilution. Additional selected OVOCs could also be introduced so that the dilution rates of the OVOCs differed. The dilution procedure was repeated once more after a two hour sampling

period for the second stage was complete, so that concentrations of some constituents fell to below 1 ppbv.

The experiment on day 3 followed the same procedure as day 2, except that water vapour was introduced into SAPHIR along with the OVOC mixture. Day 4 was similar except that ozone was added in addition to the water vapour and the OVOCs.

Day 5 offered the groups the opportunity to repeat the experiment, using the Jülich atmosphere as sample. In the first session, the SAPHIR envelope was filled from the surrounding atmosphere and no additional substances were added, while for the second session, a random mixture of OVOCs was added to the gas already in SAPHIR. There was no third session.

5.2 Logistics

Transporting the PTR-TOF-MS to Jülich was not straight forward and special arrangements had to be made to transport the equipment back and forth from Leicester. The radioactive source was shipped separately, and the remaining equipment was transported by members of the Leicester group in a hired van with a hydraulic tail-lift to help with loading heavy equipment.

5.3 The installation at Jülich

The PTR-TOF-MS was allocated space on one side of one of the customised containers which fitted under SAPHIR Figure 5.4.

5.3.1 Container

The experiments which drew input from SAPHIR could be housed in specialised containers which moved on rails and which could be moved under SAPHIR to gain access to the gas inlet manifolds. The containers were air conditioned and sufficient electric power was available inside to supply the 240V 20A current which the PTR-TOF-MS needs.

Two other experiments shared the container with the PTR-TOF-MS. Both of them required ovens, for their GC work, so that at times the air conditioner had trouble coping. However, a thermometer mounted on the PTR-TOF-MS showed that the temperature

rose by 3 °C at the most. The main instrument and its control computer fitted into the container, but all the tools, books and spare parts were kept stored in the back of the van for the duration of the experiment. The van also served for personal transportation for the period.



Figure 5.4 PTR-TOF-MS in its container shared with two other groups.

Two other groups with Gas Chromatography systems occupied the other side of the container. Space was adequate for all the equipment, although it was difficult to move around freely

The container was air conditioned, and had ample power plugs. A thermometer was taped to the body of the PTR-TOF-MS to monitor the temperature inside the container.

5.3.2 Connection to the inlet manifolds

Each container had a manifold mounted in the ceiling with user connections to SAPHIR. Users were offered a choice of sizes, the most favoured of which was 1/4" Swagelok. A valve on the connection could be closed to isolate a user or unused connection from SAPHIR. The carrier gas for the OVOCs was fed from SAPHIR via this manifold. The PTR-TOF-MS required a constant supply of N₂ with purity N7.0, and this was drawn from the liquid nitrogen supply which also supplied SAPHIR.

Two heated lines both 5.0 m long were used for the connections, one for the sample gas and the other for the nitrogen fed into a heated bubbler which supplied the PTR-TOF-MS with the reactant mixture. The lines were specially created for the ACCENT campaign with the extra heated lengths of pipeline to bring the inlet gases up to the PTR-TOF-MS operating temperature of 40 °C.

5.3.3 Radiation check

During the course of the TORCH campaign at Weybourne, concern over the radioactive source resulted in a severe disruption in the operation of the PTR-TOF-MS. Since people in the experimental container would be working in close proximity to the source, it was decided that it should be tested for potential harmful effects. The radiological department conducted their tests and proclaimed the source to be adequately shielded.

5.4 Calibration

Calculating the concentration of the OVOCs used in the intercomparison requires knowledge of the sensitivity of the PTR-TOF-MS expressed as ncps ppbv⁻¹ for each of the species used. To arrive at a figure it is necessary to measure the response of the equipment when sampling a mixture of known composition, and use the fragmentation profiles for each component to identify the peaks obtained in the resulting spectra. Chapter 3, Section 3.14 describes experiments to determine the fragmentation behaviour of several OVOCs including the species used here. The data obtained in Jülich was used in combination with fragmentation data (Section 3.14.6) to arrive at a set of sensitivities for the PTR-TOF-MS in ncps ppbv⁻¹.

There were two species, benzaldehyde and methyl acetate, for which it was not possible to obtain measured sensitivities, so assumed values were used derived from the published reaction rates for Benzaldehyde [Zhou and Zhang, 2004], or an assumed value for the reaction rate coefficient k of $3.0 \times 10^{-9} \text{ cm}^3 \text{ s}^{-1}$ for methyl acetate. The predictions turned out to be surprisingly good, but where measured sensitivities were available, the results were even better.

5.4.1 The Bristol / Apel standard

The University of Bristol group used a calibration source obtained from Apel/Riemert Incorporated in the USA and agreed for it to be used for one of the two main calibration sessions.

Table 5.2 Constituents of the Apel/Bristol calibration gas mixture.

OVOC	Mass /da	ppbv
methanol	32	522
acetaldehyde	44	453
ethanol	46	542
acrolein	55	468
Butane	58	548
propanal	58	480
acetone	58	536
1-propanol	60	532
methacrolein	70	432
MVK	70	511
butanal	72	504
MEK	73	510
1-butanol	74	491
MBO	86	540
1-butanol	74	491
pentanal	86	481
hexanal	100	476

The constituents of the gas are shown in Table 5.2 and the trace of the data accumulated during the session is shown in Figure 5.5. Thirty minutes of data was gathered from the calibration cylinder. The resulting data was summed and normalised to a hydronium count rate of 10^6 counts s^{-1} . Some of the species supplied in the standard were not present in the ACCENT intercomparison experiment, so that the overlap of acetone and propanal was avoided, but MVK and methacrolein were both present in the standard as well as in the ACCENT mixtures

5.4.2 Spectrum

When operating at an E/N of 150 Td, some fragmentation of the protonated parent species is expected, and daughter fragments from different parents can have the same mass as well. This is not surprising since when a molecule fractures, it is likely to break along lines determined by the basic structure of the parent molecule, and some fragments are more likely than others.

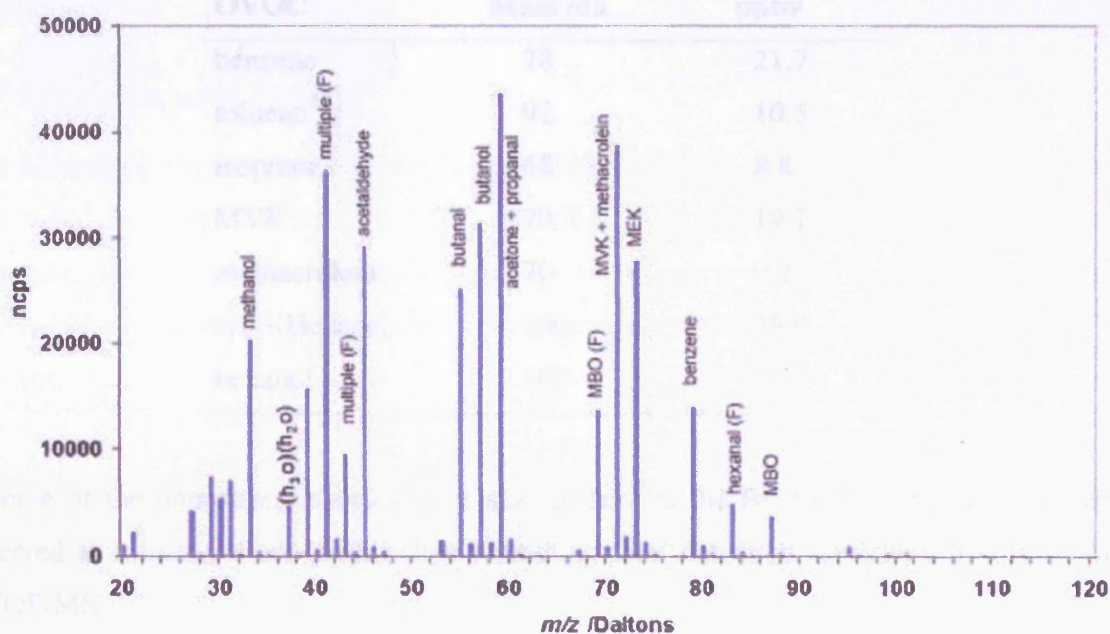


Figure 5.5 Spectrum of Bristol / Apel gas standard. A background spectrum has been subtracted so that the hydrated hydronium peak peak at $m/z = 37$ is small.

This situation is marked in the high $m/z = 30 - 40$ range, where the peaks have several offspring. Useful information can still be extracted from peaks consisting of overlapping groups, providing the components can be associated with non-overlapping peaks elsewhere in the spectrum. Several examples can be found in Table A3.1, especially for

the $m/z = 43$ group which contains 2 major component fragments from acetaldehyde and 1-propanol accounting for about 78% of the peak, and MVK, methacrolein, butanal and methyl acetate contributing to the remaining 22%.

Where the fragmentation patterns are known, it is possible to calculate the contribution of each compound to the overlapping peak and a composite peak can be partitioned between the contributing species. The Bristol/Apel standard provided the most detailed calibration data for the PTR-TOF-MS used to date.

5.4.3 Federal Atmospheric Laboratory (FAL)

The group from FAL had the means to manufacture standard OVOC mixtures using outside air or synthetic air as a carrier.

Table 5.3 FAL synthetic calibration mixture.

OVOC	Mass /da	ppbv
benzene	78	21.7
toluene	92	10.5
isoprene	68	8.8
MVK	70	19.1
methacrolein	70	9.2
cis-3-Hexanal	100	39.9
hexanol	102	19.5

Some of the component species were also present in the Bristol/Apel standard, which served as a useful cross-check when extracting their detection sensitivity by the PTR-TOF-MS.

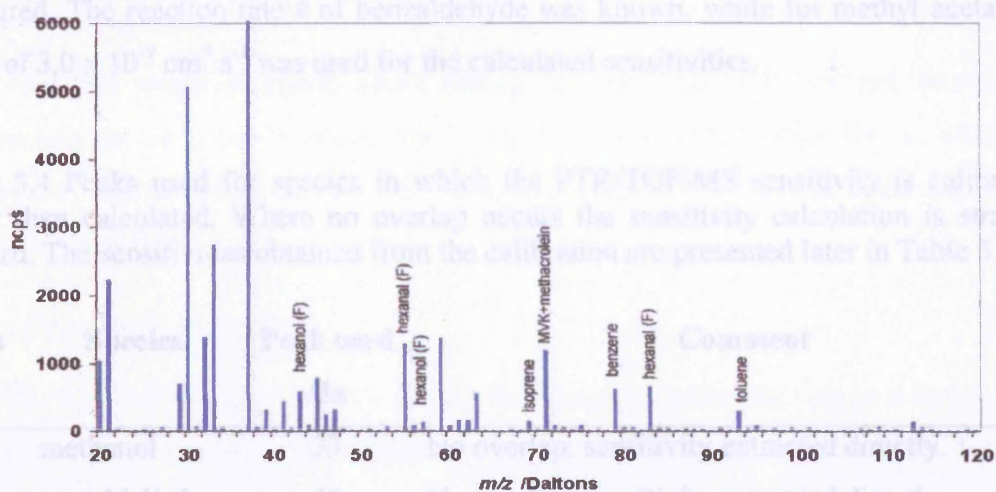


Figure 5.6 Trace taken from the FAL gas standard.

The mass spectrum is shown in Figure 5.6. There are signs of substantial fragmentation, but the peaks of interest – toluene, benzene, MVK + methacrolein are clearly defined.

5.4.4 Calibration factors

In Chapter 3 the sensitivity results for the PTR-TOF-MS are reported. The results are obtained from the calibration studies described here. As mentioned in the previous section, the species in the FAL standard served as a useful cross-check for the Apel/Bristol standard, but the OVOC concentration was about 2 orders of magnitude lower.

In the limited period in which the FAL standard could be used, the statistical errors of the peaks were greater than those obtained with the Apel/Bristol standard.

Table 5.4 contains comments on the properties of the compounds present in the Apel/Bristol standard, and the ease with which calibration figures could be obtained. When the only useful peak for a particular compound overlaps with other peaks, it is necessary to eliminate the contributions from the interfering peaks. The fragmentation data can be used to estimate the relative intensity of the interfering ion at the mass channel under investigation.

In the case of benzaldehyde and methyl acetate, no standard mixture was available, so that the sensitivity of the PTR-TOF-MS was calculated using Equation 3.11 and not

measured. The reaction rate k of benzaldehyde was known, while for methyl acetate, a value of $3.0 \times 10^{-9} \text{ cm}^3 \text{ s}^{-1}$ was used for the calculated sensitivities.

Table 5.4 Peaks used for species in which the PTR-TOF-MS sensitivity is calibrated rather than calculated. Where no overlap occurs the sensitivity calculation is straight forward. The sensitivities obtained from the calibration are presented later in Table 5.5.

Mass /da	Species	Peak used /da	Comment
32	methanol	33	No overlap; sensitivity extracted directly.
44	acetaldehyde	45	No overlap; sensitivity extracted directly.
46	ethanol	47	Not reported due to low intensity.
58	acetone propanal	59	Isobaric; normally reported together. For ACCENT, propanal was not used.
60	1-propanol	41 43	Yield obtained by subtracting contribution from interfering peak.
70	MVK methacrolein	71	Isobaric; normally reported together. Excellent agreement between Bristol/Apel and FAL
72	MEK	73	No overlap but not used in ACCENT
72	butanal	55	No overlap. Potential interference from hydronium di-hydrate negligible.
74	1-butanol	57	No overlap. Sensitivity extracted directly.
78	benzene	79	No overlap. Good agreement between Bristol/Apel and FAL. Not used in ACCENT.
86	MBO	87, 69	No overlap. Good agreement of sensitivity using either peak as base.
92	toluene	93	No overlap. Sensitivity extracted directly.
100	hexanal	83	No overlap. Sensitivity extracted directly.

The measured sensitivities are tabulated in Table 3.7 in Chapter 3 while Table 5.4 lists the actual peaks used for the sensitivity measurements and comments on the procedure used to calculate detection sensitivities.

5.5 Experimental

After the first week at Jülich spent setting up the PTR-TOF-MS and running it continuously to let it settle down, the intercomparison started officially on Monday, January 24th and ended on January 28th. The PTR-TOF-MS performed without incident for the entire period.

5.5.1 Continuous running

The PTR-TOF-MS ran continuously during the campaign gathering data in a series of 1-minute runs (1440 per day). This allowed flexibility in the choice of number and duration of the sampling periods.

5.5.2 Temperature control

To avoid the problems associated with large temperature swings such as those experienced at Weybourne, the drift-tube and all the inlets were held at a constant 40 °C. The container in which the PTR-TOF-MS was situated, had an air conditioner, which managed to restrain the ambient temperature range to 21°C to 24°C.

5.5.3 Ongoing data processing

Data captured was written to a CD after each session, while SAPHIR was being readied for the next stage of dilution. The captured data was processed offline.

First a recalibration program processed the data to ensure that time of flight shifts in the data were rectified. At Weybourne these shifts were first noticed when peaks appeared to move by as much as $m/z = 0.5$ during periods of extreme of the ambient temperature. The post-processing software re-aligns peaks in a spectrum, so that peaks of a particular mass all occupy the same mass channel.

Three 40-minute samples were chosen from the newly processed data, summed and scaled to 10^6 hydronium counts per second. For the lower concentration runs longer sample times were used since the OVOC concentration was allowed to diminish slowly until 22.00. SAPHIR was flushed early the following morning to ready it for the next day's experiment.

The same recalibration and normalising procedure was performed on the daily background data (the acquisition procedure for the background data is described in Section 5.6.3).

The normalised background was subtracted from the normalised data for each of the three sample runs. For some mass channels (particularly methanol and acetone) the contribution of the background was significant. The error for each mass channel was taken to be

$$E = (a^2 + b^2)^{1/2} \quad (5.1)$$

where a is the sample count and b is the background count at the same channel.

5.6 Results

5.6.1 Diurnal variation in the hydronium count rate

Apart from the straight-line decrease in the hydronium count rate due to contamination build-up, a cyclic component was still present despite efforts to eliminate the variation entirely. However if only the hydronium yield variation is considered for the time that data was actually gathered (Figure 5.8), then the variation drops to 2.0%.

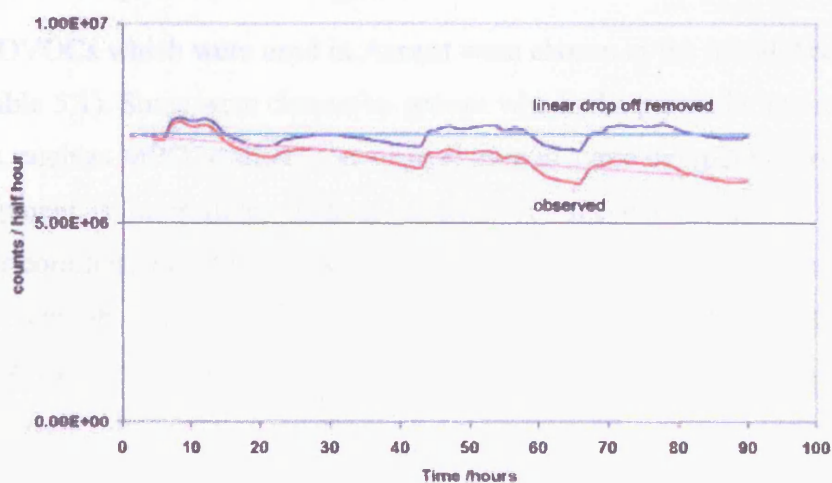


Figure 5.7 Variation in the hydronium count rate for duration of the ACCENT campaign. The lower curve depicts the experimentally observe hydronium count rate, which contains a long term linear component of the decrease in the source output as it gets dirty. In the upper curve the long term component has been removed leaving the short term yield variability.

The diurnal temperature-dependent yield variation of the hydronium yield observed during the TORCH campaign (Section 4.5.4) was 5.4%. For ACCENT the variation was found to be about 5% for the entire period of the data gathering week (Figure 5.7).

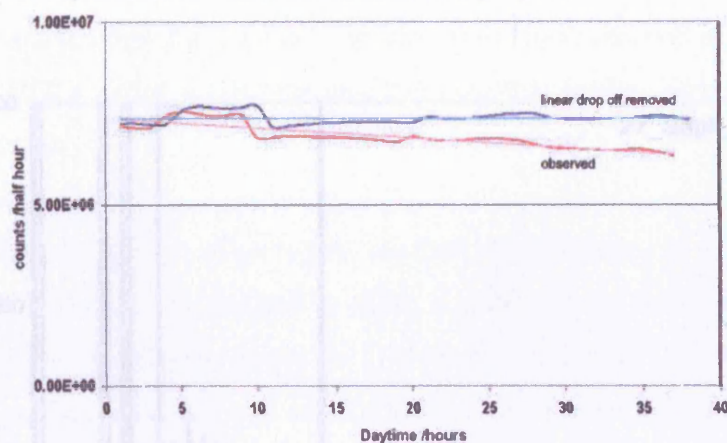


Figure 5.8 Variation in the daytime hydronium count rate for the ACCENT campaign. The lower curve represents observed data, but as the x-axis represents running time rather than true elapsed time, the slope of the long-term component is artificially exaggerated. In the upper curve the long-term component has been removed to isolate the short term yield variability.

5.6.2 List of compounds investigated

The list of OVOCs which were used in Accent were chosen at the initial Accent meeting in 2004 (Table 5.1). Some were chosen by groups who had a particular interest in certain compounds, such as MBO, while others were chosen to avoid compounds to which PTR-based equipment is insensitive, such as alkanes. All the equipment using PTR have known shortcomings, low to zero sensitivity to alcohols and alkanes, as well as an inability to separate compounds with the same m/z such as acetone and propanal or Methyl Vinyl Ketone (MVK) and methacrolein. It was also clear that no group was likely to report results for the whole range of OVOCs.

5.6.3 Background

The first official day of the intercomparison was set aside to allow the participants to measure the response of their equipment using a carrier gas with all the target compounds absent. There were three measuring sessions.

In principle, this series of experiments was intended to provide the participants with a set of base-line data, which could be used in the following days when the OVOCs mixtures were introduced into Saphir. Unfortunately, several serious leaks occurred which rendered the first day's data useless for the intended purpose.

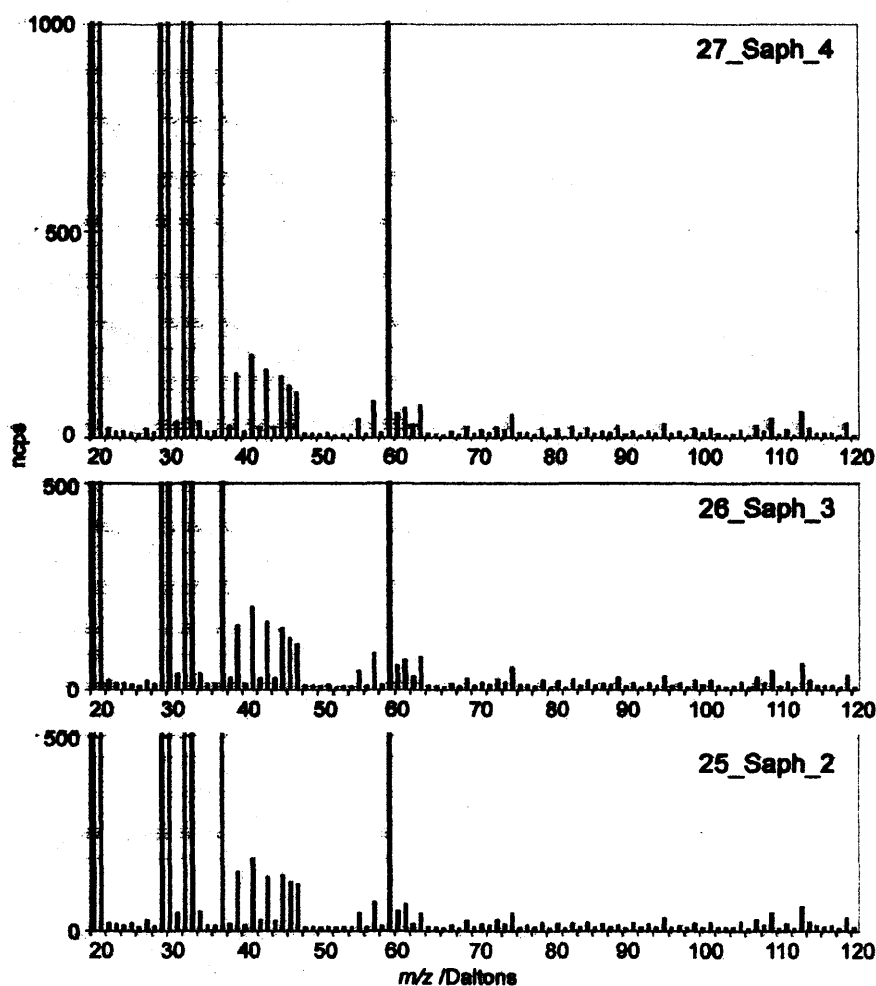


Figure 5.9 Normalised background spectra for the main measurement days January 25th to 27th 2005

As an alternative, it was decided to use the data gathered each day prior to OVOCs injection as the baseline for that day. Since the PTR-TOF-MS was running continuously, it was easy to choose data starting from the early morning period, when Saphir had been flushed in preparation for the day. The sampling periods for the 25th, 26th and 27th January were 42, 38 and 28 minutes respectively. While it would have been preferable to take more samples, the sample times used were chosen to be comparable to the sample times used for the data acquisition runs on that day. Figure 5.9 shows the background

counts traces taken on January 25th to 27th. The background contribution was quite high for some masses. The similarity in the spectra from day to day, suggests that the background spectra may be due to contamination in the PTR-TOF-MS.

On the 28th January, the first session sampled the local Jülich air, so that there was no sample to use as a baseline for the day. The second session consisted of the local air with a mixture of OVOCs added, so that the data from the first session served as the base-line data for the second.

At the end of the last session of each day, the OVOC concentration was left to diminish slowly until the chamber was flushed to make it ready for the following day. Since the flushing operation only took place in the early hours of the morning, OVOC concentration gradually fell but was initially higher than the background count registered at the start of each day.

5.6.4 Yield spectra

A quick way to demonstrate the successive dilution in OVOCs concentration is to stack the normalised spectra for a day's run as shown in Figure 5.10, where the most prominent peaks are identified to aid interpretation.

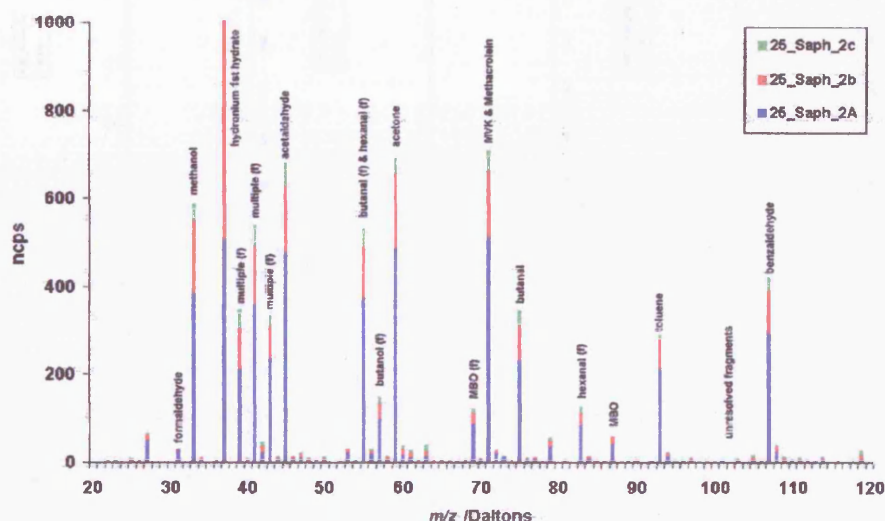


Figure 5.10 Stacked spectra for the three sessions of January 25th.

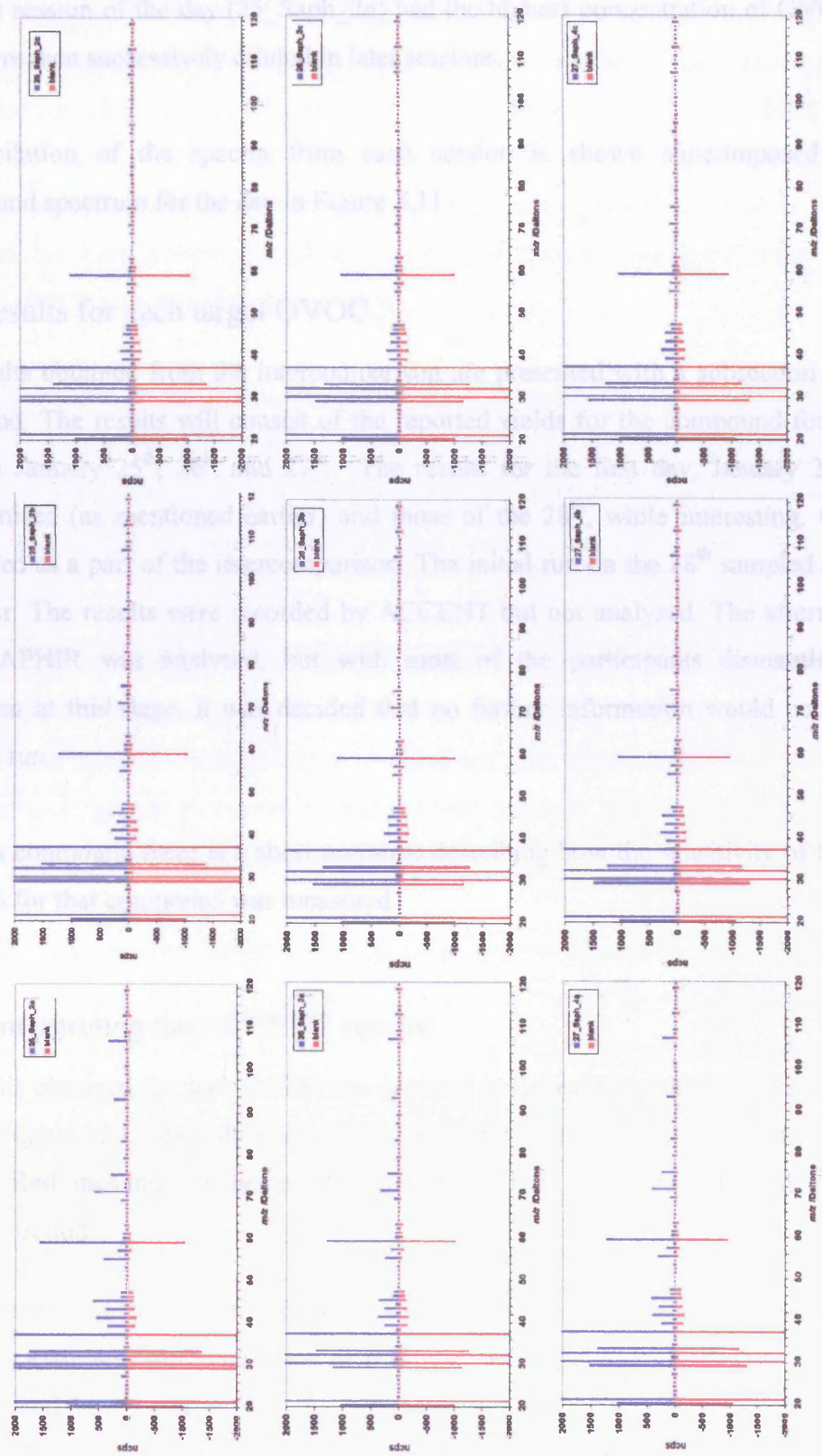


Figure 5.11 Composite spectra (+ve) and background spectra (-ve) for all three sessions for January 25th, 26th and 27th.

The first session of the day (25_Saph_2a) had the highest concentration of OVOCs and these were then successively diluted in later sessions.

A compilation of the spectra from each session is shown superimposed on the background spectrum for the day in Figure 5.11

5.7 Results for each target OVOC

The results obtained from the intercomparison are presented with a subsection for each compound. The results will consist of the reported yields for the compound for each of the days January 25th, 26th and 27th. The results for the first day, January 24th were compromised (as mentioned earlier) and those of the 28th, while interesting, were not considered as a part of the intercomparison. The initial run on the 28th sampled the local Jülich air. The results were recorded by ACCENT but not analysed. The afternoon run using SAPHIR was analysed, but with most of the participants dismantling their equipment at this stage, it was decided that no further information would be gathered from the run.

For each compound there is a short narrative describing how the sensitivity of the PTR-TOF-MS for that compound was measured.

5.7.1 Interpreting the ACCENT results

The yields obtained for each OVOC are depicted in the even-numbered series of Figure 5.12 to Figure 5.34. They show the yields for one-minute spectra for January 25th, 26th and 27th. Red lines indicate the periods during which data was extracted as three adjacent sampling periods.

Using the previously measured or calculated detection sensitivities, the measured data with error estimates were converted to ppbv and submitted to ACCENT along with the start time and duration of each sample period. In return ACCENT presented the results in two parts that are shown in the odd-numbered series Figure 5.13 to Figure 5.35.

The first part, on the left side of each diagram, consists of a plot of the reported data and a continuous curve representing the 'calculated' or reference data where the term 'calculated' is taken to mean the value of the data as measured by ACCENT midway between the start and finish time of each sampling period. The term 'calculated' used by ACCENT is unfortunate as some reaction rates were calculated as well. To avoid confusion, the term 'reference' will be used in preference to 'calculated' when referring to the ACCENT results in their present form.

In the second part of the results, shown on the right side of the diagrams, the reported data, linear regression for data and a regression line for the reference data are shown in a diagram. The experimental data and its regression is plotted as a solid line and the reference data regression line as a dotted line.

Numeric values are given for the slope, b , and intercept, $\sigma(b)$, of the reported to reference data as well as a figure for R^2 a measure of the consistency of the data points. Revised values for the detection sensitivities were obtained from these results. It is important to note that our target objective was to obtain better values of the PTR-TOF-MS detection sensitivity for the OVOCs tested in ACCENT.

It is planned to release the ACCENT data in greater numerical detail in the future, although the precise format has not yet been decided. Tables for the reported results are in Appendix 1, Tables A1.5.1 to A1.5.12. A comparison of the sensitivities, obtained by calibration, calculation and the ACCENT intercomparison are in Table 5.5.

A major benefit of the intercomparison campaign is that it generated invaluable sensitivity data for the PTR-TOF-MS, which are compared with calculated sensitivities and those obtained using the FAL and Bristol/Apel standard mixtures. All these results are summarised in Table 3.7 in Chapter 3. The fragmentation data for the species is presented in Appendix 1, Tables A1.3.1 and A1.3.2. Error considerations are discussed in Section 5.8.

5.7.2 Compounds not included

It was not possible to report on some of the component compounds included in the OVOCs cocktail used at the ACCENT intercomparison. The first of these compounds were n-butane (an alkane) which is poorly detected by the PTR-TOF-MS. Ethanol did not register sufficiently well above the background. There was no obvious reason why this should be, as the PTR-TOF-MS had no difficulty detecting its cousins methanol and 1-propanol. The detection of formaldehyde was only attempted by two groups using the Hantsch method.

5.7.3 Acetaldehyde (CH_3CHO)

The Acetaldehyde data for January 25th, 26th and 27th are shown in Figure 5.12. The group at $m/z = 45$, the full mass peak, is easily discernable above the background. The other major fragment of acetaldehyde occurs at $m/z = 43$ but since this interferes with other species, the $m/z = 45$ peak was used.

The reported concentrations for acetaldehyde (see Appendix 1, Table A1.5.1) are slightly lower than the reference values.

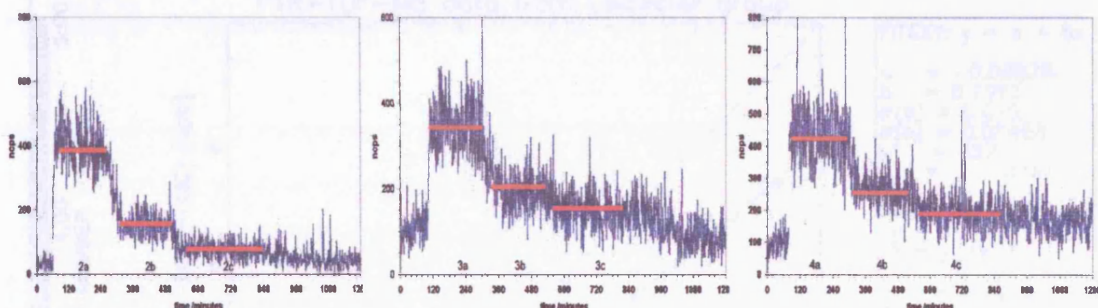


Figure 5.12 Acetaldehyde yield for the sessions January 25th, 26th and 27th.

This means that the value of the sensitivity used to calculate the reported data was higher than was actually the case. What is heartening in nearly all the results is the consistent ability of the PTR-TOF-MS to track the changes in concentration.

The observed sensitivity for acetaldehyde was $79.7 \text{ ncps ppbv}^{-1}$ which is midway between the calculated value of $43.1 \text{ ncps ppbv}^{-1}$ and the value of $102.0 \text{ ncps ppbv}^{-1}$ obtained from the calibration with the Bristol/Apel mixture. From Figure 5.13 it can be seen that the reported results are about 22% below the reference calculated concentration,

which is on the low side, but nothing like the sort of disagreement experienced at TORCH. The consistency of the results given by $R^2 = 0.99$ is very good.

5.7.4 Acetone ($(CH_3)_2CO$)

The PTR-TOF-MS had a very low detection limit for acetone, so that the acetone loading which sat on top of a fairly large background was very low. However, once sufficient data had been collected it was possible to extract the acetone signal for the acetone concentration (see Appendix J, Table A1.5.4).

Figure 5.14 Acetone yield for the sessions January 25th, 26th and 27th

Protonated acetone and acetaldehyde were separated as they are usually reported together as unresolved species, but for ACCENT, proposal was to exclude

Measurements of acetone were observed in the experiment. The acetone yield was very low and was not included in the analysis.

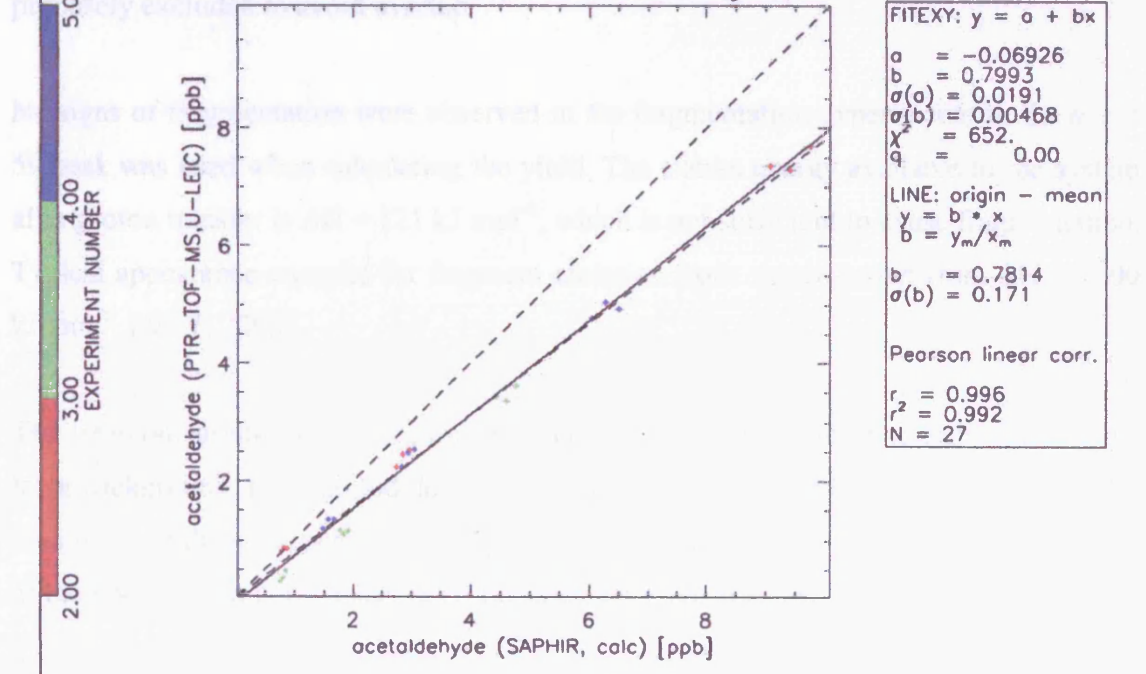


Figure 5.13 Comparison of reported values with actual concentration of acetaldehyde.

5.7.4 Acetone ((CH₃)₂CO)

The PTR-TOF-MS had some contamination in the $m/z = 59$ channel, so that the acetone loading at Jülich sat on top of a fairly large background (Figure 5.14). Nevertheless, once sufficient data had been collected it was possible to obtain meaningful figures for the acetone concentration (see Appendix 1, Table A1.5.2).

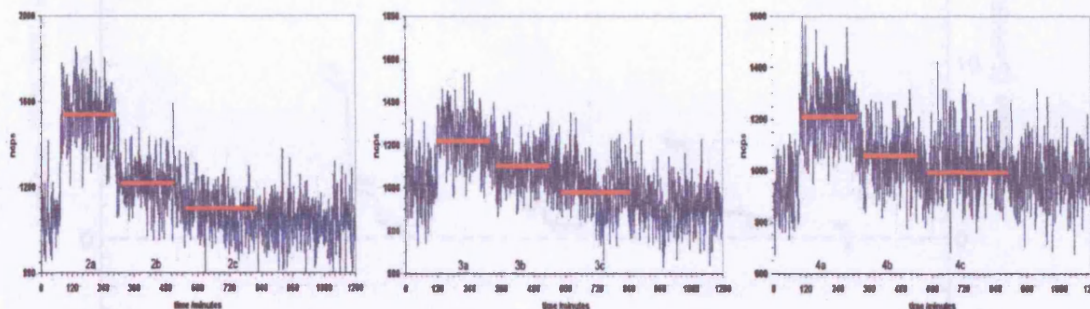


Figure 5.14 Acetone yield for the sessions January 25th, 26th and 27th.

Protonated propanal and acetone both have $m/z = 59$ and cannot be separated so they are usually reported together as unresolved species, but for ACCENT, propanal was purposely excluded to avoid overlap.

No signs of fragmentation were observed in the fragmentation experiments so the $m/z = 59$ peak was used when calculating the yield. The excess energy available to the system after proton transfer is $\Delta H = 121 \text{ kJ mol}^{-1}$, which is not sufficient to cause fragmentation. Typical appearance energies for fragment emission from acetone start from $\Delta H \geq 1000 \text{ kJ mol}^{-1}$ [NIST, 2005].

The intercomparison results shown in Figure 5.15 were satisfactory and in spite of the large background, the reported detection sensitivity values found at $61.5 \text{ npps ppbv}^{-1}$ fell within 3% of the reference value $62.6 \text{ npps ppbv}^{-1}$. The value of R^2 (0.98) is further proof of the linearity and consistency of response of the PTR-TOF-MS.

5.7.5 Benzaldehyde (C₇H₆CHO)

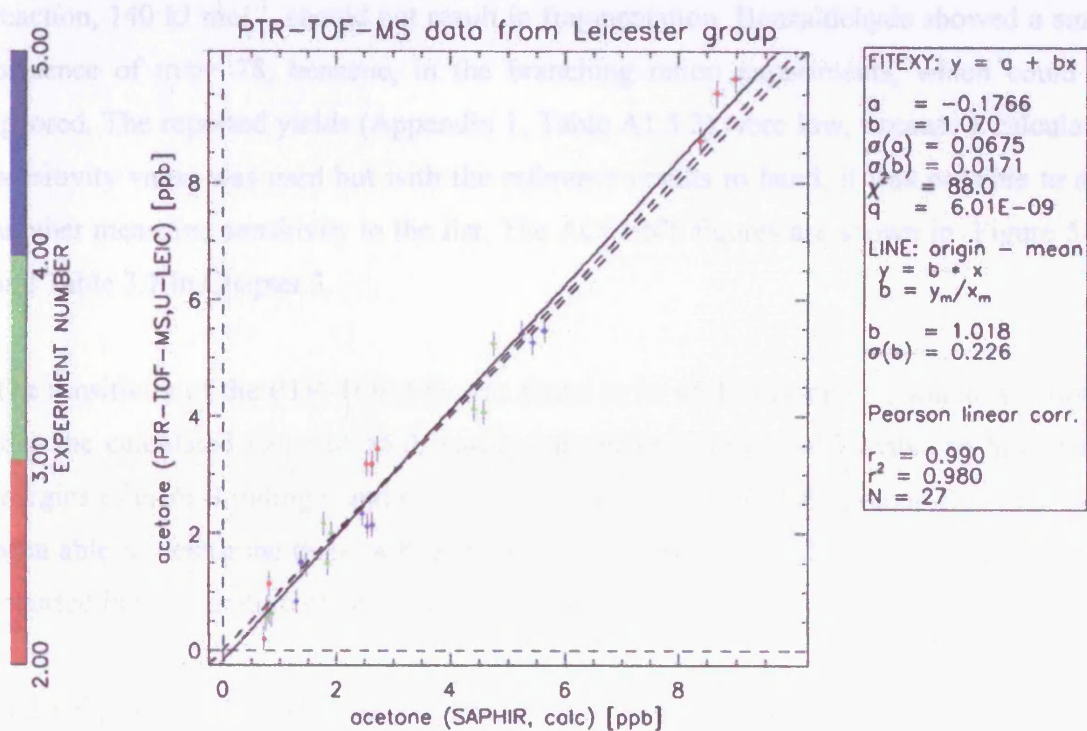
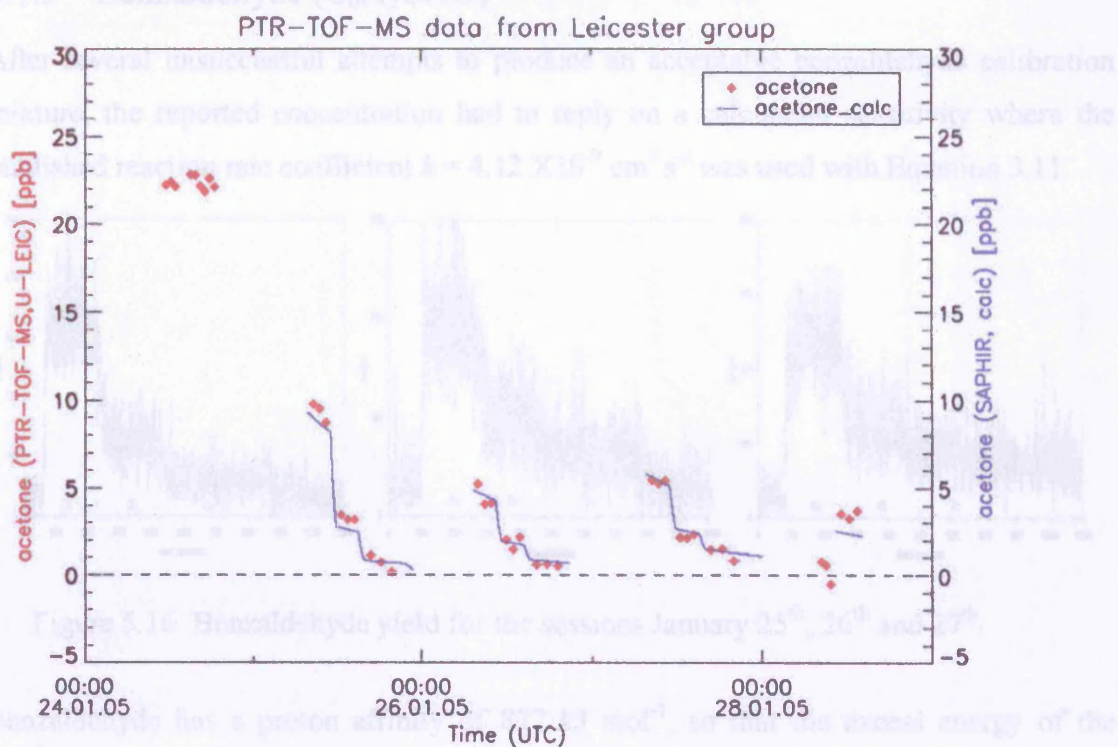


Figure 5.15 Comparison of reported values with actual concentration of acetone.

5.7.5 Benzaldehyde (C₆H₅CHO)

After several unsuccessful attempts to produce an acceptable benzaldehyde calibration mixture, the reported concentration had to rely on a calculated sensitivity where the published reaction rate coefficient $k = 4.12 \times 10^{-9} \text{ cm}^3 \text{ s}^{-1}$ was used with Equation 3.11.

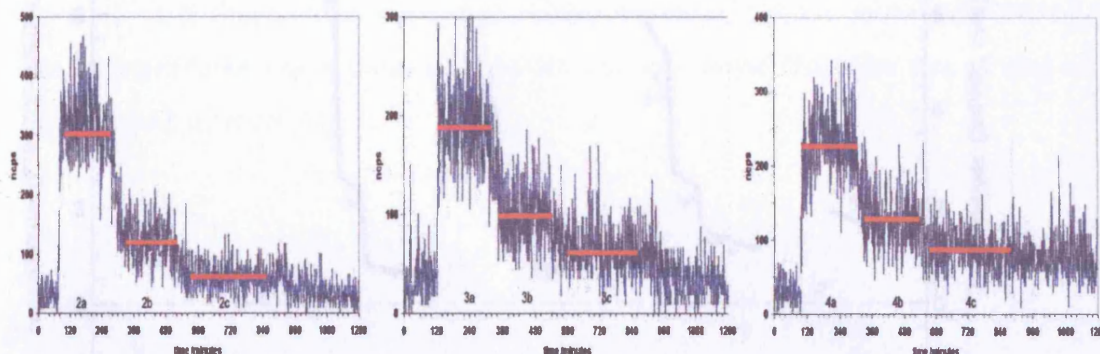


Figure 5.16 Benzaldehyde yield for the sessions January 25th, 26th and 27th.

Benzaldehyde has a proton affinity of 832 kJ mol^{-1} , so that the excess energy of the reaction, 140 kJ mol^{-1} , should not result in fragmentation. Benzaldehyde showed a small presence of $m/z = 78$, benzene, in the branching ration experiments, which could be ignored. The reported yields (Appendix 1, Table A1.5.3) were low, because a calculated sensitivity value was used but with the reference results to hand, it was possible to add another measured sensitivity to the list. The ACCENT figures are shown in Figure 5.17 and Table 3.7 in Chapter 3.

The sensitivity of the PTR-TOF-MS was found to be $45.1 \text{ ncps ppbv}^{-1}$, which was lower than the calculated value of 55.0; hardly surprising as rate coefficients can have large margins of error. Lindinger and co-workers [Lindinger *et al.*, 1998] report that they have been able to determine these with a margin of error of 15% and assert that other values reported in the literature often have margins of error approaching 30%.

Since Equation 3.11 makes no allowance for factors affecting the measured sensitivity, such as missed fragmentation daughter ions, and mass-dependent variation in sensitivity of the PTR-TOF-MS itself. The reported result for the PTR-TOF-MS sensitivity was some 18% below the reference value.

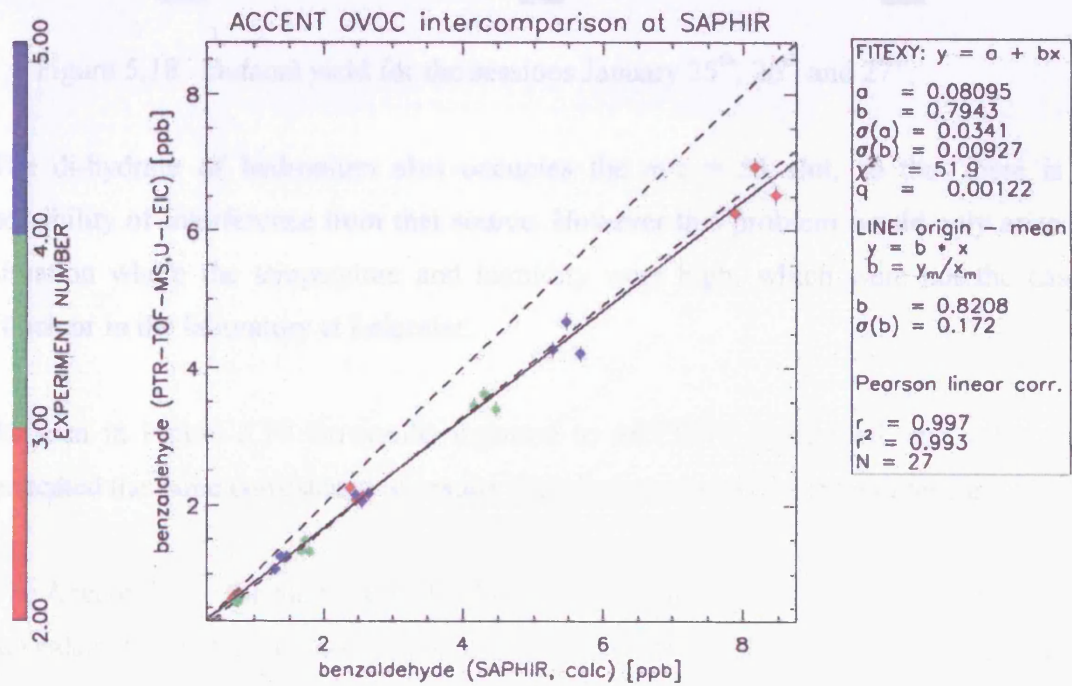
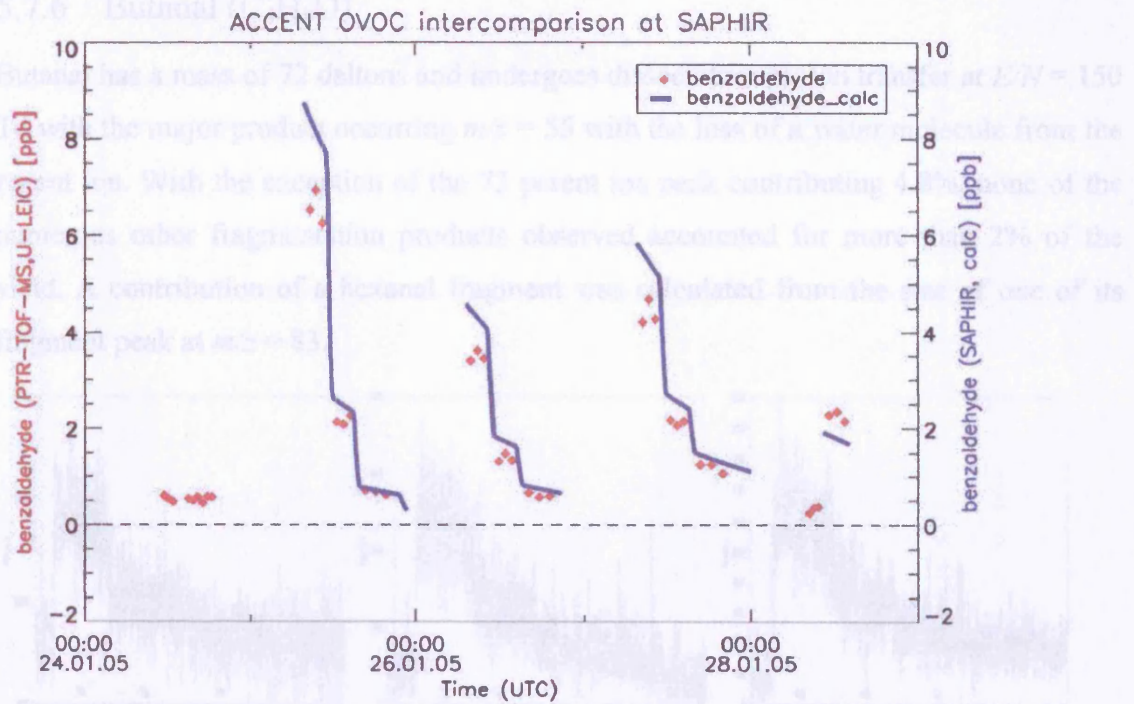


Figure 5.17 Comparison of reported values with actual concentration of benzaldehyde.

5.7.6 Butanal (C₄H₈O)

Butanal has a mass of 72 daltons and undergoes dissociative proton transfer at $E/N = 150$ Td with the major product occurring $m/z = 55$ with the loss of a water molecule from the parent ion. With the exception of the 73 parent ion peak contributing 4.8%, none of the numerous other fragmentation products observed accounted for more than 2% of the yield. A contribution of a hexanal fragment was calculated from the size of one of its fragment peak at $m/z = 83$.

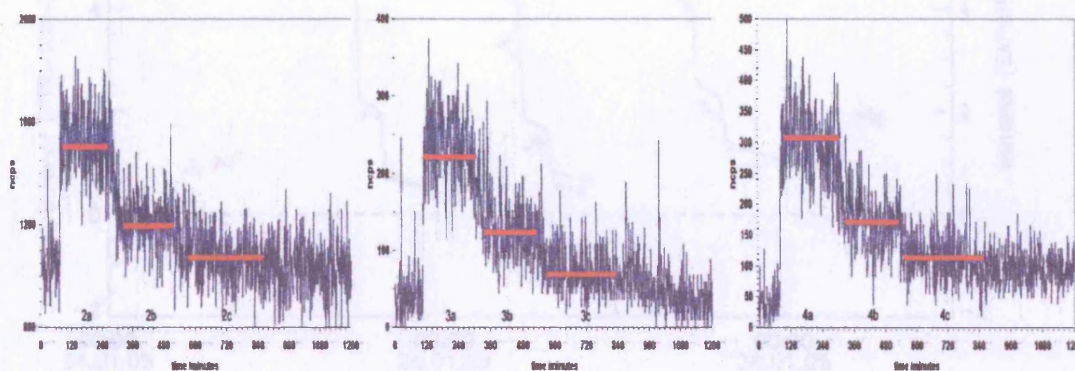


Figure 5.18 Butanal yield for the sessions January 25th, 26th and 27th.

The di-hydrate of hydronium also occupies the $m/z = 55$ slot, so that there is the possibility of interference from that source. However this problem would only arise in a situation where the temperature and humidity were high, which were not the case at Jülich or in the laboratory at Leicester.

As seen in Figure 5.19 the results reported to ACCENT agree well, and value of R^2 indicated the same consistency of results that characterise all the Accent results.

The Accent figure for the PTR-TOF-MS sensitivity for Butanal is 42.3 ncps ppbv⁻¹ while the calculated and calibration results using the Bristol /Apel mixture were 59.8 and 50.4 ncps ppbv⁻¹ respectively. The reported figures (see Appendix 1, Table A1.5.4) agree with reference values to within 17% (Figure 5.19).

5.7.7 1-butanol (C₄H₁₀O)

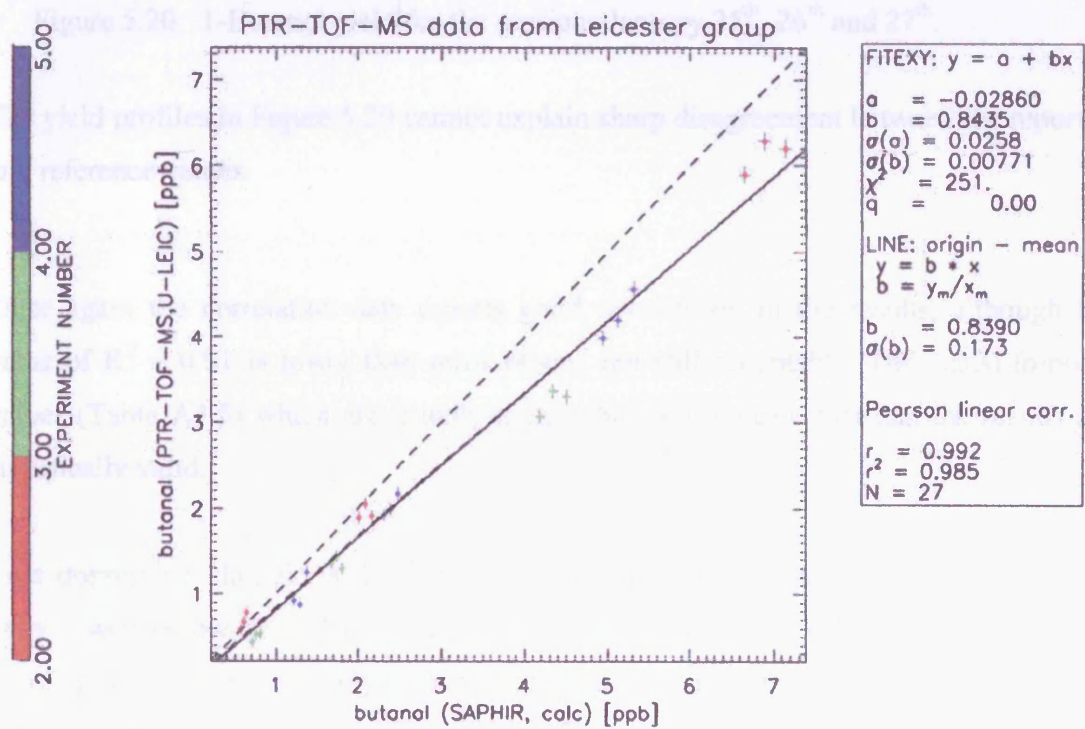
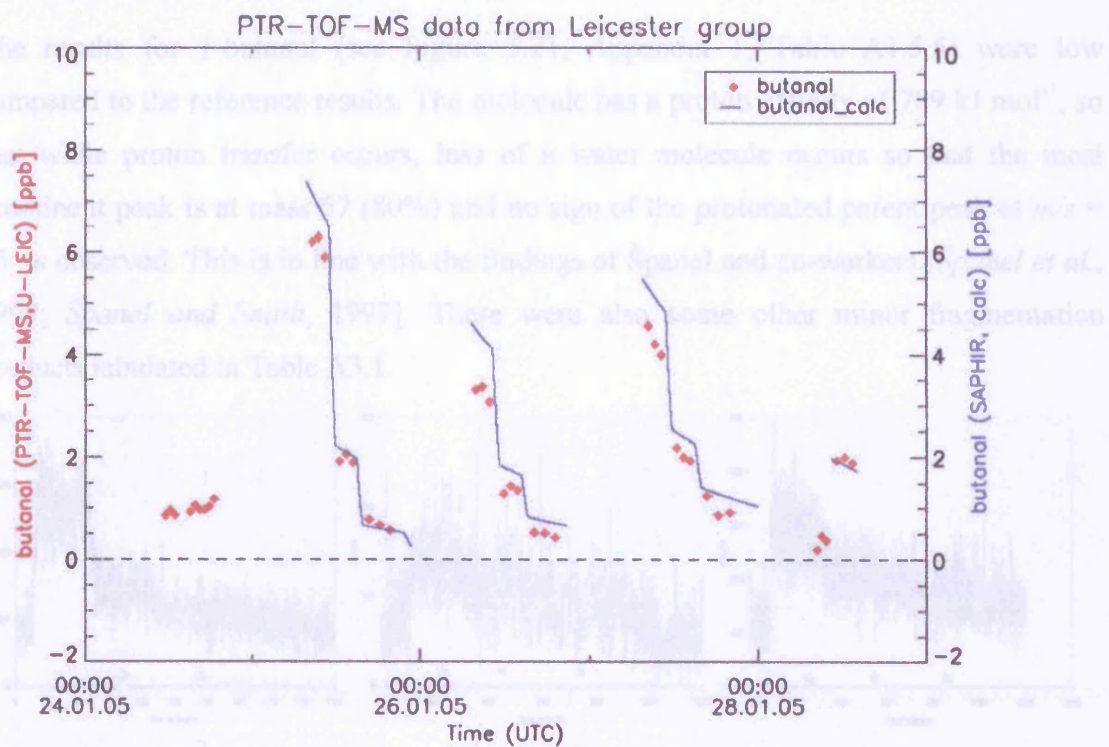


Figure 5.19 Comparison of reported values with actual concentration of butanal.

5.7.7 1-butanol (C₄H₁₀O)

The results for 1-butanol (see Figure 5.21, Appendix 1, Table A1.5.5) were low compared to the reference results. The molecule has a proton affinity of 789 kJ mol⁻¹, so that while proton transfer occurs, loss of a water molecule occurs so that the most prominent peak is at mass 57 (80%) and no sign of the protonated parent peak at $m/z = 75$ is observed. This is in line with the findings of Španel and co-workers [Španel *et al.*, 1997; Španel and Smith, 1997]. There were also some other minor fragmentation products tabulated in Table A3.1.

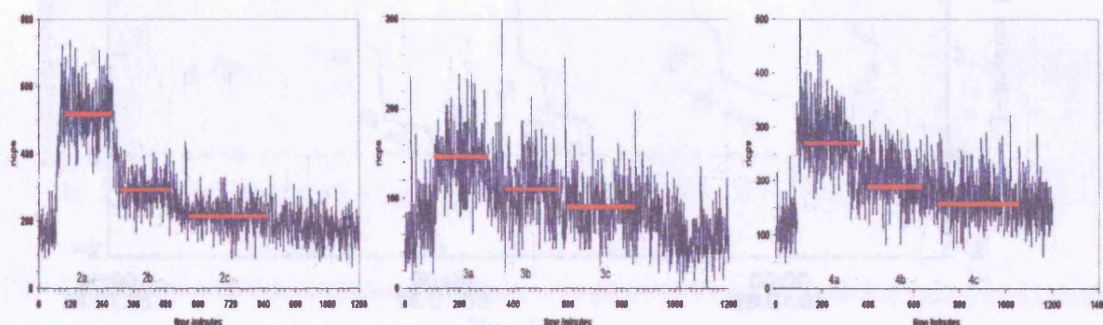


Figure 5.20 1-Butanol yield for the sessions January 25th, 26th and 27th.

The yield profiles in Figure 5.20 cannot explain sharp disagreement between the reported and reference values.

Once again the correlation data reports good consistency in the results, although the value of $R^2 = 0.91$ is lower than most others, but still acceptable. The signal-to-noise values (Table A5.5) which are usually higher than 3.0 indicate that the results are statistically valid.

Less impressive, though, is the observed sensitivity which was found to be 20.5 ncps ppbv⁻¹, well below the calculated and Apel/Bristol calibration values of 31.7 and 63.0 ncps ppbv⁻¹. The most likely explanation would be that the $m/z = 57$ channel had contributions from at least one other unidentified ion fragment.

5.7.8 Hexanal (C₆H₁₂O)

April 2005. The PTR-TOF-MS data from Leicester group shows a peak at m/z = 55 (42.0%) and a few minor peaks at m/z = 83. This peak does not overlap with other fragment ions when the m/z = 55 peak overlaps with a contribution from butanol.

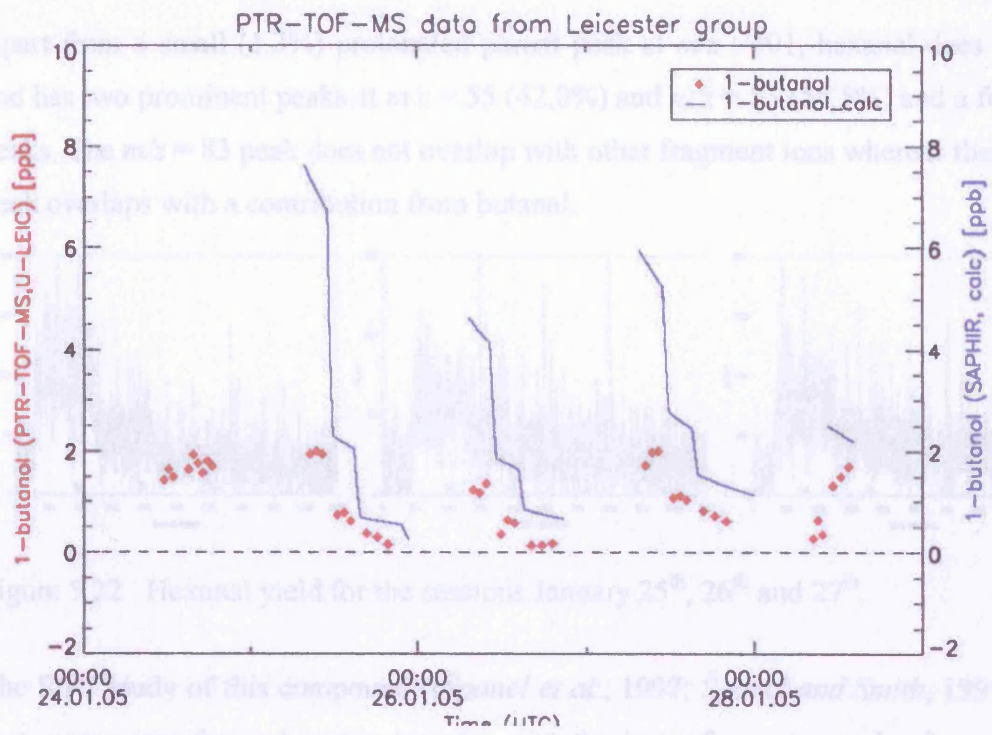


Figure 5.20 Hexanal yield for the sessions January 25th, 26th and 27th. The study of this compound (see *Journal of Agricultural and Food Chemistry*, 1997) found that proton transfer and proton transfer with the loss of a water molecule occurred in roughly equal proportions.

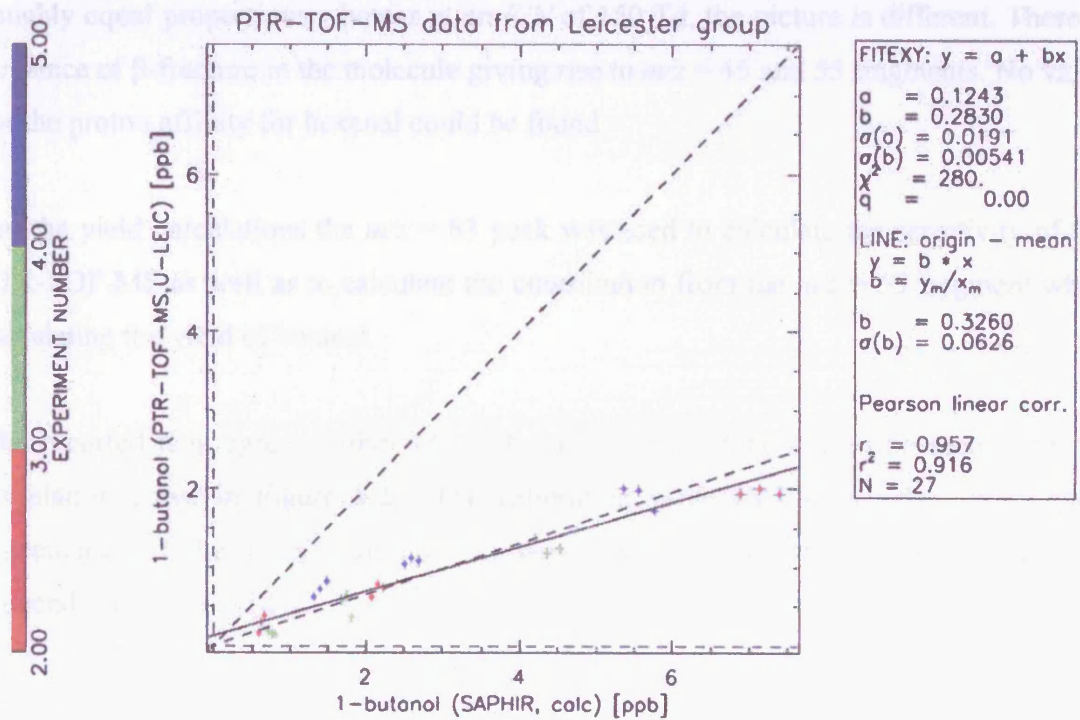


Figure 5.21 Comparison of reported values with actual concentration of 1-butanol.

5.7.8 Hexanal (C₆H₁₂O)

Apart from a small (1.3%) protonated parent peak at $m/z = 101$, hexanal does fragment and has two prominent peaks at $m/z = 55$ (42.0%) and $m/z = 83$ (55.5%) and a few minor peaks. The $m/z = 83$ peak does not overlap with other fragment ions whereas the $m/z = 55$ peak overlaps with a contribution from butanal.

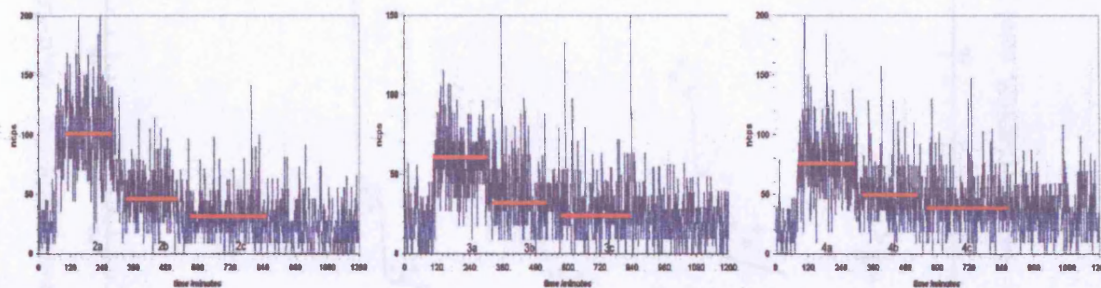


Figure 5.22 Hexanal yield for the sessions January 25th, 26th and 27th.

The SIFT study of this compound ([*Španel et al.*, 1997; *Španel and Smith*, 1997]) found that proton transfer and proton transfer with the loss of a water molecule occurred in roughly equal proportions whereas at an E/N of 150 Td, the picture is different. There is evidence of β -fracture in the molecule giving rise to $m/z = 45$ and 55 fragments. No value for the proton affinity for hexanal could be found.

For the yield calculations the $m/z = 83$ peak was used to calculate the sensitivity of the PTR-TOF-MS as well as to calculate the contribution from the $m/z = 55$ fragment when calculating the yield of butanal.

The reported data agrees within 4% with the reference data, as can be seen from the correlation curve in Figure 5.23. The calibration value 18.3 ncps ppbv⁻¹ is in good agreement with the Accent value of 19.0 ncps ppbv⁻¹. The reported results are given in Appendix 1, Table A1.5.6.

5.7.9 MBO (2-Methyl-3-buten-2-ol) (C₅H₁₀O)

The 1000s for MBO were not available, as they were as deduced from the slope of the correlation curve in Fig. 5.23.

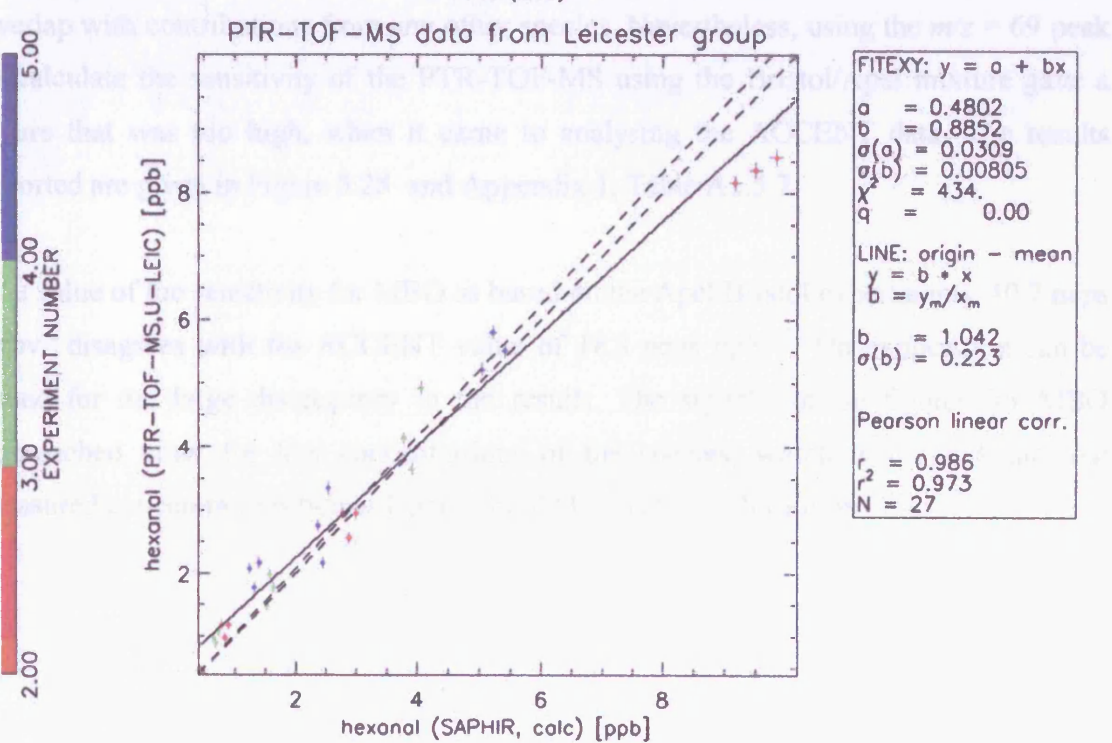
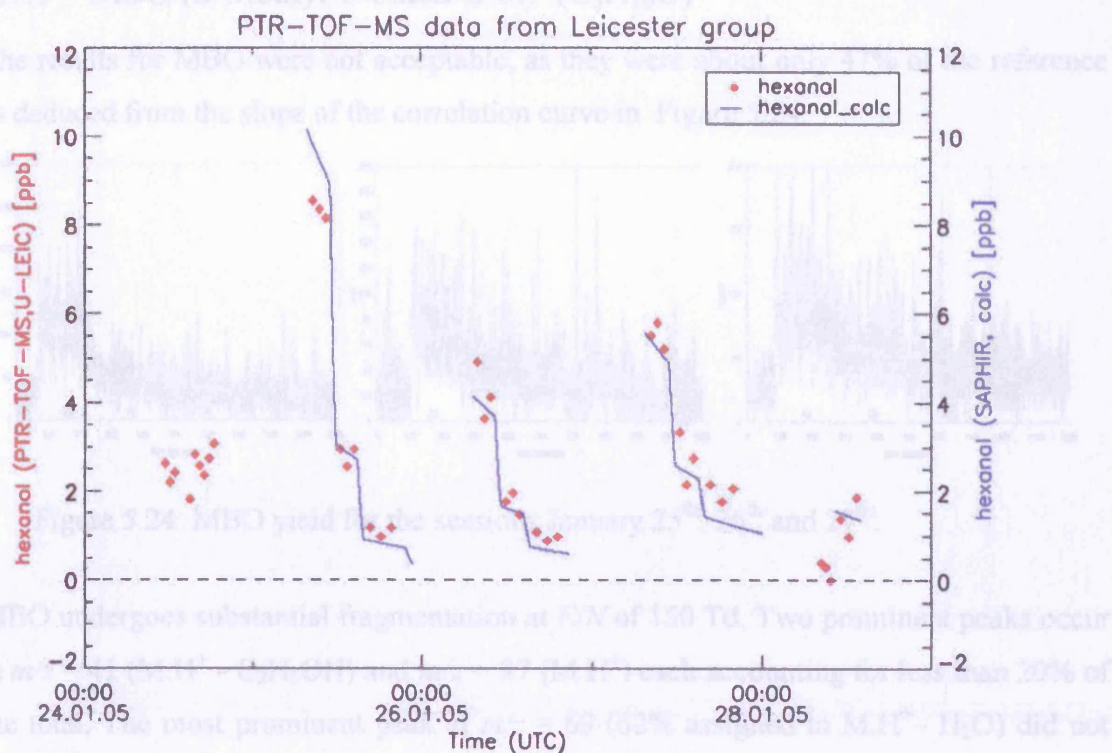


Figure 5.23 Comparison of reported values with actual concentration of hexanal.

5.7.9 MBO (2-Methyl-3-buten-2-ol) (C₅H₁₀O)

The results for MBO were not acceptable, as they were about only 47% of the reference as deduced from the slope of the correlation curve in Figure 5.24.

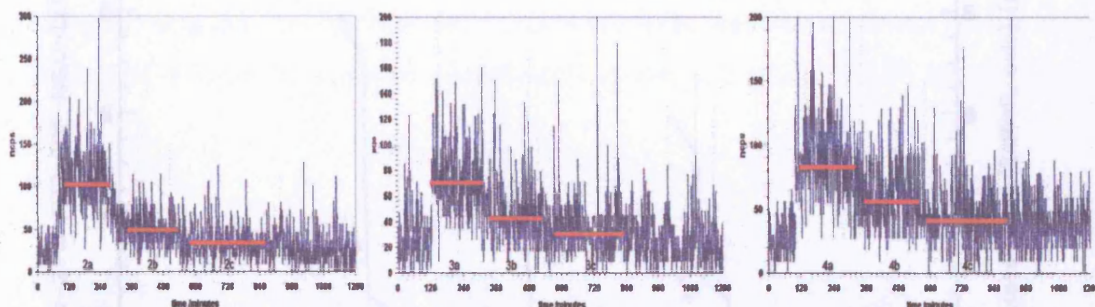


Figure 5.24 MBO yield for the sessions January 25th, 26th and 27th.

MBO undergoes substantial fragmentation at E/N of 150 Td. Two prominent peaks occur at $m/z = 41$ ($M.H^+ - C_2H_5OH$) and $m/z = 87$ ($M.H^+$) each accounting for less than 20% of the total. The most prominent peak at $m/z = 69$ (62% assigned to $M.H^+ - H_2O$) did not overlap with contributions from any other species. Nevertheless, using the $m/z = 69$ peak to calculate the sensitivity of the PTR-TOF-MS using the Bristol/Apel mixture gave a figure that was too high, when it came to analysing the ACCENT data. The results reported are given in Figure 5.25 and Appendix 1, Table A1.5.7.

The value of the sensitivity for MBO as based on the Apel/Bristol experiments, 40.7 ncps ppbv⁻¹ disagrees with the ACCENT value of 18.3 ncps ppbv⁻¹. No explanation can be found for the large discrepancy in the results. The signal-to-noise figures for MBO approached unity for low concentrations of the species, which would indicate that measured concentrations below 1 ppbv should be treated with caution.

5.7.10 Methanol (CH₃OH)

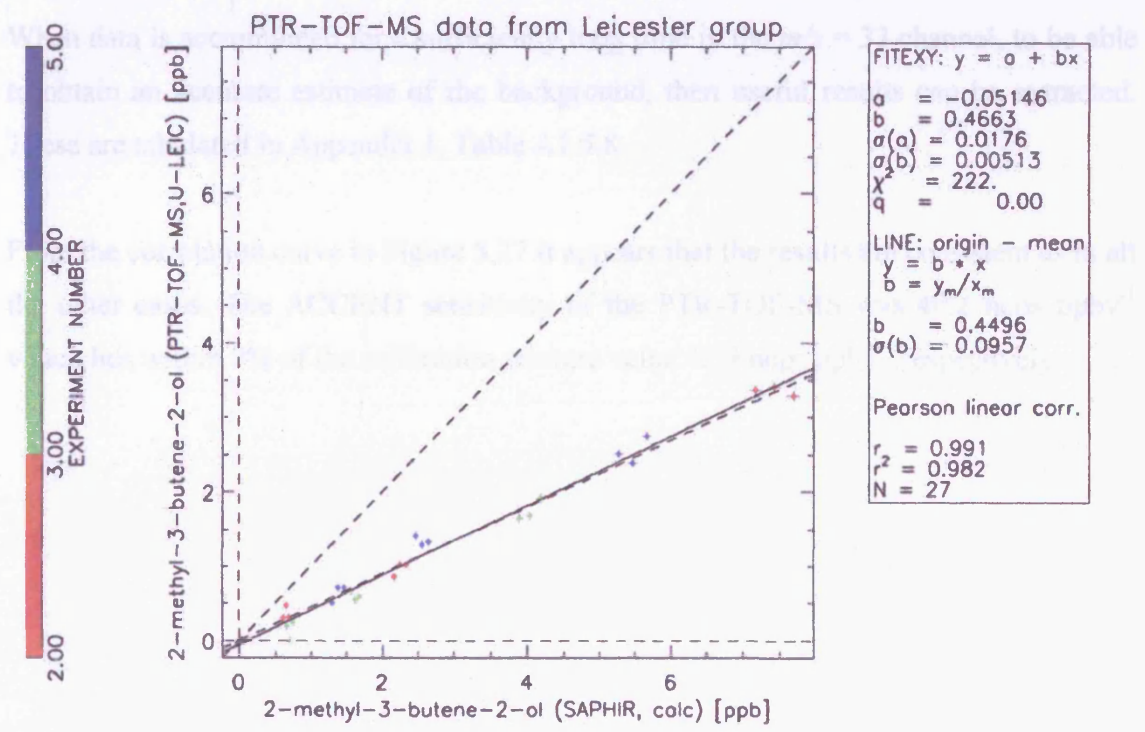
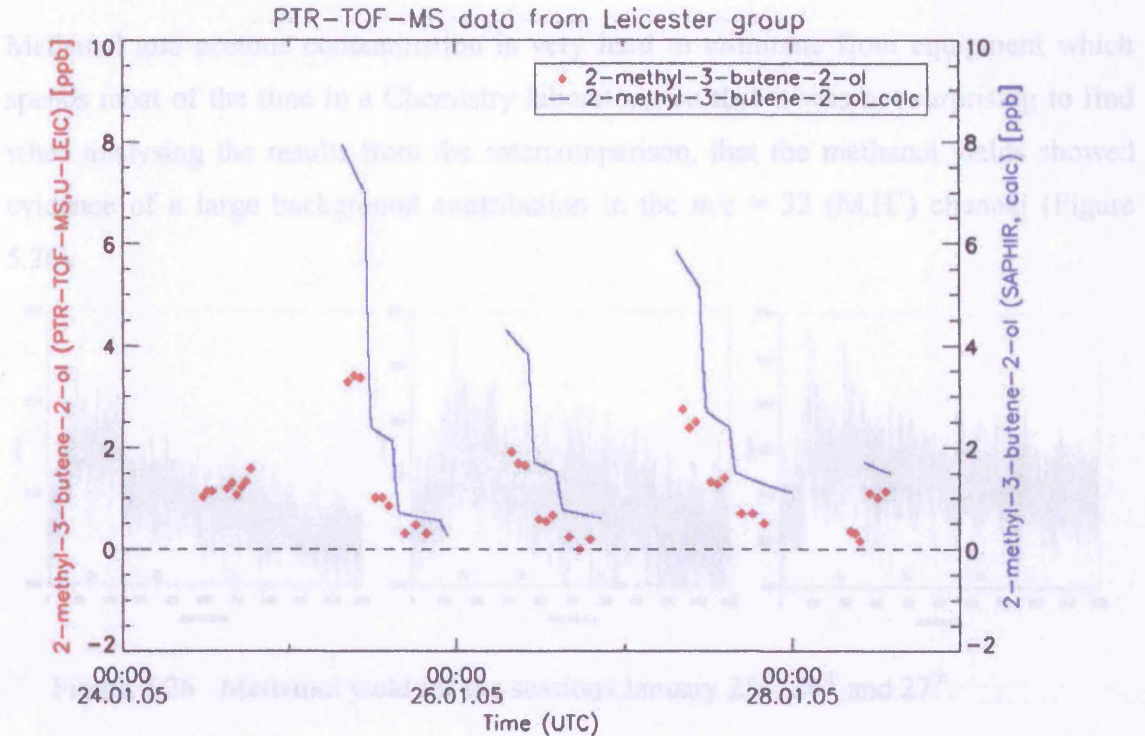


Figure 5.25 Comparison of reported values with actual concentration of MBO.

5.7.10 Methanol (CH₃ COH)

Methanol and acetone contamination is very hard to eliminate from equipment which spends most of the time in a Chemistry laboratory, so that it was not surprising to find when analysing the results from the intercomparison, that the methanol yields showed evidence of a large background contribution in the $m/z = 33$ (M.H⁺) channel (Figure 5.26).

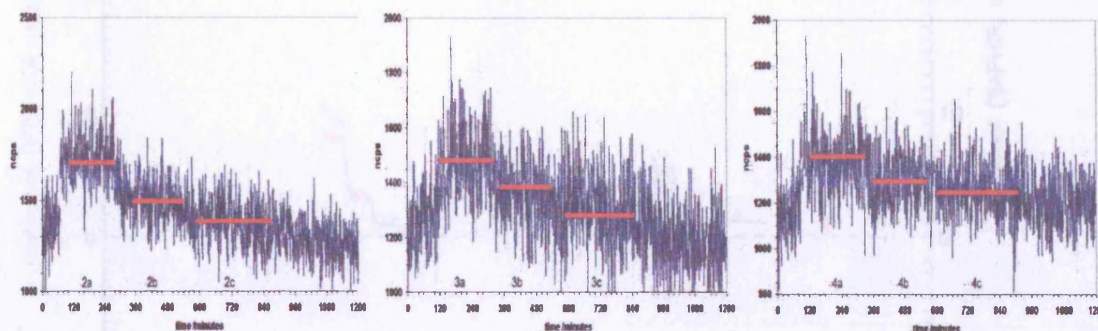


Figure 5.26 Methanol yield for the sessions January 25th, 26th and 27th.

When data is accumulated for a sufficiently long time in the $m/z = 33$ channel, to be able to obtain an accurate estimate of the background, then useful results can be extracted. These are tabulated in Appendix 1, Table A1.5.8.

From the correlation curve in Figure 5.27 it appears that the results are consistent as in all the other cases. The ACCENT sensitivity of the PTR-TOF-MS was 40.2 ncps ppbv⁻¹ which lies within 7% of the calibration mixture value 42.9 ncps ppbv⁻¹ respectively.

5.7.11 Methyl Acetate (CH3COOCH3)

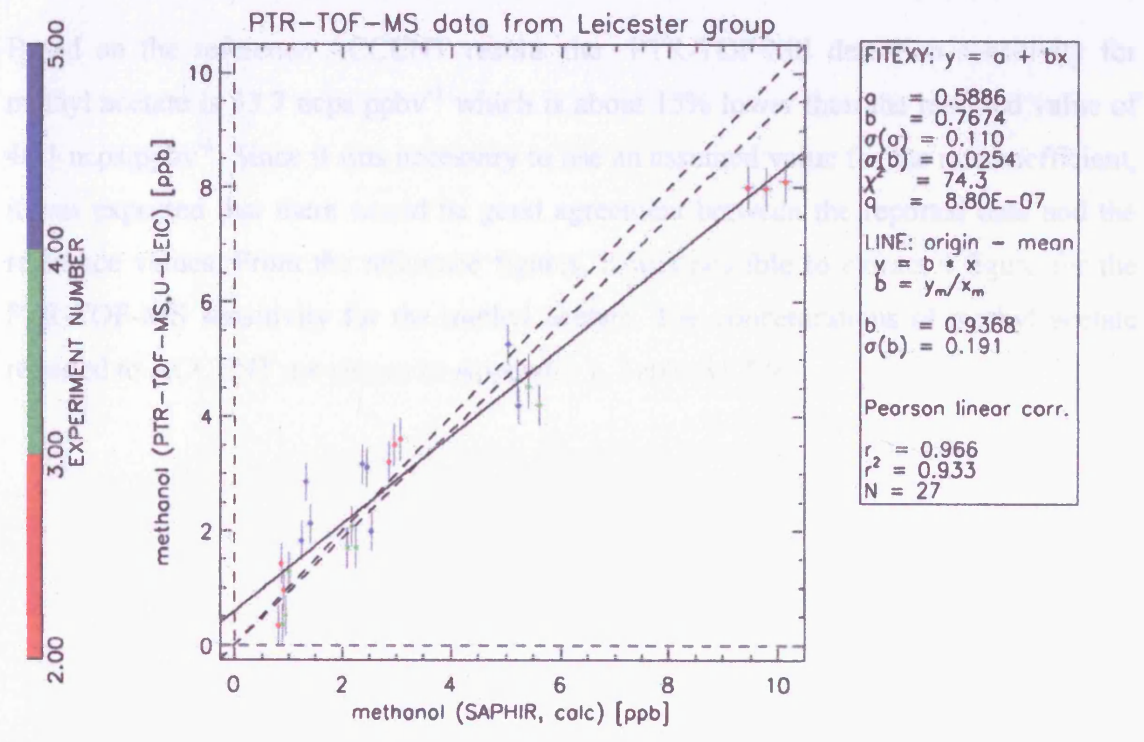
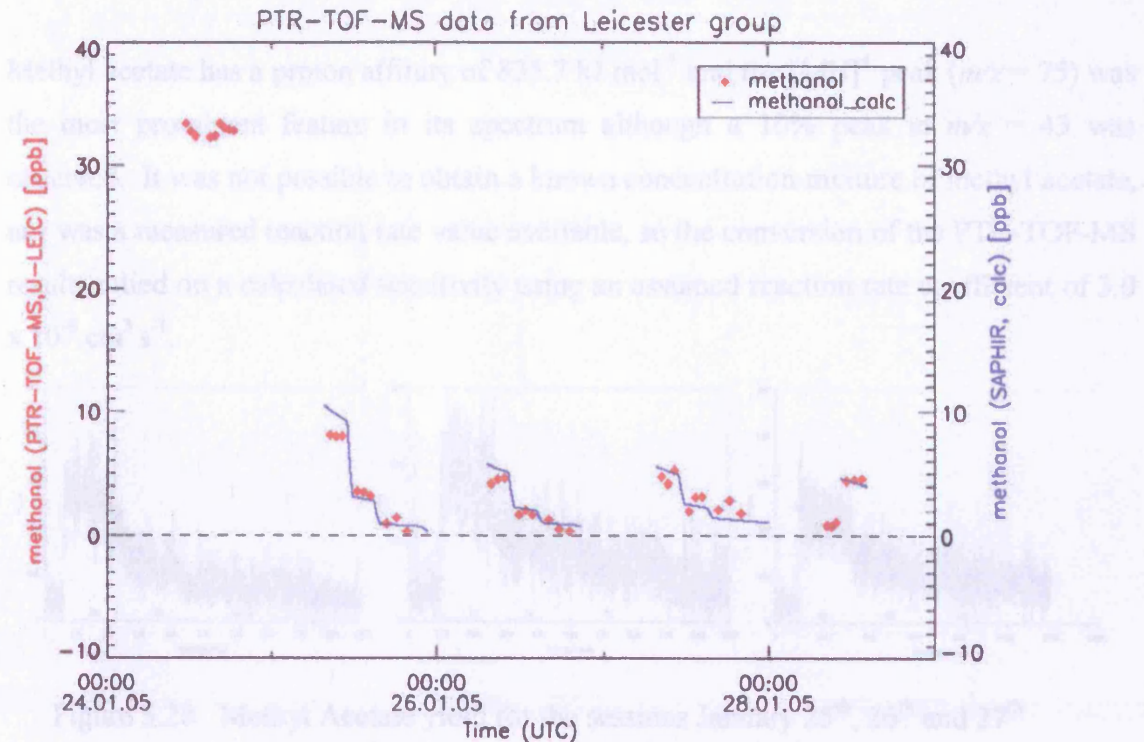


Figure 5.27 Comparison of reported values with actual concentration of methanol.

5.7.11 Methyl Acetate ($\text{CH}_3\text{COOCH}_3$)

Methyl acetate has a proton affinity of $835.7 \text{ kJ mol}^{-1}$ and the $[\text{MH}]^+$ peak ($m/z = 75$) was the most prominent feature in its spectrum although a 10% peak at $m/z = 43$ was observed. It was not possible to obtain a known concentration mixture of methyl acetate, nor was a measured reaction rate value available, so the conversion of the PTR-TOF-MS results relied on a calculated sensitivity using an assumed reaction rate coefficient of $3.0 \times 10^{-9} \text{ cm}^3 \text{ s}^{-1}$.

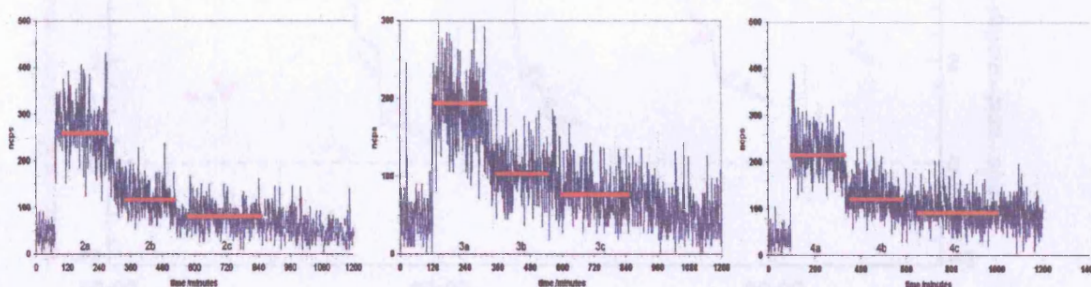


Figure 5.28 Methyl Acetate yield for the sessions January 25th, 26th and 27th.

Based on the reference ACCENT results the PTR-TOF-MS detection sensitivity for methyl acetate is $33.7 \text{ ncps ppbv}^{-1}$ which is about 15% lower than the reported value of $40.1 \text{ ncps ppbv}^{-1}$. Since it was necessary to use an assumed value for the rate coefficient, it was expected that there would be good agreement between the reported data and the reference values. From the reference figures, it was possible to extract a figure for the PTR-TOF-MS sensitivity for the methyl acetate. The concentrations of methyl acetate reported to ACCENT are shown in Appendix 1, Table A1.5.9.

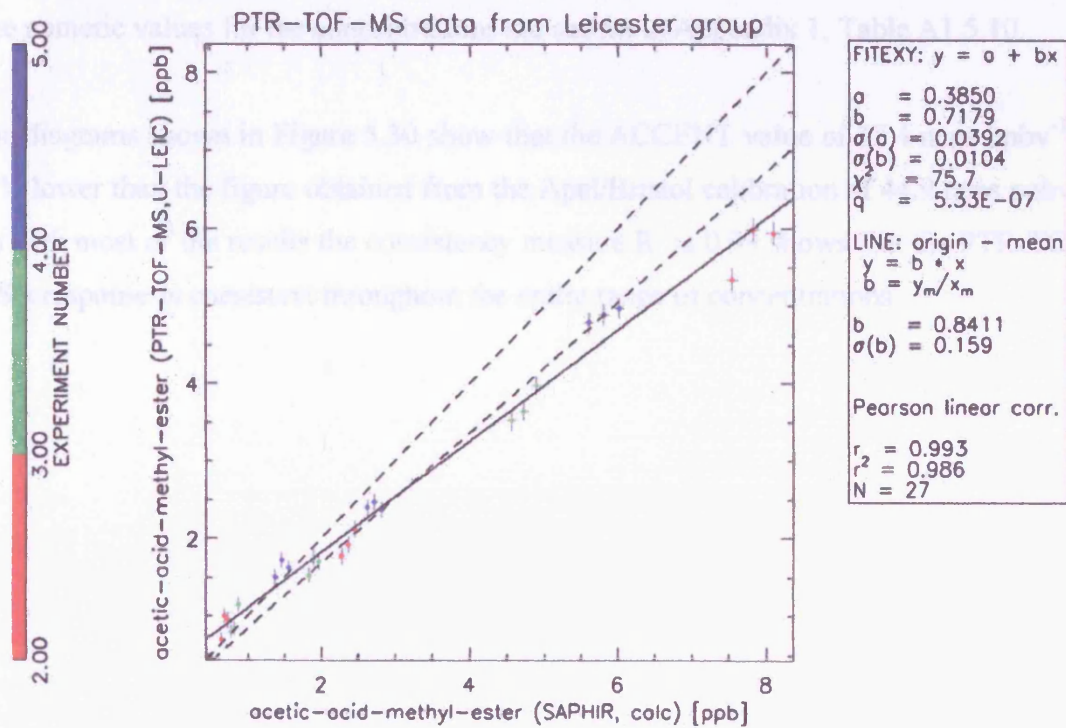
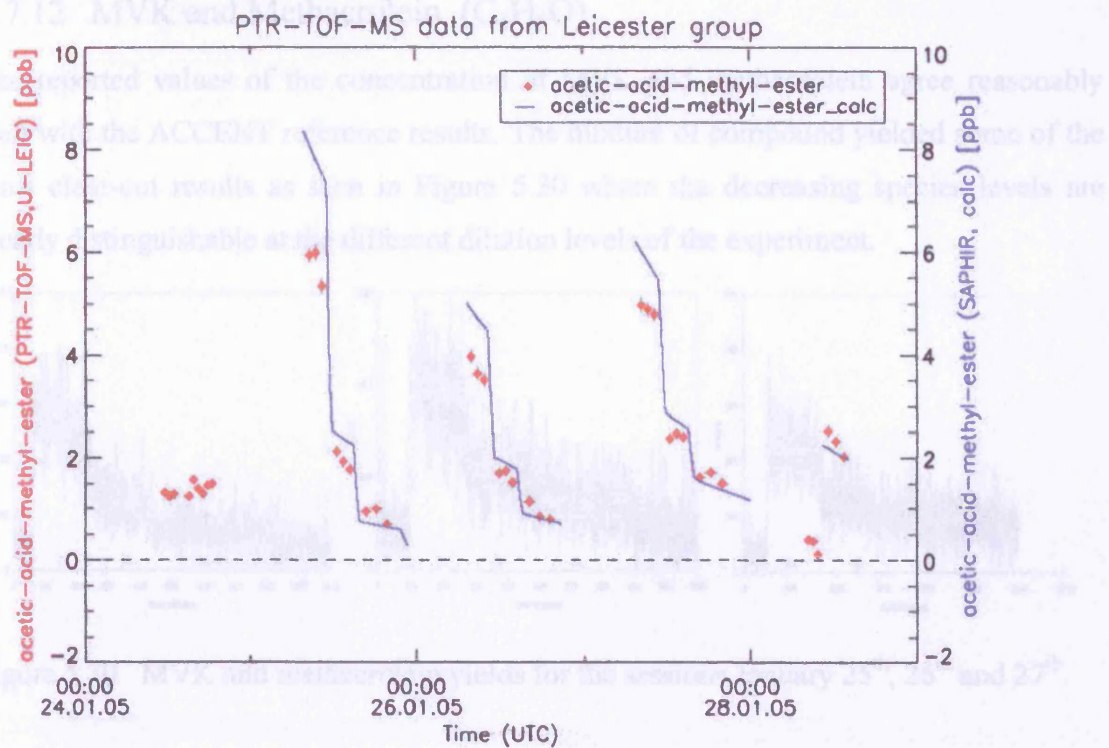


Figure 5.29 Comparison of reported values with actual concentration of methyl acetate.

5.7.12 MVK and Methacrolein (C₄H₆O)

The reported values of the concentration of MVK and methacrolein agree reasonably well with the ACCENT reference results. The mixture of compound yielded some of the most clear-cut results as seen in Figure 5.30 where the decreasing species levels are clearly distinguishable at the different dilution levels of the experiment.

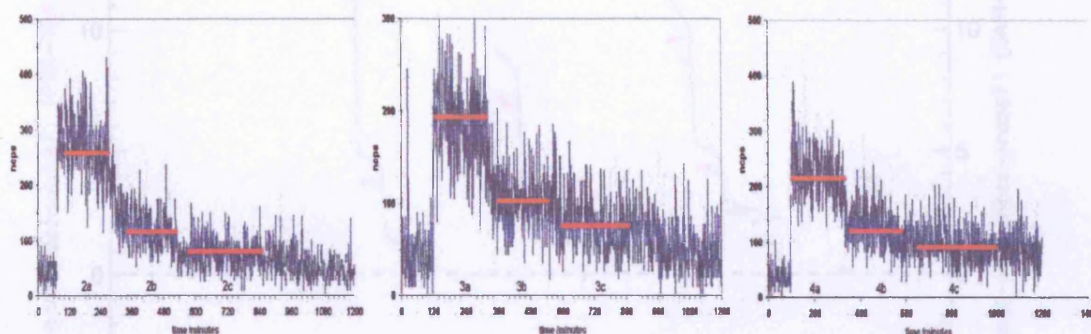


Figure 5.30 MVK and methacrolein yields for the sessions January 25th, 26th and 27th.

The numeric values for the concentrations are shown in Appendix 1, Table A1.5.10.

The diagrams shown in Figure 5.30 show that the ACCENT value of 37.4 ncps ppbv⁻¹ is 17% lower than the figure obtained from the Apel/Bristol calibration of 44.9 ncps ppbv⁻¹. As with most of the results the consistency measure R² at 0.99 shows that the PTR-TOF-MS's response is consistent throughout the entire range of concentrations.

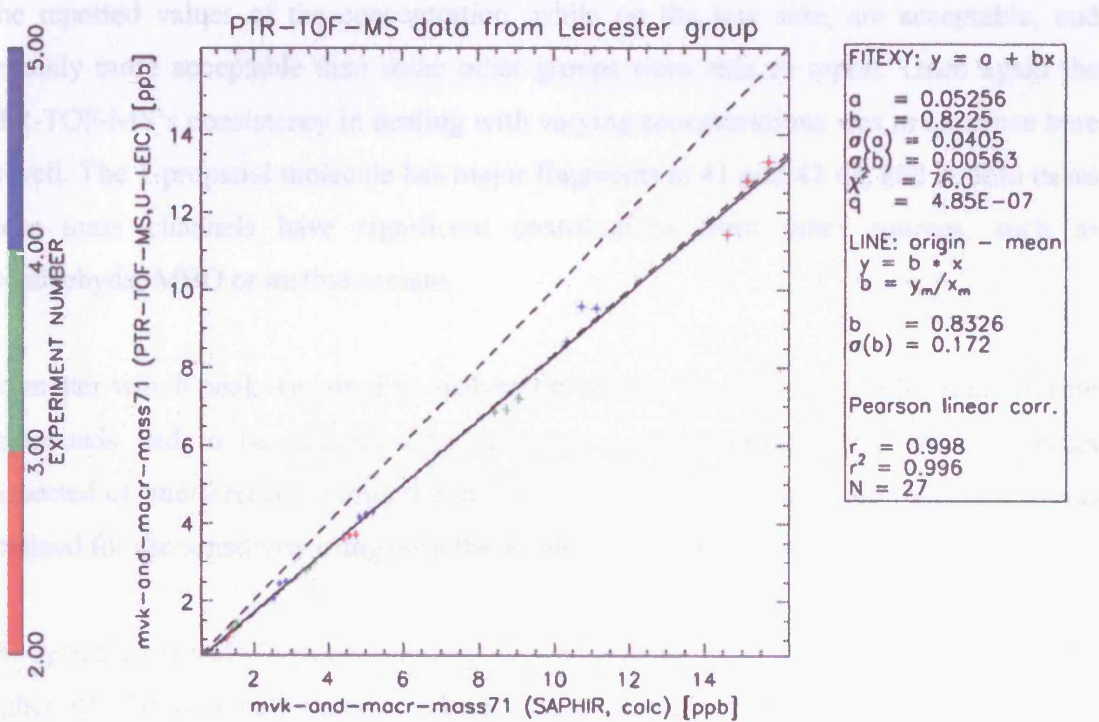
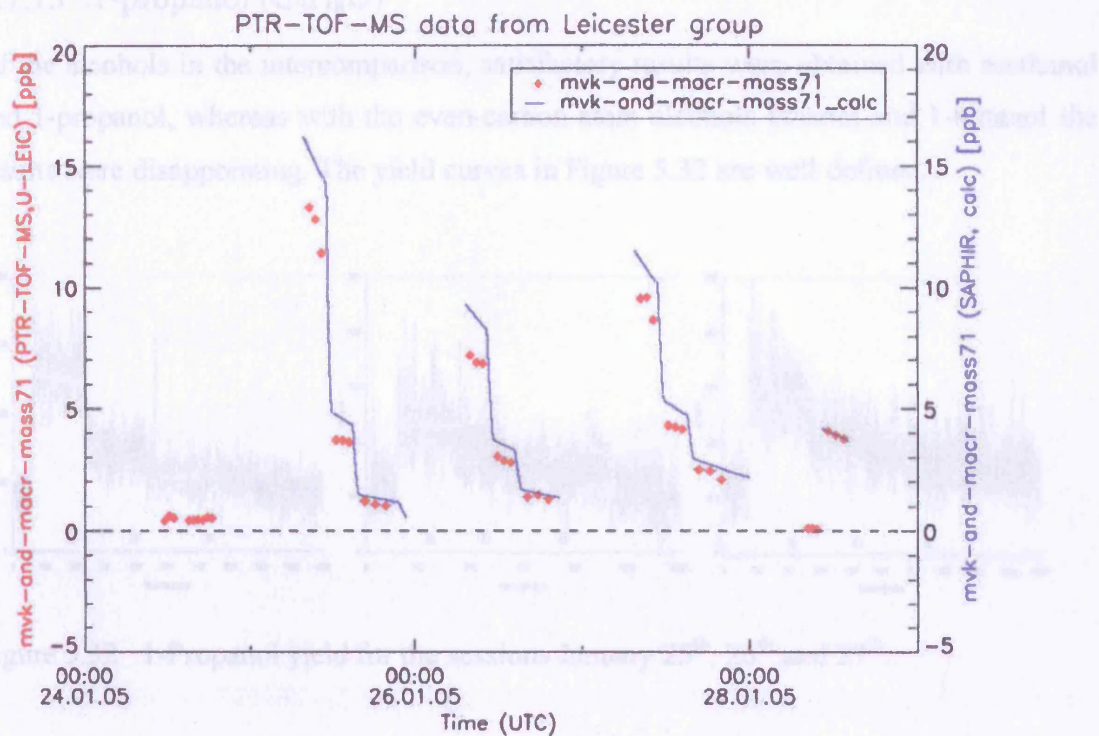


Figure 5.31 Comparison of reported values with actual concentration of MVK and methacrolein.

5.7.13 1-propanol (C₃H₈O)

Of the alcohols in the intercomparison, satisfactory results were obtained with methanol and 1-propanol, whereas with the even-carbon-atom alcohols ethanol and 1-butanol the results were disappointing. The yield curves in Figure 5.32 are well defined.

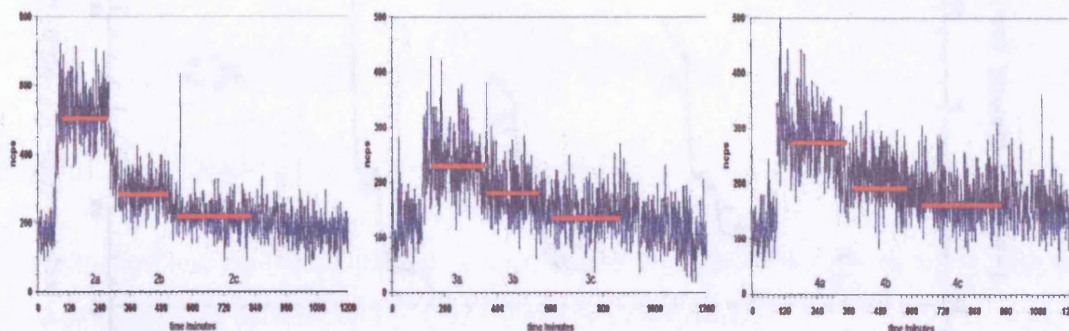


Figure 5.32 1-Propanol yield for the sessions January 25th, 26th and 27th.

The reported values of the concentration, while on the low side, are acceptable, and certainly more acceptable than some other groups were able to report. Once again the PTR-TOF-MS's consistency in dealing with varying concentrations was in evidence here as well. The 1-propanol molecule has major fragments at 41 and 43 da, and in both cases those mass channels have significant contributions from other sources, such as acetaldehyde, MBO or methyl acetate.

No matter which peak was used to analyse the results, the contribution from interfering compounds had to be calculated by referring to other prominent peaks of species suspected of interference. During the initial calibration experiment, good agreement was obtained for the sensitivity using both the 41 and 43 Dalton peaks as a basis.

The reference sensitivity for 1-propanol was 62.8 ncps ppbv⁻¹ which is 19% below the higher of the two calibration mixture values of 31.3 and 68.3 ncps ppbv⁻¹. The concentrations reported are in Table A5.11.

5.2.14 Toluene (C₇H₈)

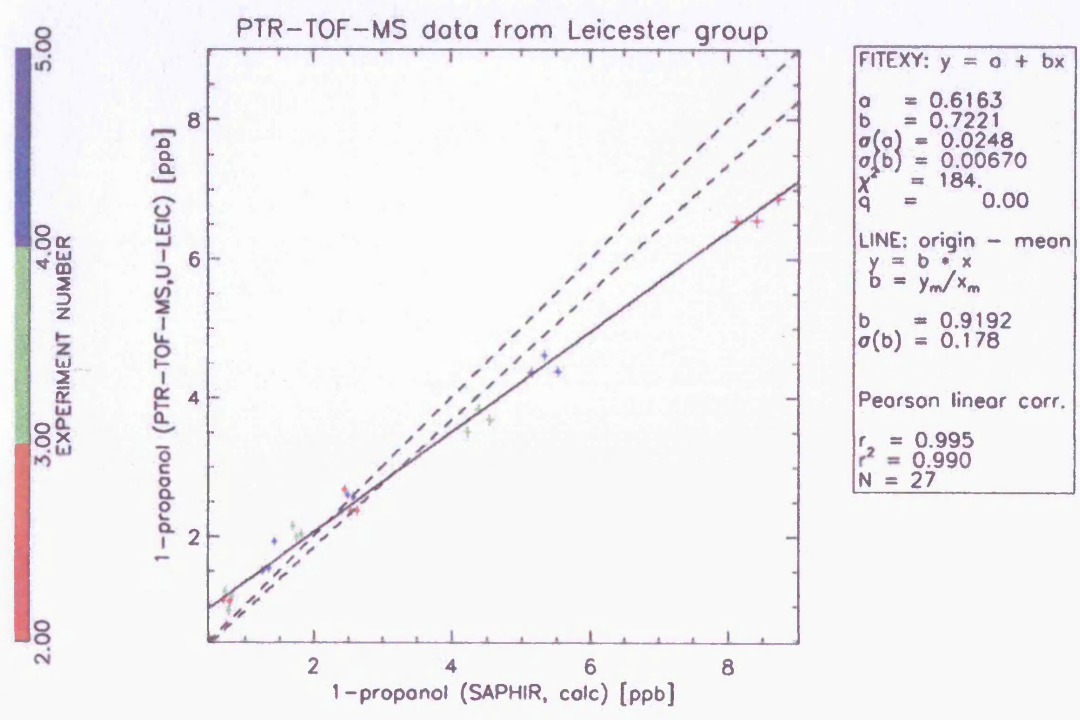
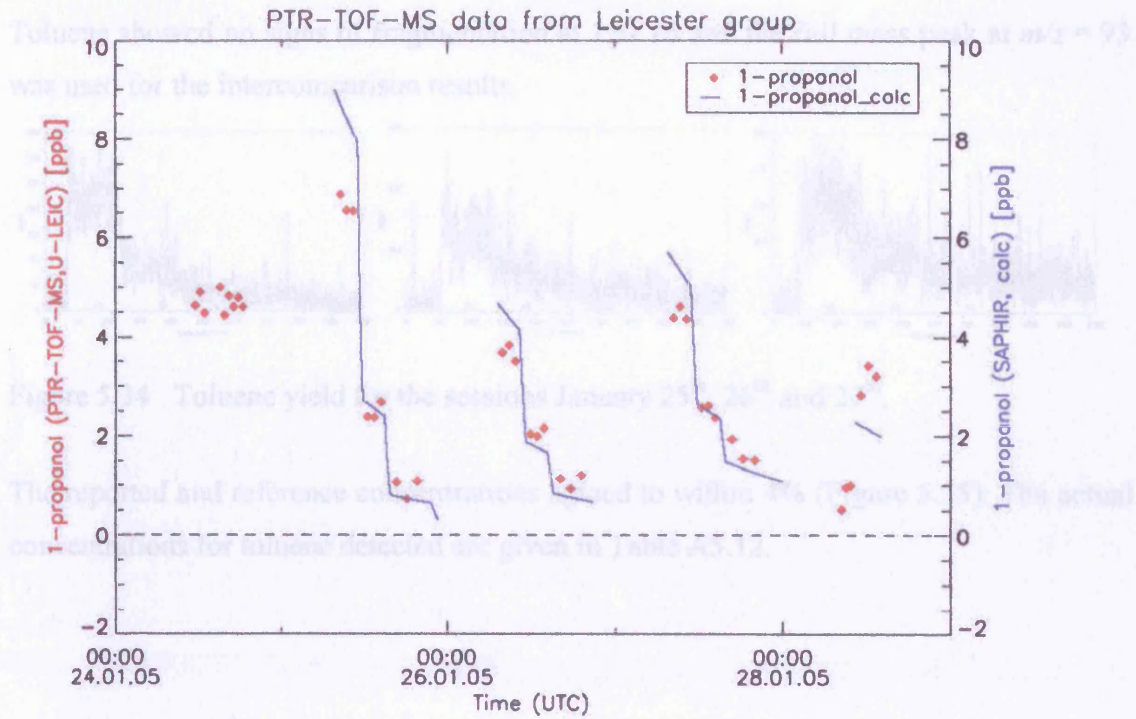


Figure 5.33 Comparison of reported values with actual concentration of 1-propanol.

5.7.14 Toluene (C₆H₅CH₃)

Toluene showed no signs of fragmentation at 150 Td and the full mass peak at $m/z = 93$ was used for the intercomparison results.

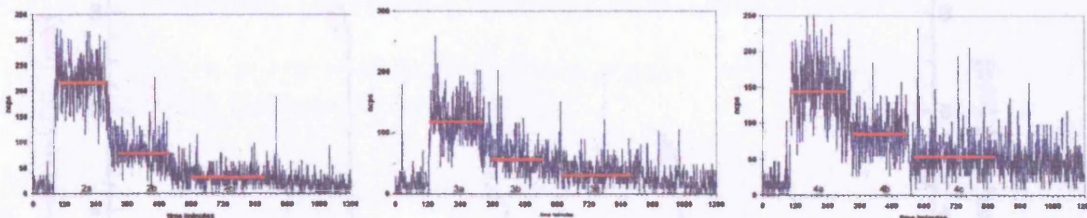


Figure 5.34 Toluene yield for the sessions January 25th, 26th and 27th.

The reported and reference concentrations agreed to within 4% (Figure 5.35). The actual concentrations for toluene detected are given in Table A5.12.



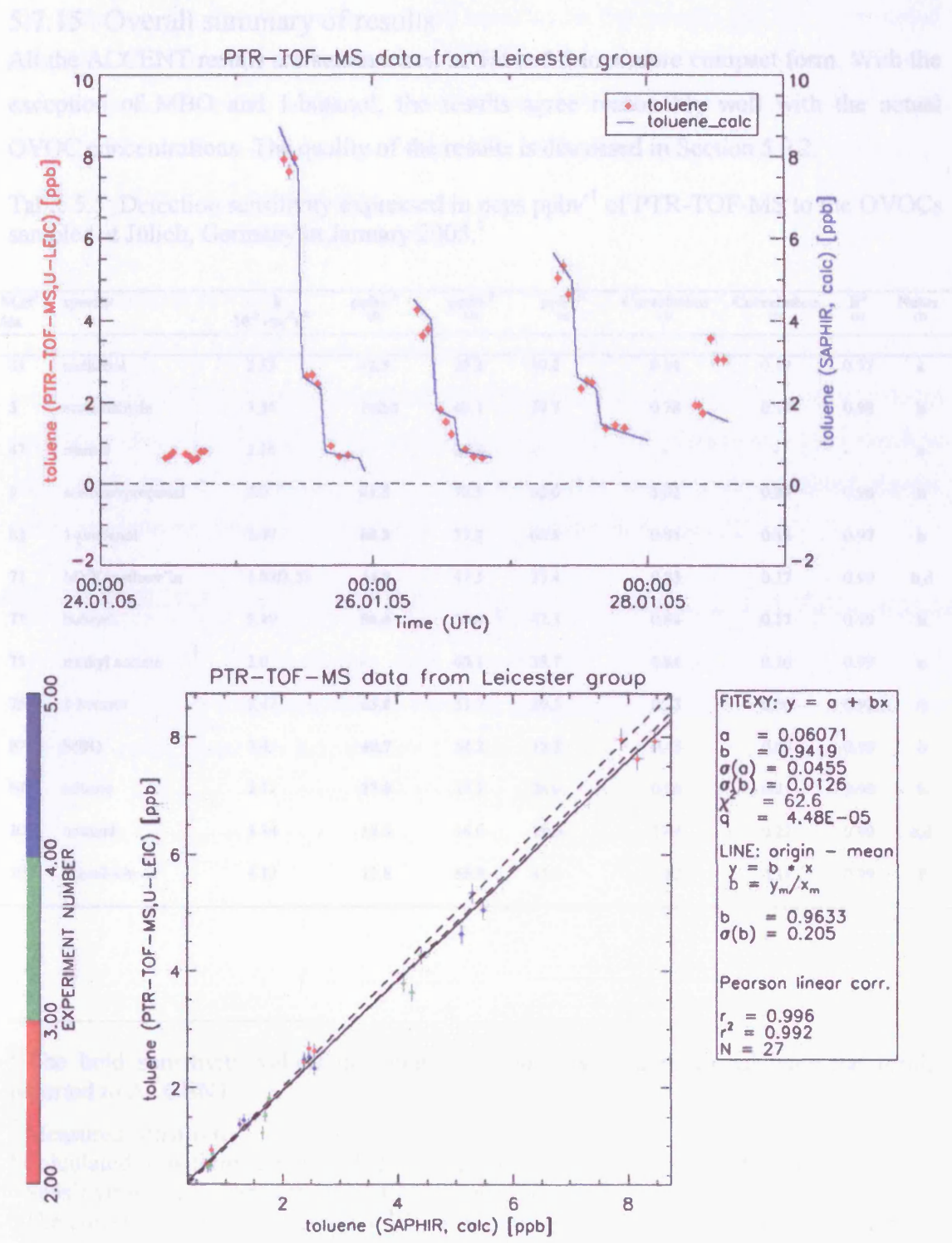


Figure 5.35 Comparison of reported values with actual concentration of toluene.

The sensitivity of the PTR-TOF-MS as measured at ACCENT was 26.0 ncps ppbv⁻¹ which compared well with values obtained from the Bristol/Apel and FAL mixtures of 27.2 and 27.0 ncps ppbv⁻¹ respectively.

5.7.15 Overall summary of results

All the ACCENT results are summarised in Table 5.5 in a more compact form. With the exception of MBO and 1-butanol, the results agree reasonably well with the actual OVOC concentrations. The quality of the results is discussed in Section 5.9.2.

Table 5.5 Detection sensitivity expressed in ncps ppbv⁻¹ of PTR-TOF-MS to the OVOCs sampled at Jülich, Germany in January 2005.¹

MH ⁺ /da	species	k 10 ⁻⁹ cm ³ s ⁻¹	ppbv ⁻¹ (²)	ppbv ⁻¹ (³)	ppbv ⁻¹ (⁴)	Correlation (⁵)	Correlation (⁵)	R ² (⁶)	Notes (⁷)
33	methanol	2.33	42.9	29.2	40.2	0.94	0.19	0.97	a
5	acetaldehyde	3.36	102.0	43.1	79.7	0.78	0.17	0.98	b
47	ethanol	2.26	-	29.9	-	-	-	-	c
9	acetone+propanal	3.0	61.5	38.5	62.6	1.02	0.23	0.98	b
61	1-propanol	2.47	68.3	31.3	62.8	0.91	0.18	0.97	b
71	MVK/methacryln	3.83/3.53	44.9	47.5	37.4	0.83	0.17	0.99	b,d
73	butanal	3.49	50.4	59.8	42.3	0.84	0.17	0.99	b
75	methyl acetate	2.0	-	40.1	33.7	0.84	0.16	0.99	e
75	1-butanol	2.47	63.0	31.7	20.5	0.33	0.06	0.92	b
87	MBO	3.4	40.7	54.2	18.3	0.45	0.09	0.99	b
93	toluene	2.12	27.0	27.2	26.0	0.96	0.21	0.99	b
101	hexanal	3.74	18.3	48.0	19.0	1.04	0.22	0.99	b,d
107	benzaldehyde	4.12	11.8	55.0	45.1	0.82	0.17	0.99	f

¹ The bold sensitivity values in columns 3 and 4 were used to calculate the results reported to ACCENT.

² Measured sensitivity

³ Calculated sensitivity using published or assumed values for rate coefficients

⁴ Sensitivities measured at the ACCENT intercomparison

⁵ The correlation slope is the ratio of the Leicester species concentrations to the reference values from ACCENT. A positive intercept is due to a small residual background count.

⁶ R² is used as a measure of the excellent consistency of the reported results.

⁷ Key to symbols:

(a) Methanol standard 10ppmv Kore Technologies; (b) Apel/Riemer standard by kind permission of the University of Bristol; (c.) Not reported; (d) FAL standard on site (e) calculated, assumed rate coefficient = 3.0x10⁻⁹ cm³ s⁻¹; (f) calculated from published rate coefficient 4.12x10⁻⁹ cm³ s⁻¹.

The effect on the detection efficiency of humidity in the sample gas has been noted elsewhere by Warneke [Warneke *et al.*, 2001] and others [Dommen *et al.*, 2003; Steinbacher *et al.*, 2006]. Judging from the values of R^2 obtained at Jülich (Table 5.5), the PTR-TOF-MS's response is not noticeably affected by the presence of both water vapour and ozone in the atmosphere.

5.8 Reporting results

The results of the intercomparison campaign were submitted to the coordinator of the campaign, Dr. Ralf Koppmann, and forwarded to the referee, Dr. Eric Apel of NCAR, for evaluation. Preliminary results were released at the ACCENT Workshop held at Jülich in June 2005. Errors in reporting were identified and a new set of corrected figures submitted. The next version of the results were received on August 31st.

The numerical values of the reported data are shown in table form in Appendix 1, Tables A1.5.1 to A1.5.12, in the format used to report the results to ACCENT. For each compound there is a column for the reported concentration in ppbv, a column for the statistical error. These are supplemented by columns listing the underlying atmospheric detail: the precision or instrumental limiting error (ILE) as described in Chapter 4, Section 4.5.8.2, and the signal-to-noise ratio for the target compounds using the grouped results.

5.8.1 Statistical errors

For the purpose of obtaining results for the reported data, one-minute runs were summed into groups ranging from 40 to 90 minutes. Background run for each day were also grouped into a single group. The statistical errors of the data and the background were calculated before they were all normalised to 10^6 ncps. The statistical variation is calculated from the expression

$$\Delta z = (\Delta X^2 + \Delta B^2)^{1/2} \quad \text{Equation 5.1}$$

where ΔX is the statistical variation of a peak and ΔB is the statistical variation of the corresponding mass channel in the background spectrum.

5.8.2 Precision

Section 4.6.7.2 describes how the precision of the measurements is derived. As a reference source the data from the Bristol/Apel calibration mixture was used. Since most of the species are present with a concentration of 400 – 500 ppbv, the counts registered in the mass channels of interest were of the order of 10^4 or more before normalising, so that the statistical error contribution to the observed standard deviation is small in comparison with the remaining effects. In most cases the values for the relative standard deviation for precision was in the region of 3%. The measure of the precision refers to the un-aggregated data.

5.8.3 Signal-to-noise ratios

The final column in each of Appendix 1, Tables A1.5.1 to A1.5.12, is the signal-to-noise ratio obtained from the one-minute runs. They are also grouped together in Appendix 1, Table A1.5.13. It is the practice in electrical measurements to regard signals where the signal-to-noise ratio exceeds 3 as acceptable [Wayne, 1994]. In more familiar terms, signal-to-noise ratios of 1, 2 and 3 correspond to uncertainty bands of 1σ , 2σ and 3σ respectively. Inspection of the signal-to-noise ratios in Table A5.13 indicate surprisingly that the variation of the signal-to-noise ratio is affected far less by concentration present, than by the type of species. Low signal-to-noise ratios are found in situations where the OVOC concentrations are low, and where contributions from background are relatively large.

The effect of collecting one-minute scans into larger groups on the signal-to-noise ratios of the worst performers in entire series, as found in sample 27_Saph_4c_1, is shown in Figure 5.36. The curves for the remaining OVOCs in the sample are not shown as they have signal-to-noise ratios greater than 3 and so would be easily distinguished in a one-minute run.

In Figure 5.36 the signal-to-noise figures of all the OVOCs shown exceed the 2σ level for two minute or greater sampling periods, while all but one would be above the 3σ level with three minute sampling periods.

5.9.2 Quality of the results

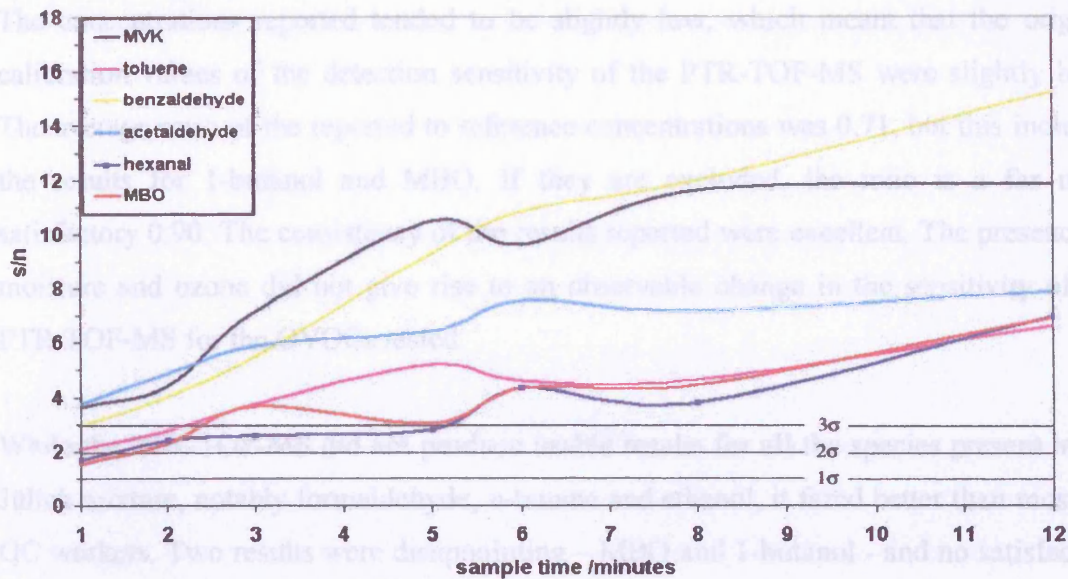


Figure 5.36 Effect of summing on the signal-to-noise ratios.

In Chapter 3, Section 3.14.7 it was observed that in order to register a single count from 1 ppbv toluene, it would take on average about 9.7 seconds, but for a statistically significant result, collecting the data for 2 minutes or longer should provide data with sufficient accuracy. For OVOCs such as ethanol and 1-butanol for which the PTR-TOF-MS was found to have a low detection efficiency, a longer accumulation time would be required to obtain a statistically significant number of events, and low signal-to-noise ratios would also indicate the minimum accumulation time.

5.9 Conclusions

5.9.1 Performance

During the ACCENT intercomparison campaign the PTR-TOF-MS performed faultlessly day and night throughout the data acquisition week. The temperature in the container did vary slightly (approx. 3 °C), but not on the scale experienced at Weybourne. No instability problems were observed during this period either, so the equipment performance was up to expectations.

5.9.2 Quality of the results

The concentrations reported tended to be slightly low, which meant that the original calibration values of the detection sensitivity of the PTR-TOF-MS were slightly high. The average ratio of the reported to reference concentrations was 0.71, but this included the results for 1-butanol and MBO. If they are excluded, the ratio is a far more satisfactory 0.90. The consistency of the results reported were excellent. The presence of moisture and ozone did not give rise to an observable change in the sensitivity of the PTR-TOF-MS for the OVOCs tested.

While the PTR-TOF-MS did not produce usable results for all the species present in the Jülich mixture, notably formaldehyde, *n*-butane and ethanol, it fared better than most the GC workers. Two results were disappointing – MBO and 1-butanol - and no satisfactory answer could be found to explain the large discrepancy between the reported and reference concentrations.

The need to stabilise the operating temperature and environment in which the PTR-TOF-MS operated at its best, has been satisfactorily addressed. Further development to increase the hydronium count rate will extend the usefulness of the machine, by reducing the sampling time need for OVOC concentrations in the sub-ppbv region.

The sensitivity of the PTR-TOF-MS was measured for several OVOCs and it was possible to prove that the sensitivity was sufficient to detect concentrations of well below 1 ppbv using a single one-minute spectrum in the best cases. The confidence in such a measurement would be increased if several spectra were summed.

In the next chapter, the experiments using NO^+ , O_2^+ and NH_4^+ as reactant gases are described in a search for a new method to distinguish between members of an isobaric doublet.

Chapter 6

Chemical Ionisation Reaction Mass Spectrometry (CIRMS)

Perplexity is the beginning of knowledge.

- Kahlil Gibran (1883-1931)

6 Chemical ionisation reaction mass spectrometry (CIRMS)

6.1 Introduction

CIRMS or chemical ionisation reaction mass spectrometry uses the techniques developed for PTR-TOF-MS but applies them to a broader range of chemical ionisation processes. CIRMS makes use of a variety of chemical reagent ions in place of the hydronium ions normally used and the types of reactions resulting usually do not involve proton transfer. The wider scope of chemical ionisation is discussed in Chapter 1, Section 1.4.2.

During the Intercomparison campaign (Chapter 5) and the headspace experiments, which followed soon thereafter (Chapter 3, Section 3.14), hexanal, methyl vinyl ketone and methacrolein were found to undergo considerable fragmentation on protonation. In addition, proton transfer reactions using H_3O^+ were unable to differentiate between the isobaric compounds methyl vinyl ketone (MVK) and methacrolein, highlighting a significant limitation of the PTR-MS technique.

In SIFT-MS reagent ions generated in a non-selective ion source are mass-selected prior to injection into the flow tube, whereas in PTR-MS in general (including the PTR-TOF-MS) no ion pre-selection is used, but the operating conditions are optimised to favour the production of a particular reagent (H_3O^+ in this case). From that stage on, many of the principles on which PTR-MS systems are based are shared with selected ion flow tube mass spectrometry (SIFT-MS) where the reagent and analyte ions mix and react in a drift-tube in PTR-MS and in the flow tube of SIFT-MS.

In recent years Smith and Španel have carried out extensive SIFT-MS work (reviewed in [Smith and Španel, 2005]) in which the reactions of H_3O^+ with a wide variety of organic analytes have been compared with other chemical ionisation precursor ions such as NO^+ and O_2^+ . To a lesser extent the rôle of NH_4^+ ions have been studied as a potential candidate for proton transfer reactions [Lindinger *et al.*, 1998; Warneke *et al.*, 1996] or adduct formation [Adams *et al.*, 2003]. From this extensive body of work, the relative rates of reactions have been deduced, as well as extensive tabulations of the resulting ion products. The reactions of NO^+ and O_2^+ have often been found to differ considerably

from those of H_3O^+ . In the case of NO^+ , hydroxy ion transfer, hydride ion transfer, electron transfer and the formation of associated M.NO products have been observed. In the case of O_2^+ disruptive fragmentation of the product ions often leads to the production of a wide variety of daughter ions. Charge transfer reaction involving NO^+ and O_2^+ have been observed to proceed at the collisional rate [Williams *et al.*, 2000]. Ammonium ions, when unable to react by proton transfer, are not energetic enough to initiate any of the previously mentioned alternative reaction routes, with the exception of the formation of associations with target molecules, usually through a stabilising termolecular process. While these changes in product identities and distributions are interesting, it not immediately clear that they have any important analytical uses.

Generally, in past PTR-MS work there have been few attempts to explore the use of alternative chemical ionisation reactions. Reagent ions which do not involve proton transfer such as NO^+ , O_2^+ and NH_4^+ (where its proton affinity precludes proton transfer) have so far not yet been employed under the conditions generally used in PTR-MS. Initially, it was not clear if sufficiently clean sources of NO^+ , O_2^+ or NH_4^+ could be obtained for work in instruments specifically designed for PTR-MS work such as the PTR-TOF-MS.

In this chapter, the possibility and indeed the feasibility of using the alternatives to H_3O^+ are explored. Using the radioactive source described in Chapter 2, NO^+ , O_2^+ and NH_4^+ ions have been successfully generated. As will be shown, relatively clean sources of the desired ions can be obtained without the need for mass pre-selection. The chemistry of these ions has been compared with that of H_3O^+ under conditions typical of the PTR-TOF-MS experiments described in Chapters 4 and 5. A few selected organic compounds were selected as trial analytes to demonstrate the chemistry. The ion-molecule chemistry is found to be similar to but not identical with that observed in SIFT-MS experiments. In particular, the use of NO^+ is found to be useful to distinguish isobaric species which are not separated when H_3O^+ is employed.

6.2 Previous investigations using alternative CI reagents

This section reviews the known ionisation processes for the alternative CI reagents considered in this chapter. Much of the information comes from the comprehensive

SIFT-MS studies by Smith, Španel and several co-workers as reviewed in [Smith and Španel, 2005].

As pointed out in the introduction to this chapter, the SIFT-MS and CI-TOF-MS share many characteristics, but there are also important differences. Most notable is the use of an accelerating electric field along the drift-tube of the PTR-TOF-MS (and CI-TOF-MS) which is absent in the SIFT-MS. This electric field and any differences in operating pressure can cause additional fragmentation of ions by collision-induced dissociation. Another point of difference between the two techniques is that in SIFT work helium is normally used as the buffer gas as opposed to nitrogen or air in the CI-TOF-MS. Ions have a longer mean free path in helium and consequently need to travel further in the flow-tube before reaching thermal equilibrium. The findings from CI-TOF-MS and SIFT-MS studies are not expected to be identical, although the latter should provide useful information for the former.

A series of experiments were carried out using NH_4^+ , O_2^+ and NO^+ as chemical ionisation reagents in the CI-TOF-MS. Before these are described, the known chemistry of these CI reagents, along with that of H_3O^+ , is briefly described.

6.2.1.1 H_3O^+

The chemistry of proton transfer reactions using H_3O^+ has been discussed in detail in Chapter 1, Sections 1.4.4 – 1.4.6, where it forms part of the introductory discussion related to the main body of the thesis. Most SIFT-MS work and all PTR-MS work is based on proton transfer reactions involving H_3O^+ . Where the analyte proton affinity permits, the reaction proceeds by proton transfer, although other exit channels, such as the expulsion of water molecules in some alcohols, have been noted [Lindinger *et al.*, 1998].

In proton transfer reactions, H_3O^+ ions donate protons to target VOC molecules M, yielding mainly protonated ions MH^+ . Some saturated aldehydes lose water molecules giving $(\text{M}-\text{H}_2\text{O})^+$ product ions, and partial dissociation occurs with longer chain alkenes. The low mass alkanes do not react with H_3O^+ while large scale fragmentation is observed with the heavier members such as nonane [Wyche, 2005]. Multihydrated clusters

$(MH^+(H_2O)_n)$ tend to form around MH^+ , but in the PTR-TOF-MS these can be minimised by operating at higher E/N values.

6.2.1.2 NH_4^+

NH_4^+ ions can act as proton donors with analytes whose proton affinities are higher than 854 kJ mol^{-1} (Section 6.2). Consequently proton transfer does not occur with most common VOCs, and so the reactions that are observed tend to proceed by association (reaction 1.32). In this case they form either a loose association or cluster or a more strongly bonded molecule depending on the form of the potential surface and the heights of the potential barriers of the reactants [Adams *et al.*, 2003]. NH_4^+ reactions, where permitted by the proton affinity of the target molecules, are usually not as exothermic as for NO^+ and O_2^+ and so large-scale fragmentation of parent ions is unlikely. Adams and co-workers using SIFT-MS reported looking for but finding no signs of fragmentation in their work. In their work with some common OVOCs, they found evidence favouring clustering or possibly adduct formation.

The main objective of Adams *et al.* was the investigation of the bonding behaviour of NH_4^+ with some OVOCs. They were interested in establishing whether the association of NH_4^+ with a series of OVOCs leads to the production of a cluster $M.NH_4^+$ or a more tightly bonded species with the same formula. In addition to cluster and adduct formation, NH_4^+ ions are able to act as proton donors to species that have a higher proton affinity than NH_3 ($854.0 \text{ kJ mol}^{-1}$). While the reaction is feasible, it is seldom used. Lindinger [Lindinger *et al.*, 1998] cites one case where the reaction was used in a PTR-MS study to distinguish between α -pinene and the isobaric twin 2-ethyl-3,5-dimethylpyrazine. Warneke and co-workers also used proton transfer from NH_4^+ to determine that a peak at $m/z = 43$ was due to a major dissociative product from protonated iso-propanol [Warneke *et al.*, 1996], thereby excluding alternative contributions from acetic acid and methyl formate. Since the target species for this thesis all have proton affinities well below that of ammonia (see Chapter 1, Table 1.8), proton transfer will be absent and cluster or adduct formation are the most likely reactions observed.

6.2.1.3 O₂⁺

O₂⁺ has been identified as a useful precursor ion [Smith and Španel, 1996] for SIFT-MS. As with NO⁺ (Section 6.2.1.4), the reactions proceed principally by means of charge transfer, non-dissociatively where the fragmentation channels are endothermic and dissociatively when exothermic.

The total energy involved in a reaction will determine which route is followed [Williams *et al.*, 2000]. The total energy is defined thus:

$$E_{\text{total}} = RE_{\text{ion}} + E_{\text{trans}} + E_{\text{rot}} + E_{\text{vib}} + E_{\text{internal}} \quad (6.1)$$

Here RE_{ion} is the recombination energy of the product ion which is the same as the ionisation energy of the analyte. If the ground state of the analyte is repulsive, then the recombination energy corresponds to the vertical recombination energy to the repulsive region of the neutral potential. The average translational energy E_{trans} is the energy imparted to the incoming ion by the drift-tube potential gradient. E_{rot} , the average analyte rotational energy is equal to $\frac{1}{2} k_{\text{B}}T$. E_{vib} is an ensemble average of the vibrational levels and E_{internal} is the corresponding average ion internal energy of the product ion. It was found that certain exit channels were sensitive to changes in a particular type of energy, as these were associated with a particular feature of the molecular structure. So, for example, by changing the recombination energy will give information on the electronic energy of the reaction [Ausloos, 1982].

The O₂⁺ ion has recombination energy of 12.06 eV. Consequently, electron transfer (reaction 1.34) is possible with molecules with lower ionisation energies, which will include almost all organic molecules. In view of the relatively high recombination energy of the precursor, several exit channels are exothermic, so that dissociative charge transfer is observed, resulting in significant fragmentation of the parent ion [Anicich, 2003]. More complicated spectra are observed since the difference in ionisation energies will deposit excess energy into the analyte molecule. Consequently the SIFT-MS studies generally show complicated spectra when O₂⁺ is employed.

6.2.1.4 NO⁺

NO⁺ has also been found to be a useful precursor ion for SIFT-MS work [*Smith and Španel, 1996*]. NO⁺ reacts with analyte molecules by electron transfer (reaction 1.34) or sometimes hydride (anion) extraction (reaction 1.33). Apart from the parent ion M⁺ production by charge transfer, reactions with these precursors often result in the production of fragments (M-H)⁺ or greater.

NO⁺ has a recombination energy of 9.6 eV, roughly comparable to those of the analyte species examined in the present study. The translational energy of about 0.3 – 0.4 eV contributed to the system by the drift-tube gradient of the PTR-TOF-MS ensures that there is some surplus energy which may open additional exit channels such as fragmentation, although not on the scale observed with O₂⁺ ions.

The main reaction products derived from SIFT-MS studies for the main classes of organic compounds are summarised in Table 6.1. Three main types of CI reaction are observed as described by reactions 1.30, 1.32, 1.33 and 1.34. Hydride ion extraction (reaction 1.33) is found with the alcohols, aldehydes, ethers and aliphatic alkanes. When NO⁺ ions react with aldehydes and ethers hydride ion transfer occurs giving (M-H)⁺ and the formation of HNO. This reaction is the only exit channel observed with saturated aldehydes. With unsaturated aldehydes the formation of associated NO⁺.M ions stabilised via termolecular reactions have been observed.

The position of the double bond in alkenes affects the course of the reaction with NO⁺. For 1-alkenes the principle reaction leads to the formation of the adduct M.NO⁺, followed by partial stabilisation and subsequent partial dissociation. In the case of 2-alkenes charge transfer occurs giving M⁺ and this is followed in some cases by hydride ion abstraction forming (M-H)⁺.

The reactions summarised in Table 6.1 have been observed to proceed mainly at or close to the gas kinetic rate [*Smith and Španel, 2005*].

Table 6.1 Processes occurring in the bimolecular and termolecular reactions of NO^+ ions and different families of hydrocarbons.¹

Species	NO^+ reactions
Alcohols	$(\text{M-H})^+$; $(\text{M-OH})^+$
Diols	$(\text{M-H})^+$; $(\text{M-OH})^+$
Phenols	M^+ ;
Aldehydes	$(\text{M-H})^+$
Ketones	$\text{NO}^+.\text{M}$; M^+
Carboxylic Acids	$\text{NO}^+.\text{M}$; $(\text{M-OH})^+$
Esters	$\text{NO}^+.\text{M}$; $(\text{M-OR})^+$
Ethers	$(\text{M-H})^+$
Organosulphur	M^+
Amines	M^+ ; $(\text{M-H})^+$
Aliphatic hydrocarbons	$(\text{M-H})^+$ (alkanes); MH^+ (alkenes)
Aromatic hydrocarbons	M^+
Monoterpenes	M^+ ; $(\text{M-R})^+$
Aliphatic halocarbons	$\text{NO}^+.\text{M}$; M^+ ; $(\text{M-X})^+$
Aromatic halocarbons	$\text{NO}^+.\text{M}$; M^+ ; $(\text{M-X})^+$

Ketones have been observed to form adducts with NO^+ for low values of E/N , but for higher values, charge transfer (M^+) and dissociative charge transfer take over. NO^+ ions show little inclination to form clusters [Fairley *et al.*, 1999].

In general, electrophilic addition (reaction 1.30) occurs with ketones and carboxylic acid.. Electron transfer (reaction 1.34) is found to occur with most species, where the ionisation energy of the analyte is less than that of NO (9.26 eV) [Lias *et al.*, 1988], [Lide, 1991].

6.3 Experimental section

6.3.1 Apparatus

¹ The reactant molecules are designated as M. M^+ is a parent radical cation and $\text{NO}^+.\text{M}$ is an adduct ion. The table is reprinted from Smith, D., and P. Španel, *Mass Spectrometry Reviews*, 25, 661-700, 2005.

The equipment used was the same as used in the headspace fragmentation experiments as described in Section 3.14. The reagents, pure O₂, ammonia or a 600 ppmv mixture of NO in N₂, were fed into the CI-TOF-MS at 50 sccm using the same mass flow controller as was used for the PTR experiments. The sample gas was fed into the CI-TOF-MS at 275 sccm.

The data taken consisted of a series of one-minute runs which were recalibrated to eliminate drifts in the time scans.

The experimental conditions for these experiments were the same as those used during the ACCENT Intercomparison campaign as described in Chapter 5: E/N was 150 Td, the drift-tube bias 2700 V and the drift-tube pressure 7.9 mbar.

The analyte and reagent lines were maintained at a constant temperature of 40 °C and the laboratory temperature remained at a constant 23 °C throughout, so that problems from temperature drifts were avoided.

6.3.2 Reagent handling

Four CI reagents were investigated, each with different characteristic reaction profiles, to demonstrate the capabilities of CIRMS: H₃O⁺, NH₄⁺, O₂⁺ and NO⁺.

For the H₃O⁺ experiments, the saturated water vapour was obtained by bubbling nitrogen (BOC 99.998%) carrier gas through a canister of demineralised water (15 MΩ cm⁻¹), as described in Section 4.5.2. The canister was maintained at 40°C. and the saturated vapour passed through a water trap before entering the instrument to remove water droplets.

Pure ammonia (BOC Special Gases, MS Grade) and pure oxygen (BOC Special Gases N5.0) were used to provide NH₄⁺ and O₂⁺ ions.

Table 6.2 Analytes chosen for investigation in the head-space fragmentation experiments.²

Item	PA / kJ mol ⁻¹	Purity	Source
Acetaldehyde	769.0	99%	Sigma Aldrich
Acetone	812.1	>95%	Sigma Aldrich
Acetonitrile	779.1	>95%	Sigma Aldrich
Benzene	750.2	>95%	Sigma Aldrich
1-Butene	746.8	1 ppm in N ₂	BOC Special Gases
Ethanol (anhydrous)	776.6	>95%	VWR International
Ethyl Acetate	-	>95%	Fisher Scientific
Hexanal	-	98%	Sigma Aldrich
Methacrolein	808.8	95%	Sigma Aldrich
Methyl Benzoate	-	>95%	Sigma Aldrich
MVK	834.7	95%	Sigma Aldrich
Toluene	784.1	>95%	Fisher Scientific

6.3.3 Analyte handling

The analytes chosen for this investigation are shown in Table 6.2. The analyte vapour was obtained by flushing a Dreschell flask containing a small quantity of analyte with nitrogen (BOC zero-grade 99.99% pure) previously dried by passing through a coil immersed in an acetone/dry ice mixture, and subsequently reheated to 40 °C by passing along a 5 m. long electrically heated tube.

6.3.4 Experimental procedure

A series of one minute spectra for the mass range of $m/z = 15$ to 200 were taken to track the declining analyte concentration. Initial runs were discarded in the analysis phase and valid data collection started once the reagent count had recovered to 90 % of its value prior to the introduction of the analyte.

² The proton affinities (PS) are listed in the column are taken from Zhou, J., and R. Zhang, *Atmos. Environ.*, 38, 2177-2185, 2004.

Background contributions to the spectra were obtained from nitrogen clean-up runs between sample changes. Clean-up spectra highlighted permanent system impurities, impurities in the nitrogen supply or long-lasting contaminations from previous samples.

6.4 Reducing interference from residual H_3O^+

Contributions from residual proton transfer reactions complicate the analysis of the results obtained when using other CI reagents. In order to remove traces of H_2O , the reagent and the carrier gases were pre-cooled by passing through cooling coils immersed in a dry ice-acetone mixture. Between runs and overnight, the cooling coils were removed from the freezing mixture and allowed to thaw. Before reconnecting them, they were flushed with dry nitrogen to remove any residual water. Trials with silica gel and molecular sieves separately or in series with pre-cooling did not produce a worthwhile effect and their use was discontinued.

All the CI gases supplied had traces of water. The reagent which was the most difficult to dry out was O_2 whereas with NH_3 and NO , the contribution of hydronium was well below that of NH_4^+ and NO^+ ions in the spectra recorded. The spectra obtained with H_3O^+ as the reagent yielded spectra were used as templates to estimate contributions from interfering proton transfer reactions (see Section 6.5.1 for details). Figure 6.1 shows the cleanliness of the ion sources. When running with NO^+ , the H_3O^+ peak was 5% of the NO^+ peak. H_3O^+ suppression was not so successful with O_2^+ where there was a 7% contribution from H_3O^+ . There was no noticeable interference from H_3O^+ in the experiments using NH_4^+ . Interference from H_2O^+ ions ($m/z = 18$) could be disregarded. In all the H_3O^+ spectra, this ion was never in evidence, and so would be even less likely to occur where H_3O^+ only appeared as a minor constituent.

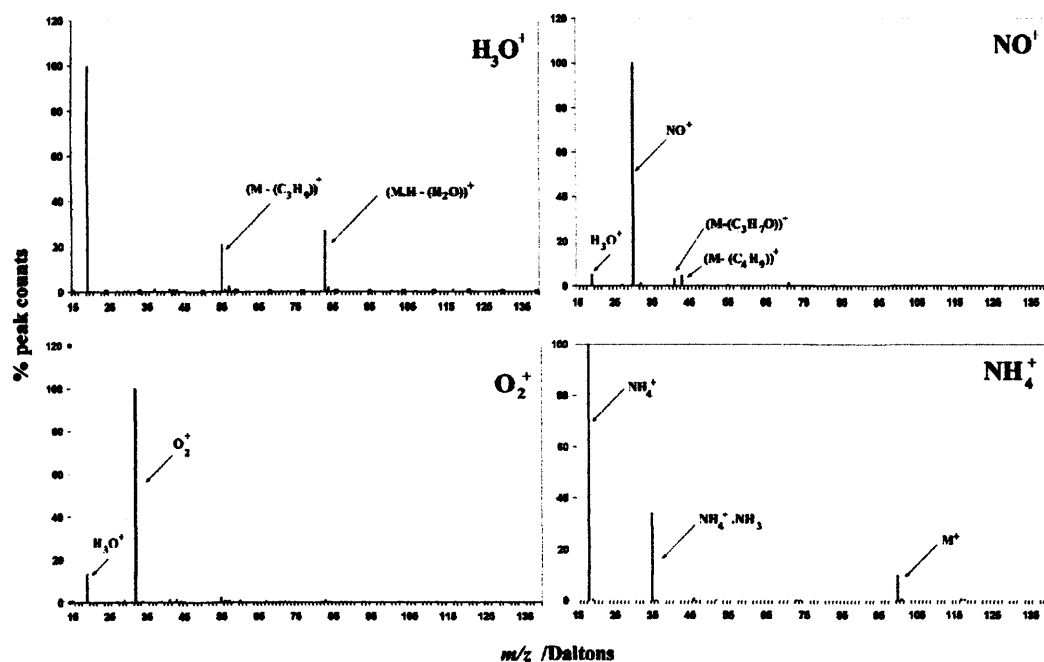


Figure 6.1 Spectra of hexanal showing the main precursor ion peak. Contributions from interfering precursors are visible but fortunately they are relatively weak.

6.5 Results

In this section we present our findings in tabular form. Of the four reagent types tried, H_3O^+ provided the cleanest and most unambiguous spectra. The yield for each mass was obtained by subtracting a background value obtained from the clean-up runs described in Section 6.3.4. As a check the peak yields were also calculated by using the peak correlation technique described in Section 3.14.4. The results obtained from the two methods agreed well. All values of ionisation energies quoted here are taken from the NIST database [NIST, 2005]. Proton affinities were also obtained from this source and the extensive work of Zhou and Zhang [Zhou and Zhang, 2004].

Sample spectra in Figure 6.2, Figure 6.5 and Figure 6.8, depict the reactions of an alkene (1-butene), a ketone (MVK) and some aldehydes (methacrolein and hexanal) with the four CI reagents H_3O^+ , NH_4^+ , NO^+ and O_2^+ . At the start of each experiment, when the analyte concentration was high enough to deplete the reagent population completely, a variety of secondary reactions took place initially that disappeared by the time the reagent count rate had returned to 90% of its value before the sample was introduced.

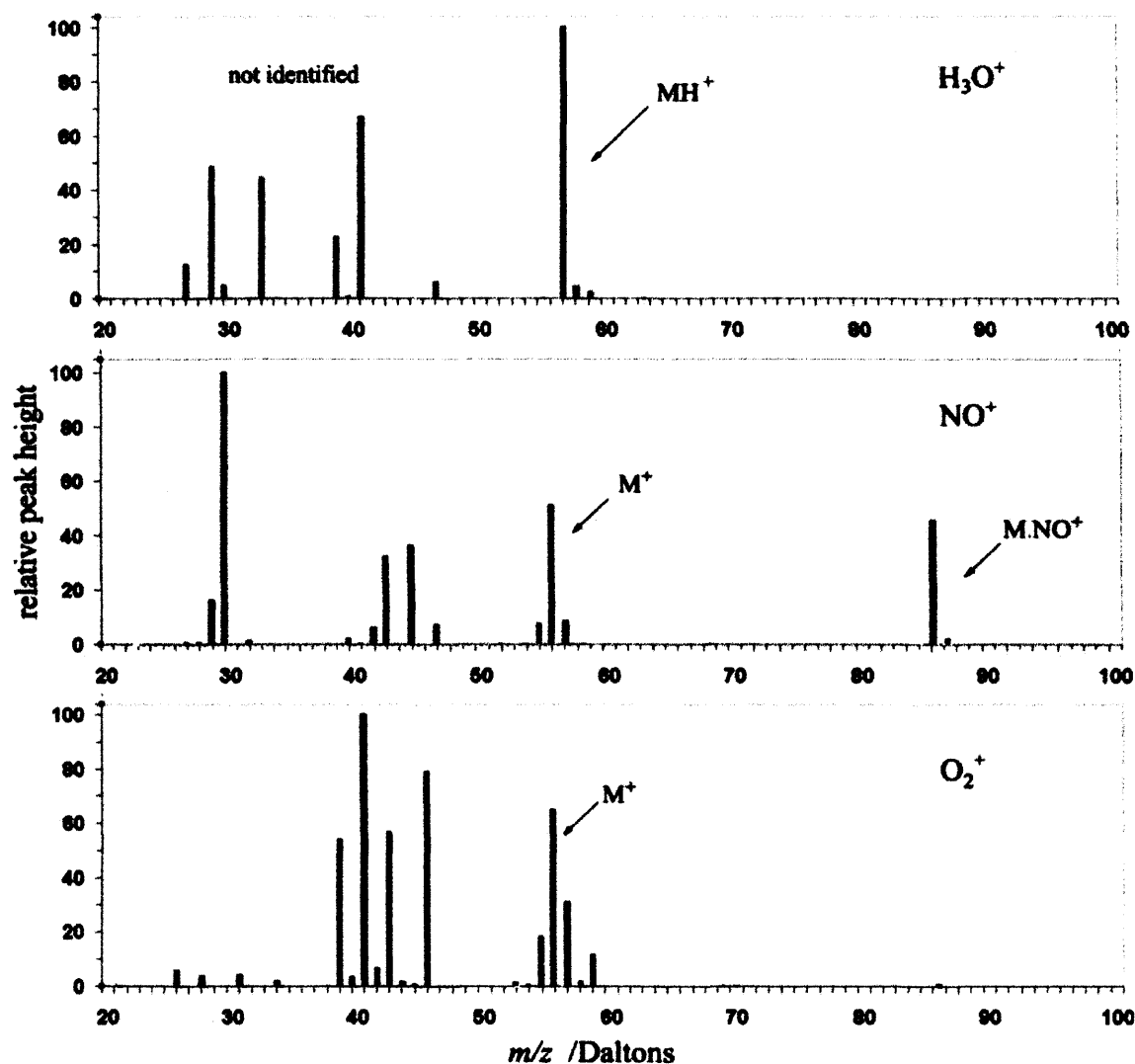


Figure 6.2 The CIRMS spectra from the reaction of 1-butene with H_3O^+ , NO^+ and O_2^+ . No products from reactions with NH_4^+ were observed.

In the cases of acetone and ethyl acetate, as an example, when working with NO^+ , strong $(\text{M}+\text{H})^+$ peaks appeared initially that were many times greater than could be accounted for by the amount of H_3O^+ ions in the system. The size of this effect decreased very rapidly initially after which it decreased in step with the analyte concentration. This phenomenon is possible evidence of self-protonation commonly observed in high concentration conditions.

6.5.1 Interference from H_3O^+ clusters

When working with O_2^+ and NO^+ it was necessary to determine to what extent proton transfer reactions from stray H_3O^+ constituted a group identification problem. Assuming that the mass peak profile is the same as running with H_3O^+ , the size of the protonated $(\text{M}+\text{H})^+$ peak in a spectrum could be used to calculate the magnitude of the interfering peaks. In the particular case of the $m/z = 55$ peak due to $\text{H}_3\text{O}^+(\text{H}_2\text{O})_2$ clusters, such interference was unlikely to exceed 5%.

6.5.2 Reactions with H_3O^+

Water has a proton affinity of 7 eV (691 kJ mol^{-1}) and easily donates a captured proton to the analytes tested. The results in Table 6.3 confirm that the predominant reaction products come from proton transfer. Among the daughter reaction products only 1-butene showed a noticeable (2.5%) monohydrate cluster.

Ethanol, ethyl acetate, hexanal, methacrolein and methyl vinyl ketone (MVK) all show signs of fragmentation. 1-butene loses a water molecule after protonation while the remainder of the samples produced the protonated $(\text{M}+\text{H})^+$ parent species. Water molecule expulsion occurs in ethanol to a minor extent (7%).

The yield of $[\text{MH}]^+$ (1% at 101 da.) for hexanal does not dominate the mass spectrum. The most prominent peak for hexanal was found at $m/z = 83$ (56%) which corresponds to the removal of a hydroxyl group from hexanal or a water molecule from protonated hexanal. The almost complete absence of this peak with the other reagents, lends some weight to the latter possibility. A large peak at $m/z = 55$ (42%) is the other main feature. This peak is most likely the result of a fracture of the carbonyl group from the alkane tail.

Protonated methacrolein and MVK show minor fragment peaks with mass 43. It is uncertain whether this occurs as a result of an ethene molecule emitted from the protonated state, or a C_2H_3 group from the parent molecule. Experiments with the other reagents show that peaks at $m/z = 43$ and 41 are much stronger than can be accounted for by interference from the protonated analytes.

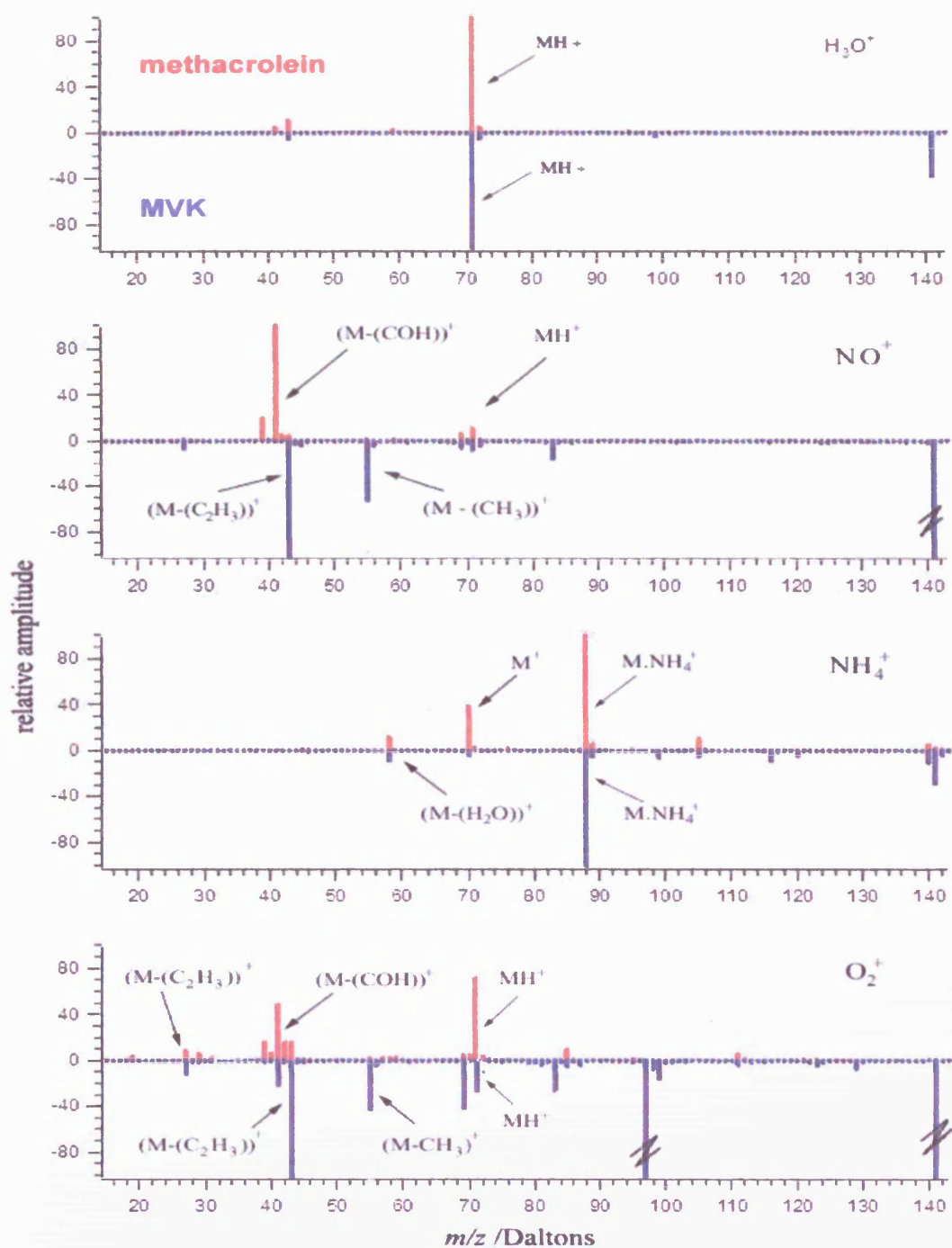


Figure 6.3 MVK (blue) and methacrolein (red) exhibit different fragmentation with NO^+ or O_2^+ reagents, but little or no differentiation with H_3O^+ or NH_4^+ . MVK has a strong tendency to dimerise. Peaks due to the dimer and its fragments are not plotted to scale so as to emphasise the relationship of the peaks derived from the fragmentation of the daughter ion.

MVK dimerises and exhibits very strong peaks at $m/z = 140$ with all the reagents. Methacrolein by contrast shows little inclination to form a dimer or cluster.

Table 6.3 Ion products from reactions with H_3O^+ for $E/N = 150$ Td.

Compound	MW	M	m/z	Branching	Ion	%
Acetaldehyde	44	$\text{C}_2\text{H}_4\text{O}$	45	M.H^+	$\text{C}_2\text{H}_5\text{O}$	100
Acetone	58	$\text{C}_3\text{H}_6\text{O}$	59	M.H^+	$\text{C}_3\text{H}_7\text{O}$	100
Acetonitrile	41	$\text{C}_2\text{H}_3\text{N}$	42	M.H^+	$\text{C}_2\text{H}_4\text{N}$	100
Benzene	78	C_6H_6	79	M.H^+	C_6H_7	100
1-Butene	56	C_4H_8	55	$(\text{M} - (\text{H}))^+$	C_4H_7	97
			73	$(\text{M} - (\text{H}).\text{H}_2\text{O})^+$	$\text{C}_4\text{H}_7.\text{H}_2\text{O}$	3
Ethanol	46	$\text{C}_2\text{H}_6\text{O}$	47	M.H^+	$\text{C}_2\text{H}_7\text{O}$	93
			29	$(\text{M} - (\text{H}_2\text{O}))^+$	C_2H_4	7
Ethyl Acetate	88	$\text{C}_4\text{H}_8\text{O}_2$	89	M.H^+	$\text{C}_4\text{H}_9\text{O}_2$	5
			61	$(\text{M} - (\text{C}_2\text{H}_3))^+$	$\text{C}_2\text{H}_5\text{O}_2$	74
			43	$(\text{M} - (\text{C}_2\text{H}_3\text{O}))^+$	$\text{C}_2\text{H}_5\text{O}$	21
Hexanal	100	$\text{C}_6\text{H}_{12}\text{O}$	101	M.H^+	$\text{C}_6\text{H}_{13}\text{O}$	1
			83	$(\text{M.H} - (\text{H}_2\text{O}))^+$	C_6H_{11}	56
			55	$(\text{M} - (\text{C}_3\text{H}_9))^+$	$\text{C}_3\text{H}_3\text{O}$	42
Methacrolein	70	$\text{C}_4\text{H}_6\text{O}$	71	M.H^+	$\text{C}_4\text{H}_7\text{O}$	88
			43	$(\text{M} - (\text{C}_2\text{H}_3))^+$	$\text{C}_2\text{H}_3\text{O}$	9
			41	$(\text{M} - (\text{CHO}))^+$	C_3H_5	4
Methyl Benzoate	136	$\text{C}_8\text{H}_8\text{O}_2$	137	M.H^+	$\text{C}_8\text{H}_9\text{O}_2$	100
MVK	70	$\text{C}_4\text{H}_6\text{O}$	71	M.H^+	$\text{C}_6\text{H}_{13}\text{O}$	95
			43	$(\text{M} + (\text{H}) - (\text{C}_2\text{H}_4))^+$	$\text{C}_2\text{H}_3\text{O}$	5
Toluene	92	C_7H_8	93	M.H^+	C_7H_9	100

Whether we are looking at a cluster or some closer alliance is not clear as some (but not all) fragment peaks are observed. This points to a cluster of two MVK molecules with one of them undergoing fragmentation.

The intensity of the cluster is dependent on the concentration of MVK in the sample, and its intensity does not follow that of the protonated peak. There are clearly several competing processes at work here.

The strong appearance of an $m/z = 55$ group in the fragmentation in 1-hexanal is most likely caused by an alkyl tail (C_3H_9) splitting off from the carbonyl group with some rearrangement of hydrogen. The $m/z = 55$ peak corresponds, amongst others, to a cluster of $H_3O^+(H_2O)_2$ but judging from the low intensity of this peak seen during the clean-up runs, interference from this source is minimal.

6.5.3 Reactions of NH_4^+

Table 6.4 summarises the ion products from reactions with NH_4^+ in the CI-TOF-MS experiments. The proton affinities of the analytes were less than that of Ammonia (8.8 eV or 854 kJ mol^{-1}) so that proton transfer was inhibited. The H_3O^+ peak in the output was between 4% - 5% of the NH_4^+ peak and the spectra produced did not have any characteristics of proton transfer reactions. In Section 6.4 the possibility of interference by H_2O^+ ions was shown to be unimportant.

Adams and co-workers found that cluster formation with ammonia [*Adams et al.*, 2003] was the predominant reaction mechanism with organic molecules, although some minor peaks could be evidence of the formation of an adjunct with NH_4^+ . In the CIRMS experiment, cluster formation was low as would be expected in conditions of mid to high E/N . Although energetically forbidden, M^+ peaks suggestive of charge transfer were found with acetaldehyde, hexanal and methacrolein and ethanol. Initially this was thought to be due to the presence of another reagent such as O_2^+ , or even H_2O^+ . O_2^+ was considered an unlikely cause, as the observed fragmentation patterns were not the same as those where O_2^+ was the reagent. H_2O^+ has never been observed where H_3O^+ was the main reagent, and since there were no sign of contributions from H_3O^+ , this possibility was also unlikely here. In the case of acetaldehyde and methacrolein, strong dimer groups were observed, so that it is possible that the observed groups could be the result of asymmetric collisional break-up of dimers. Signs of dimer formation were not seen in hexanal and ethanol.

Table 6.4 Reaction products with NH_4^+ . Its recombination energy is 4.76 eV.

Compound	MW	M	<i>m/z</i>	Branching	Ion	%
Acetaldehyde	44	$\text{C}_2\text{H}_4\text{O}$	61	$(\text{M} \cdot (\text{NH}_3))^+$	$\text{C}_3\text{H}_7\text{O} \cdot (\text{NH}_3)$	2
Acetone	58	$\text{C}_3\text{H}_6\text{O}$	76	$(\text{M} \cdot (\text{NH}_3))^+$	$\text{C}_3\text{H}_6\text{O} \cdot (\text{NH}_3)$	91
			93	$(\text{M} + (\text{NH}_4) \cdot (\text{NH}_3))^+$	$\text{C}_3\text{H}_6\text{O} \cdot \text{NH}_4 \cdot (\text{NH}_3)$	9
Acetonitrile	41	$\text{C}_2\text{H}_3\text{N}$	59	$(\text{M} \cdot (\text{NH}_3))^+$	$\text{C}_2\text{H}_3\text{N} \cdot (\text{NH}_3)$	95
			76	$(\text{M} + (\text{NH}_4) \cdot (\text{NH}_3))^+$	$\text{C}_2\text{H}_3\text{N} \cdot \text{NH}_4 \cdot (\text{NH}_3)$	5
Benzene	78	C_6H_6		None observed		
1-butene	56	C_4H_8		None observed		
Ethanol	46	$\text{C}_2\text{H}_6\text{O}$		None observed		
Ethyl Acetate	88	$\text{C}_4\text{H}_8\text{O}_2$	106	$(\text{M} \cdot (\text{NH}_3))^+$	$\text{C}_4\text{H}_8\text{O}_2 \cdot (\text{NH}_3)$	94
			123	$(\text{M} (-\text{H}) + (\text{NH}_4) \cdot (\text{NH}_3))^+$	$\text{C}_4\text{H}_8\text{O}_2 \cdot \text{NH}_4 \cdot (\text{NH}_3)$	5
Hexanal	100	$\text{C}_6\text{H}_{12}\text{O}$	117	$(\text{M} \cdot (\text{NH}_3))^+$	$\text{C}_6\text{H}_{12}\text{O} \cdot (\text{NH}_3)$	100
Methacrolein	70	$\text{C}_4\text{H}_6\text{O}$	88	$(\text{M} \cdot (\text{NH}_3))^+$	$\text{C}_4\text{H}_6\text{O} \cdot (\text{NH}_3)$	91
			105	$(\text{M} + (\text{NH}_4) \cdot (\text{NH}_3))^+$	$\text{C}_4\text{H}_6\text{O} \cdot \text{NH}_4 \cdot (\text{NH}_3)$	9
Methyl Benzoate	136	$\text{C}_8\text{H}_8\text{O}_2$	154	$(\text{M} \cdot (\text{NH}_3))^+$	$\text{C}_8\text{H}_8\text{O}_2 \cdot \text{NH}_3$	90
			171	$(\text{M} + (\text{NH}_4) \cdot (\text{NH}_3))^+$	$\text{C}_8\text{H}_8\text{O}_2 \cdot \text{NH}_4 \cdot (\text{NH}_3)$	10
MVK	70	$\text{C}_4\text{H}_6\text{O}$	88	$(\text{M} \cdot (\text{NH}_3))^+$	$\text{C}_4\text{H}_6\text{O} \cdot \text{NH}_3$	95
			105	$(\text{M} + (\text{NH}_4) \cdot (\text{NH}_3))^+$	$\text{C}_4\text{H}_6\text{O} \cdot \text{NH}_4 \cdot (\text{NH}_3)$	5
Toluene	92	C_7H_8		None observed		

Generally reaction yields were low compared to those obtained with H_3O^+ . Whereas reactions with H_3O^+ were observed to proceed at close to the collisional rate, association reactions involving NH_4^+ involve slower three-body reactions.

6.5.4 Reactions of O_2^+

Reactions with the O_2^+ ion follow the general pattern seen with H_3O^+ and as seen with NO^+ in the next section, except that fragmentation was more extensive as a result of the

strongly exothermic nature of the reactions resulting in a proliferation of the daughter ions. The reactions with O_2^+ thus proceed along the route of non-dissociative charge transfer resulting in the formation of parent radical cations M^+ , or by dissociative charge transfer resulting in the formation of several fragment daughter ions. The fragmentation products resulting from using O_2^+ as the reagent gas is summarised in Table 6.6.

Charge transfer was found to occur for benzene, 1-butene, methyl benzoate, methacrolein, MVK and toluene. In acetaldehyde, ethanol, methacrolein, methyl benzoate and MVK this was followed by the ejection of a hydrogen atom in line with the findings of Smith and Španěl from SIFT-MS []. Acetone and ethanol lose a methyl group while acetone and 1-hexanal have a slight tendency to lose H_2O molecules. [Gross, 2004].

Table 6.5 Reaction products with O_2^+ . Its recombination energy is 12.06 eV.

Compound	MW	M	m/z	Branching	Ion	%
Acetaldehyde	44	C_2H_4O	43	$(M-H)^+$	C_2H_3O	100
Acetone	58	C_3H_6O	43	$(M-CH_3)^+$	C_2H_3O CH_3O	100
Acetonitrile	41	C_2H_3N		No reaction		-
Benzene	78	C_6H_6	78	M^+	C_6H_6	100
1-Butene	56	C_4H_8	56	M^+	C_4H_8	100
Ethanol	46	C_2H_6O	45	$(M-H)^+$	C_2H_5O	64
			29	$(M-(CH_3))^+$	CH_3O	33
			27	$(M-(H_2O))^+$	C_2H_4	3
Ethyl acetate	88	$C_4H_8O_2$	61	$(M-(C_2H_5O_2))^+$	C_2H_3	61
			55	$(M-(CH_3O))^+$	C_3H_3O	5
			45	$(M-(C_2H_5O))^+$	C_2H_5O	12
			43	$(M-(COOH))^+$	C_2H_3O	22
1-Hexanal	100	$C_6H_{12}O$	82	$(M-(H_2O))^+$	C_6H_{10}	5

Compound	MW	M	<i>m/z</i>	Branching	Ion	%
			71,72,73	(M - (CHO)) ⁺	C ₅ H ₁₁	2,5,2
			60	(M - (C ₃ H ₄)) ⁺	C ₃ H ₈ O	5
			55,56,57	(M - (C ₃ H ₆)) ⁺	C ₃ H ₃ O	15,12,11
			43,44,45	(M - (C ₄ H ₆)) ⁺	C ₂ H ₃ O	14,7,6
			41	(M - (C ₃ H ₇ O)) ⁺	C ₃ H ₅	16
Methacrolein	70	C ₄ H ₆ O	70	M ⁺	C ₄ H ₆ O	3
			69	(M - H) ⁺	C ₄ H ₅ O	3
			43	(M - (C ₂ H ₃)) ⁺	C ₂ H ₃ O	16
			41	(M - (COH)) ⁺	C ₃ H ₅	58
			39	(M - (CH ₃ O)) ⁺	C ₃ H ₃	18
Meth. Benzoate	136	C ₈ H ₈ O ₂	136	M ⁺	C ₄ H ₆ O	2.7
			135	(M - H) ⁺	C ₆ H ₅ CH ₂ CO ₂	3.3
			105	(M - (CH ₃ O)) ⁺	C ₆ H ₅ CO	85
			91	(M - (CHO ₂)) ⁺	C ₆ H ₅ CH ₂	6
MVK	70	C ₄ H ₆ O	70	M ⁺	C ₄ H ₆ O	< 2
			69	(M - H) ⁺	C ₄ H ₅ O	19
			55	(M - (CH ₃)) ⁺	C ₃ H ₃ O	18
			43	(M - (C ₂ H ₃)) ⁺	C ₂ H ₃ O	47
			41	(M - (COH)) ⁺	C ₃ H ₅	10
			27	(M - (C ₂ H ₃ O)) ⁺	C ₂ H ₃	6
MVK dimer	70/70		140	M.M ⁺	(C ₄ H ₆ O) ₂	63
			97	(M.M - (C ₂ H ₃ O)) ⁺	C ₄ H ₆ O.C ₃ H ₃	37
Toluene	92	C ₇ H ₈	92	M ⁺	C ₇ H ₈	100

The $m/z = 43/27$ and the $m/z = 41/39$ pairs feature strongly, often with the exclusion of one or the other. With the strongly exothermic reactions characteristic of oxygen, there are several peripheral peaks clustered around the main fragmentation peaks observed with other reagents.

The $m/z = 55$ peak seen in ethyl acetate, 1-hexanol and MVK is thought to be a $(C_3H_3O)^+$ fragment split off from the parent ions. It would also have clashed with the dihydrate hydronium cluster $H_3O^+(H_2O)_2$, had it been a problem. In Section 6.5.5 the origin of the peaks at $m/z = 43, 41, 39$ and 27 is discussed as well as the exclusion mechanism which determines how they form groups.

6.5.5 Reactions of NO^+

In this section it will be shown that NO^+ has proved to be the most versatile alternative to proton transfer reactions using H_3O^+ . In Table 6.1 there is a list of all the possible reaction mechanisms that can occur using NO^+ as the reagent, for the most part, the only one or two of these are involved per reaction, easing the interpretation of the results.

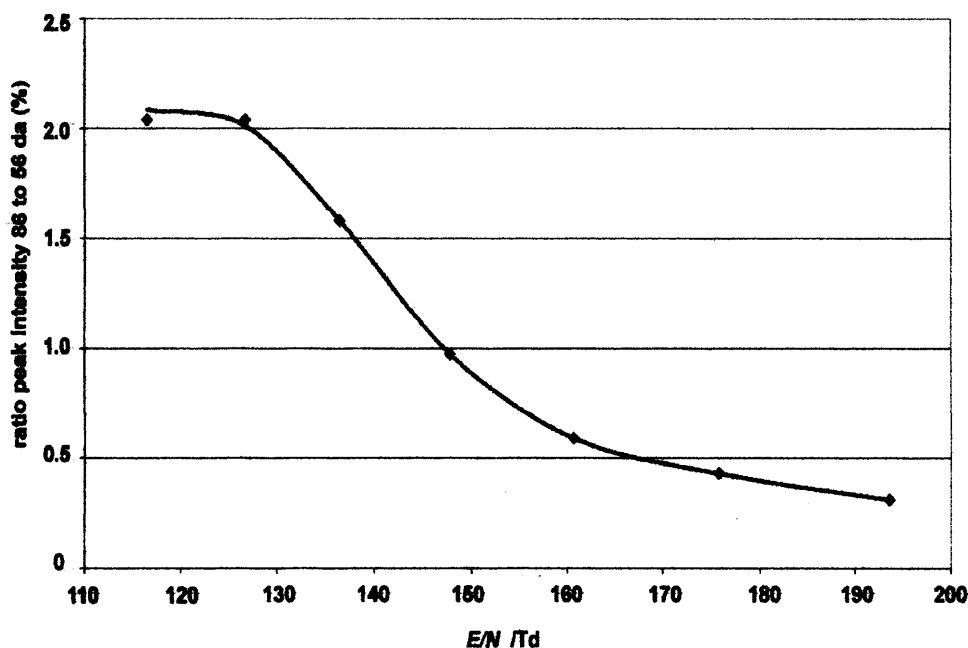


Figure 6.4 Relative intensity of adduct/cluster at $m/z = 86$ in 1-butene decreases as a function of E/N .

The reactions of NO^+ yield a simpler set of products than those seen from O_2^+ , as summarised in Table 6.6.

Table 6.6 Reaction products with NO⁺. its recombination energy is 9.26 eV.

Compound	MW	IE /eV	M	<i>m/z</i>	Branching	Ion	%
Acetaldehyde	44	10.23	C ₃ H ₇ O	43	(M - H) ⁺	C ₃ H ₆ O	100
Acetone	58	9.70	C ₃ H ₆ O	43	(M - (CH ₃)) ⁺	C ₂ H ₃ O CH ₃ O	100
Acetonitrile	41	8.72	C ₂ H ₃ N		No reaction		-
Benzene	78	9.24	C ₆ H ₆	78	M ⁺	C ₆ H ₆	100
1-Butene	56	9.55	C ₄ H ₈	56	M ⁺	C ₄ H ₈	53
				86	M.NO ⁺	M.NO ⁺	47
Ethanol	46	10.48	C ₂ H ₆ O	45	(M - (H)) ⁺	C ₂ H ₅ O	66
				29	(M - (CH ₃)) ⁺	CH ₃ O	34
				27	(M - H ₂ O) ⁺	C ₂ H ₄	3
Ethyl Acetate	88	10.01	C ₄ H ₈ O ₂	61	(M - (C ₂ H ₅ O ₂)) ⁺	C ₂ H ₃	61
				55	(M - (CH ₃ O)) ⁺	C ₃ H ₃ O	5
				45	(M - (C ₂ H ₃ O)) ⁺	C ₂ H ₅ O	12
				43	(M - (COOH)) ⁺	C ₂ H ₃ O	22
Hexanal	100	9.72	C ₆ H ₁₂ O	82	(M - H ₂ O) ⁺	C ₆ H ₁₀	6
				72	(M - (CHO)) ⁺	C ₅ H ₁₁	15
				55	(M - (C ₃ H ₉)) ⁺	C ₃ H ₃ O	15
				43	(M - (C ₄ H ₉)) ⁺	C ₂ H ₃ O	30
				41	(M - (C ₃ H ₇ O)) ⁺	C ₃ H ₅	20
Methacrolein	70	9.65	C ₄ H ₆ O	70	M ⁺	C ₄ H ₆ O	1
				41	(M - (COH)) ⁺	C ₃ H ₅	79
				39	(M - (CH ₃ O)) ⁺	C ₃ H ₃	15
Methyl benzoate	136	N/A	C ₈ H ₈ O ₂	136	M ⁺	C ₈ H ₆ O	3
				135	(M - (H)) ⁺	C ₆ H ₅ CH ₂ CO ₂	3
				105	(M - (CH ₃ O)) ⁺	C ₆ H ₅ CO	85
				91	(M - (CHO ₂)) ⁺	C ₆ H ₅ CH ₂	6
MVK	70	9.65	C ₄ H ₆ O	70	M ⁺	C ₄ H ₆ O	2
				55	(M - CH ₃) ⁺	C ₃ H ₃ O	31
				46	unidentified	-	11
				43	(M - (C ₂ H ₃)) ⁺	C ₂ H ₃ O	41

Compound	MW	IE /eV	M	<i>m/z</i>	Branching	Ion	%
				27	(M - (C ₂ H ₃ O)) ⁺	C ₂ H ₃	4
MVK dimer	70+70	-		140	M.M ⁺	(C ₄ H ₆ O) ₂	63
				97	(M.M - (C ₂ H ₃ O)) ⁺	C ₄ H ₆ O.C ₃ H ₃	37
Toluene	92	8.83	C ₇ H ₈	92	M ⁺	C ₇ H ₈	100

Cluster formation with NO⁺, which is dependent on pressure, was not prominent except for the case of 1-butene. In an inconclusive experiment made to determine whether NO⁺ formed a cluster or a closer association, it was found that C₄H₈.NO decreased with rising *E/N* (Figure 6.4). This behaviour is certainly to be expected with a cluster, but it could apply to a more closely-bound product. The *m/z* = 43/27 and the *m/z* = 41/39 pairs of groups are of interest as they appear to be structure-related. Both appear in hexanal, whereas the former dominates in MVK while the other one features in methacrolein.

Although MVK and methacrolein have identical chemical composition, they differ structurally (Figure 6.7) which determines which fragmentation route taken. Unless the reagent ion opens up an additional reaction channel it serves principally to energise the analyte to proceed with fragmentation along preferred lines.

When comparing the results of this study with the work the effect of applying a large *E/N* becomes apparent as the resultant ion mix observed differs from that obtained in a SIFT. Fragmentation is prominent and the contribution of the unfragmented species diminishes strongly in the aldehydes. This is illustrated by the results for hexanal in Figure 6.5. In the H₃O⁺ work, the MH⁺ peak is barely present with a 1% contribution, while the *m/z* = 82 and 55 predominate. In the NO⁺ work, the (M-H)⁺ hydride extraction peak is 5% of the total. The prominent peaks are at *m/z* = 70, 41 and 43. Minor peaks which appear at *m/z* = 82 and 55 could be due to H₃O⁺ contamination. O₂⁺ gave rise to large numbers of daughter ions whereas the only major peak observed with NH₄⁺ as the reagent corresponds to M⁺ or the result of charge transfer. This origin of this peak is puzzling, because if one were to assume that it is due to charge transfer due to contaminant O₂⁺ reagent ions, the absence of the structure characteristic of O₂⁺ contradicts this possibility.

No reaction of benzene with NO^+ was observed. Toluene was immune to fragmentation and its peak at $m/z = 92$ is most likely due to charge transfer. Toluene has an ionisation energy of 8.83 eV and NO^+ one of 9.26 eV, so that charge transfer is exothermic.

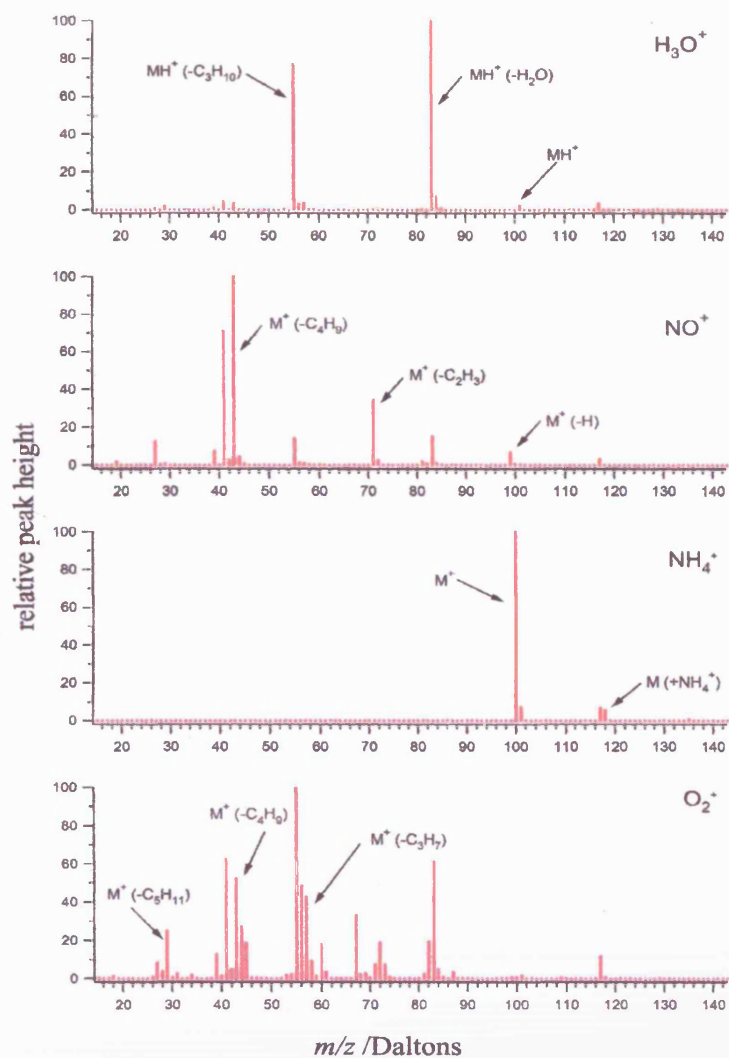


Figure 6.5 Mass spectra from reactions of hexanal with various CI reagents.

6.5.6 1-butene sensitivity measurements with some CI reagents

A series of experiments were carried out to measure the sensitivity of 1-butene to the CI reagents H_3O^+ , NO^+ and O_2^+ . While the choice of 1-butene for the comprehensive set of experiments would appear arbitrary, at the time when the multi-reagent CI experiments

were performed, it was the only mixture available in our laboratory containing a single hydrocarbon component with known concentration (1 ppmv).

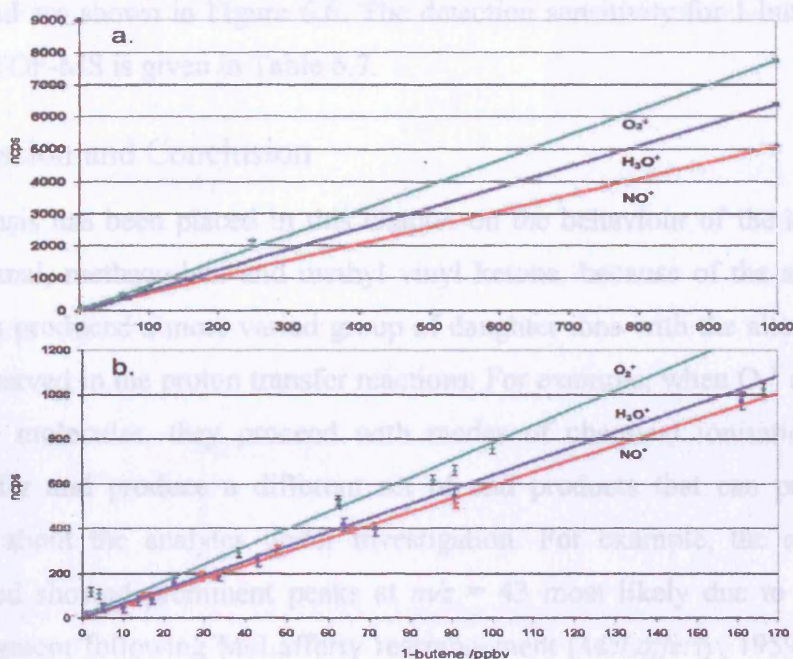


Figure 6.6 This figure is reproduced from Chapter 3. It shows the CI-TOF-MS sensitivity obtained for 1-butene. The top plot (a) shows the full range of dilutions used, while (b) shows the lower end of the plots in more detail.

It was used to measure the linear response and the low-end sensitivity of the CI-TOF-MS using all the CI reagents under study. The experimental procedure involved the use of a home-made diluter and was described in Chapter 3, Section 3.1.2.

Table 6.7 Sensitivity for detection of 1-butene using H₃O⁺, NO⁺ and O₂⁺ as reagents. This table is copied from Table 3.4 in Chapter 3.

Reagent	Ncps ppbv ⁻¹
H ₃ O ⁺	6.5
NO ⁺	5.9
O ₂ ⁺	7.7

NH_4^+ did not have a measurable reaction with 1-butene, while with the other reagents the CI-TOF-MS showed a linear response for a range of concentrations from 1 ppmv down to 1 ppbv and are shown in Figure 6.6. The detection sensitivity for 1-butene observed with the CI-TOF-MS is given in Table 6.7.

6.6 Discussion and Conclusion

Much emphasis has been placed in this chapter on the behaviour of the aldehydes and ketones hexanal, methacrolein and methyl vinyl ketone, because of the all target ions, these species produced a more varied group of daughter ions with the alternate reagents than was observed in the proton transfer reactions. For example, when O_2^+ and NO^+ react with analyte molecules, they proceed with modes of chemical ionisation other than proton transfer and produce a different set of end products that can provide further information about the analytes under investigation. For example, the aldehydes and ketones tested showed prominent peaks at $m/z = 43$ most likely due to the $(\text{C}_2\text{H}_3\text{O})^+$ carbonyl fragment following McLafferty rearrangement [McLafferty, 1959], [Silverstein *et al.*, 1963] and [Glagovich, 2005]. The experiments with NO^+ demonstrated this mechanism most clearly.

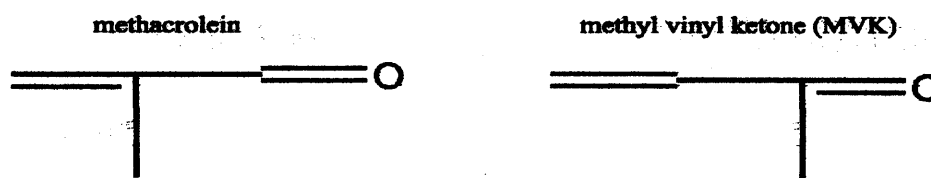


Figure 6.7 The position of the $\text{C}=\text{O}$ group determines the behaviour of the two molecules.

Alkenes usually form fragments corresponding to $\text{C}_n\text{H}_{2n+1}^+$, $\text{C}_n\text{H}_{2n}^+$, and $\text{C}_n\text{H}_{2n-1}^+$. [Glagovich, 2005] The peaks at $m/z = 43$ and 41 occurring in Methacrolein and MVK while not alkenes show signs of similar behaviour. The different location of $\text{C}=\text{O}$ group in these species result in two entirely different fragmentation routes Figure 6.7. Strong peaks at $m/z = 43$ in ethyl acetate, hexanal, methacrolein and MVK (Figure 6.8) are linked to the detachment of degraded carboxyl groups COOH and the acyl groups in the aldehydes and ketones which undergo McLafferty rearrangement [Glagovich, 2005].

The results obtained for the reactions with NO^+ were similar to those published by Smith and Španel [Smith and Španel, 2005] in Table 6.1, but with smaller contributions from the parent species because of the disruptive influence of operating at an E/N of 150 Td.

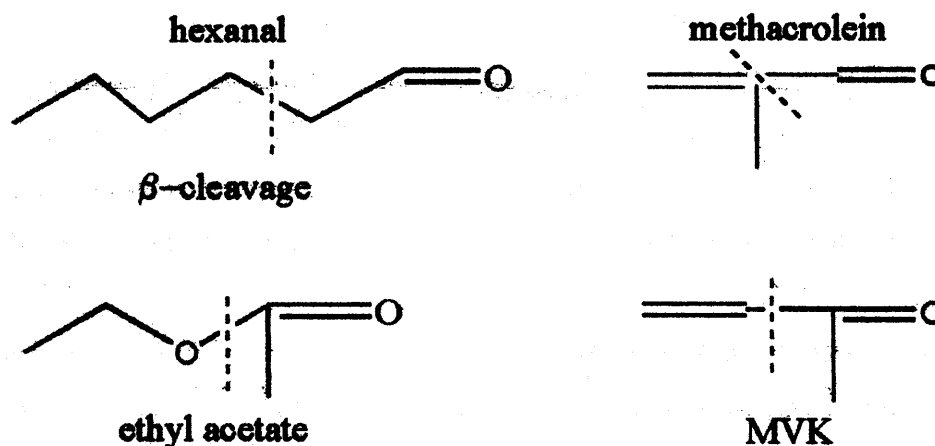


Figure 6.8 Fragmentation processes leading to peaks at $m/z = 43$.

The $m/z = 41$ peak (Figure 6.9) originates from a C_3H_5 group split off from the alkyl tail as in 1-hexanal (γ -cleavage?) and as a result of α -cleavage in methacrolein.

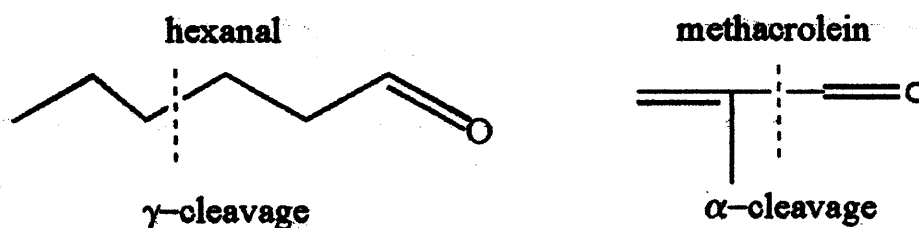


Figure 6.9 Cleavage in hexanal and methacrolein both leading to $m/z = 41$ fragments

Using O_2^+ as the CI reagent resulted in a complicated collection of reaction products which hindered interpretation, although many of the peaks noted with NO^+ were present.

Two of the CI reagents were found to be the most useful for future work. Of the four reagents tried, H_3O^+ and NO^+ gave the most satisfactory results that were also easier to interpret. NO^+ reactions highlighted fragmentation alternatives without creating over-busy spectra.

The cleanest spectra were obtained with H_3O^+ . In terms of yield, the proton transfer reaction is by far the most prolific, judging from the problems in eliminating interference from low concentrations H_3O^+ present during the NH_4^+ , O_2^+ and NO^+ work.

Proton transfer reactions were not observed with NH_4^+ . There was evidence of cluster formation and to a lesser extent, signs of a closer association. Even at an E/N of 150 Td, the NH_4^+ ions were not able to excite the analyte into the sort of fragmentation behaviour experienced with NO^+ and O_2^+ . The prominent M^- peaks found with several analytes are difficult to explain, as charge transfer between NH_4^+ and the analytes is not possible.

Stephenson's rule [Stephenson, 1946] indicates when a fracture occurs the positive charge will reside on the fragment with the lower ionisation energy. In the case of the other analytes the energy gained from the electrical gradient in the drift-tube was insufficient to enable charge transfer. By contrast, O_2^+ caused fragmentation on such a large scale that by comparison interpreting the NO^+ spectra proved more straightforward.

Several criteria were set out in the introduction of this chapter that would show whether the CI-TOF-MS was a suitable device for working with CI reactions.

The first one was to establish whether sufficient NO^+ , O_2^+ and NH_4^+ ions would be generated by the ^{241}Am source to be able to perform useful CI investigations. In all cases count rates of the precursor ions were comparable to those obtained with H_3O^+ ions.

The second criterion was to see whether useful work could be done in the absence of the mass pre-selection process that is used with SIFT-MS. It was found that pure ammonia severely contaminated the CI-TOF-MS, to the extent that it will never be used again. The main source of interference with the CI reagents, NO^+ and O_2^+ , came from H_3O^+ ions, but as was seen in Section 6.3 these could be effectively controlled. In future where interference from proton transfer reactions cannot be ignored, contributions from that source can be estimated from the profiles obtained from the H_3O^+ experiments (Section 6.5.1). So while the problem of interference cannot be eliminated, it is possible to take their effects into account. The second criterion has also been met.

The third criterion was to determine whether the new CIRMS technique would provide new chemistry insights in areas where proton transfer reactions cannot. Apart from the real-time data acquisition advantages already realised with the proton transfer work, the use of other CI reagents has been shown to address its inability to distinguish readily between isobaric compounds. It was shown that using NO^+ as a reagent, the isobaric methacrolein and MVK molecules could be induced to fragment in recognisably different ways. This difference in fragmentation patterns as the reagent is switched from H_3O^+ to NO^+ holds promise as a means of distinguishing these isobaric compounds. This idea may be applicable to other isobaric compounds and is currently being investigated. The third criterion has thus been met.

The ability of the PTR-TOF-MS to provide real-time multiple views of a large range of masses has been demonstrated in the proton transfer work with which it was engaged for over a year. Using the built in time-coherence of related reaction products, it provides a useful means for estimating the relative contributions of fragmentation products and even estimating interfering background events.

The ^{241}Am ion source coped well with the various reactants and apart from the problem of the ammonia contamination, the PTR-TOF-MS in its new rôle as CI-TOF-MS has performed satisfactorily.

All in all, there are clear advantages of having the option of working with more than one reagent. The CI-TOF-MS, with its time-coherent data gathering characteristics, is a powerful tool for investigating the role of VOCs and OVOCs in the air in greater depth and detail than formerly possible.

In the next chapter, the final one of the thesis, several areas are mentioned where future work could profitably be done.

Chapter 7

Summary and Future work

The only source of knowledge is experience.

- Albert Einstein (1879 -1955)

7 Final comments

The work described in this thesis concentrates on the development and commissioning of the PTR-TOF-MS as a tool for the detection of a wide range of hydrocarbons in the troposphere and in the laboratory. The main features of the equipment, positive and negative are discussed in this chapter. The proton transfer reaction mechanism will remain as the main chemical ionisation technique used, but alternative chemical ionisation precursors have been tested for their usefulness as complementary extensions. It was hoped that at least one of the reagents tested would be able to distinguish clearly isobaric compounds and O_2^+ and particularly NO^+ were found to be promising. Further developments in the field of chemical ionisation reaction mass spectrometry (CIRMS) will make use several types of chemical ionisation. The term CI-TOF-MS would describe the function of the PTR-TOF-MS more accurately in future. While the instrument is now fully operational, there are areas left for future work where its performance could be improved.

7.1 Development Achievements

In the foregoing chapters, the task of bringing the PTR-TOF-MS into service, and proving its worth as a research instrument was described with each chapter dealing with a separate phase of its development and implementation.

7.1.1 Hardware development

The CI-TOF-MS is now fully operational, and following the ACCENT Intercomparison (Chapter 5) and the initial CIRMS work to investigate matters arising from the ACCENT Intercomparison, it is now entering service as a general purpose research tool. It is available to other workers in the laboratory for a variety of different applications. It is also now in regular service monitoring the atmosphere near the centre of Leicester as well.

7.1.2 Ease of operation

Starting up the CI-TOF-MS is straightforward, although the start-up and closing-down procedure requires that all the steps be done in the correct sequence and a few critical precautions are observed. The two most important of these relate to the drift-

tube bias and avoidance of excess moisture. Firstly the drift-tube bias may not be applied before the operating pressure in the instrument has been reached otherwise premature sparking can occur. Secondly, water in droplet form should not be let into the instrument. Either of these events can result in extended down times.

No adjustment of the controls is needed once the system is running. From time to time the ion source gets dirty and the reagent count rate drops. The ion source and drift-tube assembly should be dismantled from the TOF-MS for cleaning on a regular basis, on average once every two months.

7.1.3 Detection sensitivity

The yield for each VOC and OVOC depends on the count rate of the CI reagent being used, which is in the region of 4000 counts per second. In Section 3.14.7 it was found that a single normalised count of a compound with a concentration of 1 ppbv and for which the PTR-TOF-MS's detection efficiency was $25.7 \text{ ncps ppbv}^{-1}$ could be gathered in 9.7 seconds. In Section 4.6.2 it was shown that when monitoring the troposphere composition near Leicester, it was possible to measure NMHC concentrations in the region of 200 – 500 pptv using ten-minute scans.

7.1.4 Managing fragmentation, temperature effects and time shifts

In proton transfer reaction work, if fragmentation is a problem, reducing E/N can be useful, but apart from isolated look-to-see situations, changes in the operating E/N is best avoided. Moving to a new standard value of E/N entails repeating all the sensitivity and headspace measurements described in Chapters 3 and 6 for the new value of E/N . Future events may make such a move worth the effort.

It became apparent early on that the equipment was sensitive to the ambient temperature. In section 3.10 it was found that the temperature of the drift-tube affected the hydronium count rate and that this appeared to be due to variations in the number density of the gas in the drift-tube. In later work, it was found that the problem could be avoided by maintaining the drift-tube and the inlet feeds at a constant 40 °C.

Eliminating shifts in the time-of-flight of the ions is handled by taking all data as a series of one-minute scans, followed by offline recalibration of the traces before summing them into groups of longer sampling times.

7.2 Scientific achievements

7.2.1 Detection sensitivity

As a consequence of the ACCENT Intercomparison a useful set of data has been obtained for the detection efficiencies of some of the most common OVOCs occurring in the atmosphere. The results were of particular importance as it showed that the PTR-TOF-MS could hold its own against other PTR-MS equipment and had a linear response over a range of OVOC concentrations ranging from several ppbv to concentrations of less than 1 ppbv. In the case of benzaldehyde and methyl acetate, where it had not been able to obtain standard mixtures for calibration, the reference figures from ACCENT have provided values that can be added to the list of compounds for which calibration values are known. In the future further results will be added to the portfolio.

7.2.2 Accuracy

The PTR-TOF-MS performed satisfactorily at the ACCENT Intercomparison where it was able to report accurately sample OVOC concentrations for ten out of the twelve samples for which results were submitted. In two cases, the results were not acceptable and it is believed that problems with the initial calibration may lie at the root of the problem. In all cases the PTR-TOF-MS was able to follow the steps of successive dilution demonstrating the inherent accuracy of response of the equipment in the range 10 ppbv to less than 1 ppbv.

7.2.3 The Leicester atmosphere

In a series of experiments monitoring the atmosphere around the University of Leicester Chemistry Department the effect of the VOC and OVOC loading was found to increase by day and diminish at night. On weekends the daily increase was found to be substantially less than during the weekdays. The concentration of some species were found to vary rapidly throughout the day, features which would be missed by

equipment relying on techniques with a lower sampling rate such as gas chromatography.

7.2.4 CIRMS

In chapter 6 it was shown that the other CI precursor ions frequently used in SIFT-MS could be successfully implemented on the PTR-TOF-MS and as a consequence the equipment would henceforth be known as CI-TOF-MS. Ion yields from NO^+ , O_2^+ and NH_4^+ were found to be comparable to those obtained with H_3O^+ . Problems arising from contamination by unwanted precursor ions, particularly H_3O^+ , could be kept to manageable proportions. It was found that by using an alternate reagent ion such as NO^+ , it was possible to distinguish between the components of an isobaric compound mixture, in this case methyl vinyl ketone and methacrolein.

7.2.5 Insensitivity to detection

The equipment was found to be insensitive to the lighter alkanes ethane, propane and butane. Similarly the detection ability for alcohols varied widely: methanol and 1-propanol were detected without problem whereas ethanol and butanol were not (Chapter 5). Aldehydes and ketones were detected without problem.

7.3 Ongoing challenges

7.3.1 Preamplifier failures

The preamplifier feeding the signal from the MCP detector to the time-to-digital converter was prone to unannounced failures, although the frequency of failure was reduced if the equipment ran continuously. The repair is simple – two chips have to be replaced, but access when the equipment is *in situ* is can be difficult.

The manufacturers of the TOF-MS, KORE Technology, do not currently have a solution to the problem, so several sets of replacement chips are always held in stock.

7.3.2 Transportation, formalities and red tape

The PTR-TOF-MS is not easy to transport. It is heavy and has to be partially dismantled for transport. The radioactive source has to be removed and transported by an approved transport organisation, and although safe, requires additional paperwork and pre-approval before it can be moved.

The MCP detector is not easily removed and can deteriorate if left at atmospheric pressure and traces of water vapour for extended periods. Ideally it should be maintained in an oil-free vacuum and kept away from moist atmospheres at all times. So far it has been found to suffer no damage when the ion source is removed; the rest of the equipment is evacuated to 10^{-8} mbar, and then sealed. It was found that after transporting the equipment for journeys lasting up to 24 hours there was no noticeable deterioration in performance.

The PTR-TOF-MS will soon be installed in specifically designed transportation along with other equipment (see section 7.2.3). This will eliminate many of the transport problems, but the equipment will have to be re-evacuated at regular intervals on a long journey. The radioactive source will still have to be removed and travel separately.

7.4 Future development

Several areas have been identified where further work would improve the performance of the PTR-TOF-MS.

7.4.1 Improving the hydronium count rate

The highest hydronium count rate achieved thus far is 4500 s^{-1} , so there is room for substantial improvement. Currently the ion source and drift-tube assembly is mounted on an intermediate pumping chamber which allows the drift-tube and the body of the TOF-MS to be maintained at a sufficiently large pressure differential, to be within the operating range of the installed turbo-molecular pumps. The exit aperture of the drift-tube should be close to the first element of the input einzel lens of the CI-TOF-MS. At the moment emergent ions have to traverse a 3 cm field-free gap to reach this first element of the ion lens.

New simulation tests have shown that the ion beam leaving the drift-tube is scattered by the air molecules in the intermediate pumping chamber. Further simulations have shown that performance can be improved by inserting an additional einzel lens, between the drift-tube and the input of the CI-TOF-MS.

Another alternative would be to redesign the transfer chamber area to bring the final aperture closer to the input einzel lens of the TOF-MS. A further option would be to try a stronger ^{241}Am source in place of the current source but commercial suppliers of such a source has not been found.

Demand for time on the PTR-TOF-MS has precluded further development work on the hollow cathode ion source, which may prove to be another viable alternative to the ^{241}Am -powered ion source. Initial experiments with this discharge source yielded H_3O^+ count rates more than an order of magnitude higher than the radioactive source. Further work on the discharge source may be able to raise the count rate even further. The discharge source would also have the benefit of not requiring separate and costly transportation when the instrument is moved.

7.4.2 Online standards

While it was possible to obtain some useful OVOC detection efficiencies for the PTR-TOF-MS at the ACCENT Intercomparison campaign, it was still necessary to use a standard mixture obtained from other groups working there. In the future the laboratory will need a means of providing standard gas mixtures easily and cheaply to fit the changing demands of future projects.

Several alternatives are available, some based on permeation tubes. Permeation tubes are less expensive than mixtures of standard gases, so that it would be possible to maintain a battery of permeation tubes covering the range of VOCs and OVOCs targeted for study.

7.4.3 Dedicated instrument

For the purposes of monitoring the troposphere, an instrument with the mass resolution of the current PTR-TOF-MS (better than 0.3 da.) is more than adequate and an instrument with a lesser specification would still suffice. Ideally, such an instrument would be dedicated to the task of monitoring the troposphere only. The current equipment has had to work with a wide variety of analytes, some of which are known to be 'sticky'. They have contaminated the equipment for extended periods and rendered it beyond use for atmospheric work during the long decontamination process. The successful implementation of the CI-TOF-MS has created a demand for

it to be used on a variety of different projects, and monitoring the troposphere is, alas, only one of them.

7.5 Finally

The writer left the academic world to find fame and fortune in the commercial world in 1970 but he always retained a lingering desire to return to Academia. Upon his retirement in 2002, it became apparent that progress in the field in which he had originally qualified, low energy nuclear physics, was stationary, as nothing new had really happened in the intervening years in that particular branch of the subject. Certainly the advances in technology offered bigger, better and faster equipment but the nature of the work done now, thirty years later, had not really changed and so presented no new challenge. Consequently, a change of direction was indicated, and since he lived in Leicester, it seemed a natural place to start looking. Here he was fortunate to meet up with the colleagues with whom he has been working for the last three years, and to have worked on a project that has turned out successfully. The success of the project can be greatly ascribed to the help, guidance and advice received from colleagues, the academic and technical staff at the University of Leicester.

Appendices

Appendix 1 Tables

A1.3 Characterisation

Table A1.3. 1 OVOC fragmentation table using H_3O^+ as the reagent. This table is the first of two parts and covers fragmentation products in the range 27 to 57 da.

Mass	Item	27	29	31	33	39	41	43	45	47	55	57
31	formaldehyde			100.0								
33	methanol				100.0							
45	acetaldehyde							37.6	62.4			
47	ethanol		14.7							85.3		
59	acetone											
59	propanal			18.9			7.6					
61	1-propanol	2.8				6.0	51.4	39.1				
71	methacrolein						3.8	8.4				
71	MVK							4.9				
73	butanal	1.2	3.3			2.0	2.0	2.2			87.6	
76	1-butanol		3.1			1.4	15.9					80.3
76	m. acetate							10.0				
87	MBO						20.4					
93	toluene											
101	hexanal		1.2								42.0	
107	benzaldehyde											
Mass		27	29	31	33	39	41	43	45	47	55	57

Table A1.3. 2 OVOC fragmentation table using H_3O^+ as the reagent. This table is the second of two parts and covers fragmentation products in the range 59 to 107 da.

Mass	Item	59	69	71	73	75	79	83	87	89	93	101	106	107
31	formaldehyde													
33	methanol													
45	acetaldehyde													
47	ethanol													
59	acetone	100.0												
69	propanal	73.5												
61	1-propanol	0.6												
71	methacrolein	1.3		86.5										
71	MVK			95.1										
73	butanal			1.2	4.2									
75	1-butanol													
75	m. acetate					90.0								
87	MBO		62.9						16.7					
93	toluene										100.0			
101	hexanal							55.5				1.3		
107	benzaldehyde						2.9							87.1
Mass		59	69	71	73	75	79	83	87	89	93	101	106	107

A1.5 ACCENT intercomparison

The results of the ACCENT intercomparison campaign are tabulated in tables A5.1 to A5.12.. The yields are in ppbv, and the errors, statistical, atmospheric and precision (columns 3,4,5 and 6) are in the same units.

The final column the signal to noise is the ratio of the mean value of the one-minute runs divided by the standard deviation of the same set of runs. The ratio measures how well established a peak can be identified using one minute runs alone. Aggregating one-minute runs reduces the standard deviation to that the signal to noise ratio is improved.

Table A1.5. 1 The ACCENT Intercomparison campaign results for Acetaldehyde.

<u>Experiment</u>	<u>Ext.</u>	<u>Acetaldehyde</u>	<u>statistical</u>	<u>atmospheric</u>	<u>precision</u>	<u>signal/noise</u>
		ppbv	ppbv	ppbv	ppbv	
25-Saph-2a	-1	7.70	0.05	0.92	0.04	8.38
25-Saph-2a	-2	7.29	0.05	1.01	0.04	7.23
25-Saph-2a	-3	7.36	0.05	1.08	0.04	6.80
25-Saph-2b	-1	2.53	0.04	0.53	0.01	4.77
25-Saph-2b	-2	2.45	0.04	0.50	0.01	4.85
25-Saph-2b	-3	2.24	0.04	0.64	0.01	4.05
25-Saph-2c	-1	0.85	0.03	0.23	0.00	3.76
25-Saph-2c	-2	0.86	0.03	0.22	0.00	3.92
25-Saph-2c	-3	0.80	0.03	0.21	0.00	3.76
26-Saph-3a	-1	3.62	0.04	0.20	0.02	18.57
26-Saph-3a	-2	3.36	0.04	0.06	0.02	53.46
26-Saph-3a	-3	3.44	0.04	0.25	0.02	13.64
26-Saph-3b	-1	1.15	0.03	0.41	0.01	2.78
26-Saph-3b	-2	1.10	0.03	0.04	0.01	29.77
26-Saph-2b	-3	1.16	0.03	0.08	0.01	15.37
26-Saph-3c	-1	0.47	0.03	0.16	0.00	2.93
26-Saph-3c	-2	0.35	0.03	0.10	0.00	3.51
26-Saph-3c	-3	0.30	0.03	0.06	0.00	5.32
27-Saph-4a	-1	4.93	0.04	0.23	0.02	21.31
27-Saph-4a	-2	5.04	0.05	0.46	0.03	10.94
27-Saph-4a	-3	4.77	0.04	1.73	0.02	2.76
27-Saph-4b	-1	2.54	0.04	0.31	0.01	8.30
27-Saph-4b	-2	2.48	0.04	0.06	0.01	40.77
27-Saph-4b	-3	2.24	0.04	0.47	0.01	4.80
27-Saph-4c	-1	1.35	0.03	0.14	0.01	9.88
27-Saph-4c	-2	1.35	0.03	0.09	0.01	14.84
27-Saph-4c	-3	1.19	0.03	0.09	0.01	13.74

Table A1.5. 2 The ACCENT Intercomparison campaign results for Acetone.

Experiment	Ext.	Acetone	statistical	atmospheric	precision	signal/noise
		ppbv	ppbv	ppbv	ppbv	
25-Saph-2a	-1	9.77	0.22	1.08	0.13	9.07
25-Saph-2a	-2	9.52	0.22	1.02	0.12	9.29
25-Saph-2a	-3	8.71	0.22	0.95	0.11	9.21
25-Saph-2b	-1	3.45	0.21	0.30	0.04	11.70
25-Saph-2b	-2	3.19	0.21	0.27	0.04	11.76
25-Saph-2b	-3	3.19	0.21	0.36	0.04	10.66
25-Saph-2c	-1	1.13	0.20	0.12	0.01	9.48
25-Saph-2c	-2	0.73	0.20	0.07	0.01	10.70
25-Saph-2c	-3	0.19	0.20	0.02	0.00	10.91
26-Saph-3a	-1	5.24	0.21	0.05	0.07	102.09
26-Saph-3a	-2	4.07	0.21	0.79	0.05	5.17
26-Saph-3a	-3	4.13	0.21	0.06	0.05	65.89
26-Saph-3b	-1	2.01	0.20	0.16	0.03	12.66
26-Saph-3b	-2	1.48	0.20	0.15	0.02	10.17
26-Saph-2b	-3	2.17	0.20	0.41	0.03	5.29
26-Saph-3c	-1	0.61	0.20	0.06	0.01	10.39
26-Saph-3c	-2	0.64	0.19	0.02	0.01	29.79
26-Saph-3c	-3	0.54	0.20	0.04	0.01	13.80
27-Saph-4a	-1	5.47	0.20	0.53	0.07	10.35
27-Saph-4a	-2	5.26	0.20	0.20	0.07	26.69
27-Saph-4a	-3	5.43	0.20	0.26	0.07	21.10
27-Saph-4b	-1	2.15	0.20	0.13	0.03	16.24
27-Saph-4b	-2	2.13	0.20	0.20	0.03	10.81
27-Saph-4b	-3	2.34	0.20	0.53	0.03	4.42
27-Saph-4c	-1	1.46	0.19	0.07	0.02	19.51
27-Saph-4c	-2	1.50	0.19	0.31	0.02	4.88
27-Saph-4c	-3	0.83	0.19	0.12	0.01	6.71

Table A1.5. 3 The ACCENT Intercomparison campaign results for Benzaldehyde.

<u>Experiment</u>	<u>Ext.</u>	<u>Benzaldehyde</u>	<u>statistical</u>	<u>atmospheric</u>	<u>precision</u>	<u>signal/noise</u>
		<u>ppbv</u>	<u>ppbv</u>	<u>ppbv</u>	<u>ppbv</u>	
25-Saph-2a	-1	6.53	0.13	1.65	0.88	4.0
25-Saph-2a	-2	6.94	0.13	1.75	0.93	4.0
25-Saph-2a	-3	6.26	0.13	1.68	0.84	3.7
25-Saph-2b	-1	2.13	0.08	0.66	0.28	3.2
25-Saph-2b	-2	2.08	0.08	0.69	0.28	3.0
25-Saph-2b	-3	2.26	0.09	2.28	0.30	3.2
25-Saph-2c	-1	0.72	0.06	0.30	0.10	2.4
25-Saph-2c	-2	0.69	0.06	0.29	0.09	2.4
25-Saph-2c	-3	0.63	0.06	0.28	0.08	2.2
26-Saph-3a	-1	3.40	0.10	0.34	0.46	10.0
26-Saph-3a	-2	3.62	0.11	1.59	0.49	2.3
26-Saph-3a	-3	3.45	0.10	0.22	0.46	15.4
26-Saph-3b	-1	1.32	0.08	0.00	0.18	1.4
26-Saph-3b	-2	1.48	0.08	1.06	0.20	1.4
26-Saph-2b	-3	1.34	0.08	0.82	0.18	1.6
26-Saph-3c	-1	0.67	0.07	0.31	0.09	2.1
26-Saph-3c	-2	0.58	0.07	0.00	0.08	2.3
26-Saph-3c	-3	0.60	0.07	0.24	0.08	2.5
27-Saph-4a	-1	4.21	0.11	0.25	0.56	16.8
27-Saph-4a	-2	4.68	0.12	0.38	0.63	12.4
27-Saph-4a	-3	4.27	0.11	1.84	0.57	2.3
27-Saph-4b	-1	2.17	0.09	0.65	0.29	3.3
27-Saph-4b	-2	2.06	0.09	0.11	0.28	19.3
27-Saph-4b	-3	2.15	0.09	1.51	0.29	1.4
27-Saph-4c	-1	1.25	0.08	0.27	0.17	4.6
27-Saph-4c	-2	1.25	0.08	1.00	0.17	1.3
27-Saph-4c	-3	1.07	0.07	0.26	0.14	4.1

Table A1.5. 4 The ACCENT Intercomparison campaign results for Butanal.

Experiment	Ext.	Butanal	statistical	atmospheric	precision	signal/noise
		ppbv	ppbv	ppbv	ppbv	
25-Saph-2a	-1	6.20	0.10	1.06	0.09	5.9
25-Saph-2a	-2	6.29	0.10	1.10	0.09	5.7
25-Saph-2a	-3	5.90	0.09	1.14	0.09	5.2
25-Saph-2b	-1	1.91	0.06	0.44	0.03	4.4
25-Saph-2b	-2	2.05	0.06	0.53	0.03	3.9
25-Saph-2b	-3	1.89	0.06	0.92	0.03	4.1
25-Saph-2c	-1	0.78	0.05	0.27	0.01	2.8
25-Saph-2c	-2	0.67	0.05	0.26	0.01	2.5
25-Saph-2c	-3	0.58	0.05	0.25	0.01	2.4
26-Saph-3a	-1	3.31	0.08	0.86	0.05	3.8
26-Saph-3a	-2	3.37	0.08	1.61	0.05	2.1
26-Saph-3a	-3	3.07	0.07	0.00	0.05	1.0
26-Saph-3b	-1	1.29	0.06	0.56	0.02	2.3
26-Saph-3b	-2	1.44	0.06	0.36	0.02	4.0
26-Saph-2b	-3	1.36	0.06	0.36	0.02	3.7
26-Saph-3c	-1	0.53	0.05	0.05	0.01	10.9
26-Saph-3c	-2	0.52	0.05	0.04	0.01	11.7
26-Saph-3c	-3	0.43	0.05	0.12	0.01	3.6
27-Saph-4a	-1	4.56	0.09	0.48	0.07	9.4
27-Saph-4a	-2	4.20	0.08	0.09	0.06	45.2
27-Saph-4a	-3	3.99	0.08	1.20	0.06	3.3
27-Saph-4b	-1	2.17	0.07	1.62	0.03	1.3
27-Saph-4b	-2	1.99	0.06	0.41	0.03	4.8
27-Saph-4b	-3	1.92	0.06	0.32	0.03	6.0
27-Saph-4c	-1	1.25	0.06	0.27	0.02	4.6
27-Saph-4c	-2	0.87	0.03	0.10	0.01	8.4
27-Saph-4c	-3	0.92	0.05	0.60	0.01	1.5

Table A1.5. 5 The ACCENT Intercomparison campaign results for 1-butanol.

Experiment	Ext.	Butanol	statistical	atmospheric	precision	signal/noise
		ppbv	ppbv	ppbv	ppbv	
25-Saph-2a	-1	1.94	0.06	0.61	0.04	3.2
25-Saph-2a	-2	2.00	0.06	0.68	0.04	2.9
25-Saph-2a	-3	1.94	0.06	0.59	0.04	3.3
25-Saph-2b	-1	0.74	0.05	0.23	0.01	3.2
25-Saph-2b	-2	0.78	0.05	0.24	0.01	3.3
25-Saph-2b	-3	0.62	0.05	0.31	0.01	2.7
25-Saph-2c	-1	0.38	0.05	0.14	0.01	2.7
25-Saph-2c	-2	0.30	0.05	0.11	0.01	2.8
25-Saph-2c	-3	0.16	0.05	0.05	0.00	3.0
26-Saph-3a	-1	1.24	0.06	0.11	0.02	11.4
26-Saph-3a	-2	1.18	0.06	0.05	0.02	22.5
26-Saph-3a	-3	1.36	0.06	0.00	0.03	1.0
26-Saph-3b	-1	0.36	0.05	0.16	0.01	2.2
26-Saph-3b	-2	0.64	0.06	0.18	0.01	3.6
26-Saph-2b	-3	0.58	0.06	0.07	0.01	8.8
26-Saph-3c	-1	0.14	0.05	0.03	0.00	4.4
26-Saph-3c	-2	0.14	0.05	0.09	0.00	1.6
26-Saph-3c	-3	0.18	0.05	0.05	0.00	3.5
27-Saph-4a	-1	1.72	0.06	0.07	0.03	23.2
27-Saph-4a	-2	1.98	0.06	0.08	0.04	25.4
27-Saph-4a	-3	2.00	0.06	0.16	0.04	12.9
27-Saph-4b	-1	1.08	0.06	0.41	0.02	2.7
27-Saph-4b	-2	1.12	0.06	0.41	0.02	2.7
27-Saph-4b	-3	1.04	0.05	0.11	0.02	9.1
27-Saph-4c	-1	0.82	0.05	0.40	0.02	2.1
27-Saph-4c	-2	0.72	0.05	0.28	0.01	2.6
27-Saph-4c	-3	0.62	0.05	0.25	0.01	2.4

Table A1.5. 6 The ACCENT Intercomparison campaign results for Hexanal.

Experiment	Ext.	Hexanal	statistical	atmospheric	precision	signal/noise
		ppbv	ppbv	ppbv	ppbv	
25-Saph-2a	-1	8.56	0.11	5.43	0.29	1.6
25-Saph-2a	-2	8.36	0.11	5.43	0.28	1.5
25-Saph-2a	-3	8.16	0.11	5.76	0.28	1.4
25-Saph-2b	-1	2.95	0.08	1.34	0.10	2.2
25-Saph-2b	-2	2.56	0.08	1.34	0.09	1.9
25-Saph-2b	-3	2.95	0.08	4.11	0.10	1.9
25-Saph-2c	-1	1.18	0.07	0.66	0.04	1.8
25-Saph-2c	-2	0.98	0.07	0.59	0.03	1.7
25-Saph-2c	-3	1.18	0.07	0.84	0.04	1.4
26-Saph-3a	-1	4.92	0.09	0.92	0.17	5.3
26-Saph-3a	-2	3.64	0.08	0.42	0.12	8.7
26-Saph-3a	-3	4.13	0.08	1.29	0.14	3.2
26-Saph-3b	-1	1.77	0.07	1.28	0.06	1.4
26-Saph-3b	-2	1.97	0.07	0.00	0.07	1.5
26-Saph-2b	-3	1.48	0.07	0.88	0.05	1.7
26-Saph-3c	-1	1.08	0.06	1.25	0.04	0.9
26-Saph-3c	-2	0.89	0.06	0.84	0.03	1.1
26-Saph-3c	-3	0.98	0.06	0.70	0.03	1.4
27-Saph-4a	-1	5.51	0.10	2.81	0.19	2.0
27-Saph-4a	-2	5.80	0.10	0.00	0.20	3.5
27-Saph-4a	-3	5.21	0.10	0.90	0.18	5.8
27-Saph-4b	-1	3.34	0.09	0.78	0.11	4.3
27-Saph-4b	-2	2.16	0.08	0.32	0.07	6.7
27-Saph-4b	-3	2.75	0.08	1.08	0.09	2.5
27-Saph-4c	-1	2.16	0.08	0.97	0.07	2.2
27-Saph-4c	-2	1.77	0.08	1.44	0.06	1.2
27-Saph-4c	-3	2.07	0.08	0.97	0.07	2.1

Table A1.5. 7 The ACCENT Intercomparison campaign results for MBO.

Experiment	Ext.	MBO	statistical	atmospheric	precision	signal/noise
		ppbv	ppbv	ppbv	ppbv	
25-Saph-2a	-1	3.29	0.06	1.83	0.10	1.8
25-Saph-2a	-2	3.41	0.06	1.84	0.10	1.9
25-Saph-2a	-3	3.37	0.06	2.03	0.10	1.7
25-Saph-2b	-1	1.02	0.04	0.41	0.03	2.5
25-Saph-2b	-2	1.02	0.04	0.47	0.03	2.2
25-Saph-2b	-3	0.86	0.04	0.18	0.03	2.5
25-Saph-2c	-1	0.31	0.04	0.19	0.01	1.6
25-Saph-2c	-2	0.47	0.04	0.28	0.01	1.7
25-Saph-2c	-3	0.31	0.04	0.17	0.01	1.9
26-Saph-3a	-1	1.92	0.05	0.31	0.06	6.2
26-Saph-3a	-2	1.69	0.05	0.29	0.05	5.8
26-Saph-3a	-3	1.65	0.05	0.57	0.05	2.9
26-Saph-3b	-1	0.59	0.04	0.59	0.02	1.0
26-Saph-3b	-2	0.55	0.04	0.40	0.02	1.4
26-Saph-2b	-3	0.67	0.04	0.00	0.02	1.0
26-Saph-3c	-1	0.24	0.04	0.05	0.01	1.0
26-Saph-3c	-2	0.21	0.04	0.05	0.01	4.7
26-Saph-3c	-3	0.20	0.04	0.09	0.01	2.3
27-Saph-4a	-1	2.75	0.05	0.25	0.08	10.0
27-Saph-4a	-2	2.39	0.05	0.53	0.07	4.5
27-Saph-4a	-3	2.51	0.05	0.18	0.08	14.0
27-Saph-4b	-1	1.33	0.05	0.57	0.04	2.4
27-Saph-4b	-2	1.29	0.05	0.57	0.04	2.3
27-Saph-4b	-3	1.41	0.05	1.46	0.04	1.0
27-Saph-4c	-1	0.71	0.04	0.21	0.02	3.4
27-Saph-4c	-2	0.71	0.04	0.31	0.02	2.3
27-Saph-4c	-3	0.51	0.04	0.17	0.02	3.0

Table A1.5. 8 The ACCENT Intercomparison campaign results for Methanol.

Experiment	Ext.	Methanol	statistical variation	atmospheric	precision	signal/noise
		ppbv	ppbv	ppbv	ppbv	
25-Saph-2a	-1	8.10	0.37	0.93	0.14	8.75
25-Saph-2a	-2	7.98	0.37	0.88	0.14	9.11
25-Saph-2a	-3	8.00	0.37	0.91	0.14	8.75
25-Saph-2b	-1	3.60	0.36	0.26	0.06	13.74
25-Saph-2b	-2	3.50	0.36	0.32	0.06	10.87
25-Saph-2b	-3	3.20	0.36	0.35	0.05	11.75
25-Saph-2c	-1	0.96	0.35	0.09	0.02	11.17
25-Saph-2c	-2	1.42	0.35	0.15	0.02	9.66
25-Saph-2c	-3	0.34	0.35	0.03	0.01	9.72
26-Saph-3a	-1	4.19	0.35	0.32	0.07	12.97
26-Saph-3a	-2	4.52	0.35	0.23	0.08	19.85
26-Saph-3a	-3	4.63	0.35	0.21	0.08	21.82
26-Saph-3b	-1	1.70	0.34	0.06	0.03	30.58
26-Saph-3b	-2	2.07	0.34	0.04	0.04	54.19
26-Saph-2b	-3	1.70	0.34	0.15	0.03	11.34
26-Saph-3c	-1	1.28	0.34	0.03	0.02	42.12
26-Saph-3c	-2	0.52	0.34	0.02	0.01	32.93
26-Saph-3c	-3	0.36	0.34	0.07	0.01	5.14
27-Saph-4a	-1	4.75	0.34	0.46	0.08	10.44
27-Saph-4a	-2	4.19	0.33	0.10	0.07	41.46
27-Saph-4a	-3	5.26	0.34	0.05	0.09	108.47
27-Saph-4b	-1	1.99	0.33	0.50	0.03	3.99
27-Saph-4b	-2	3.10	0.33	0.20	0.05	15.36
27-Saph-4b	-3	3.16	0.33	0.08	0.05	39.95
27-Saph-4c	-1	2.12	0.33	0.02	0.04	96.53
27-Saph-4c	-2	2.85	0.33	0.19	0.05	15.13
27-Saph-4c	-3	1.82	0.33	0.06	0.03	30.85

Table A1.5. 9 The ACCENT Intercomparison campaign results for Methyl Acetate.

Experiment	Ext.	Methyl Acetate	statistical	atmospheric	precision	signal/noise
		ppbv	ppbv	ppbv	ppbv	
25-Saph-2a	-1	5.94	0.14	1.45	0.05	4.1
25-Saph-2a	-2	5.99	0.14	1.49	0.05	4.0
25-Saph-2a	-3	5.34	0.14	1.35	0.04	4.0
25-Saph-2b	-1	2.12	0.10	0.64	0.02	3.3
25-Saph-2b	-2	1.92	0.10	0.63	0.02	3.1
25-Saph-2b	-3	1.77	0.10	1.09	0.01	3.1
25-Saph-2c	-1	0.95	0.09	0.37	0.01	2.6
25-Saph-2c	-2	1.00	0.09	0.36	0.01	2.8
25-Saph-2c	-3	0.70	0.08	0.28	0.01	2.5
26-Saph-3a	-1	3.97	0.12	1.14	0.03	3.5
26-Saph-3a	-2	3.64	0.12	1.11	0.03	3.3
26-Saph-3a	-3	3.52	0.12	0.49	0.03	7.2
26-Saph-3b	-1	1.70	0.10	0.21	0.01	8.0
26-Saph-3b	-2	1.75	0.10	0.42	0.01	4.2
26-Saph-2b	-3	1.52	0.09	0.71	0.01	2.1
26-Saph-3c	-1	1.15	0.09	0.27	0.01	4.3
26-Saph-3c	-2	0.85	0.08	0.18	0.01	6.0
26-Saph-3c	-3	0.80	0.08	0.14	0.01	5.6
27-Saph-4a	-1	4.97	0.13	0.14	0.04	35.6
27-Saph-4a	-2	4.89	0.13	0.28	0.04	17.8
27-Saph-4a	-3	4.79	0.13	0.24	0.04	20.0
27-Saph-4b	-1	2.37	0.10	0.12	0.02	20.1
27-Saph-4b	-2	2.47	0.10	0.72	0.02	3.5
27-Saph-4b	-3	2.40	0.10	0.35	0.02	6.8
27-Saph-4c	-1	1.62	0.09	1.06	0.01	1.5
27-Saph-4c	-2	1.72	0.09	0.65	0.01	2.7
27-Saph-4c	-3	1.50	0.09	0.21	0.01	7.1

Table A1.5. 10 The ACCENT Intercomparison campaign results for MVK & Methacrolein.

Experiment	Ext.	MVK+ Methacrolein	statistical	atmospheric	precision	signal/noise
		ppbv	ppbv	ppbv	ppbv	
25-Saph-2a	-1	13.30	0.16	1.91	0.24	6.97
25-Saph-2a	-2	12.81	0.15	1.78	0.23	7.19
25-Saph-2a	-3	11.42	0.15	1.65	0.21	6.91
25-Saph-2b	-1	3.72	0.09	1.08	0.07	3.45
25-Saph-2b	-2	3.70	0.09	0.94	0.07	3.94
25-Saph-2b	-3	3.63	0.09	2.41	0.07	4.43
25-Saph-2c	-1	1.22	0.06	0.53	0.02	2.33
25-Saph-2c	-2	1.10	0.06	0.50	0.02	2.20
25-Saph-2c	-3	1.03	0.06	0.44	0.02	2.35
26-Saph-3a	-1	7.20	0.12	1.75	0.13	4.12
26-Saph-3a	-2	6.91	0.11	0.57	0.12	12.03
26-Saph-3a	-3	6.86	0.11	0.57	0.12	11.96
26-Saph-3b	-1	3.04	0.08	0.41	0.05	7.47
26-Saph-3b	-2	2.87	0.08	1.61	0.05	1.78
26-Saph-2b	-3	2.79	0.08	0.27	0.05	10.51
26-Saph-3c	-1	1.37	0.06	0.34	0.02	4.07
26-Saph-3c	-2	1.45	0.06	0.41	0.03	3.49
26-Saph-3c	-3	1.30	0.06	0.12	0.02	10.48
27-Saph-4a	-1	9.53	0.13	2.48	0.17	3.84
27-Saph-4a	-2	9.58	0.13	1.53	0.17	6.25
27-Saph-4a	-3	8.65	0.13	2.87	0.16	3.01
27-Saph-4b	-1	4.31	0.09	0.15	0.08	29.67
27-Saph-4b	-2	4.24	0.09	0.73	0.08	5.82
27-Saph-4b	-3	4.16	0.09	0.44	0.07	9.56
27-Saph-4c	-1	2.50	0.08	0.28	0.04	9.06
27-Saph-4c	-2	2.45	0.07	0.82	0.04	2.97
27-Saph-4c	-3	2.08	0.07	0.96	0.04	2.17

Table A1.5. 11 The ACCENT Intercomparison campaign results for 1-propanol.

Experiment	Ext.	Propanol	statistical	atmospheric	precision	signal/noise
		ppbv	ppbv	ppbv	ppbv	
25-Saph-2a	-1	6.87	0.08	0.71	0.10	6.78
25-Saph-2a	-2	6.55	0.08	0.64	0.10	5.36
25-Saph-2a	-3	6.54	0.08	0.64	0.10	5.17
25-Saph-2b	-1	2.38	0.06	0.09	0.04	3.92
25-Saph-2b	-2	2.37	0.06	0.08	0.04	4.16
25-Saph-2b	-3	2.68	0.06	0.11	0.04	3.97
25-Saph-2c	-1	1.07	0.06	0.02	0.02	3.75
25-Saph-2c	-2	0.73	0.06	0.01	0.01	3.71
25-Saph-2c	-3	1.09	0.06	0.02	0.02	3.78
26-Saph-3a	-1	3.68	0.07	0.20	0.06	3.03
26-Saph-3a	-2	3.83	0.07	0.22	0.06	1.60
26-Saph-3a	-3	3.51	0.07	0.18	0.05	6.34
26-Saph-3b	-1	2.03	0.06	0.06	0.03	2.43
26-Saph-3b	-2	1.99	0.06	0.06	0.03	5.76
26-Saph-2b	-3	2.15	0.06	0.07	0.03	7.23
26-Saph-3c	-1	1.14	0.06	0.02	0.02	4.58
26-Saph-3c	-2	0.94	0.06	0.01	0.01	3.52
26-Saph-3c	-3	1.21	0.06	0.02	0.02	23.33
27-Saph-4a	-1	4.38	0.07	0.29	0.07	7.13
27-Saph-4a	-2	4.61	0.07	0.32	0.07	7.38
27-Saph-4a	-3	4.36	0.07	0.28	0.07	44.17
27-Saph-4b	-1	2.57	0.06	0.10	0.04	2.68
27-Saph-4b	-2	2.60	0.06	0.10	0.04	3.36
27-Saph-4b	-3	2.37	0.06	0.08	0.04	5.43
27-Saph-4c	-1	1.93	0.06	0.06	0.03	9.54
27-Saph-4c	-2	1.54	0.06	0.04	0.02	4.52
27-Saph-4c	-3	1.51	0.06	0.03	0.02	2.08

Table A1.5. 12 The ACCENT Intercomparison campaign results for Toluene.

Experiment	Ext.	Toluene	statistical	atmospheric	precision	signal/noise
		ppbv	ppbv	ppbv	ppbv	
25-Saph-2a	-1	7.93	0.18	2.54	0.10	3.1
25-Saph-2a	-2	7.63	0.18	2.48	0.09	3.1
25-Saph-2a	-3	7.96	0.18	2.61	0.10	3.0
25-Saph-2b	-1	2.63	0.12	0.79	0.03	3.3
25-Saph-2b	-2	2.67	0.12	0.69	0.03	3.9
25-Saph-2b	-3	2.44	0.11	3.22	0.03	2.1
25-Saph-2c	-1	0.93	0.09	0.54	0.01	1.7
25-Saph-2c	-2	0.67	0.08	0.40	0.01	1.7
25-Saph-2c	-3	0.70	0.08	0.38	0.01	1.8
26-Saph-3a	-1	4.26	0.14	1.41	0.05	3.0
26-Saph-3a	-2	3.63	0.14	0.98	0.04	3.7
26-Saph-3a	-3	3.78	0.14	0.78	0.05	4.8
26-Saph-3b	-1	1.81	0.11	1.21	0.02	1.5
26-Saph-3b	-2	1.52	0.10	0.32	0.02	4.8
26-Saph-2b	-3	1.22	0.10	1.04	0.01	1.2
26-Saph-3c	-1	0.85	0.09	0.09	0.01	4.1
26-Saph-3c	-2	0.67	0.09	0.12	0.01	5.5
26-Saph-3c	-3	0.63	0.09	0.25	0.01	2.5
27-Saph-4a	-1	5.04	0.15	1.09	0.06	4.6
27-Saph-4a	-2	5.33	0.16	0.44	0.06	12.2
27-Saph-4a	-3	4.63	0.15	0.21	0.06	21.8
27-Saph-4b	-1	2.33	0.11	0.39	0.03	6.0
27-Saph-4b	-2	2.52	0.12	1.17	0.03	2.1
27-Saph-4b	-3	2.48	0.12	0.20	0.03	12.7
27-Saph-4c	-1	1.37	0.10	0.17	0.02	8.1
27-Saph-4c	-2	1.44	0.10	0.17	0.02	8.6
27-Saph-4c	-3	1.37	0.10	0.69	0.02	2.0

Table A1.5. 13 Summary of signal-noise ratios obtained for the target OVOCs for the Jülich experiments for the days January 25th, 26th and 27th, 2005.

Experiment	Ext	acetaldehyde	acetone	benzaldehyde	butanal	1-butanol	hexanal	MBO	methyl acetate	methanol	MVK methacrolein	1-propanol	toluene
25-Saph-2a	-1	8.60	10.93	5.83	5.8	4.0	3.34	2.51	4.82	11.98	6.93	6.72	4.93
25-Saph-2a	-2	7.32	11.34	5.29	5.7	3.5	3.09	2.14	4.64	13.00	7.16	5.31	5.02
25-Saph-2a	-3	6.87	11.12	5.38	5.2	4.3	2.45	2.34	4.85	12.01	6.97	5.12	4.51
25-Saph-2b	-1	4.75	11.69	3.24	4.4	3.2	2.22	1.52	3.29	13.73	3.45	3.92	3.27
25-Saph-2b	-2	4.85	11.68	3.01	3.8	3.3	1.92	1.22	3.02	10.87	3.94	4.10	3.84
25-Saph-2b	-3	4.04	10.66	3.21	4.0	2.7	1.89	1.40	3.06	11.75	4.41	3.95	2.07
25-Saph-2c	-1	3.72	9.51	2.37	2.8	2.6	1.79	1.28	2.59	11.16	2.33	3.75	1.70
25-Saph-2c	-2	3.89	10.63	2.38	2.5	2.8	1.66	1.15	2.80	9.64	2.19	3.71	1.68
25-Saph-2c	-3	3.76	10.82	2.24	2.4	3.0	1.41	1.67	2.48	9.72	2.34	3.78	1.85
26-Saph-3a	-1	5.49	10.07	5.81	5.0	4.1	2.63	1.83	4.26	10.35	4.51	3.87	3.42
26-Saph-3a	-2	6.36	9.18	4.24	4.4	3.3	2.37	1.90	4.24	11.76	5.27	4.96	3.39
26-Saph-3a	-3	4.88	9.45	4.19	5.6	3.7	3.25	1.83	3.71	10.77	5.19	3.90	3.86
26-Saph-3b	-1	3.76	11.21	2.93	3.3	3.1	1.70	1.54	3.01	12.25	3.62	4.05	2.10
26-Saph-3b	-2	3.79	10.59	2.96	2.9	2.8	1.65	1.45	3.81	10.14	3.24	3.65	2.40
26-Saph-3b	-3	4.03	10.36	3.46	3.4	3.7	1.62	1.71	3.45	10.60	3.18	3.84	2.30
26-Saph-3c	-1	3.32	9.10	2.50	2.5	3.1	1.56	1.42	2.83	10.29	2.46	3.58	1.75
26-Saph-3c	-2	2.99	7.75	2.00	2.4	3.2	1.62	1.31	2.69	8.99	2.53	3.53	1.39
26-Saph-3c	-3	3.38	8.22	2.52	2.4	2.9	1.22	1.39	2.40	9.27	2.66	3.67	1.96
27-Saph-4a	-1	5.13	9.39	4.67	5.3	3.6	2.53	2.04	4.39	9.21	5.81	4.66	3.58
27-Saph-4a	-2	5.19	10.55	6.27	5.9	4.3	2.43	2.15	4.90	11.90	5.54	4.51	3.98
27-Saph-4a	-3	4.61	9.95	4.74	5.3	3.9	3.01	2.11	5.42	9.22	5.61	5.86	3.63
27-Saph-4b	-1	4.91	10.68	3.37	3.6	3.0	2.14	1.71	3.47	9.08	4.38	4.85	2.76
27-Saph-4b	-2	4.91	10.07	3.84	3.5	3.5	1.80	1.64	2.86	9.44	4.03	4.78	3.16
27-Saph-4b	-3	5.03	9.06	3.56	4.6	3.8	2.17	1.50	3.89	11.39	4.50	4.23	2.64
27-Saph-4c	-1	4.03	7.76	2.87	3.3	3.0	1.78	1.00	3.10	11.28	2.91	4.34	1.68
27-Saph-4c	-2	3.15	8.16	3.20	2.7	3.1	1.75	1.48	3.26	8.67	3.09	4.07	2.19
27-Saph-4c	-3	3.87	9.93	2.89	2.7	2.8	2.07	1.40	2.58	10.53	2.87	3.44	1.87

Appendix 2. Publications

A2.1 Articles

1. Demonstration of Proton-Transfer Reaction Time-of-Flight Mass Spectrometry for Real-Time Analysis of Trace Volatile Organic Compounds
R.S. Blake, C. Whyte, C.O. Hughes, A. M. Ellis and P. S. Monks
Anal. Chem. 2004, 76, 3841-3845
2. Proton transfer reaction time-of-flight mass spectrometry: a good prospect for diagnostic breath analysis?
R. S.Blake, C. Whyte, P. S. Monks and A. M. Ellis
Proc. 1st International Conference Breath Analysis, Dornbirn, Austria (2004)
- 3.. Intercomparison of Oxygenated Volatile Organic Compound (OVOC) Measurements
¹R. Koppmann, ¹T. Brauers, ¹J. Bossmeyer, ¹C. Holzke, ¹R. Tillmann, ¹R. Wegener, ²A. Brunner, ²M. Jocher, ²T. Ruuskanen, ²C. Spirig, ³R. Steinbrecher, ³R. Meier, ³D. Steigner, ⁴E. Gómez Alvarez, ⁵K. Müller, ⁶S. J. Solomon, ⁷D. Young, ⁸J. Hopkins, ⁹G. Legreid, ¹⁰A. Wisthaler, ¹¹R. Blake, ¹¹K. Wyche, ¹²A. Bjerke, ¹³E. Apel

¹Forschungszentrum Jülich, Jülich; Germany, ²FAL Agroscope, Reckenholz, Switzerland; ³Forschungszentrum Karlsruhe, IMK-IFU, Garmisch-Partenkirchen, Germany; ⁴CEAM, Valencia, Spain; ⁵Institut für Troposphärenforschung, Leipzig, Germany; ⁶Universität Bremen, Bremen, Germany; ⁷University of Bristol, Bristol, UK, ⁸University of York, York, UK; ⁹EMPA, Dübendorf, Switzerland; ¹⁰Universität Innsbruck, Innsbruck, Austria; ¹¹University of Leicester, Leicester, UK; ¹²NILU, Kjeller, Norway; ¹³NCAR, Boulder, CO, USA

Accent Symposium, Urbino 2005
4. Differentiation of isobaric compounds using chemical ionization reaction mass spectrometry.
K. P Wyche, R. S Blake, K. A Willis, P. S. Monks and A. M Ellis
Rapid Commun. Mass Spectrom. 2005; 19: 1-7

A2.2 Letters, Posters and Short Communications

5. R. S. Blake, C. Whyte, C. O. Hughes, A. M. Ellis and P. S. Monks
EGU Conference, Nice 2004 (Poster).
6. Chemical-ionisation processes in time-of-flight mass spectrometers for real-time analysis of atmospheric trace species.

R. S. Blake, A. M. Ellis, K. Willis, C. Whyte, K. P. Wyche and P. S. Monks
EGU Conference, Vienna 2005 (Poster)

7. Chemical ionisation reaction time-of-flight mass spectrometry for real-time analysis of atmospheric trace species.

R. S. Blake, A. M. Ellis, P. S. Monks, K. A. Willis and K. P. Wyche
ACCENT Symposium, Urbino 2005 (Poster)

8. Performance of a Chemical Ionisation Reaction Time-of-flight Mass Spectrometer During the ACCENT Oxygenated Volatile Organic Compound (OVOC) Measurement Intercomparison, Jülich 2005.

K. P. Wyche, R. S. Blake, A. M. Ellis and P. S. Monks.
ACCENT Symposium, Urbino 2005 (Poster)

References

References

Chapter 1

- Adams, N., and D. Smith, *Int. J. Mass Spectrom. Ion Physics*, 21, 349, 1976.
- Albritton, D., T. Miller, D. Martin, and E. McDaniel, *Phys. Rev.*, 171, 94, 1969.
- Baldwin, M., Peptides and proteins studied using mass spectrometry, in *Encyclopaedia of spectroscopy and spectrometry*, edited by J. Lindon, G. Tranter, and J. Holmes, Academic Press, London, 1999.
- Blake, R., C. Whyte, C. Hughes, A. Ellis, and P. Monks, Demonstration of Proton-Transfer Reaction Time-of-Flight Mass Spectrometry for Real-Time Analysis of Trace Volatile Organic Compounds, *Anal. Chem.*, 76, 3841-3845, 2004.
- Brasseur, G., J. Orlando, and G. Tyndall, *Atmospheric Chemistry and Global Change*, Oxford University Press, 1999.
- Cantrell, C., in *Challenges on photochemistry workshop*, GAAC, NCAR, Boulder, 1998.
- Caprioli, R., and M. Suter, *Int. J. Mass Spectrom. Ion Processes*, 118/119, 449-476, 1992.
- Ehhalt, D., *Phys Chem Phys*, 24, 5401-8, 1999.
- Fairley, D., D. Milligan, C. Freeman, M. McEwan, P. Spanel, and D. Smith, *Int. J. Mass Spectrom.*, 193, 35-43, 1999.
- Fehsenfeld, F., E. Ferguson, and A. Schmeltekopf, *J. Chem. Phys.*, 44, 3022, 1966.
- Fehsenfeld, F., W. Lindinger, H. Schiff, and E. Ferguson, *J. Chem. Phys.*, 64, 4887, 1976.
- Ferguson, E., F. Fehsenfeld, and A. Schmeltekopf, in *Advances in Atomic and Molecular Physics ed. DR Bates and I Estermann*, pp. 1-56, 1969.
- Friedrich, B., W. Trafton, A. Rockwood, S. Howard, and J. Futrell, *J. Chem. Phys.*, 80, 2537, 1984.
- Glosik, J., A. Jordan, V. Skalsky, and W. Lindinger, *Int. J. Mass Spectrom. Ion Processes*, 129, 109-116, 1993.
- Haagen-Smit, A., *Eng. and Sci. (Calif. Inst. of Technology)* (December), 1-7, 1950.
- Haagen-Smit, A., *Ind. Eng. Chem*, 44, 1342, 1952.
- Hansel, A., A. Jordan, R. Holzinger, W. Vogel, and W. Lindinger, *Int. J. Mass Spectrom. Ion Processes*, 149/150, 609-619, 1995.

- Hierl, P., V. Pacak, and Z. Herman, *J. Chem. Phys.*, **67**, 2678, 1977.
- Howorka, F., W. Lindinger, and M. Pahl, *Int. J. Mass Spectrom. Ion Physics*, **12**, 67-77, 1973.
- Hunter, P., and S. Lias, *J. Phys Chem*, **27** (3), 413-656, 1998.
- Jackson, A., Sources of Air pollution, in *handbook of Atmospheric Science*, edited by C. Hewitt, and A. Jackson, pp. 124-155, 2003.
- Lagg, A., J. Taucher, A. Hansel, and W. Lindinger, *Int. J. Mass Spectrom. Ion Processes*, **134**, 55-60, 1994.
- Lindinger, W., A. Hansel, and A. Jordan, On-line monitoring of volatile organic compounds at pptv levels by means of Proton-Transfer-Reaction Mass Spectrometry (PTR-MS) Medical applications, food control and environmental research, *Int. J. Mass Spectrom. Ion Processes*, **173**, 191-241, 1998.
- Mann, M., *Organic Mass Spectrometry*, **25**, 575-587, 1990.
- Märk, T., and H. Oskam, *Phys Rev A*, **A4**, 1445, 1971.
- McFarland, M., D. Albritton, F. Fehsenfeld, E. Ferguson, and A. Schmeltekopf, *J. Chem. Phys.*, **59**, 6610-6619, 1973.
- Middleton, P., Source and Pollutants, in *Composition, Chemistry and Climate of the Atmosphere*, edited by H. Singh, Van Nostrand Reinhold, 1995.
- Monks, P., Tropospheric Photochemistry, in *Handbook of Atmospheric Science*, edited by C. Hewitt, and A. Jackson, pp. 156-187, 2003.
- Munson, B., *Int. J. Mass Spectrom.*, **200**, 243 -251, 2000.
- Munson, B., and F. Field, *J. Am. Chem. Soc.*, **88**, 2621-2630, 1966.
- NIST, Standard Reference Database Number 69 (June 2005), National Institute of Standards and Technology, 2005.
- Pahl, M., W. Lindinger, and F. Howorka, *Z. Naturforsch.*, **27a**, 678-692, 1971.
- Phelps, A., and S. Brown, *Phys. Rev.*, **86**, 102, 1952.
- Praxmarer, C., A. Hansel, A. Jordan, H. Kraus, and W. Lindinger, *Int. J. Mass Spectrom. Ion Processes*, **129**, 121, 1993.
- Prazeller, P., P. Palmer, E. Boscaini, and T. Jobson, *Rapid Commun. Mass Spectrom.*, **17**, 1593-1599, 2003.
- Smith, D., and P. Španel, *Mass Spectrometry Reviews*, **25**, 661-700, 2005.
- Su, T., and J. Chesnavich, *J. Chem. Phys.*, **76**, 5183, 1982.

- Talrose, V., and A. Ljubimova, *Int. J. Mass Spectrom. Ion Processes*, **33**, 502-504, 1998 (reprint from 1952).
- Teloy, E., and D. Gerlich, *Chem. Phys*, **4**, 417, 1974.
- Warneke, C., C. Van der Veen, S. Luxembourg, J. de Gouw, and A. Kok, *Int. J. Mass Spectrom.*, **207**, 167-182, 2001.
- Wyche, K., *Private Communication*, 2005.
- Zhou, J., and R. Zhang, *Atmos. Environ.*, **38**, 2177-2185, 2004.

Chapter 2

- Alikanov, S., *Sov Phys JETP*, **4**, 452, 1957.
- Bergmann, T., T. Martin, and H. Schaber, *Rev. Sci. Instr.*, **60**, 347 & 792, 1989.
- Boesl, U., R. Weinkauff, and E. Schlag, *Int. J. Mass Spectrom. Ion Processes*, **112**, 121, 1992.
- Boesl, U., R. Weinkauff, C. Weickhardt, and E. Schlag, *Int. J. Mass Spectrom. Ion Processes*, **131**, 87, 1994.
- Boschetti, A., F. Biasioli, M. van Opbergen, C. Warneke, A. Jordan, R. Holzinger, P. Prazeller, T. Karl, A. Hansel, W. Lindinger, and S. Iannotta, *Int. J. Mass Spectrom.*, **17**, 143-151, 1999.
- Critchley, A., T. Elliott, G. Harrison, C. Mayhew, J. Thompson, and T. Worthington, *Int. J. Mass Spectrom.*, **239**, 235-241, 2004.
- de Gouw, J., C. Warneke, T. Karl, G. Eeredekens, C. Van der Veen, and R. Fall, *Int. J. Mass Spectrom.*, **223-334**, 365-382, 2003a.
- de Gouw, J., C. Warneke, B. Kuster, P. Goldan, and N. Lovejoy, pp. 44-47, Institut für Ionenphysik der Universität Innsbruck, Igls/Innsbruck, 2003b.
- Dupeyrat, G., B. Rowe, D. Fahey, and D. Albritton, *Int. J. Mass Spectrom. Ion Physics*, **44**, 1-118, 1982.
- Fishman, V., and J. Grabowski, *Int. J. Mass Spectrom.*, **177**, 175-186, 1998.
- Hansel, A., A. Jordan, R. Holzinger, W. Vogel, and W. Lindinger, *Int. J. Mass Spectrom. Ion Processes*, **149/150**, 609-619, 1995.
- Hanson, D., J. Greenberg, B. Henry, and E. Kosciuch, *Int. J. Mass Spectrom.*, **223-224**, 507-518, 2003.
- Howorka, F., W. Lindinger, and M. Pahl, *Int. J. Mass Spectrom. Ion Physics*, **12**, 67-77, 1973.

- Lindinger, W., *Phys Rev A*, 7 (1), 328-333, 1973.
- Lindinger, W., in *Gaseous ion chemistry and mass spectrometry*, edited by J. Futrell, pp. 141-154, Wiley, New York, 1986.
- Lindinger, W., A. Hansel, and A. Jordan, *Chem. Soc. Rev.*, 27, 347-354, 1998a.
- Lindinger, W., A. Hansel, and A. Jordan, On-line monitoring of volatile organic compounds at pptv levels by means of Proton-Transfer-Reaction Mass Spectrometry (PTR-MS) Medical applications, food control and environmental research, *Int. J. Mass Spectrom. Ion Processes*, 173, 191-241, 1998b.
- Mamyrin, B., D. Karataev, D. Shmikk, and V. Zagulin, *Sov Phys JETP*, 37, 45, 1973.
- Opsal, R., K. Owen, and J. Reilly, *Anal. Chem*, 57, 1884, 1985.
- Pahl, M., W. Lindinger, and F. Howorka, *Z. Naturforsch.*, 27a, 678-692, 1971.
- Španel, P., and D. Smith, *J. Phys. Chem.*, 99, 15551-15556, 1995.
- Prazeller, P., P. Palmer, E. Boscaini, and T. Jobson, *Rapid Commun. Mass Spectrom.*, 17, 1593-1599, 2003.
- Smith, D., and P. Španel, *Rapid Commun. Mass Spectrom.*, 10, 1183-1198, 1996.
- Soppart, O., and J. Baumbach, *Mass Sci. Technol.*, 11, 1473-1479, 2000.
- Stephenson, W.E., *Phys. Rev*, 69, 691, 1946.
- Warneke, C., C. Van der Veen, S. Luxembourg, J. de Gouw, and A. Kok, *Int. J. Mass Spectrom.*, 207, 167-182, 2001.
- Weickhardt, C., F. Moritz, and J. Grotemeyer, *Mass Spectrometry Reviews*, 15, 139-162, 1996.
- Whyte, C., *Private Communication*, 2003.
- Wiley, W., and I. McLaren, *Rev. Sci. Instr.*, 26, 1150, 1955.

Chapter 3

- Cunningham, A., J. Payzant, and P. Kebarle, *J. Am. Chem. Soc.*, 94, 7627, 1972.
- de Gouw, J., C. Warneke, T. Karl, G. Eerdekens, C. Van der Veen, and R. Fall, *Int. J. Mass Spectrom.*, 223-224, 365-382, 2003a.
- de Gouw, J., C. Warneke, B. Kuster, P. Goldan, and N. Lovejoy, pp. 44-47, Institut für Ionenphysik der Universität Innsbruck, Igls/Innsbruck, 2003b.

- Dotan, I., D. Albritton, W. Lindinger, and M. Pahl, *J. Chem. Phys.*, **65**, 5028-5029, 1976.
- Gilmore, I., and M. Seah, *Int. J. Mass Spectrom.*, **202**, 217, 2000.
- Kore Technology, TOF Handbook, 2003.
- Lau, Y., S. Ikuta, and J. Kebarle, *J. Am. Chem. Soc.*, **104**, 104, 1982.
- Warneke, C., J. de Gouw, W. Kuster, P. Goldan, and R. Fall, *Environ. Sci. Technol.*, **37**, 2494-2501, 2003.
- Zhou, J., and R. Zhang, *Atmos. Environ.*, **38**, 2177-2185, 2004.

Chapter 4

- Dommen, J., et al. (2003), paper presented at 1st International Conference on Proton Transfer Reaction Mass Spectrometry and its Applications, Institut for Ionenphysik der Universitat Innsbruck, Igls-Innsbruck.
- Dotan, I., et al. (1976), *J. Chem. Phys.*, **65**, 5028-5029.
- Hopkins, J. (2004), Analysis of C2-C7 NMHC, lightweight oxygenated VOC and DMS by Dual Channel GC-FID, *UFAM/ University of York*.
Leicester CC Report Why worry about fireworks?
- Lindberg, V. (2000), Uncertainties and Error Propagation (part 1), *Report Renslaer Institute of Technology*.
- Lindinger, W., et al. (1998), *Int. J. Mass Spectrom. Ion Processes*, **173**, 191-241.
- Steinbacher, M., et al. (2006), *Int. J. Mass Spectrom.*, **219**, 117-128.
- Warneke, C., et al. (2001), *Int. J. Mass Spectrom.*, **207**, 167-182.
- Wayne, R. (1994), Chemical Instrumentation, *Oxford Chemical Primers*, 65 - 69.

Chapter 5

- Dommen, J., M. Steinbacher, A. Prévôt, and N. A., in *1st International Conference on Proton Transfer Reaction Mass Spectrometry and its Applications*, edited by A. Hansel, and T. Mark, pp. 10-13, Institut for Ionenphysik der Universitat Innsbruck, Igls-Innsbruck, 2003.
- Ennis, C., Private Communication, *University of York*, 2004.
- Lindinger, W., A. Hansel, and A. Jordan, On-line monitoring of volatile organic compounds at pptv levels by means of Proton-Transfer-Reaction Mass Spectrometry (PTR-MS) Medical applications, food control and

- environmental research, *Int. J. Mass Spectrom. Ion Processes*, 173, 191-241, 1998.
- NIST, Standard Reference Database Number 69 (June 2005), National Institute of Standards and Technology, 2005.
- Španel, P., Y. Ji, and D. Smith, *Int. J. Mass Spectrom.*, 165-166, 25-37, 1997.
- Španel, P., and D. Smith, *Int. J. Mass Spectrom. Ion Processes.*, 167-168, 375-388, 1997.
- Steinbacher, M., J. Dommen, C. Ammann, C. Spirig, A. Neftel, and A. Prevot, *Int. J. Mass Spectrom.*, 219, 117-128, 2006.
- Warneke, C., C. Van der Veen, S. Luxembourg, J. de Gouw, and A. Kok, *Int. J. Mass Spectrom.*, 207, 167-182, 2001.
- Wayne, R., Chemical Instrumentation, *Oxford Chemical Primers*, 65 - 69, 1994.
- Zhou, J., and R. Zhang, *Atmos. Environ.*, 38, 2177-2185, 2004.

Chapter 6

- Adams, N., L. Babcock, T. Mostefaoui, and M. Kerns, *Int. J. Mass Spectrom.*, 223-224, 459-471, 2003.
- Anicich, V., *An index of the literature for bimolecular gas phase cation-molecule kinetics*, NASA, Pasadena, 2003.
- Ausloos, P., *J. Am. Chem. Soc.*, 104, 5259, 1982.
- Fairley, D., D. Milligan, C. Freeman, M. McEwan, P. Španel, and D. Smith, *Int. J. Mass Spectrom.*, 193, 35-43, 1999.
- Glagovich, N., Spectrometry Course Notes, Central Connecticut State University, 2005.
- Gross, J., *Mass Spectrometry - a Textbook*, Springer, 2004.
- Lias, S., J. Bartmess, J. Liebman, R. Levin, and W. Mallard, *J. Chem. Phys Ref Data*, 17 ((suppl 1)), 1-861, 1988.
- Lide, D., in *Handbook of Chemistry and Physics*, CRC, Boca Raton, 1991.
- Lindinger, W., A. Hansel, and A. Jordan, On-line monitoring of volatile organic compounds at pptv levels by means of Proton-Transfer-Reaction Mass Spectrometry (PTR-MS) Medical applications, food control and environmental research, *Int. J. Mass Spectrom. Ion Processes*, 173, 191-241, 1998.

- McLafferty, F., *Anal. Chem.*, **31**, 82, 1959.
- NIST, Standard Reference Database Number 69 (June 2005), National Institute of Standards and Technology, 2005.
- Silverstein, R., G. Bassler, and T. Morrill, Mass spectrometry, in *Spectrometric identification of organic compounds*, John Wiley & Sons Inc, USA, 1963.
- Smith, D., and P. Španel, *J. Chem. Phys.*, **104**, 1893, 1996.
- Smith, D., and P. Španel, *Mass Spectrometry Reviews*, **25**, 661-700, 2005.
- Stephenson, W.E., *Phys. Rev.*, **69**, 691, 1946.
- Warneke, C., J. Kuczinski, A. Hansel, A. Jordan, W. Vogel, and W. Lindinger, *Int. J. Mass Spectrom. Ion Processes*, **154**, 61, 1996.
- Williams, S., A. Midey, S. Arnold, R. Morris, A. Viggiano, and M. Berman, *J. Phys Chem A*, **104**, 10336-10346, 2000.
- Wyche, K., *Private Communication*, 2005.
- Zhou, J., and R. Zhang, *Atmos. Environ.*, **38**, 2177-2185, 2004.